DEVELOPMENT OF NANOCRYSTALLINE DIAMOND LATERAL VACUUM FIELD EMISSION DEVICES

By

Karthik Subramanian

Dissertation

Submitted to the Faculty of the

Graduate School of Vanderbilt University

in partial fulfillment of the requirements

for the degree of

DOCTOR OF PHILOSOPHY

in

Electrical Engineering

August, 2008

Nashville, Tennessee

Approved:

Professor Weng P. Kang

Professor Jim L. Davidson

Professor Bharat L. Bhuva

Professor Alvin M. Strauss

Professor Norman H. Tolk

To my dearest wife, Anu

To my beloved parents, Mrs. & Mr. Subramanian, and brother, Mouli

And

To our just-born baby boy, Vrushab

ACKNOWLEDGMENTS

I am deeply thankful to my dissertation advisor, Prof. Weng Poo Kang for offering me the opportunity to work on this research, and continuously guiding me through the course of my graduate study. His technical inputs helped me clearly understand the objectives of the research and develop problem-solving skills on more occasions than one. He has expertly guided my growth in this field of research and beyond and set targets for me to accomplish, which galvanized me to improve my thought process and work attitude. I express my heartfelt gratitude to Prof. Jim L. Davidson for his always prompt and sound technical assistance, constant encouragement and camaraderie. He has played a great role in defining and widening the scope of this research, in the process setting up exciting objectives to focus on during the progress of my work. I would also like to thank Profs. Bharat L. Bhuva, Norman H. Tolk, and Alvin M. Strauss for serving on my Ph.D. committee. Their valuable technical suggestions were instrumental in giving a well-defined shape to this research work. I am thankful to all my present and ex-colleagues in the Diamond Microelectronics Research Group, especially Dr. Yong Mui (Kelvin) Wong, Mr. Mick Howell, Dr. Bo Kyoung Choi, Rohit Takalkar, Supil Raina, and Dr. William H. Hofmeister for contributing vital suggestions through multiple discussions, along with Dr. Anurat Wisitsora-at for indirectly providing me help through his previous work on diamond vacuum field emission devices.

I thank Mr. Charles Ellis for allowing me to use the microfabrication facility at Auburn University, Alabama, especially the ICP-RIE system for the nanodiamond etch process. I would like to thank Mr. Ron Schroeder at the Honeywell Kansas City Plant for his collaboration in package development for the diamond lateral device. My gratitude goes to fellow graduate

students at Vanderbilt University, Jonathan Jarvis in the department of Physics and Astronomy for his involvement with field emission simulations, and Sriram Dixit in the Material Sciences program for helping me perform AFM and RBS measurements on nanodiamond samples. I would also like to thank Dr. Yunlong Cui of Fisk University for offering assistance with Raman Spectroscopy and the Vanderbilt Institute of Nanoscale Science and Engineering (VINSE) for providing its Clean Room facility for research. My acknowledgments also go to our administrative assistants, Janell Lees, and Lauren Fox for their efficient handling of the procurement of all lab supplies required for this research, and also to Lori Schmidt and Linda Koger, Department of Electrical Engineering and Computer Science for their administrative help throughout the course of my graduate program here at Vanderbilt.

This work would not have been possible without the financial support, in terms of research assistantship, from Tennessee Valley Authority (Diamond microtips program) and Army Research Labs (ACNP program). I am thankful to the Graduate School at Vanderbilt University for travel grants, which helped me attend and present my work at various international conferences. I express my appreciation to the participants at the conferences, especially Dr. Heinz Busta (Prairie Prototypes, LLC), Dr. David Hsu (Naval Research Labs), and Prof. Robert Nemanich (Arizona State University) for some useful suggestions, constructive criticism, and opinion regarding this work.

I owe a lot to my wife, Anupama for playing a significant role in my completion of this dissertation. She, also being a PhD student at Vanderbilt, has been incredibly supportive all through the course of my graduate studies, ensuring my confidence level is always at its high, creating the most conducive atmosphere for me to focus on my research, leaving other family

concerns out of my mind all the while. I would like to thank her for being there for me through this memorable journey.

My parents, Mr. & Mrs. Subramanian and my brother, Mouli Subramanian have instilled the importance of education in me right from a very young age and positively encouraged me the same way during the highs and lows of my educational career. They have devoted themselves at every possible stage in my life so far to ensure I do not compromise with my education, for which I cannot thank them enough. I am grateful to my parents-in-law, Dr. & Mrs. Balasubramanian, sister-in-law, Anitha and her spouse, Vijay Chandramouli, for listening to me with endless patience whenever I talk to them about my research.

I am indebted to my friends Sivakumar Pasupathy, Suresh Ramakrishnan, Santh Rajagopalan, Shankar Rajaraman, Saumitra Vajandar, Sameer Mahajan, Nikkon Ghosh, Siyu Wei, Kah Leng Soh, Sriram Balasubramanian, Balachandar Raghavan, Visweswaran Sundararaman, Ravivarman Periasamy, Narayanan Chandrasekaran, Anand Natarajan, Madhusudhan SN, Kumaran Ramasamy, Hariharan Kannan, Prakash Ragothamachar, my closest cousin, Mrs. Latha Ravichandran, my aunt and uncle, Mrs. and Mr. Jayashankar Bharadwaj, Vivek Devadevan, Gopinath Madhavan, Dennis Amon, Arun David, and others, who have contributed in their own unique ways during this period and always.

Above all, my heartfelt salutation to Mother Nature for creating infinite avenues to continuously explore, learn, and contribute to the development of science and technology, and in effect, life on this fascinating planet.

TABLE OF CONTENTS

LIST OF TABLES

Table Page

LIST OF FIGURES

Figure Page

CHAPTER I

INTRODUCTION

This chapter introduces the subject dealt with in this research. An overview of the field of vacuum microelectronics, in particular, its history and present research focus, is provided. The need for nanocrystalline diamond as a cold field emission material and the motivation behind the development of lateral emitter device technology are presented. Last, the specific objectives of the proposed research are outlined, followed by the organization of this dissertation.

1.1 Overview of vacuum microelectronics and vacuum field emission devices

Vacuum microelectronics is an emerging technology [1] that will lead to the development of electronic devices and device components with much better performance and higher operational limits than those found in solid-state devices [2]. Vacuum microelectronic devices rely on ballistic electron transport in vacuum for their operation, a fundamental difference from that of solid-state technology, in which the electron transport is impeded by the crystal lattice, placing a limit on both the miniaturization and the switching speed of active electronic devices. The interest in the field of vacuum microelectronics has grown greatly over the last decade.

The invention of solid-state transistors in the late 1940s [3], and the development of integrated circuits in the 1960s [4,5] had led people to believe that the time of using vacuum tubes was over. They were large, fragile, and inefficient then, requiring a vacuum to operate, with a cathode heated to over 1000 °C to generate the electrons. However, the rebirth of the vacuum tube in micron-sized forms has generated renewed interests in the utilization of vacuum microelectronic devices (VMDs) for many new applications. Present micro/nanofabrication

techniques have enabled the miniaturization of vacuum devices to nanoscale dimensions, specifically the field emission cathodes upon which the devices are based [6-8]. These vacuum electron source devices now offer several advantages over their solid-state counterparts. The ballistic transport of free electrons in vacuum is more efficient than the collision-dominated and mobility-limited transport in solid-state semiconductors, with no dissipation of energy and a very small electron transport time. The speed of electrons in solid-state medium is limited by the carrier saturation velocity of the solid (~10^7 cm/s in silicon) because of optical and acoustic phonons scattering, while in vacuum, it is limited only by the speed of light. Particularly, the operational characteristics of field emitter devices are essentially independent of the ambient temperature and are insensitive to radiation damage, unlike most solid-state devices that are primarily dominated by electron scattering transport in semiconductors, junction leakage at high temperature, and damage to the semiconductor crystal structure at high radiation, leading to spurious signals and general performance degradation. Also, the "junction-free" vacuum devices possess high-speed and long lifetime. As prominent issues of noise and leakage gain priority in solid-state circuits with technology scaling towards the sub-nanometer mode, vacuum-based nanoelectronics has the potential to become the technology of the future. These characteristics are conducive to employing vacuum microelectronics in many applications such as high-speed, high-power switches in power systems, active elements in integrated circuits, high-power amplifiers, microwave tubes and plasma electronics, field emitter arrays for flat panel displays and efficient light sources, instrumentation in space, aviation and communication systems, novel sensors/NEMS, electron microscopy and e-beam lithography, and x-ray generators [2,9,10].

Vacuum microelectronic devices principally utilize cold cathodes based on field-electron emission in contrast to the conventional electron tubes that exclusively employ cathodes based

on thermionic electron emission, thereby bringing certain unique aspects to device performance. Cold cathode devices can be turned on instantaneously, without a tedious warm-up period, and can operate at room temperature. In addition, electron field emission can provide higher current density than thermionic emission. By keeping vacuum as the signal carrier medium, these devices should hold high temperature and radiation tolerance, high reliability and long life properties as thermionic vacuum tubes do. Also, because of their small size, VMDs can operate much faster than the traditional vacuum tubes. **Table 1.1** summarizes the device properties of vacuum microelectronic devices and solid-state devices for potential applications.

Table 1.1 Comparison of vacuum microelectronic & solid-state electronic devices [1]

Property	**Solid-state devices**	**Vacuum micro/nano electronic devices**	**Comparison S-same; D-different; B-better; P-poor**
Structure	Solid/solid interface	Solid/vacuum	D
Size	Micron/nano-scale range	Micron/nano-scale range	S
Current density	10^4-10^5 (A/cm^2)	4 x 10^4 (A/cm^2)	S
Voltage (V_{op})	> 0.1 V	> a few (V)	D
Electron transport - medium - ballistic - coherence	 Solid < 0.1 μm, Low temp. Length < 0.1 μm Time < 10^{-13} s at RT	 Vacuum 100 % ballistic Length >> 0.1 μm Time >> 10^{-13} s	 B B B B
Electron energy	< 0.3 eV	Several to 1000 eV	D
Cutoff frequency	< 20 GHz (Si) < 100 GHz (GaAs)	< 100-1000 GHz	B
Power	Small	Large	B
Speed	Moderate	Very fast	B
Radiation hardness	Poor	Excellent	B
Temperature sensitivity	-30 to +50 °C	< 500 °C	B
Reliability	Fair	Good	B
Lifetime	Medium	Long	B
Technology	Very well established	Recently developing	P

The basic ideas that led to the development of microfabricated field emitter array (FEA) were conceived by Kenneth Shoulders and Dudley Buck at MIT in the 1950s [11]. They proposed to employ thin film deposition and micromachining techniques to fabricate integrated vacuum field-effect devices. To be seen in proper perspective, this was done before the advent of solid-state integrated circuits. Shoulders brought these basic concepts to the Stanford Research Institute (SRI International) and initiated a research program to develop microfabricated vacuum integrated circuits [12]. In 1961, he designed vacuum field emission device structures of micron size, and predicted their performance in terms of switching speed, operating voltage, lifetime, temperature and radiation tolerance, and envisaged certain applications for them, thus forming the genesis of the vacuum microelectronic technology, which is now being researched in essentially every industrial country of the world. It was Capp Spindt, also of SRI, in 1968, who materialized Shoulders' vision by developing a manufacturing scheme and microdevice, now popularly referred to as the Spindt emitter array [13-14], shown in **Figure 1.1**. The field then burgeoned in 1985, when the Spindt-developed field emission technology was used in flat panel displays by LETI CENG of Grenoble, France [15], and when Greene, Gray, and Campisi of the Naval Research Laboratory (NRL) presented their stimulating work on the gated silicon pyramid triode, marking the rebirth of interest in vacuum electronics [16]. The cross section of the latter device, as in **Figure 1.2**, was chosen as the logo for the International Vacuum Microelectronics Conference (IVMC), first held in Williamsburg, Virginia, which has been an annual event since then. The conference was renamed as the International Vacuum Nanoelectronics Conference (IVNC) in 2003, as the field embraced the advent of nanotechnology in vacuum field emission.

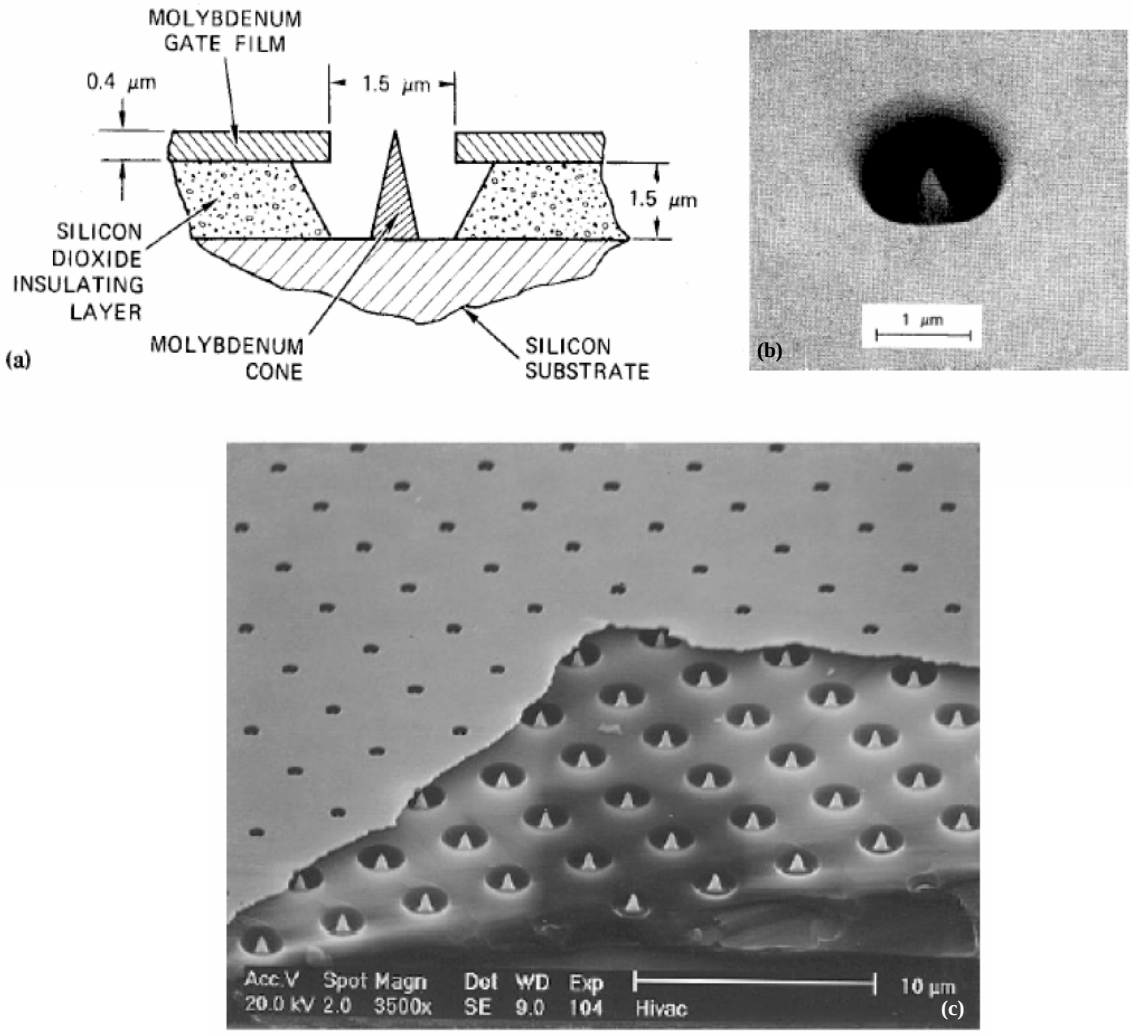

Figure 1.1 The Spindt microfabricated Molybdenum field emitter array structures [14].

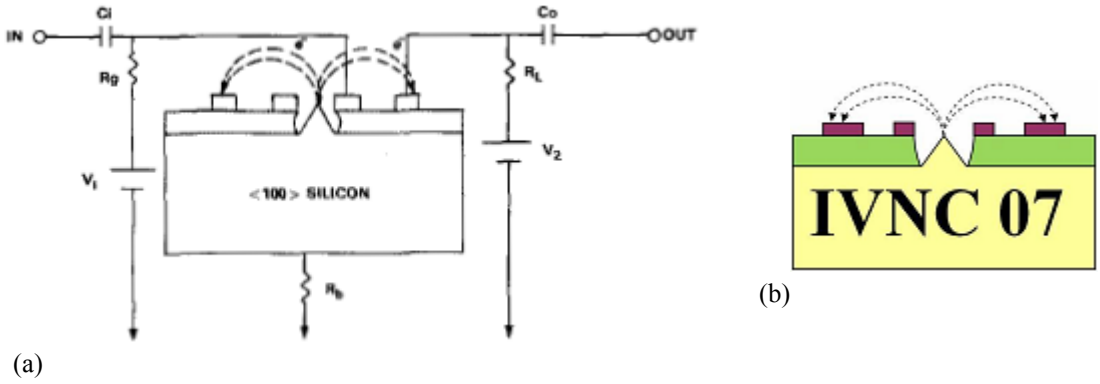

Figure 1.2 Cross-section of the integrated silicon field emitter array vacuum FET (Field effect transistor) developed by Greene et al, which was adopted as logo for the IVNC [16].

In the meantime, the core research of vacuum microelectronics has been the search for electron field emission devices with low operating voltage, high and stable emission current at practical vacuum levels for potential applications. A majority of the last decade has been focused on the development of new cathode materials and structures with better and more reliable performance for practical vacuum micro/nanoelectronic applications. These include the use of electric field enhancement on sharp micro/nanotips, and low work function wide band gap (WBG) emitter materials. Besides metal [13-14, 17-26] and silicon field emitter devices [16, 27-44], electron field emission from diamond, diamond-coated surfaces, and carbon related materials specifically carbon nanotubes (CNTs) has been the major subject of interest. These carbon-derived emitters have emerged as appealing candidates for the present generation of vacuum nanoelectronic devices.

Chemical vapor deposited (CVD) diamond has been shown experimentally to yield large emission currents at low electric fields relative to that of metals or narrow band-gap semiconductors. CVD diamond is an excellent electron emitter with a very low electron affinity, which allows for a very small threshold electric field [45-56] and subsequently a low turn-on voltage in an appropriately designed emitter vacuum device configuration. In addition, diamond has superior mechanical and chemical properties suitable for vacuum microelectronic applications. Diamond, being the hardest material known and also chemically inert, is immune to ion bombardment and chemical adsorption. Hence, the diamond emitters can operate with relatively good stability even at medium or practical vacuum levels achievable in a packaged environment. In addition, diamond has strong crystal structure, and hence field emission devices made of diamond should be able to operate with long life with no vacuum arcing even at high electric fields. The high thermal conductivity of diamond [57-59] prevents over-heating of the

emitters tips and maintains a very large current density. The wide band-gap (WBG) property permits the diamond emitters to have operational temperature immunity, which combined with its radiation tolerance characteristics, signifies a reliable material and device for harsh environments. The strongly bound crystal structure of diamond, its high electrical breakdown field and high thermal conductivity offer advantages over other materials, circumventing emitter tip erosion encountered at high current densities, as high and stable emission current requirements assume paramount importance in the potential application of vacuum micro/nanoelectronics for flat panel displays, intense electron sources for microwave generation, and other high power electronic devices, as illustrated by **Figure 1.3**.

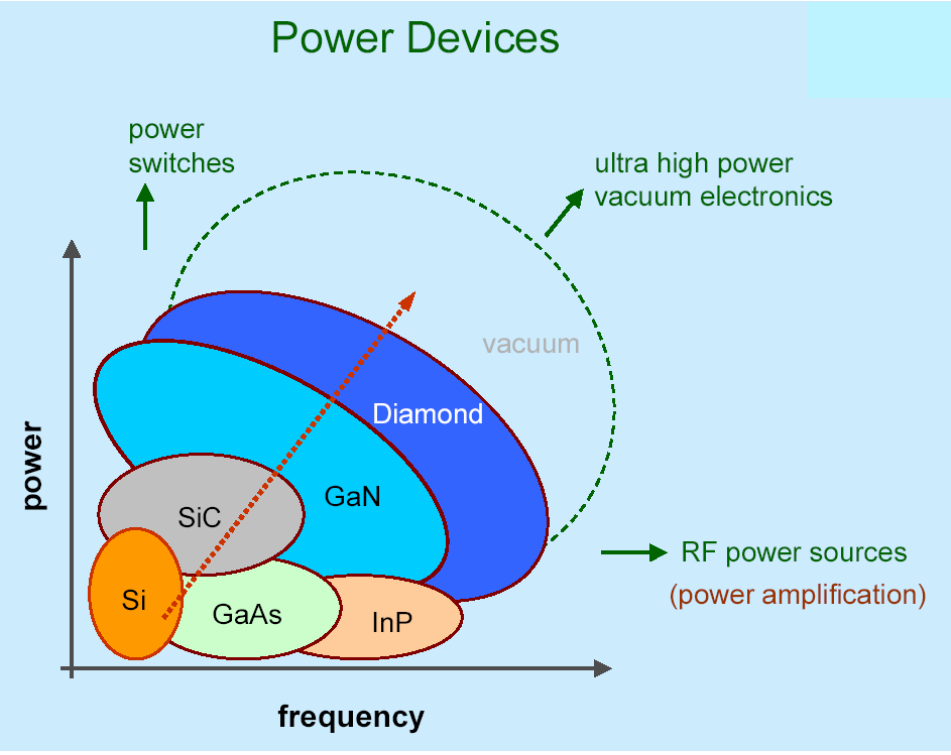

Figure 1.3 Illustration of the potential of diamond vacuum microelectronic technology for high power, high-frequency applications [60].

Table 1.2 summarizes the material properties of diamond, silicon and metal for field emission applications [61].

Table 1.2 Material properties of diamond, silicon and metal for field emission applications [61]

Property	**Diamond**	**Silicon**	**Metal**	**Advantages of diamond**
Electron affinity (eV)	Low EA and NEA on some facets	4.05	4-6	Low operating voltage
Electrical breakdown field (V/cm)	1×10^7	2.5×10^5	N/A	High power application
Thermal conductivity (W/cm-°C)	20	1.5	5-0.5	High emission current/current density
Carrier mobility (cm^2/V.s)	1.5×10^3	2.0×10^3	10^2-10^3	High carrier saturation velocity
Surface chemical stability	Relatively inert to adsorption	Very sensitive to adsorption	Quiet sensitive to adsorption	High stability, larger emitting area
Vacuum requirement (Torr)	Relatively low vacuum (10^{-5}-10^{-6})	Very high vacuum (10^{-10} – 10^{-11})	Very high vacuum (10^{-9}-10^{-11})	Practical vacuum environment
Process Technology	Recently developing	Well established	Well established, but with slow progress	Technology rapidly advancing

However, capturing the coveted properties of diamond reliably in thin film form has been challenging. Also, the utilization of these properties in device configurations has been hindered by the process difficulty in integrating diamond films with other materials (semiconductors, metals, oxides). The scarcity of appropriate wet, dry, or plasma etch techniques for diamond micropatterning has, so far, been a barrier to the successful realization of real diamond devices, especially in the case of cold cathode structures, where the emitter geometry directly affects

device performance. Incorporation of n-type donor impurities into diamond is required to directly populate the conduction band with electrons and induce emission with a very small electric field, taking advantage of the low or negative electron affinity surface of the material. It has not been an easy practice to introduce impurities especially donors into diamond since diamond is a wide band gap material with very tight lattice structure, and high activation energy. Further, there are very few reports of monolithic diamond emission devices, with feasibility of integration into vacuum ICs, such as diodes with built-in anode and triodes with built-in gate and anode, meeting the low operating voltage requirement of IC-compatible applications. From a fabrication perspective, batch-processing techniques for multiple field emission devices in wafer process technology have not been explored, especially with diamond. Importantly, the significant advantages offered by the properties of diamond for unaffected emitter device operation in hostile environments of high radiation, in addition to high temperatures, have not yet been utilized to realize the inherent potential of the vacuum technology for extreme-environment electronics. These issues are addressed in this research.

1.2 Introduction to nanocrystalline diamond

Nanocrystalline diamond or "nanodiamond" is one of the emerging materials, offering a wide range of applicability over the conventional CVD microcrystalline diamond. The properties of materials with nanometric dimensions are significantly different from those of atoms or bulk materials. Appropriate control of the properties of nanometer-scale structures can lead to new science as well as new devices, technologies, and products. Nanocrystalline diamond is evoking interest for vacuum electron devices [62-72], high-frequency surface acoustic wave (SAW) devices, and other applications in nanoelectronics [73-77], NEMS [78-79], biosensors,

electrochemistry and other varied fields [80-82]. Apart from the robust chemical, mechanical, and thermal properties of the conventional CVD microcrystalline diamond films, nanodiamond possesses certain distinct properties including smaller grain size (1 nm-100 nm), higher volume density of grain boundaries, smoother and more uniform surface morphology, n-type electrical conductivity at room temperature from nitrogen incorporation, increased (but still minute) degree of sp^2-bonded carbon content, hardness and lowered internal stress, and a wider latitude for integration with other materials associated with active electronic devices, viz., semiconductors, metals, and insulators. These properties of nanocrystalline diamond have been found to be capable of being effectively controlled and reproduced. The grain size, sp^2-carbon and n-type dopant are strong field enhancement factors (explained in detail in Chapter III), elevating the utility of diamond for vacuum nanoelectronic device applications.

1.3 Background & motivation behind lateral field emitter devices

This research focuses on the design, fabrication and characterization of nanodiamond lateral field emission devices, owing to the immense potential of the combination for practical vacuum micro/nanoelectronic devices. To date, the proposed and fabricated field emission devices have been largely divided into two categories, viz., vertical and lateral structures. Planar lateral field emission devices offer significant advantages in high-speed and high-frequency applications [83-103]. The first concept of a vacuum microelectronic device, proposed by Shoulders in 1961, included a "single-layer type" lateral emitter structure with a tetrode configuration (shown in **Figure 1.4 (a)**), having a switching time of ~ 10^{-10} s [12]. It was Busta, in 1989, who microfabricated the first lateral device using NiCr on a glass substrate, the device structure shown in **Figure 1.4 (b)** [83]. A *laterally configured* device, with the cathode, gate, and

anode lying on the same plane, can be easily designed to have a small electron path length resulting in reduced transit times [85]. Capacitance, a critical factor in determining the device speed is inherently small due to the small interelectrode overlapping area. Precise lithography-controlled micron and sub-micron interelectrode spacings enable a significant reduction in device operating voltages, enhancing the practicality of applying the device in vacuum integrated circuits. Low voltage operation, in addition to reducing the power requirements, can minimize destructive effect caused by ion sputtering. Ochiai et al. [100] and Oro et al. [85] have achieved interelectrode gaps as small as 10 nm and 20 nm respectively assisted by focused ion beam (FIB) and electron beam lithography (EBL) techniques in planar lateral emitter device structures. If an appropriate lateral device fabrication process is identified for nanodiamond, the low threshold electric field potential of the material can be best utilized to develop a vacuum microelectronic device with a turn-on voltage lower than or comparable to that of solid-state devices, offering a potential replacement for semiconductor devices, especially in high-speed, high-frequency applications.

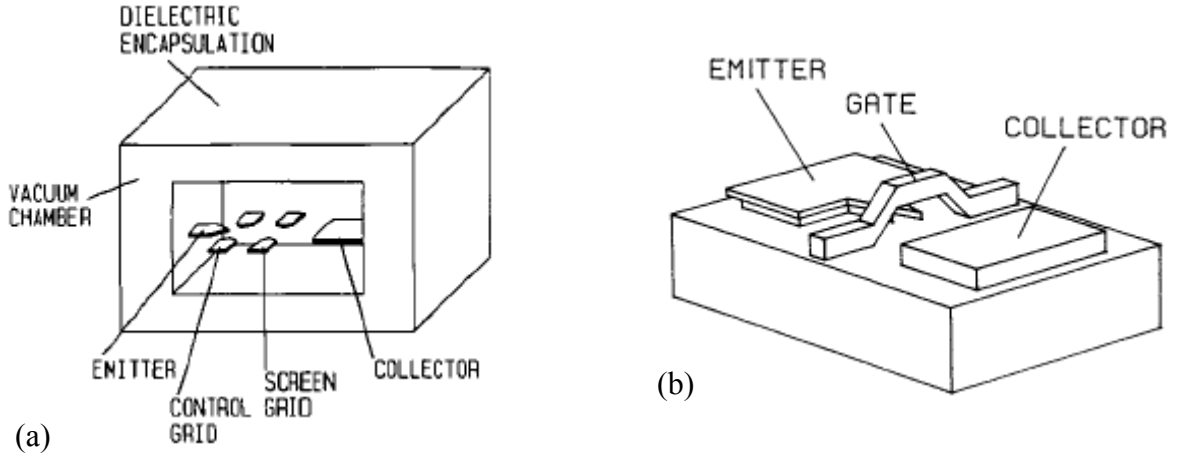

Figure 1.4 (a) Tunnel effect vacuum tetrode: single-layer type (lateral device) structure first proposed by Shoulders [12]; (b) A perspective view of the first fabricated lateral device using a NiCr emitter on a glass substrate [83].

One of the major challenges faced today in vacuum nanoelectronics is the development of emitter arrays delivering uniform emission current over a large area. A lateral device, with the emitter geometry and interelectrode gap defined by a high-resolution CAD-derived mask (layout) and transferred onto the emitting material by lithography process control, constitutes a versatile array construct suited for the generation of uniform current densities resulting in reliable array operation. Application of CVD diamond for lateral emitters can enhance the utility of the vacuum device for high power applications, owing to the high current per tip capability of the material. Moreover, the lateral configuration greatly reduces the processing complexity in monolithically integrating the anode, cathode and gate electrodes to achieve a complete field emission device, which can, in turn, be easily integrated with a driving circuit, such as CMOS circuits. This chip-type device architecture offers straight forward, conventional approaches to design performing electronic logic functions completely equivalent to conventional silicon devices except faster, more *rugged* and harder. The construct is also well suited for packaging with no device assembly issues involved. The application of the lateral emitters can extend to sensors and micro/nanoelectromechanical (MEMS/NEMS) systems, where the approach offers direct integration with MEMS actuators which provide a *mechanical tuning* feature. Milanović et al. [102] have shown that electrodes can be placed at closer, arbitrary distances by lateral actuation using comb drive, gap-closing, or thermal actuators, demonstrating a range of novel applications.

Lateral field emission diode and triode devices, based on a variety of materials other than diamond including silicon and metal cathodes, have been investigated with different emitter geometries following simpler micro/nanofabrication processes compared to vertically configured emission devices. Some of the common patterning techniques employed to build these fully

integrated device configurations are focused ion beam-enabled nanopatterning, UV/e-beam lithography, standard wet and dry chemical etch processing, orientation dependent etching (ODE), local oxidation of silicon (LOCOS), and thermal stress-controlled nanogap formation for possible use in integrated circuits, RF systems, sensors and MEMS, and flat panel displays. Sub-micron gate-cathode and anode-cathode spacings (0.1-0.4 μm) have been utilized to result in device turn-on voltages of 10-20 V and higher in some cases. However, the emission characteristics demonstrated deny practical applications due to high applied electric fields [85, 86, 99, 100, 104-111] and voltages resulting in relatively low emission currents, and possible leakage through the supporting oxide layer when the device is operated over time at high electric fields. Also, emitter tip degradation and destruction at current densities required for use in applications have been reported [112-113]. The turn-on voltage and maximum current capability are limited by the properties of the material applied and the processes employed to fabricate the devices. As the interelectrode gap cannot be reduced much further, it is imperative to decrease the electric field required to extract the electrons. With CVD diamond, having a low electron affinity and strong mechanical and thermal properties, and in particular, nanocrystalline diamond possessing suitable field enhancement factors and low work function with nitrogen incorporation, efficient and reliable nanodiamond lateral field emitters functioning at extremely low turn-on and operating electric fields and voltages generating high emission currents can be achieved. But, very less work has been reported [114] on diamond lateral devices due to the difficulty in realizing device-level, micron/submicron scale diamond patterning. In this research, we have identified a nanodiamond process technology for the development of lateral field emission devices.

1.4 Objective of the research

The purpose of this research is to develop reliable and consistent process techniques to deposit and micropattern nanocrystalline diamond thin films and integrate them in the fabrication of monolithic lateral electron field emission devices, operable at low voltage and electric field with high emission current for IC-compatible and extreme-environment applications in vacuum microelectronics.

This study is focused on the following:

- Development of a consistent process technique for the deposition of nanodiamond films;
- Identification of material factors contributing to field emission enhancement and the suitable optimization of the properties of nanodiamond;
- Development of a well-controlled diamond patterning scheme to realize useful micro/nanostructures for a wide range of applications;
- Design and fabrication of micropatterned nanodiamond field emission cathode, monolithic diode and triode devices in lateral configuration;
- Electrical characterization and analysis of nanodiamond lateral emitter devices as vacuum diodes and triodes.

1.5 Organization of the dissertation

There are seven chapters in this dissertation and they are organized in the following topics:

- *Chapter I* provides an overview of vacuum microelectronics and electron field emission devices. Need for the development of field emission devices and the advantages of nanocrystalline diamond as a material for vacuum devices are described. The

background and motivation behind the focus of this research on lateral electron emitters with nanodiamond is clearly outlined. Finally, the goal of the research is stated.

- *Chapter II* contains a theoretical background of basic electron emission in vacuum, and field emission from metal, silicon, and specifically diamond. This chapter also provides an extensive survey of recent theoretical and experimental work on diamond field emission.
- *Chapter III* is written to introduce the new material, nanocrystalline diamond, and its unique properties, with emphasis on its applicability to vacuum micro/nanoelectronics.
- *Chapter IV* explains the proposed research and the methodological approaches used to achieve the objectives.
- *Chapter V* describes the details of experimental conducted in this research, consisting of material and device processing, with the corresponding results.
- *Chapter VI* presents the vacuum electrical characterization techniques and the field emission performance of the devices developed.
- *Chapter VII* concludes the results of the proposed research, with recommendations provided for further work that can be explored in the area of study.

CHAPTER II

OVERVIEW OF ELECTRON FIELD EMISSION

In this chapter, the theoretical aspects of cold field emission have been discussed in detail. The possible mechanisms of field emission from CVD diamond and some of the important results reported so far from diamond emitters and devices are highlighted.

2.1 Basic principle of electron emission in vacuum

Electron emission is the process of emitting electrons from a solid surface into vacuum. The most common processes of electron emission are thermionic emission, thermionic-field emission, and field emission. In these processes, energies in form of heat and/or electric field are exerted to induce electron emission. The mechanisms for these processes can be explained by considering the energy band diagram of a metal-vacuum system as shown in **Figure 2.1**.

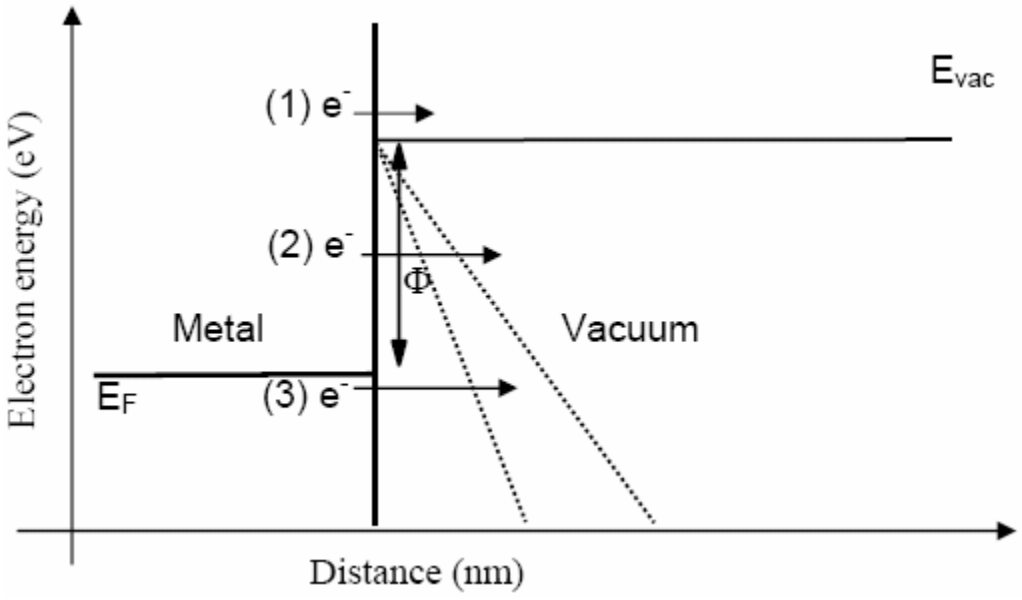

Figure 2.1 Mechanisms for thermionic (1), thermionic-field (2), and field emission (3) [115].

For thermionic emission, electrons emit into vacuum mainly due to heat application. At 0 K, all electrons in metal have energy below the Fermi level (E_F). As temperature increases, some electrons gain kinetic energy and have total energy above Fermi level. If temperature is sufficiently high, some electrons can have total energy higher than vacuum level (E_{vac}). These electrons ((1) e^- in **Figure 2.1**) are readily to emit into vacuum with no applied potential. Thermionic emission from metal is normally obtained at very high temperature of 1500-2500 °C depending on the metal work function.

At moderate temperature, some electrons have total energy above Fermi level but below vacuum level. These electrons ((2) e^- in **Figure 2.1**) are not readily to emit into vacuum. In order for these electrons to emit into vacuum, a moderate electric field must be applied to thin down the potential barrier as illustrated in **Figure 2.1**. This thermal-field activated emission process, via quantum-mechanical tunneling, is called thermionic-field emission. Depending on the metal work function, thermionic-field emission from metal can be observed at moderate temperature of 700-1500 °C.

Electron field emission is a unique quantum-mechanical effect of electrons tunneling from a condensed matter (solid or liquid) into vacuum. At low temperature, most of electrons have total energy below Fermi level. A strong external electric field must be applied to thin down the potential barrier (width of ~ 1.5 nm) at the solid/vacuum interface, thereby allowing electrons ((3) e^- in **Figure 2.1**) to quantum-mechanically tunnel into vacuum. This is called field emission because electric field is the main energy source that induces electron emission.

Electron emission can also occur by other methods such as light excitation (photoelectric electron emission), external electron energy (secondary electron emission), and internal polarization switching (ferroelectric electron emission). These interesting electron emission

phenomena are beyond the scope of this research. The efficiency of the field emission process is tens of millions of times higher than in other known emission processes. The extremely high current density in field emission and the fact that no energy is consumed by the emission process afford exceptionally wide possibilities for practical application of this effect. Theory and aspects of field emission as the main topic of this research are dealt with in the following sections.

2.2 Fowler-Nordheim theory of field emission

The electron field emission from cold cathodes with flat surface has been verified theoretically and experimentally to obey the Fowler-Nordheim equation, proposed in 1928 [116]:

$$J = (I/A) = K_1(E^2/\Phi)\exp(-K_2\,\Phi^{3/2}/E) \tag{2.1}$$

where K_1 and K_2 are constants: $K_1=1.54\text{x}10^{-6}$ A•eV/V^2, $K_2 = 6.83\text{x}10^7$ V/(cm•(eV)$^{3/2}$), J is the emission current density (A/cm^2), Φ is the work function of the emitting surface (eV) and E (V/cm) is the electric field across the parallel plates, which is given by:

$$E = V/d \tag{2.2}$$

where V is the anode-cathode voltage and d is the anode-cathode spacing.

It should be noted that Eq. 2.1 was derived for a metal cathode. From the equation, the emission characteristic strongly depends on the work function of the cathode. Material with lower work function gives a higher emission current at a given applied electric field. Considering the absolute value in the exponent of the equation, Φ is usually around 4-6 eV for metals, thus $\Phi^{3/2}$ and the exponential factor are approximately 10 and $10^{-3x10^8/E}$ respectively. Therefore, an applied field greater than 3×10^6 V/cm is needed to make any sensible emission measurement from a planar metal cathode [117].

In order to reach these high fields at reasonable voltages, it is customary to machine the field emitters into protruding objects to take advantage of the field enhancement of regions of high curvature. Hence, let us consider the sharp cone structure, generally referred as the "Spindt cathode", which has been developed using various types of metal materials. The sharp cone structure results in *non-uniform* electric field. The electric field is highest at the tip apex and rapidly decreases outward to the anode. Thus, the F-N equation, Eq. (2.1), which is derived for planar cathode with an assumption that there is uniform electric field in the vacuum gap, cannot be precisely applied. The precise calculation of potential distribution, electric field, and emission current for a sharp microstructure involves numerical calculation of 3-dimensional Poisson equation and Schrodinger equation for electron emission [118-120]. However, the emission current for a sharp microstructure can be obtained with a simple modification of Fowler-Nordheim equation for a planar metal cathode by replacing the parallel electric field in Eq. (2.2) with electric field at the apex of the sharp microstructure that is:

$$E = \beta V/d \tag{2.3}$$

where β is defined as the geometrical field enhancement factor, which is the factor of which electric field is increased due the sharp microstructure relative to the planar structure. The Fowler–Nordheim current of an array of emitters is then given by:

$$I = n\alpha \frac{1.54x10^{-6}(\beta E)^2}{\phi} \exp\left(-6.83x10^7 \frac{\phi^{3/2}}{\beta E}\right) \tag{2.4}$$

where n is the number of emitters in the array, and α the emitting area per tip in cm^2. This F-N equation, Eq. (2.4) can be rewritten as [7]:

$$\ln\left(\frac{I}{E^2}\right) = \ln\left(1.54x10^{-6} \frac{n\alpha\beta^2}{\phi}\right) - 6.83x10^7 \frac{\phi^{3/2}}{\beta E} \tag{2.5}$$

Thus, by plotting the emission current in the form of $\ln(I/E^2)$ versus $1/E$, a straight line should be obtained with a slope proportional to $\Phi^{3/2}/\beta$ and an intercept proportional to $n\beta^2/\Phi$.

It is well known that the geometrical field enhancement factor increases with sharpness of the tip and the field at the apex of the tip is inversely proportional to the tip radius. This simple approximation implies that the emission current for a sharp microstructure is equivalent to the emission current of a planar cathode of the same vacuum gap but the effective electric field is increased by the factor of β. This agrees very well with experimental results because the electric field of a sharp tip is strongest at the apex and reduced rapidly for the region away from the apex and thus it can be assumed that most of emission current arises from electron tunneling within the vicinity of this highest electric field region. Even with the sharp cone structure, the operating voltage of the cathode is still high, since the field enhancement factor is limited to 100-500 by the technology of making the sharp metal tips.

The sharp cone concept was later extended to silicon cathode structure. The silicon cathode is usually heavily doped (n^+) to achieve low work function for silicon ($\Phi \approx \chi = 4.12$ eV) and good ohmic contact with metal. The potential drop across the depletion region in the n^+ silicon (V') is generally very small compared to the potential drop across the vacuum gap because only small voltage is required for electrons to quantum-mechanically tunnel through the thin depletion potential barrier into the conduction band of n+ silicon. Thus, it is practical to assume that most of the potential drop across the vacuum gap and the enhanced electric field $E=\beta V/d$ is established at the apex of the tip. The enhanced electric field at the apex allows electrons in conduction band of silicon to quantum-mechanically tunnel through the silicon-vacuum potential barrier into the vacuum. Finally, electrons are accelerated by the electric field and collected at the anode.

Silicon emitters [16, 27-44] have shown some improvements over the metal cathodes. Since the work function of silicon is in the same order of magnitude as metal work function, the improvement obtained from silicon emitter is the increasing in the geometrical field enhancement factor due to the availability of advanced silicon technology for making sharper tips. In addition, the well-established IC technology allows the fabrication of more complex triode device structures and makes mass production of the emitters possible. However, silicon emitters have limited applications, because the operating voltage of the silicon cathode is still high compared to that of a solid-state device. Also, a silicon emitter is prone to surface adsorption, which leads to instability and reproducibility problem. The life of the emitter is short owing to tip destruction under high electric field.

2.3 Electron field emission from diamond

The presence of low electron affinity on diamond surfaces, coupled with the practical chemical vapor deposition (CVD) of diamond as a thin film on a variety of substrates, has promoted further interest in the use of diamond and diamond-like carbon materials as field emitters [121]. Experimentally, diamond has been observed to emit electrons at relatively low electric fields and generate useful current densities [56,122-123].

Diamond is one of the main crystalline allotropes of carbon, as shown in **Figure 2.2** [121]. It is the high-pressure form of carbon with an sp^3-tetrahedral bonded cubic structure. Diamond has low electron affinity, which is a measure of the energy barrier that electrons must overcome to escape into vacuum. This combination of low surface barrier to electron emission in an otherwise robust material has attracted attention to diamond's promise as a high performance cold cathode material. Diamond is an indirect wide band-gap material with E_g =5.45 eV. Three

distinct types of diamond surfaces have been widely studied [45-55, 61]. For hydrogen-free diamond surfaces, the electron affinity is small and positive as shown in **Figure 2.3(a)**. Partially hydrogenated (111) and (100) diamond surfaces have effective negative electron affinity (NEA), as illustrated in **Figure 2.3(b)**. The hydrogen is deposited as ionic species to form an affinity lowering surface dipole. This reduction in electron affinity, together with a short characteristic band bending at the surface results in the effective NEA surface. Furthermore, diamond surface coated with a thin layer of metal such as Zirconium (Zr) [124], Cobalt (Co) [124-125], Ni [126], and (111)-(2x1) Diamond-TiO surface [127] also exhibit effective NEA property. Last, the diamond (100)-(2x1):H and completely hydrogenated surface is believed to be a true NEA surface as illustrated in **Figure 2.3(c).** In addition, it is believed that a true NEA surface also exists on Cesium or Cesium oxide coated diamond (100) surface [128]. The occurrence of the true NEA has not been found for conventional semiconductor materials and is thought by many to never occur.

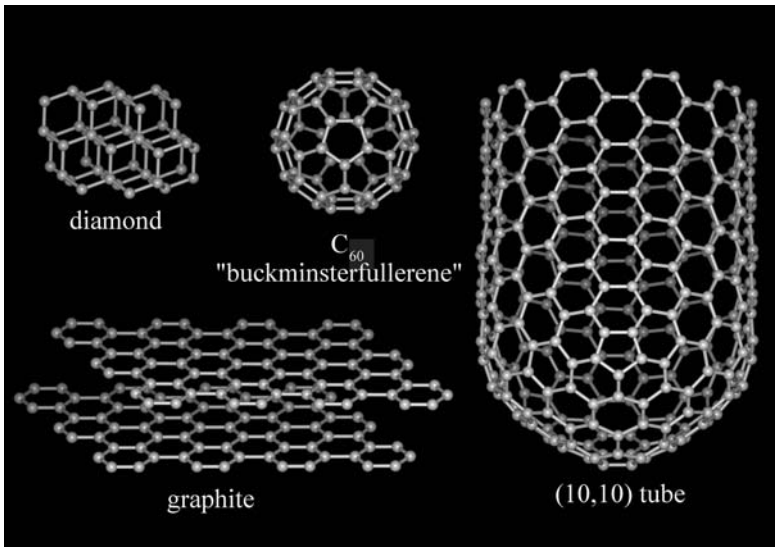

Figure 2.2 The allotropes of carbon, diamond, graphite, C_{60}, and carbon nanotubes [121].

2.3.1 Energy band diagram of diamond

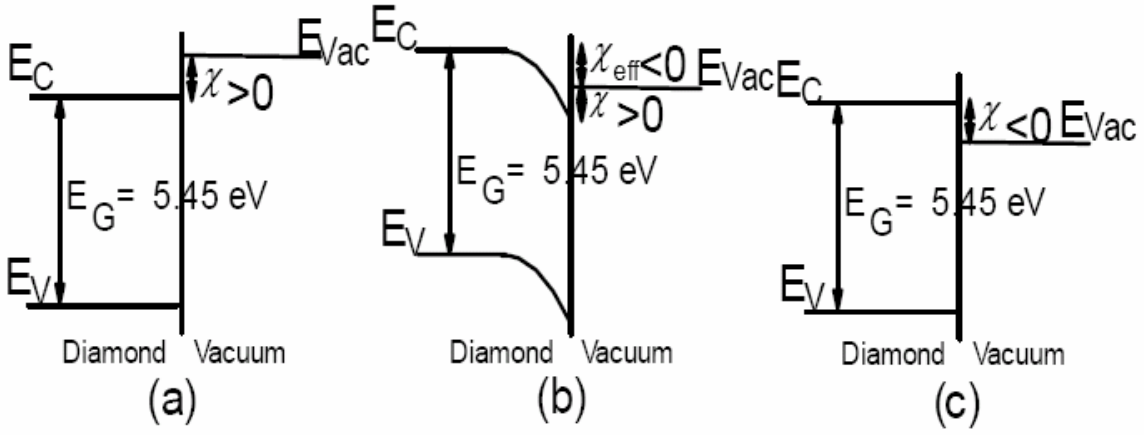

Figure 2.3 Energy band diagrams of diamond: (a) Positive electron affinity; (b) Effective negative electron affinity; (c) True negative electron affinity [115].

Assuming a small positive electron affinity for diamond surface, a complete energy band diagram for electron emission from the surface may be drawn as shown in **Figure 2.4** [115]. For electron emission to occur, electrons must quantum-mechanically tunnel through the potential barrier at metal-diamond interface into diamond. Electrons will then drift through diamond bulk and go over a small potential barrier at diamond-vacuum interface into vacuum.

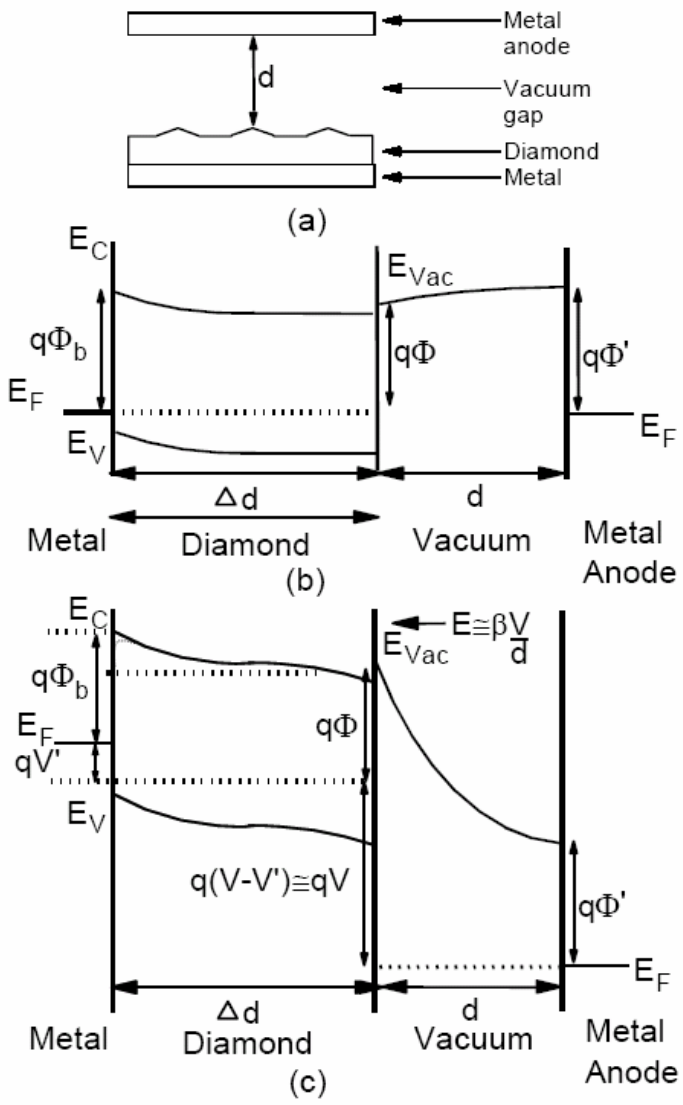

Figure 2.4 Diamond cathode structure and energy band diagrams. (a) Diamond cathode structure; (b) Energy band diagram at thermal equilibrium; (c) Energy band diagram under forward bias [115].

Small electron affinity of diamond is believed by many to be responsible for observed low field emission from diamond because small electron affinity would allow electrons from the conduction band to emit into vacuum easily with low applied electric field. However, electron in the conduction band of diamond is limited because diamond is a wide band gap material, unless

n-type doping is performed. Thus, electrons must be injected from metal into conduction band of diamond in order for emission to occur. High electric field should be required for electrons to tunnel through metal-diamond interface because the potential barrier at metal-diamond interface would be as high as work function of silicon or metals. Thus, the basic energy band diagram as described is inadequate for the explanation of the observed low field emission from diamond.

In order to understand the field emission mechanism from diamond, a better knowledge of carrier transport through diamond-metal interface and the diamond film is needed. In addition, a more complete energy band structure, which includes the effect of grain boundary and defects of polycrystalline diamond, also needs to be studied. Furthermore, unknown characteristics of diamond surfaces such as sharp facets of as-grown diamond with unknown field enhancement factor further complicated the emission mechanisms from diamond surfaces. A considerable amount of experimental and theoretical works has been carried out to reveal the field emission mechanism in CVD diamond. Several field emission enhancement models for various types of diamond emitters have been proposed. The following section summarizes some of the proposed theories and models.

2.3.2 Emission mechanisms

While the low electron affinity property of diamond surfaces may be important and can make diamond an efficient photoemitter, it is not adequate by simply invoking this property to explain why diamond is a good field emitter. For field emission to occur, and more importantly to sustain, there must be a continuous supply of electrons and a sustainable transport mechanism for the electrons to reach the surface. Moreover, the energy levels of these electrons relative to the vacuum level are critical in determining the threshold field required for emission. A small

electron affinity surface is practically useful in reducing the barrier for electron emission only when the energy levels of some occupied states or bands, including surface states, are positioned sufficiently close to the conduction band minimum in diamond.

Simple field enhancement model

Among the various models, the simplest and the most obvious argument cites the classic field emission theory, described earlier in this chapter, by noting that there are local field enhancements on sharp morphological features protruding on the diamond surface. The electric field at a given applied potential is enhanced by these sharp microstructures [129] and thereby electron tunneling is enhanced. Field emission from micropatterned diamond microtips exhibits significant enhancement both in total emission current and stability compared to planar diamond emitter. To apply the simple field enhancement model, the microstructure must have certain geometry with a smooth surface. The geometrical field enhancement factor β depends only on the geometry of the microstructure. The field enhancement factor β for various shapes of microstructure [1] has been estimated based on electrostatic theory and shown in **Figure 2.5**. The electric field at the surface of a sphere, **Figure 2.5 (a)**, of a rounded whisker can be evaluated using elementary electrostatic theory and expressed in closed form as a function of polar angle θ as [1]:

$$E=(V/d)(h/r+3\cos\theta) \tag{2.6}$$

$$\beta= h/r+3\cos\theta \tag{2.7}$$

where h is the height of the sphere from the base, r is the radius of the tip, V and d are defined previously.

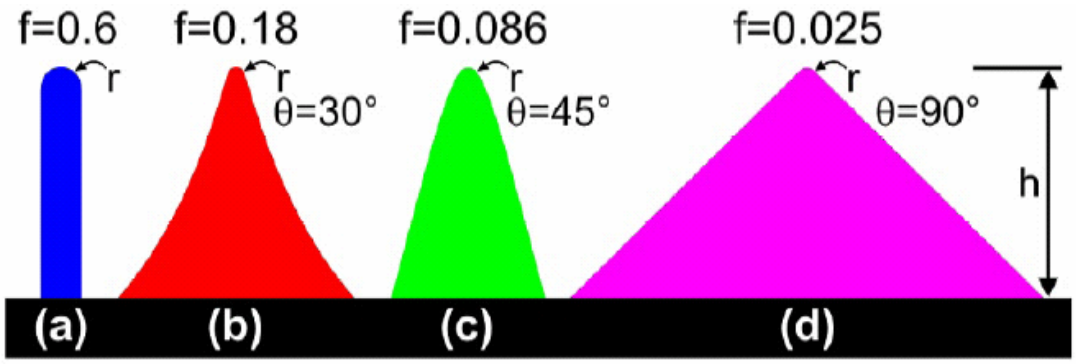

Figure 2.5 Various shapes of field emitters: (a) Rounded whisker; (b) Sharpened pyramid; (c) Hemi-spheroidal; (d) Pyramid [1].

For h>>r, $E \approx (h/r)(V/d)$ and $\beta \approx h/r$, it has been shown that the field at the apex of a rounded whisker shape is approximately equal to that of a floating sphere and is given by $E = (h/r)(V/d)$. Thus, it has primarily been concluded that the round whisker shape is the closest to the "ideal" field emitter. On the contrary, a wide-angle pyramidal shape is not an optimum field emitter even though its thermal and mechanical stability is excellent. In addition, it was primarily found that a wedge molybdenum shape emitter [17] has an effective emitting area about 100 times greater than a conical shape emitter and a correspondingly larger current density. However, wedge-shape diamond tip arrays fabricated by mold transfer technique, reported later, did not exhibit significant field emission enhancement compared to the pyramidal shape one [130].

Two step field enhancement (TSFE) model

This model is a modified version of the simple field enhancement model developed to account for the complicated morphology of diamond surface. The emitting surface may be thought of as a number of small protrusions act as tiny tips. The emitting tip with height h_1 and sharpness of radius r_1 is assumed to consist of a number of tiny tips with height h_2 and sharpness of radius r_2 as shown in **Figure 2.6**.

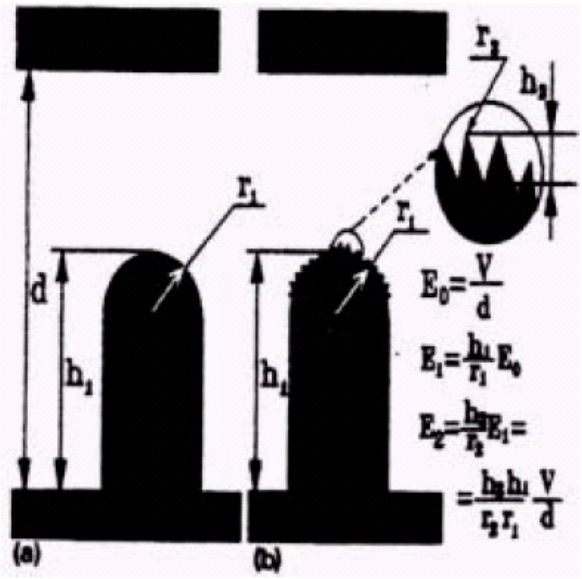

Figure 2.6 Geometry of emitters: (a) The simple field enhancement approach; (b) The TSFE approach [115].

The electric field on the blunt tip is equal to:

$$E_1 = (h_1 / r_1)(V/d) \tag{2.8}$$

and the field enhancement at the end of protrusions is equal to:

$$E2 = (h_2 / r_2)\, E_1 = (h_1\, h_2 / r_1\, r_2)(V/d) \tag{2.9}$$

where V and d are defined previously.

The TSFE model was applied to analyze electron emission from diamond coated silicon field emitters [131]. The emission current were calculated using the F-N analysis on diamond coated silicon field emitters based on the TSFE model and found to be in good agreement with experimental data. It has been proposed that the ultrasharp protrusions may be formed under the assumption that the diamond particles are relatively large (of micrometer range) and thus they are not truly smooth or spherical but have microstructures with some spikes of deep-submicrometer sizes. The (111) surface on the spike microstructure may be thought of as spikes

of deep-submicrometer sizes or ultra sharp protrusions because (111) part of the surface with NEA could be the only actively emitting spot.

The TSFE model has also been well applied to explain the increase in the geometrical field enhancement of sharpened pyramidal diamond microtips [115]. In this case, the sharpened diamond microtip was modeled as a large conical tip with tip height of h_1 and tip radius curvature of r_1, superimposed with a sharp tiny conical tip with tip height of h_2 and tip radius curvature of r_2, as shown in **Figure 2.7**. The electric field at the sharpened tip apex arises from a two-cascaded tip structure. In the first step, the electric field at the apex of large conical tip is enhanced by the factor of h_1/r_1 from the planar base, while in the second step, the electric field at the apex of the sharp tiny conical tip is enhanced by the factor of h_2/r_2 from the apex of large conical tip. Thus, the total geometrical field enhancement factor of the diamond microtip was taken as the product of field enhancement factors of the two cascaded tip structure:

$$\beta_g = \left(\frac{h_1}{r_1}\right)\left(\frac{h_2}{r_2}\right) \tag{2.10}$$

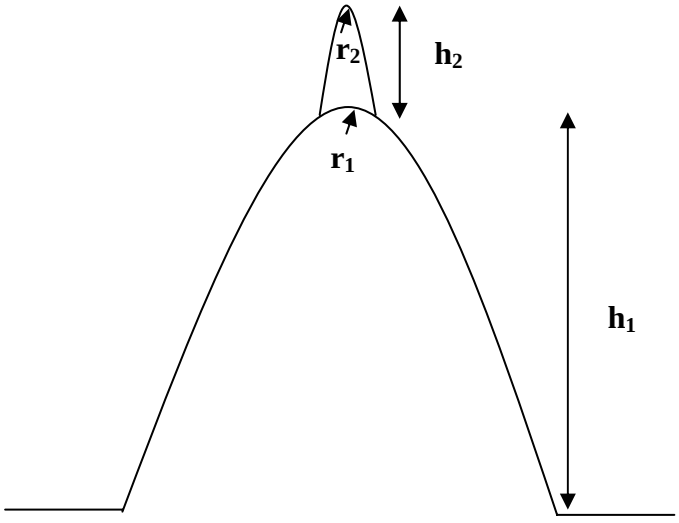

Figure 2.7 Illustration of the two-step field emission enhancement (TSFE) model applied to explain the geometrical field enhancement in diamond microtips [115].

The geometrical field enhancement estimated using the model was found to be in good agreement with the result obtained from F-N analysis. These field enhancement models could certainly be a working and contributing mechanism, but it addresses neither the source of electrons in the wide-bandgap diamond nor the issue of effective electron transport to the surface of diamond.

Defect/impurity theory

The defect/impurity theory suggests that structural defects and impurities can form energy states within the band gap of diamond [132-136]. When the defect density is sufficiently high, the electronic states of various defects can interact and form energy bands. If these bands are wide enough or closely placed, the electron hopping mechanism within the bands, similar to the Poole-Frenkel conduction mechanism or the Hill type conduction [137-138] could easily provide a steady flow of electrons to the surface and sustain a stable electron emission. The electrons can either be excited into the conduction band or unoccupied surfaces states from these defect/impurity bands and emit, or tunnel directly from the defect/impurity bands and emit. For example, photoelectron yield spectroscopy detected sub-bandgap emission associated with the presence of graphite in diamond [139]. The defects/impurities essentially raise the Fermi level by acting as donors of electrons and thus reduce the tunneling barrier. This theory is supported by overwhelming experimental data indicating that defective or lower quality diamonds have better emission properties.

Role of sp^2-carbon content in the diamond film

In regard to the role of graphite in the electron emission from diamond, Athwal et al. [140], and Xu and Latham [141] suggested a field-induced hot electron emission process from isolated graphitic inclusions in diamond, citing an antenna effect that leads to field concentrations on a "floating" conductive particle (i.e., graphite) embedded in an insular matrix (i.e., diamond). This model is based on the observation that active emission sites correspond to discrete location of defects or graphite inclusions on the diamond surface [142-146]. To sustain a continuous emission current, electrons are assumed to be supplied to the emitting surface through conduction channels formed in diamond via an electroforming process at high electric fields [147-148]. Grain boundaries in diamond films [149-150] and hydrogenated diamond surfaces [146, 151] have also been suggested to function as conduction channels.

Developing from the hot electron emission model, Wisitsorat-at [115,122] proposed that isolated conducting sp^2 nano-particles in the diamond film form a series of cascaded MIM (metal-insulator-metal) microstructures, which enhance the electric field inside the diamond film, thereby increasing the field enhancement factor. The image effect at the diamond-sp^2 interface causes band bending in the conduction band of diamond as illustrated in **Figure 2.8**. The enhanced electric field decreases the width of tunneling distance, W, at the metal-diamond interface significantly, and thereby increases the electron tunneling probability from metal into the conduction band of diamond. The electrons in the conduction band of diamond are then accelerated toward the next floating sp^2 particle under the induced electric field. Thus, the sp^2 particles would enhance diamond field emission.

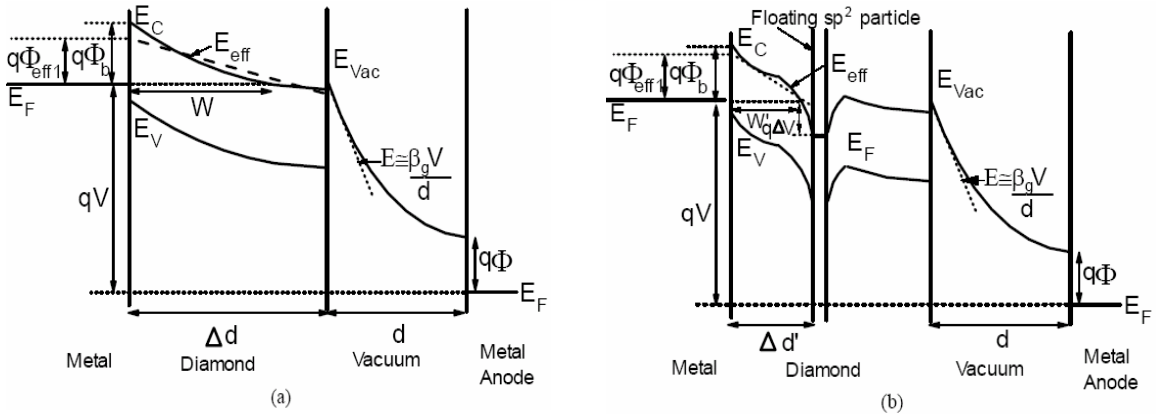

Figure 2.8 Mechanism of sp^2-carbon in diamond film as a field enhancement factor [115].

Similarly along this mechanism, Cui et al. [139] concluded from their photoelectron sub-bandgap emission study that the diamond phase provides a thermally and mechanically stable matrix with a comparatively low work function, and graphitic phases provide the transport path for electrons to reach the surface and emit.

Field emission enhancement via doping

In theory, the addition of n-type donor impurities into diamond is the best approach to enhance electron emission from diamond. Since diamond has low electron affinity, if the conduction band can be directly populated with electrons via donors, very small electric field is sufficient to induce electron emission. In practice, it is not easy to introduce impurities especially donors into diamond since diamond is a wide band gap material with very tight lattice structure. Diamond film doping with various group V elements, n-type dopants, such as phosphorous (P) and nitrogen (N) has been shown to be possible [71,132,152-156]. Ion implantation is the first successful method to introduce n-type dopants into diamond [71]. N and P have been

successfully incorporated into CVD diamond films by the addition of various dopant gases such as nitrogen (N_2), ammonia (NH_3), urea ($(NH_3)_2CO$), and phosphine (P_2H_5) into H_2 plasma [152,156]. A very high concentration of 2×10^{20} cm^{-3} N-incorporated nanocrystalline diamond film has been achieved by a plasma-enhanced CVD technique using N_2/CH_4 plasma [154].

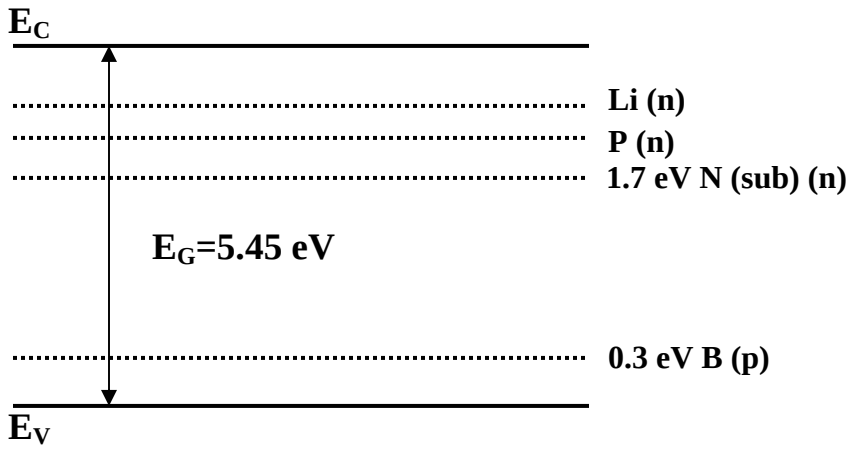

Figure 2.9 Energy band of diamond with dopants' energy levels [115].

The n-type dopants such as N, Li and P provide donor levels within the energy gap as illustrated in **Figure 2.9**. The energy levels associated with Li and P dopants are still unknown, but it has been found that the substitutional nitrogen forms a donor level ~ 1.7 eV below the conduction band. Assuming NEA property on diamond surface, the vacuum energy level is ~ 0.7 eV below the conduction band. Thus, the nitrogen donor level is 1 eV below the vacuum level, which means that the work function is approximately 1 eV. Therefore, a low electric field is sufficient for electron emission. The effect of nitrogen doping for electron emission enhancement has been confirmed by experiment with O-Cs treatment to lower electron affinity [132,155]. The nitrogen-doped diamond field emitter with Cs treatment exhibits electron emission at the lowest

reported electric field <0.2 V/μm [132]. Furthermore, other theoretical calculations for nitrogen-doped diamond field emitter have quantitatively verified experimental results [157-158]. Other experiments [71,152,154,156] using phosphorous and nitrogen as n-type dopants with no Cs treatment have independently confirmed that a diamond emitter with n-type dopants shows a better emission characteristic than a p-type (boron-doped) diamond emitter. One of the main objectives of this research is to develop a reproducible technique to achieve room temperature n-type electrical conductivity in nanocrystalline diamond for enhanced electron field emission. The process technique employed, the mechanism behind the n-type conductivity behavior, and the subsequent enhancement realized in electron field emission by n-type dopant (nitrogen) incorporation are discussed in this dissertation.

Other interesting models

Various other proposed models include electron injection over a Schottky barrier at the back-contact interface between a metallic substrate and diamond as the controlling mechanism [159], field concentrations induced by chemical inhomogeneity (such as hydrogen termination) on the surface [151], dielectric breakdown that provides conductive channels in diamond [148], surface arcing that results in the formation of tips and protrusions and thus provide additional geometric field enhancement [160], space charge limited conduction current through the bulk of the diamond [161], and surface conduction enhanced electron emission [146]. All these mechanisms are not necessarily mutually exclusive, because each addresses a particular part of a overall complex field emission process that includes the critical steps of supplying electrons to diamond, transporting them through the bulk to the surface, and emitting them into vacuum.

2.3.3 Reported emission characteristics of diamond

Although the NEA property of diamond was reported by Himpsel et al. [46] in 1979, investigations of field emission properties of diamond did not start in earnest until the early 1990s, when diamond films and coatings with controlled quality on many different substrates became widely available due to the emergence of low pressure CVD techniques. The many published reports show irrefutable evidence indicating that diamond and diamond-like carbon (DLC) materials are good field emitters, with low turn-on fields and useful emission current densities. Electron emission has been observed from many different types of diamond materials, including synthetic single crystals and powders, vapor-deposited islands and films with varying surface morphologies and crystallite sizes, and nanocrystalline coatings, as shown in **Figure 2.10**.

Early reports on diamond field emission include Wang et al. [142] who reported low-field (< 3 V/μm) electron emission from undoped CVD polycrystalline diamond films, Geis et al. [162] who measured emission currents from a diamond diode structure consisting of a p-type diamond substrate and a carbon ion implanted diamond surface, and Djubua et al. [19] who showed that arrays of diamond-like carbon cones formed by plasma polymerization required the lowest operating voltage for emission when compared to arrays of Mo and Hf tips. Most of these diamond materials are found to emit electrons efficiently under applied fields.

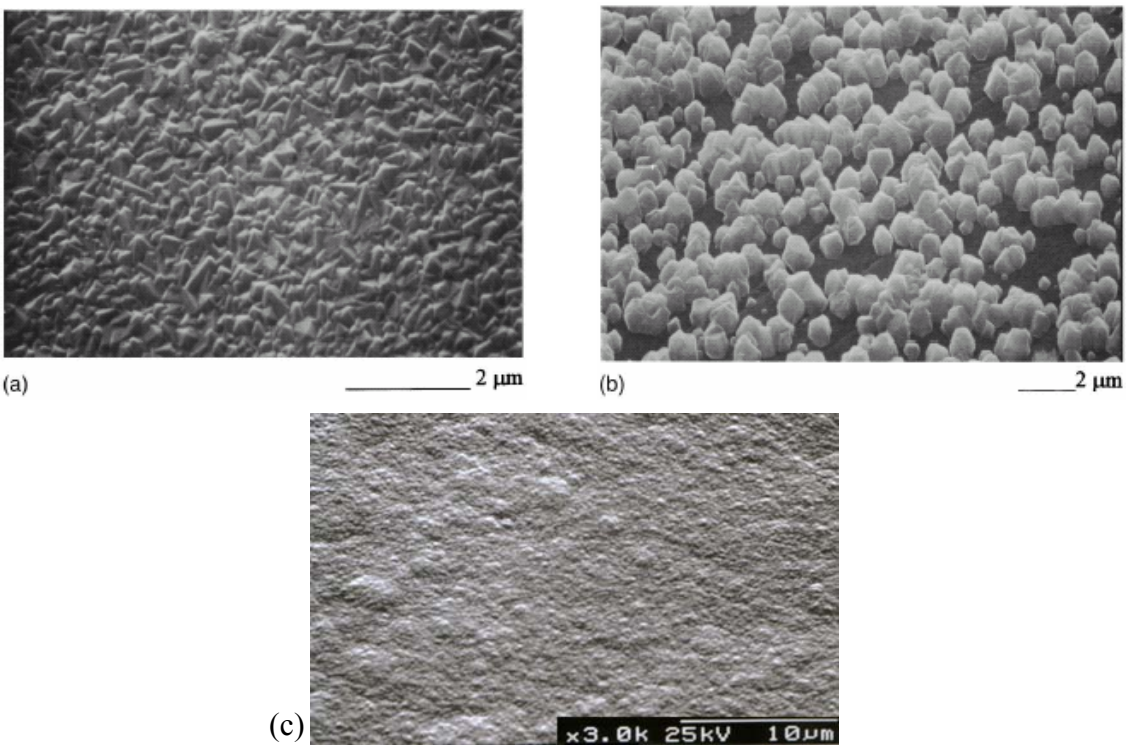

Figure 2.10 Scanning electron micrographs of diamond cold cathodes of (a) continuous film-type, (b) island-type, and (c) nanostructured diamond coating [121].

While the low electron affinity behavior of diamond has been effectively utilized, its ability to emit large amounts of electrons without consuming heating energy which is necessary in the cases of hot electron cathodes has been explored for low-voltage, high-current applications. Vanderbilt University introduced a patented mold-transfer process [163] for creating high density diamond microtip arrays (30 million tips/cm^2) and demonstrated the superior performance of the material as a cold cathode and further developed efficient vacuum diode and triode devices using the tip array structure [123,164-165]. A typical diamond pyramidal field emitter array (FEA) microstructure is shown in **Figure 2.11**, with its electrical performance in device forms given in **Figure 2.12** and **Figure 2.13**.

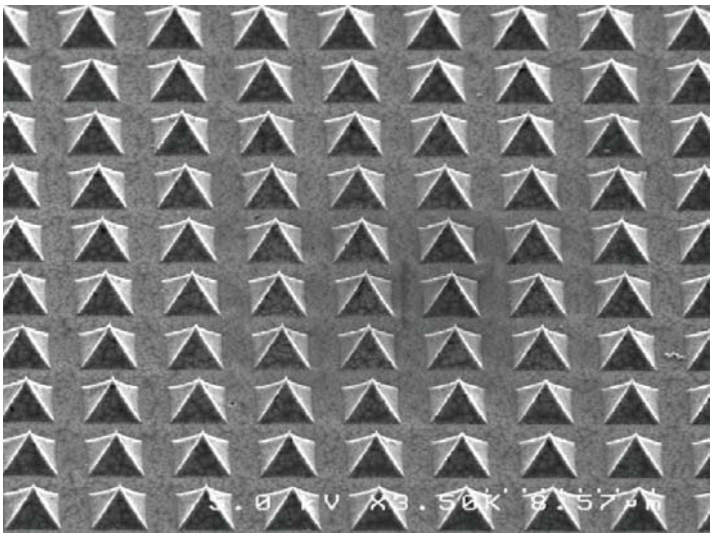

Figure 2.11 Scanning electron micrograph of CVD diamond pyramidal microtip array cathode fabricated from inverted Si molds by Vanderbilt [115].

The diamond diode, utilizing a flat-surfaced highly doped n-type Si anode, shows a rectifying behavior with an exponential increase in the emission current with increasing electric field in forward bias and zero current in reverse bias. The corresponding Fowler-Nordheim plots of $\ln(I/E^2)$ vs. $1/E$ are characterized with a negative linear slope, confirming field emission-type behavior of the current through the diamond diode device. Also, a diamond field emission diode with a high emission current of 22 mA at an electric field of 16 V/μm has been shown [123], indicating that microtip arrays fabricated from diamond are promising candidates for high current cathodes.

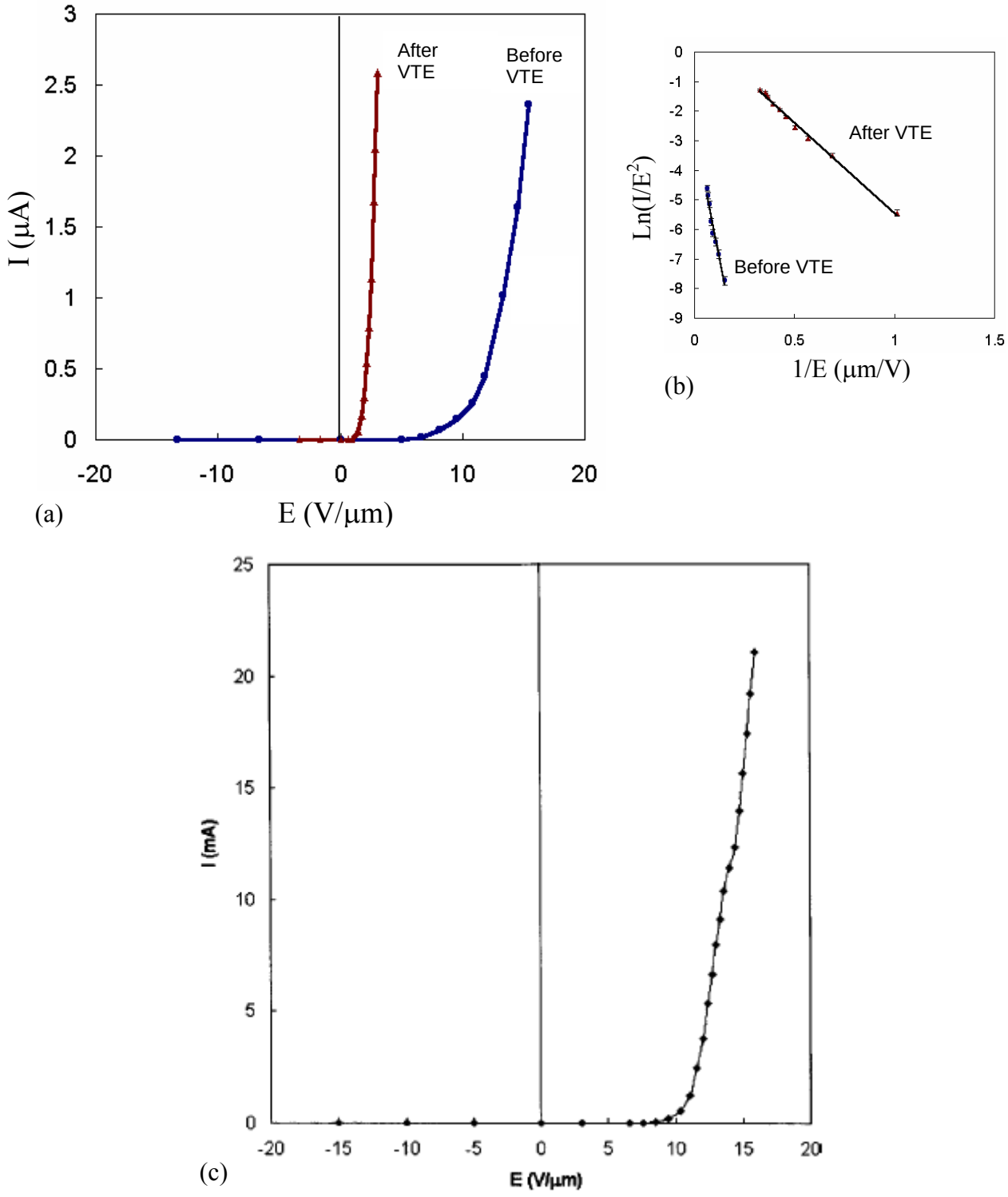

Figure 2.12 Typical field emission behavior reported from the Vanderbilt CVD diamond pyramidal microtip array diode before and after vacuum-thermal-electric (VTE) treatment: (a) Current vs. Electric field (I-E) characteristics; (b) corresponding Fowler-Nordheim plots; (c) High current field emission characteristics (I-E) of the diamond diode [115,123].

A triode is the three-terminal vacuum equivalent of a field effect transistor device, in which electrons are emitted from the cathode into vacuum, and a gate electrode varies the electric field between the cathode and gate to control the emission current. The electrons pass through apertures in the gate, accelerate toward the anode, and are collected to give a current through the device. A substantial output current gain (I_a) can be achieved if the gate intercepts only a small fraction of the emitted current. As this gate-controlled current goes to the anode and passes through an external load, it can produce a voltage larger than the control voltage at the gate, resulting in a voltage gain ($\Delta V_a/\Delta V_g$). Therefore, a correct device geometry should yield an overall power gain. The performance characteristics of a vacuum field emitter triode developed with the pyramidal diamond microtip array [164] are illustrated in **Figure 2.13**. Transistor characteristics are obtained from the device in common emitter configuration**,** demonstrating good gate control and modulation of the anode current with well-defined cut-off, linear, and saturation regions, similar to that of a solid-state transistor. The plot shows that at a constant gate voltage, V_g, the anode or collector current, I_a, increases in the beginning with increasing anode voltage, V_a, but saturates at $V_a > 60$ V. Also, as V_g increases, the anode current in the triode device increases exponentially, illustrating that the emission behavior of the device is controlled by the gate, and is quite insensitive to applied anode voltage. The figure indicates a low gate turn-on voltage of 22 V and a high emission current of 200 μA. A high transconductance ($\partial I_a/\partial V_g$) and high DC voltage gain ($\partial V_a/\partial V_g$) of 800 evident from the figure represent the best reported vacuum transistor behavior in literature [165]. Further, when an AC signal is superimposed on the input gate voltage of the triode amplifier, an AC voltage gain is obtained by connecting a load to the output. The characteristics of the diamond field emission triode show a high AC voltage gain of ~ 65 with a high output voltage of ~ 100 V for an input voltage of 1.5 V,

operating at I_a = 120 μA, V_g = 31 V and V_a = 400 V, thereby displaying a very promising prospect for signal amplification applications. For comparison, the theoretical AC voltage gain obtainable from a Spindt-type vacuum microelectronic triode is 13.8 or 23 dB [166].

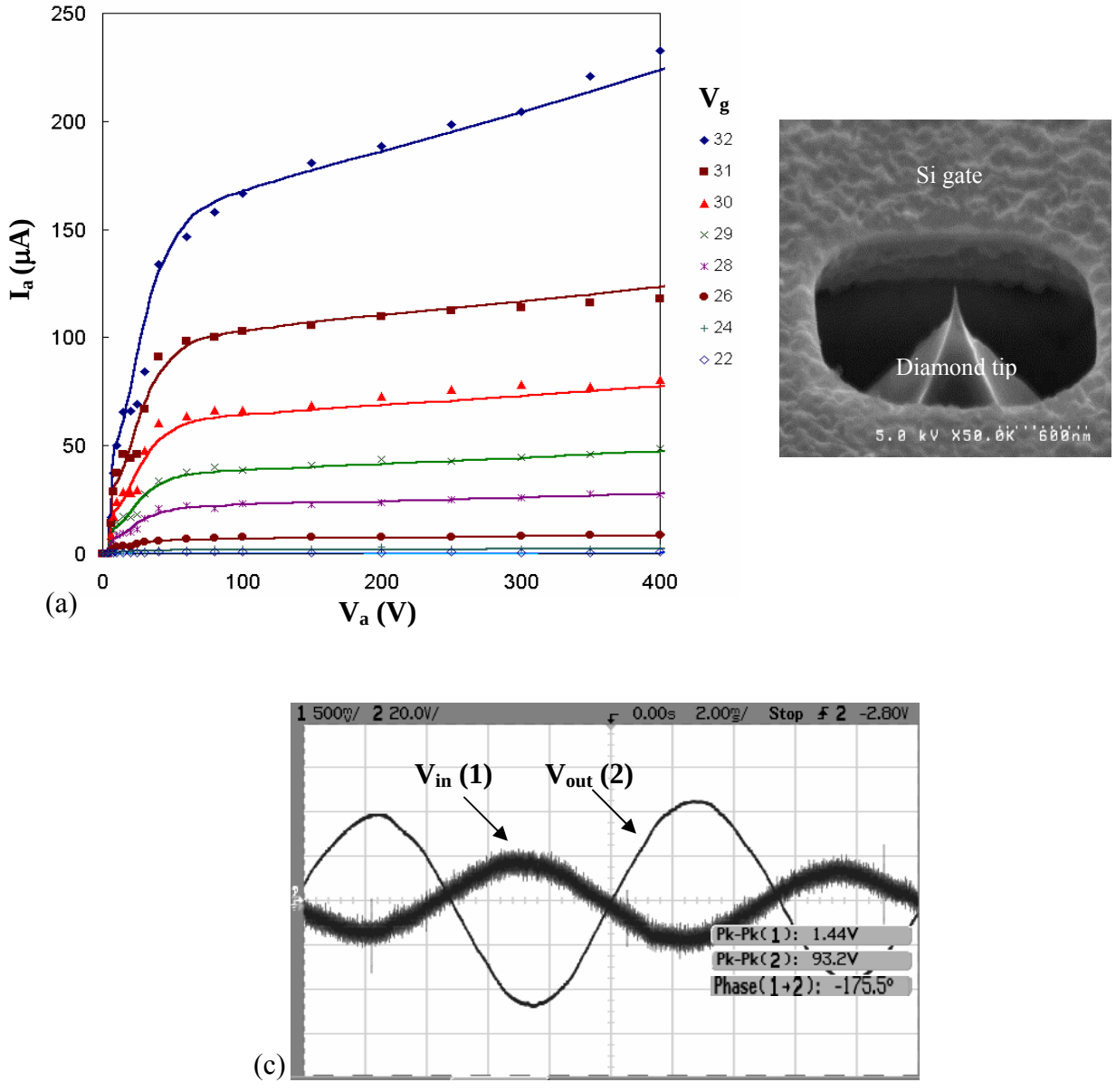

Figure 2.13 Transistor characteristics of the Vanderbilt self-aligned gated diamond microtip array vacuum triode: (a) I_a-V_a-V_g DC plots; (b) device structure; (c) AC characteristics [165].

The Spindt-type cold cathode structure, with sharp emitter tips surrounded by the gate electrodes to control the electron emission, has also been applied to diamond by Nishibayashi et al. at Sumitomo Electric Industries, Ltd. (Japan), and is being investigated for high current electron beam applications [167]. Cone-shaped diamond emitter tips, each with a surrounding gate electrode within a distance of 1 μm, was fabricated using a self-align process, yielding a high-density diamond emitter device with 390000 emitter tips in a 1 mm square area. The device structure is included in **Figure 2.14**.

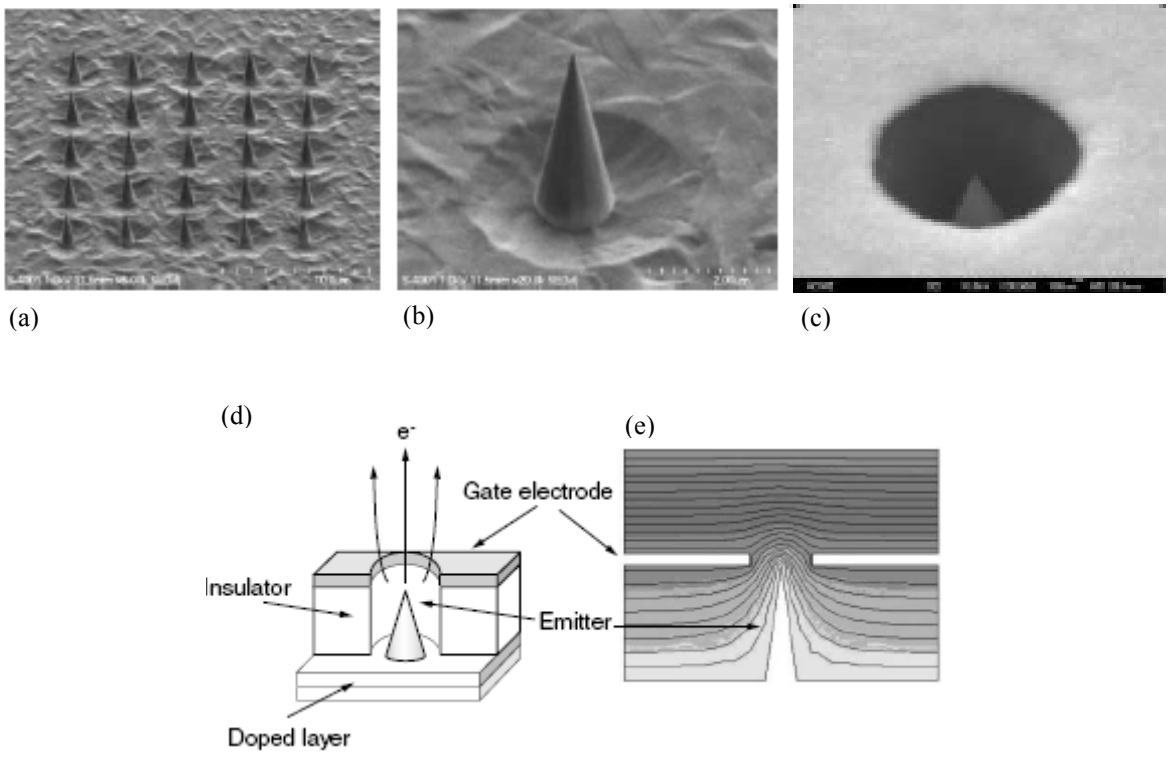

Figure 2.14 Diamond vertical field emitters fabricated by Nishibayashi et al for high current electron emission: (a) Emitter tip array; (b) Appearance of cone-shaped diamond tip; (c) Emitter with gate electrode; (d) Diamond device structure; and (e) Electric field diagram when positive bias is applied on gate electrode [167].

When a positive voltage is applied to the gate electrode, the electric field is concentrated around the apex of the emitter tip so that electrons are pulled out from the emitter tip (**Figure 2.14 (e)**). In such a strong electric field, electrons are emitted out of diamond by a tunneling effect. The sharper the emitter tip is, the lower the threshold voltage for electron emission. Gated diamond emitter devices with electron emission areas ranging from 5 to 500 μm-square were fabricated, and the emission current was found to increase as the emission area grew (**Figure 2.15**). A maximum current density of 265 mA/mm^2 has been achieved by the group [167]. Such high current densities enable diamond to be used as an ideal material for applications like electron microscopy, electron beam lithography, microwave tubes and integrated micro vacuum devices. Nishibayashi et al. report that the obtained results are from polycrystalline p-type diamond emitter devices and confirm that electron emission properties can be improved by using n-type diamond.

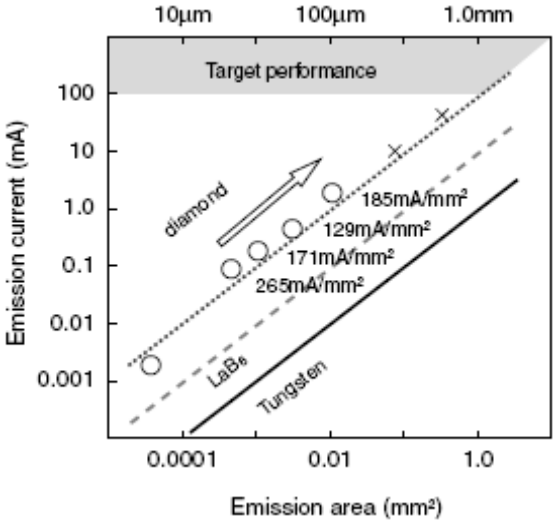

Figure 2.15 Emission current vs. emission area plot of diamond emitter device: Electron currents >100 mA/mm^2 were obtained in emitter devices of various sizes; total emission current above 100 mA is expected to be achieved by enlarging the emission area. The solid and broken lines show emission current density upper limits for tungsten (W) and lanthanum hexaboride (LaB6), conventional hot cathode materials, which are 1 mA/mm^2 and 10 mA/mm^2, respectively [167].

It is important to mention, while discussing about the high power potential of vacuum microelectronics, that the largest total emission current produced so far from a microfabricated field emitter device is 300 mA (40 A/cm^2), achieved by Schwoebel, Spindt, and Holland at SRI International using a 50,000 tip Molybdenum emitter array [168]. Efforts by different teams are primarily concentrated on improving the emission uniformity over an emitter array in the cathode to realize the potential of microfabricated field emitters for very high current densities (> 100 A/cm^2) and total emission currents (> 1 A).

Diamond materials with small grain sizes and high defect densities generally emit better than those with large crystallite sizes and low defect contents, as reflected in the data in **Figure 2.16**. Heavy doping, n-type or p-type in nature, enhances emission. Outstanding emission properties are discovered in both ultrafine diamond powders containing 1- 20 nm crystallites produced by explosive synthesis and nanocrystalline or ultra-nanocrystalline diamond films (composed of ~1-100 nm crystallites) [154,169-173]. Emission has been found to originate from sites that are associated with defect structures in diamond [142, 173, 143-145]. Compared with conventional Si or metal microtip emitters, diamond emitters show lower threshold fields, improved emission stability, and robustness in low/ medium vacuum environments. Attempts have also been made to apply diamond coatings on tips of silicon or metal-emitter arrays to further enhance the emission characteristics [131, 170, 174-178]. High emission currents of 60-100 μA per tip have been measured for Si tips conformally coated with nanocrystalline diamond films [63].

Nanocrystalline diamond, a strongly emerging form of CVD diamond material, has generated significant interest for vacuum micro/nanoelectronics in recent years. The properties of nanodiamond and its reported emission characteristics are discussed in the next chapter.

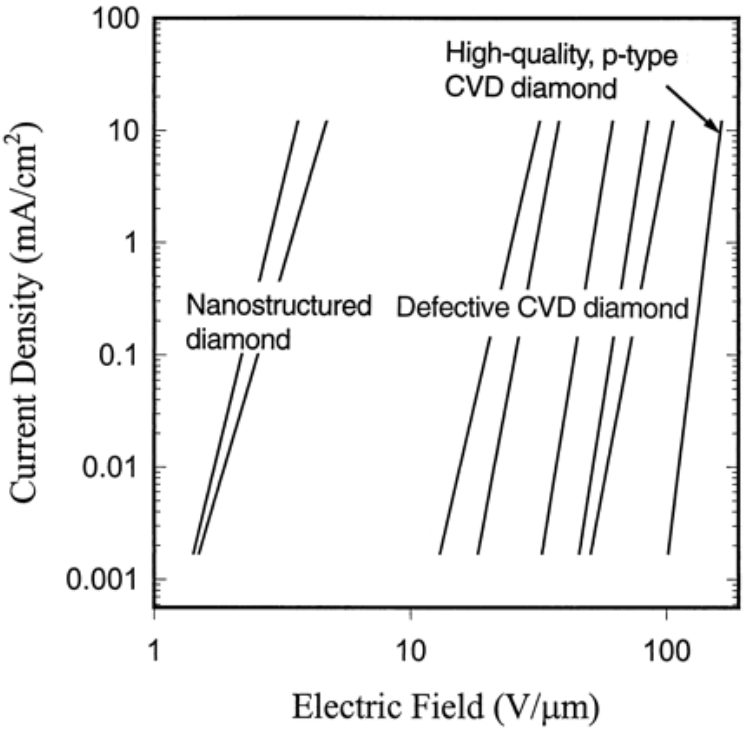

Figure 2.16 Emission current density vs. applied electric field for various types of diamond emitters [121].

CHAPTER III

NANOCRYSTALLINE DIAMOND

With this research oriented towards the development of a promising cold cathode material, nanocrystalline diamond, it would be appropriate to dedicate a chapter to introduce the material and update the rapid advancements perpetuated by its properties in various fields including vacuum nanoelectronics, NEMS, biomedicine, electrochemistry, optics, and beyond, with particular emphasis on its utility as an electron emitter.

A unique combination of high thermal conductivity, low electron affinity, high chemical stability, and high resistance to particle bombardment makes CVD diamond, a suitable candidate for applications varying from electronics to tribology [179]. Uses based on the physical strength and hardness of diamond such as cutting tools, protective coatings and composite additives have been in practice and available in the market. At the same time, the conventional CVD microcrystalline diamond is not used widely for applications in micro/nanoelectronic devices, optical devices and coatings, nanoelectromechanical systems (NEMS), and thermal management devices. It is very important to tailor this material to cater to many applications. In this direction, the processing challenges and the difficulties encountered in applying the properties of diamond in thin film and device forms can be neutralized by the development of nanocrystalline diamond, often referred to as “nanodiamond”.

A diamond film is termed as “nanocrystalline” if it possesses a grain size in the nanometer scale between 1 nm and 100 nm. Nanocrystalline diamond, while holding the meritorious nature of the conventional CVD microcrystalline diamond in its mechanical, thermal and electrical properties, offers certain unique properties, brought about by its small grain size

and large network of grain boundaries. Nanodiamond has great surface smoothness, n-type dopant incorporation, higher (but minute) degree of sp^2-bonded carbon content, hardness, reflectivity, lowered internal stress and friction coefficient, and a large scope for materials processing and integration. These properties of nanodiamond are experimentally confirmed to be controllable over a broad range.

3.1 Morphology of nanocrystalline diamond

The grain size of a nanocrystalline diamond film can be typically controlled to be as small as 2 nm. For example, Ultrananocrystalline diamond (UNCD), first developed by Argonne National Labs (ANL), has ultra-small (2-5 nm) grains and atomically abrupt (~ 0.5 nm) high energy grain boundaries [79]. **Figure 3.1 (a)** displays a high resolution transmission electron microscope (TEM) image of the UNCD [180], while **Figures 3.1 (b)** and **(c)** show the scanning electron microscope (SEM) picture of nanocrystalline diamond, having a typical cluster morphology with grain size of 15-20 nm [65,70]. The morphology change in the diamond film brings with a large increase in the utility of the material. With respect to field emission, the nanodiamond grain size results in the formation of sharp tips with small radius of curvature, leading to a high geometrical field enhancement factor, while the increased grain boundary network, acting as conduction channels, augment the electrical conductivity of the entire film, thereby enhancing the electron transport through the diamond. Nanodiamond films overcome most of the drawbacks of traditional, microcrystalline diamond films as they are smooth, dense, and can be conformally coated on a wide variety of materials with high-aspect-ratio structures [181]. One of the effective deposition techniques to achieve nanocrystalline diamond, and the effect of controlling the plasma chemistry and associated process parameters on the morphology

and electrical properties of the diamond film have been explored in this research, which is elaborated in detail in chapter V.

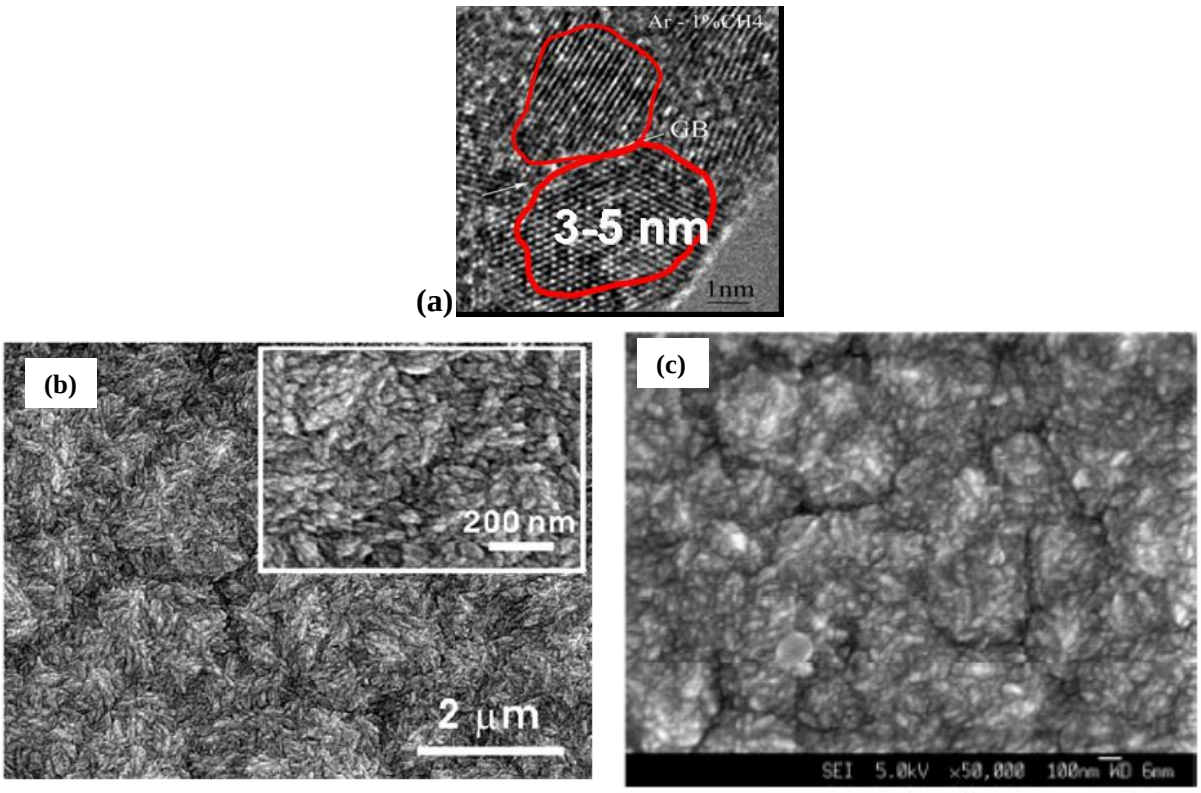

Figure 3.1 (a) TEM image of the UNCD film with 3-5 nm grain size [180]; (b and c) SEM pictures of nanodiamond films deposited by $CH_4/H_2/N_2$ [70] and CH_4/Ar [65] microwave plasma deposition techniques respectively.

The surface roughness (100-400 nm) of the CVD microdiamond film is considered to be high for many applications. For example, diamond is well suited for use as protective optical coatings but diamond films with high surface roughness cause attenuation and scattering of the transmitted signals restricting their use in optical coatings. In order to overcome the problem of surface roughness of diamond films either post-polishing should be adopted, or naturally smooth films should be grown without compromising their hardness and other useful properties. However, post-polishing is expensive and time consuming. Nanocrystalline diamond has a very

smooth and uniform surface morphology with a typical RMS surface roughness about 20 nm [80]. The smoothness of the thin film is directly related to its mechanical properties like coefficient of friction relevant to MEMS, and is also a very critical factor in several cases such as micropatterning of diamond films to realize useful structures, and integration of different materials with diamond.

3.2 sp^2/sp^3 composition of nanocrystalline diamond

Nanodiamond is highly sp^3-bonded in nature. Due to the decrease in the grain size and increase in the volume density of grain boundaries, nanodiamond films also encompass an increased sp^2-bonded non-diamond carbon content, preferentially in the grain boundaries.

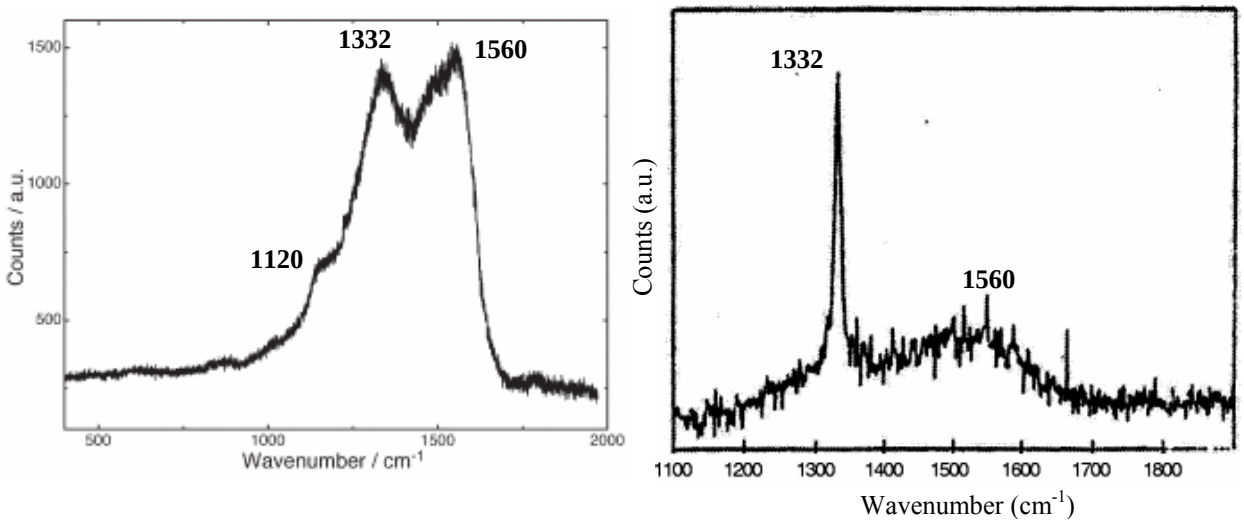

Figure 3.2 (a) Visible Raman spectrum of a ultrananocrystalline diamond film with 3-5 nm grain size [182]; (b) Typical Raman spectrum of a microcrystalline diamond film.

It is known that the intensity and broadening of Raman peaks are directly correlated to the crystallinity (crystal size) of films. A broad sp^3-diamond peak (1332 cm^{-1}) and higher sp^2-carbon shoulder (1560-1580 cm^{-1}) are typical characteristics of the Raman spectrum obtained from a nanodiamond film, as shown in **Figure 3.2 (a)**, in comparison with that of a conventional

microdiamond film (grain size: 1 μm-3 μm), featuring a sharp sp^3-diamond peak and a very small sp^2-carbon signature, **Figure 3.2 (b)**. The use of visible excitation often gives rise to an intense background photoluminescence that can mask the Raman line in nanodiamond, even in films with low amounts of sp^2–bonded carbon. Also, Raman scattering in visible range is about 50 times more sensitive to the sp^2-bonded carbon than the sp^3-bonded carbon [80]. For reference, it can be noted that UV Raman spectroscopy and synchrotron based near-edge x-ray absorption fine structure measurements (NEXAFS) were used to identify the presence of about 5 % sp^2 bonding in a typical UNCD film [183]. The role of sp^2-carbon as a strong field enhancement factor for electron emission from diamond has been discussed in Chapter II.

The visible Raman spectroscopy is mainly suitable to monitor the sp^2-carbon behavior and follow the evolution of sp^2-carbon phase. UV–Raman spectroscopy using higher photons energy (shorter wavelength) can characterize the nature of sp^3-bond in the films more clearly [184]. **Figures 3.3 (a)** and **(b)** show the typical visible and UV Raman spectra of nanocrystalline diamond films respectively. The peak at 1332 cm^{-1}, characteristic to sp^3-bonding, which is not easily resolvable in visible Raman spectroscopy, is clearly observed in **Figure 3.3 (b)**.

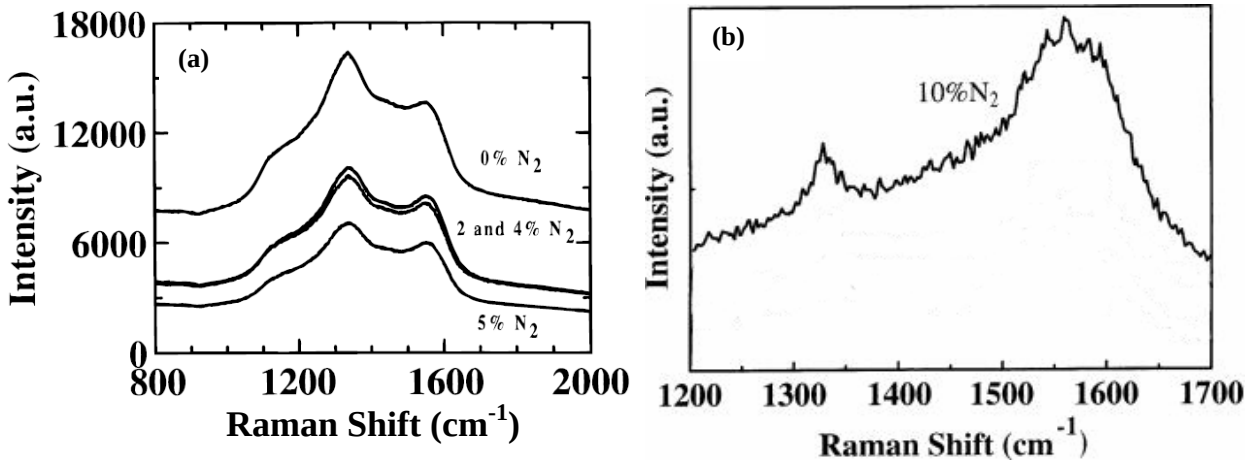

Figure 3.3 (a) Visible Raman spectra of nanocrystalline diamond films deposited from 0, 2, 4, and 5% N_2 in $CH_4/Ar/N_2$ source gas mixture; (b) UV Raman spectra of nanocrystalline diamond films deposited from 10% N_2 in $CH_4/Ar/N_2$ source gas mixture [80].

In **Figure 3.3 (a)**, showing a series of visible Raman spectra for films deposited with and without N_2 in the source gas mixture, three bands are observed for all four nanocrystalline films: 1125, 1332, and 1560 cm^{-1}. The broad band at ~ 1332 cm^{-1} is assigned to the first-order phonon mode for diamond, reflective of the sp^3-bonded diamond nanocrystallites. Normally, microcrystalline diamond films have a sharp peak at 1332 ± 2 cm^{-1} with a line-width of 5 to 8 cm^{-1} (**Figure 3.2 (b)**). The significantly broadened diamond line (broadening of the full width at half-maximum (FWHM) of the 1332-cm^{-1} diamond peak) for the nanocrystalline films results from the decreasing grain size to the nanometer scale. To a first approximation, the line-width is a measure of the phonon lifetime. The more defects (*e.g.,* grain boundaries) and impurities (*e.g.,* nitrogen) there are, the shorter the phonon lifetime and the broader the line-width [80]. The non-diamond sp^2-bonded carbon peak at 1560 cm^{-1} results from the π-bonded carbon atoms in the grain boundaries. The position and intensity of this broad peak depends on the deposition conditions used, the wavelength of the excitation photon, the relative amount of the sp^2-bonded carbon phase in the optically probed volume, and how microstructurally ordered or disordered the phase is. The spectra also contain a feature centered at 1125 cm^{-1}, which has been observed in nanodiamond films in the vicinity of 1120-1190 cm^{-1} by different researchers [65,67,70,80,185,186]. Definitive assignment of this peak has not been made yet. It is possible that the band arises from the effects of small crystallites or disorder in the tetrahedral carbon network of diamond [80].

It can be seen that the ratio of the diamond (1332 cm^{-1}) to the nondiamond (1560 cm^{-1}) band intensities, is large for the film deposited without any added N_2 and decreases for the films deposited with the gas. However, the ratio is independent the of N_2 level. One of the suggested theories to explain the decrease in this sp^3/sp^2 band intensity ratio when N_2 is added is the

decrease in the average grain size. In other words, increasing the N_2 in the source gas mixture causes an increase in the relative number of grain boundaries in the film, and it is at these grain boundaries that the sp^2-bonded carbon atoms exist [80].

The signal for diamond is expected to increase relative to that for amorphous or graphitic carbon as the excitation wavelength is shifted toward the UV due to an increase in the scattering cross section. For example, the spectrum for a 1% CH_4/1% N_2/98% Ar nanocrystalline diamond film, given in **Figure 3.3 (b)**, exhibits a moderately intense diamond line at 1332 cm^{-1} with a line-width of 25 cm^{-1} [80]. No band was detected at 1125 cm^{-1} (this region of the spectrum is not shown), but a broad band centered near 1550 cm^{-1} is present due to the sp^2-bonded carbon atoms in the grain boundaries. The band intensities for the diamond and nondiamond carbon are roughly the same, but the peak area for the latter is significantly larger. In essence, it is evident that nanocrystalline diamond films have a significant diamond crystal component, with a relatively increased sp^2-bonded carbon.

3.3 Nitrogen as an n-type dopant in nanocrystalline diamond

The success in fabricating diamond-based electronic devices has been limited mainly due to the difficulty in achieving the effective n-type conductivity of diamond. The problem lies in the difficulty of finding a way to dope diamond so that it's ambient temperature conductivity and carrier mobility are sufficiently high to make diamond-based devices work at room temperature. Nitrogen is among a few suitable dopants for nanocrystalline diamond. But, traditional doping with nitrogen does not work, since nitrogen atoms at substitutional sites introduce a deep donor level 1.7 eV below the conduction band, and thus is not thermally activated at room temperature [70,181,187]. This is due to the fact that nitrogen is very reluctant to insert into the diamond

lattice, and all efforts to dope microcrystalline diamond with electrically active nitrogen have to date met with very limited success. Unlike nitrogen doped single crystal diamond, nitrogen doped ND/UNCD films exhibit significant electrical conductivity at room temperature. This has been achieved in-situ by the addition of N_2 to gas plasmas generated in CH_4/Ar and CH_4/H_2 mixtures during the thin film growth.

In contrast to diamond single crystals or microcrystalline films, nanodiamond, due to its small grain size and thereby a high density of grain boundaries, allows for easier incorporation of nitrogen impurities [188-192]. Secondary ion mass spectroscopy (SIMS) data has shown that the content of nitrogen in the ultrananocrystalline diamond (UNCD) film saturates at $2x10^{20}$ atoms/cm^3 (~ 0.2 % total nitrogen content in the film), when the nitrogen concentration in the plasma is 5 % [188]. The conductivity at room temperature increases dramatically with nitrogen concentration, from 0.016 (1 % N_2) to 143 $\Omega^{-1}cm^{-1}$ (20 % N_2) [188,193]. This is to be compared with the best values reported previously, which are 10^{-6} $\Omega^{-1}cm^{-1}$ for nitrogen-doped microcrystalline diamond and 0.33 $\Omega^{-1}cm^{-1}$ for phosphorous-doped microcrystalline diamond films. These obtained results with the UNCD by researchers at Argonne are illustrated in **Figure 3.4** [154,188]. Temperature dependent conductivity and Hall measurements performed on UNCD films are indicative of multiple, thermally activated conduction mechanisms with very low, effective activation energies of < 0.1 eV [181]. This behavior is similar to highly boron-doped microcrystalline diamond. Hall measurements of the carrier mobility report reasonably high room-temperature carrier mobilities of 10 cm^2/V-s [188]. The negative value of the Hall coefficients indicates that electrons are the majority carriers in nitrogen-doped nanodiamond films.

Several other works have reported successful nitrogen incorporation and high electrical conductivity in nanocrystalline diamond. SIMS measurements on nanocrystalline diamond films having a grain size of about 10 nm deposited by N_2/CH_4 plasma CVD process, were conducted by N.S. Xu et al [67], who found that the nitrogen distribution is uniformly high in the film with a concentration reaching up to 10^{21} atoms/cm^3. K.L. Ma et al [70] have reported that the introduction of nitrogen to CH_4/H_2 in the nanodiamond growth plasma significantly reduces the resistivity of the film by six orders of magnitude. Further, the nitrogen incorporation has been confirmed to be consistent through the depth of the film, shown by the profiles of the carbon and nitrogen concentrations as a function of depth for a nanocrystalline diamond film in **Figure 3.5** [80]. X-ray photoelectron spectroscopy (XPS) information obtained from nanodiamond film grown in a nitrogen-rich $CH_4/H_2/N_2$-mixture plasma CVD process is shown in **Figure 3.6** [65]. The N 1s spectrum of the diamond film detected by XPS shows a clear peak located at 398 eV corresponding to nitrogen, denoting the existence of nitrogen atoms incorporated in the film.

Researchers have proposed that in the case of nitrogen incorporation in nanodiamond, conduction occurs via the grain boundaries and not the grains. Density-functional based tight-binding molecular dynamics simulations have shown that nitrogen incorporation into the grain boundaries is favored by 3-5 eV over substitution into the bulk. Nitrogen increases the amount of three-coordinated carbon atoms in the grain boundary and leads to additional electronic states near the Fermi level, causing it to shift upward (toward the conduction band). Thus, nearest-neighbor hopping or other thermally activated conduction mechanisms could occur in the grain boundaries and result in greatly enhanced electron transport. The conduction may occur via the new carbon states in the band gap. Hence, it is proposed that grain boundary conduction

involving carbon π-states in the grain boundaries is responsible for the high electrical conductivities [154,181,188,194,80].

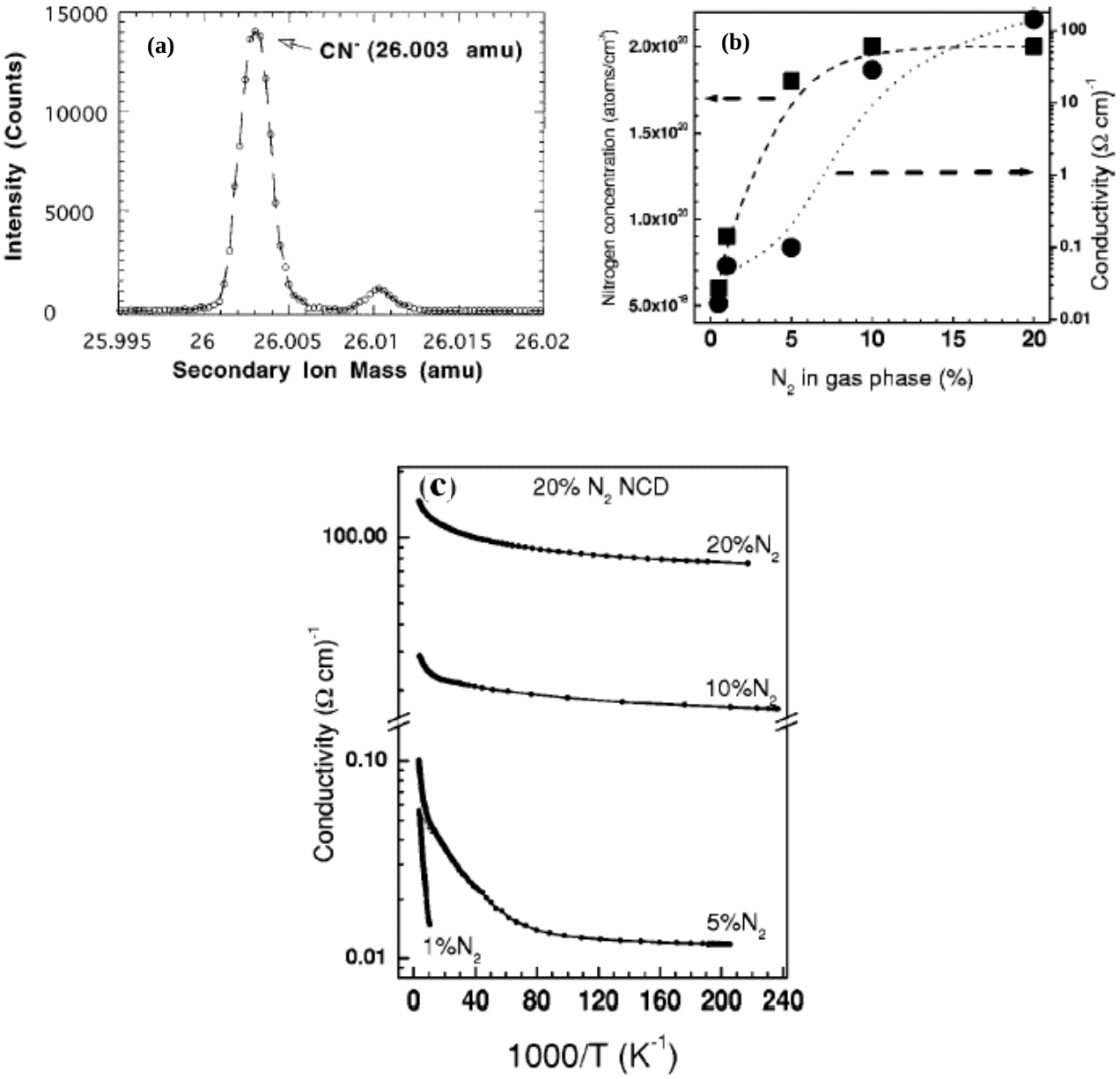

Figure 3.4 (a) High-resolution SIMS spectra of the ultrananocrystalline diamond film revealing the incorporation of nitrogen with a CN^- secondary ion peak with a mass of 26.0030 amu; (b) Total nitrogen content and room-temperature conductivity as a function of nitrogen in the plasma; (c) Arrhenius plot of conductivity data obtained in the temperature range 300–4.2 K for UNCD films synthesized using different nitrogen concentrations in the plasma [154,188].

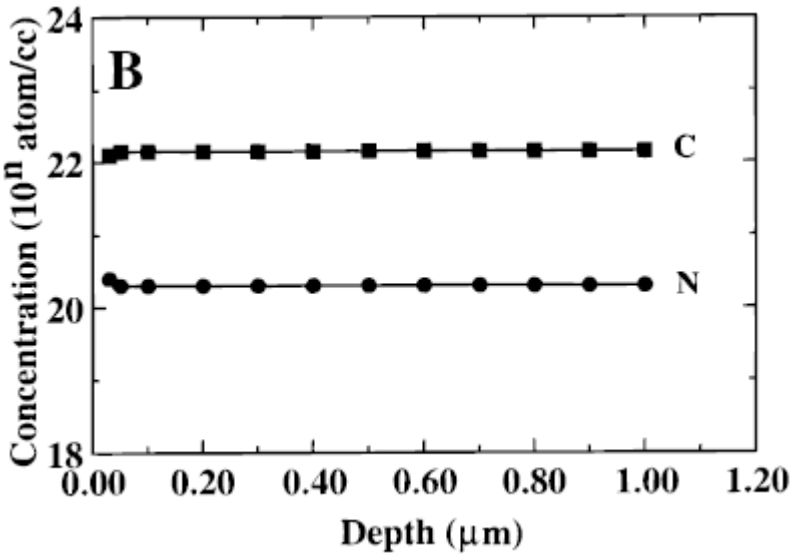

Figure 3.5 Depth profiles for the atomic carbon and nitrogen concentrations in a 1 μm-thick nanocrystalline diamond film deposited from 1% CH_4/5% N_2/95% Ar [80].

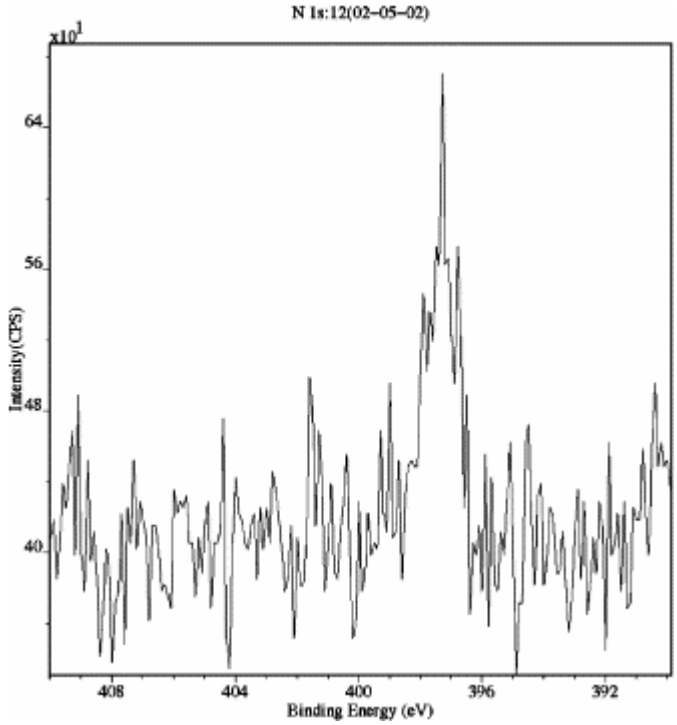

Figure 3.6 The XPS N 1s core-level electron spectrum for nanodiamond film deposited in $CH_4/H_2/N_2$ mixture, clearly showing the nitrogen peak at 398 eV [65].

3.4 Growth temperature

Most diamond CVD processes require the substrate temperature to be above 700 °C to obtain high quality crystalline diamond films, as the nucleation and growth of diamond is not an easy task at a lower substrate temperature (< 500 °C). Though the typical substrate temperature for nanodiamond growth is 700-800 °C, different researchers [195-196] have shown successful synthesis at temperatures as low as 400 °C. It has been reported that the nanodiamond growth process plasma chemistry exhibits much less temperature dependence than the conventional microcrystalline diamond deposition process. **Figure 3.7** shows dense and continuous UNCD films obtained at 400 °C substrate temperature using an optimized ultrasonic seeding process [195].

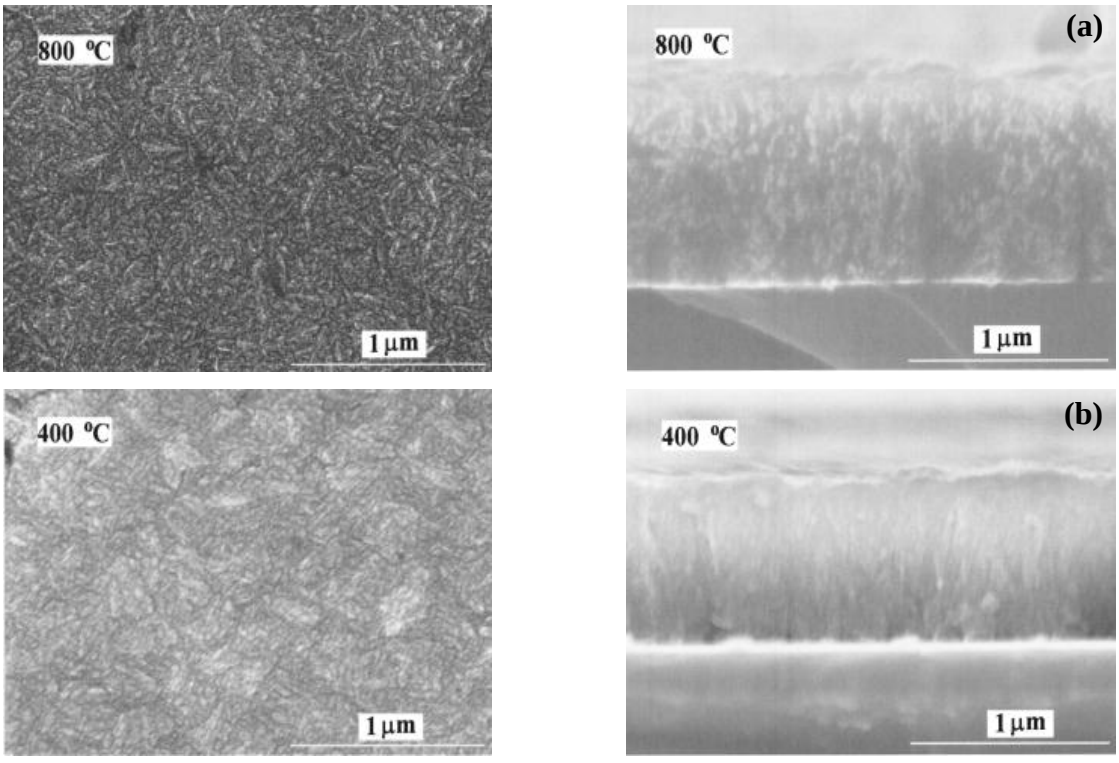

Figure 3.7 SEM pictures of the surface morphology and cross-section of UNCD films deposited at (a) 800 °C and (b) 400 °C [195].

Deposition at temperatures compatible with standard semiconductor manufacturing processes can enhance the feasibility of combining diamond with other materials including metals, semiconductors, and oxides, pitchforking its use in integrated circuits and other applications, such as microelectromechanical systems (MEMS) (see **Figure 3.8**) [195].

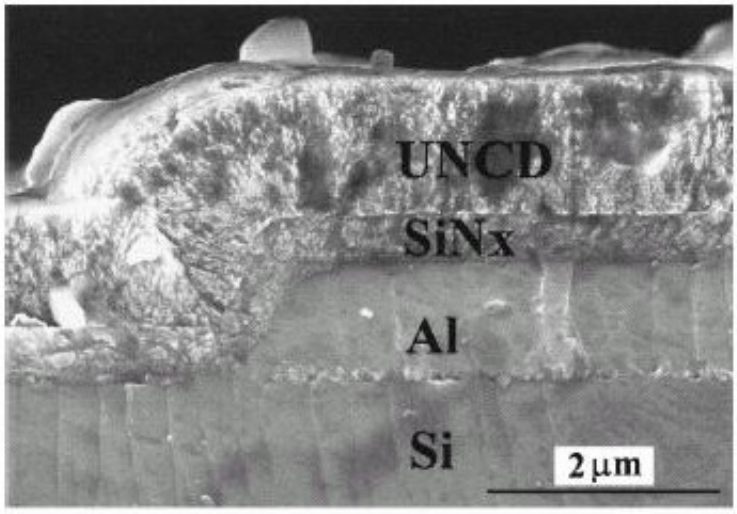

Figure 3.8 Low-temperature UNCD as hermetic coating for BioMEMS [195].

3.5 Micropatterning of diamond

The mechanical hardness of diamond warrants a robust and controlled etch process to micropattern the material uniformly and realize useful structures for any given application. The surface roughness is a critical parameter for lithographically patterning a thin film. The smoother surface morphology and uniformly controllable thickness properties of nanodiamond can overcome many lithography problems. The nanodiamond reactive ion etch technique developed in this research offering selectivity, yield and reproducibility, while maintaining a good etch rate, is detailed in chapter V. The feasibility of film micropatterning in CVD diamond technology can help form various robust and useful structures suited for a wide range of applications.

3.6 Ultrananocrystalline diamond (UNCD)

A summary of the features of ultrananocrystalline diamond (UNCD) [180,181,197] would provide a comprehensive shape to this chapter on nanodiamond. UNCD refers to a diamond film with the smallest ever grain size of 2-5 nm. Originally developed by Argonne National Laboratories, UNCD is synthesized using a microwave plasma chemical vapor deposition technique in hydrogen-poor plasma chemistries, with CH_4 or C_2H_2 as the carbon source gas. Argon-methane plasmas produce C_2 dimers that lead to the growth of phase-pure nanocrystalline diamond (more than 95% sp^3-bonded carbon). UNCD films have been deposited at temperatures as low as 350 °C, and on a wide variety of substrates, including Si, SiO_2 (thin oxide films, quartz, Corning glass), refractory metals (Ti, Ta, W, Mo), as well as SiC and SiN. Continuous films have been grown to render the substrate impervious to chemical attack from strong acid solutions such as HF and HNO_3. Deposition of reliable, high-quality ohmic contacts has been possible on n-type conductive nitrogen-doped UNCD [198], useful for electronic devices. With recent advances in plasma technology, UNCD films have been deposited on 200 mm substrates.

The material properties of UNCD™, commercialized by Advanced Diamond Technologies, Inc., are outlined as follows (as reported in [180]):

Mechanical Properties: The hardness, Young's modulus, fracture toughness and strength of UNCD have been found to be essentially equivalent to natural diamond.

Tribological Properties: UNCD exhibits friction coefficients as low as 0.03 in air. This, combined with the extreme hardness, good adhesion properties, and low film stress, allows for a wide range of applications of UNCD as a tribomechanical coating.

Transport Properties: The electrical conductivity of UNCD films can be changed over eight orders of magnitude, by altering the deposition process. Nitrogen-doped UNCD films have been reported to exhibit the highest n-type conductivity for a phase-pure diamond film and are more conductive than any doped microcrystalline diamond film or diamond-like carbon film.

Electrochemical Properties: Ultrathin UNCD films have been shown to exhibit the same superior electrochemical properties as heavily doped microcrystalline diamond films. Very thick films of microcrystalline diamond, however, are needed due to the columnar microstructure and low-energy grain boundaries which gives rise to large leakage currents. Due to the high renucleation rate, equiaxed microstructure, and high-energy grain boundaries, UNCD films as thin as 100 nm can be used for electrochemical applications.

Electron Field Emission Properties: Low threshold electric fields (2-3.2 V/μm) [62,154] have been reported from UNCD for electron emission. When deposited conformally on high aspect-ratio Si tip emitters, as shown in **Figure 3.9**, field emission studies showed a substantial reduction in the emission turn-on voltage and a large enhancement of emission current for diamond-coated tips, as compared to the values of the uncoated Si tips [63]. Emission currents of 60-100 μA from a single UNCD-coated silicon microtip and as high as 1 mA from conformally-coated arrays of silicon microtips have been observed [63,121,180]. In addition, the field electron emission is reported to be very stable even when the surface is exposed to 10^{-4} Torr of oxygen or hydrogen [199-200].

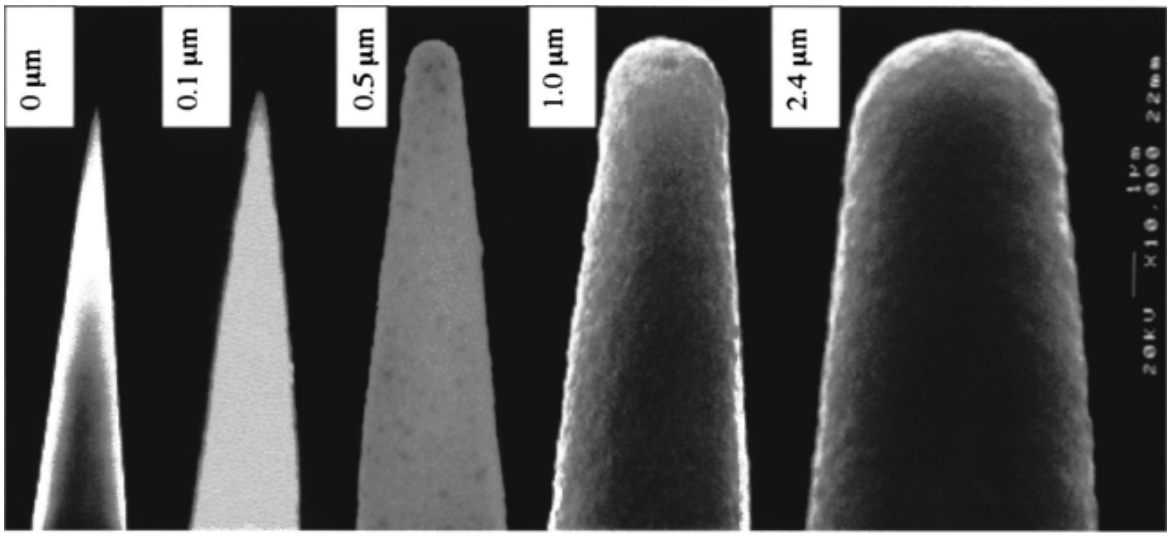

Figure 3.9 Series of SEM images of a 25 nm diameter Si tip emitter coated with a UNCD film with incremental coating thickness. The tip on the left is uncoated and successive images represent coatings ranging from 100 nm to 2.4 µm in thickness [63].

3.7 Nitrogen-incorporated nanocrystalline diamond for enhanced electron field emission

This section elucidates how the unique properties of nanodiamond can be favorable for electron field emission. For a semiconducting field emitter such as diamond, the emitting electrons can originate from either the conduction band, the valence band, and/or surface states. Diamond has a wide bandgap (~ 5.5 eV), and undoped diamond is thus generally thought to be unable to produce sustained electron emission because of its insulating nature. Although electrons emitting from surface states in diamond can occur, there are no obvious mechanisms by which electrons can be transported through the undoped bulk to the surface states. Either the bulk or the surface of diamond must be made conductive in order to sustain the emission process. Furthermore, to fully take advantage of diamond's small electron affinity to realize electron emission at low applied fields, the Fermi level must be close to the conduction band. This would require the diamond to be n-type doped. Although p-type diamond can be readily made available

by boron doping, very high electric fields are needed for emission to occur, because the emitting electrons reside deep (> 5 eV) below the vacuum level in p-type diamond, unless sp^2 content is included to improve electron transport and emission [115]. An ideal emitting structure may, therefore, consist of an n-type doped semiconducting diamond with a true NEA surface.

Nitrogen-incorporated nanocrystalline diamond offers excellent field enhancement factors with its small grain size, increased and controlled sp^2-carbon content and n-type electrical conductivity, thereby serving as a suitable electron emitting material. The tiny grain size of nanodiamond is instrumental in achieving an electron emitter tip with ultra-small radius of curvature. The small grain size provides a more localized field enhancement site at the tip apex, yielding a good figure of merit and high geometrical field enhancement factor, thereby allowing easier electron tunneling. The nitrogen dopant and sp^2-carbon promote field emission by significantly enhancing the electron transport through the nanodiamond to the vacuum interface and reducing the energy barrier that the electrons must tunnel through for emission [62,65-66]. The considerable increase in the electrical conductivity of the nanocrystalline diamond film by n-type conductivity indicates a reduction in the work function [64-65,68], a critical parameter in electron emission, governed by the F-N phenomenon. The energy states induced by nanocrystalline boundary and nitrogen incorporation in the CVD diamond have been calculated by quantum theory [67], which reveals that the interface-related states form a shallow band of 0.29 eV below the conduction band edge. This boundary band, if occupied under an applied field or under some other appropriate mechanism, could supply significant electrons to sustain stable emission. Thus, nitrogen-incorporation to nanocrystalline diamond makes it electronically active, while retaining the thermal and mechanical stabilization properties of the diamond material, yielding an efficient and reliable electron emitter.

CHAPTER IV

PROPOSED RESEARCH AND APPROACH

The purpose of this research is to develop reliable and consistent process techniques to deposit and micropattern nanocrystalline diamond thin films and integrate them in the fabrication of lateral electron field emission devices, operable at low voltage and electric field with high emission currents for IC-compatible and extreme-environment applications in vacuum microelectronics. To achieve this goal, the research has been focused on two main areas. First is the development of well-controlled processes for the growth and micropatterning of nanodiamond films to realize useful emitter structures. This part of the research deals with the study, processing, characterization and experimental analysis of field enhancement factors in diamond for electron emission, realization of CVD nanocrystalline diamond material with properties suited for electron field emission, and development of a highly selective diamond etch technique to fabricate versatile electron emitter structures of nanodiamond. The second part of the research involves the design, microfabrication, and characterization of monolithic nanodiamond field emission diodes and triodes in lateral configuration by the application of the material and process techniques developed in the first part. The specifics of device design, fabrication schema, characterization techniques employed, and results achieved are presented in chapters V and VI.

4.1 Part I: Development of nanocrystalline diamond for use as an electron field emitter

4.1.1 Analysis of field emission from diamond

An understanding of the physics of diamond field emission is essential for the development of an efficient diamond field emitter. **Figure 4.1** conceptually summarizes the mechanism of nanodiamond field emission described in chapters II and III.

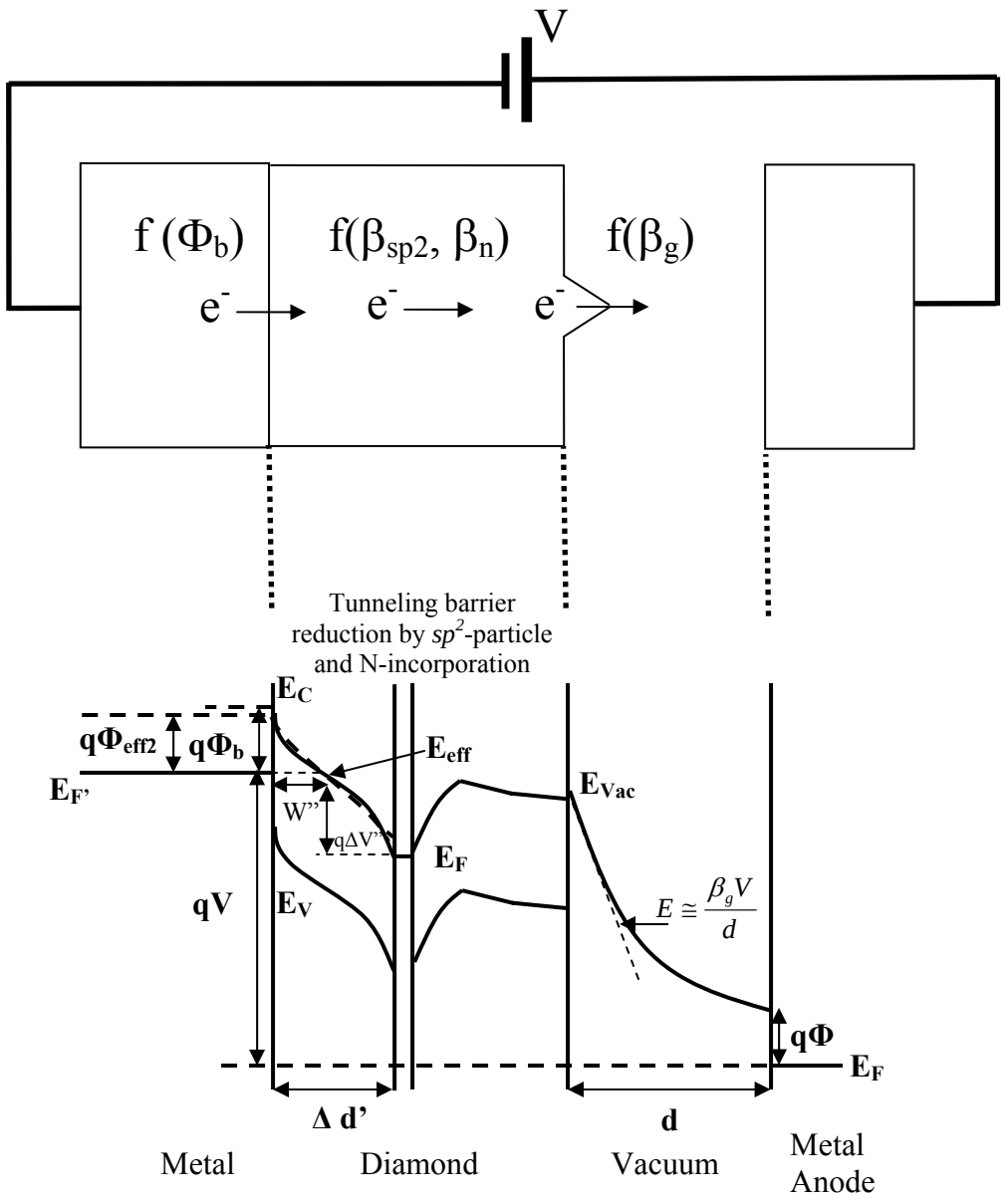

Figure 4.1 Summary of the mechanism of nanodiamond field emission.

For electron field emission from diamond to occur, electrons must [115]:

1) Tunnel through the metal-diamond interface. Electron tunneling at the metal-diamond interface depends on the barrier height, Φ_b, and hence the choice of metal contact.

2) Conduction through the diamond layer. The conduction through diamond plays an important role in the diamond field emission characteristics and this conduction is primarily controlled by diamond's composition (sp^2/sp^3 and doping).

3) Tunneling through the diamond-vacuum interface. The geometry of diamond emitter controls the electric field and the electron tunneling probability through the diamond-vacuum interface. The electron emission from the diamond emitters obeys the modified Fowler-Nordheim equation:

$$\mathrm{Ln}(I/E_0^2) = \mathrm{Ln}(A^* K_1 * \beta^2/\Phi) - (K_2 * \Phi^{1.5}/\beta)(1/E_0) \quad (4.1)$$

where K_1 and K_2 are constants, I is the emission current, Φ is the work function of the emitting surface (in eV), β is the total field enhancement factor, A is the emitting area, and E_0 is the macroscopic applied electric field (Volts/cm). $E_0 = V_D/d$ where V_D and d are the anode-cathode voltage and spacing, respectively.

Through experimental analysis, we have identified the unique behavior of the total field enhancement factor β of the diamond emitter. The β can be expressed as the product of the following field enhancement components:

$$\beta = \beta_g \, \beta_{sp2} \, \beta_n \quad (4.2)$$

where β_g, β_{sp2}, and β_n are field enhancement components due to the emitter geometry, sp^2-carbon content, and nitrogen doping, respectively. As discussed in the previous chapter, the nitrogen-incorporated nanocrystalline diamond, developed in this research, was found to be a promising form of CVD diamond, offering the field enhancement factors outlined in equation 4.2.

4.1.2 Development of nanocrystalline diamond film growth technique

The nanodiamond growth plasma chemistry can be effectively controlled to define the grain size, sp^2-carbon content, and the nitrogen-induced n-type conductivity in the thin film. We have identified a suitable process technique involving $CH_4/H_2/N_2$ microwave plasma enhanced chemical vapor deposition (MPECVD) to grow nitrogen-incorporated nanodiamond films on various substrates including silicon. Effective seeding techniques, applicable for diamond device-level processing, were utilized to augment the diamond nucleation site density. Through a comprehensive set of trials, the microwave plasma growth parameters, viz., gas flow rates of methane, hydrogen and nitrogen, microwave power and reactant pressure, and in effect, the growth rate were varied to determine the ideal set of process parameters giving the best film continuity and uniformity, small grain size, optimal sp^2-carbon content, low electrical resistance, and low surface roughness in the nanodiamond film. These nanodiamond films were electrically tested for vacuum field emission to consolidate the approach. The experiment led to the development of a reliable process technique yielding nanodiamond films with the required properties.

4.1.3 Development of nanodiamond micropatterning technique

The development of a robust micropatterning technique for nanodiamond is critical to utilize its strong properties and realize applicable structures and devices from the material. Non-uniform diamond emitter microstructures can result in uncontrolled randomly scattered emission sites, inconsistent emission behavior and no long-term stability. Hence, practical engineering design and control of the uniformity and microstructure of diamond emitters for device applications assumes paramount importance. If a deposition-etch selective micropatterning

process technique is developed for diamond thin films, it will be much more advantageous and less complicating than a selective diamond growth technique to realize useful micro/nanostructures and monolithic devices from the material. With this regard, a nanodiamond etch process has been developed using the ICP-RIE (inductively coupled plasma-reactive ion etch) technique in oxygen plasma with good selectivity, etch rate, and reproducibility to yield different micropatterns defined with the material for application as a field emitter. Experimental trials involving different plasma technology sources, etchant gas chemistries, power and pressure conditions, and masking materials of varied thicknesses were explored to establish the nanodiamond micropatterning process.

4.2 Part II: Design and development of monolithic nanodiamond lateral vacuum diodes and triodes

The development of practical vacuum microelectronic devices operating with high emission currents at low electric fields and voltages is the target of this research. There are four physical ways of improving the emission performance of a vacuum microelectronic device:

(i) Reducing the cathode material work function;

(ii) Enhancing the effective field at the emitter tip through sharpening;

(iii) Decreasing the inter-electrode distance;

(iv) Increasing the number of emitter tips for a given area, i.e., tip density.

Our fabrication process efforts are directed at simple ways of optimizing all of the above.

Novel and efficient device designs and fabrication schemes have been developed to utilize the potential of the nanodiamond material as an electron emitter, by integrating the cathode with electrodes controlling the motion of electrons. The field emitter devices were designed to operate in a planar lateral configuration. This lateral-type vacuum device is a

complete field emission device, with a nanodiamond pointed finger-like emitter array, integral anode and insulator involving a small interelectrode gap. The Vanderbilt Diamond Laboratory has built the first diamond lateral emitter using mold transfer technique [114]. In this research, we introduce a controllable and consistent processing scheme, similar to that used with very large scale integrated (VLSI) wafer technology, for monolithic nanodiamond lateral field emission devices utilizing the reactive ion etching (RIE) technique. The entire arsenal of deposition, micromachining and other material processing techniques developed in Part I were integrated to microfabricate these devices. Simple lithography-assisted single-mask and advanced dual-mask batch-processing methods have been used to fabricate nanodiamond lateral emitter devices on silicon-on insulator (SOI) and aluminum nitride substrates.

The motivation behind the development of a nanodiamond lateral emitter was to build a reliable, low voltage- and low electric field-operating monolithic field emission device applicable in integrated circuits, taking advantage of its small interelectrode gap distance, low input and negligible parasitic capacitance structure, along with the field emission potential of nanodiamond. One of the key parameters for an electronic device design is the operating voltage. For IC-compatible and general vacuum microelectronic applications, the turn-on and operating voltages should be as low as possible, as it offers better power and thermal management, apart from minimizing device reliability issues caused by ion sputtering, the sputter coefficient for ions in the energy range of the cathode to gate/anode voltage being negligible. Since the turn-on voltage depends on the turn-on electric field of cathode and the anode-cathode spacing, it is desired that a diamond cathode be fabricated to meet these two requirements. The lateral device configuration, with a simpler fabrication technique than the vertical assembly, allows for versatile electrode geometries, thereby paving the way for the nitrogen-incorporated

nanodiamond cathode to have a high field enhancement factor (β) resulting in a low turn-on electric field. Very small anode-cathode spacing in the micron or even sub-micron range can be realized in a lateral device, as the anode, cathode and the insulator are integrated, with the interelectrode separation defined by fine lithography. The small grain size and smooth surface of nanodiamond, coupled with its materials integration feasibility, enable uniform micropatterning of the diamond thin film to delineate the lateral device features using conventional photolithography and RIE process techniques. The lateral emitter arrays can also form a sound candidate for high power applications. In comparison with vertical field emitters, the smaller and more consistent interelectrode spacing of the lateral devices can result in electrical characteristics of higher current and higher transconductance at low operating voltages. The possibility of obtaining uniform current densities is appealing for high current, even though, lateral devices occupy more "real estate" than vertical devices, resulting in relatively lower packing densities. High density nanodiamond lateral comb array devices were fabricated to pursue this potential.

4.2.1 Design of monolithic nanodiamond lateral vacuum diodes

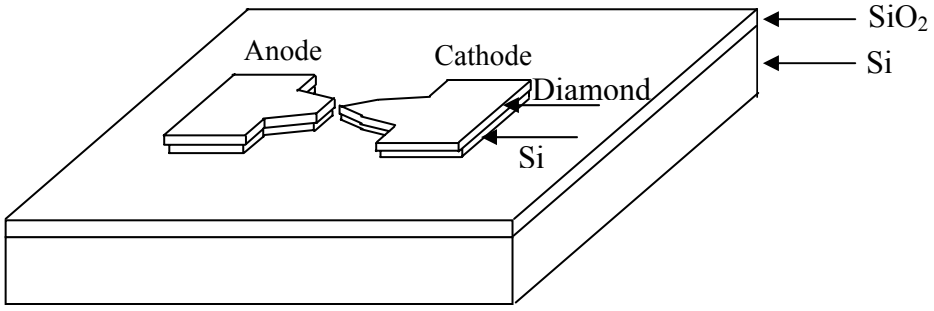

Figure 4.2 Basic design of a nanodiamond lateral field emission diode.

The basic design of the nanodiamond lateral field emission diode is presented in **Figure 4.2**. The nanodiamond cathode is equipped with an array of uniformly spaced high aspect-ratio *finger-like* emitters with sharp apexes for geometrical field enhancement. The anode has a straight edge structure, and its material is either nanodiamond or a metal with high work function (Φ) to obtain rectifying diode characteristics. The electrodes are separated by a distance as small as 2 μm, determining the turn-on voltage of the diode, per a specific nanodiamond composition and diode configuration. Diamond lateral vacuum devices should operate at compatible voltages with photolithographically defined micron-scale spacings, owing to the low electric field emission characteristic of the cathode material. A silicon layer supports the diamond electrode structures on an insulating substrate of SiO_2, which serves as the isolation material. A silicon-on-insulator (SOI) wafer is the substrate on which the lateral devices are built.

4.2.2 Design of monolithic nanodiamond lateral vacuum triodes

Lateral device design is one of the suitable approaches to achieve a completely integrated three-terminal field emission device. An uncomplicated process technique can be utilized to batch-fabricate lateral triodes on the same substrate, notably with very small lithographically defined gate-cathode spacing. Furthermore, devices with multiple gate electrodes such as tetrodes and pentodes can be easily achieved with the lateral design. An important parameter for triode design is the gate voltage. For most applications, the gate turn-on and modulating voltages are desired to be small. Similar to the diamond vacuum diode, the gate voltage relies on the turn-on electric field of diamond cathode and the gate-cathode spacing. The nitrogen-incorporated nanodiamond lateral device approach, with 2 μm gate-cathode gap design, is suitable to achieve the desired goals. **Figure 4.3** represents the nanodiamond vacuum microtriode design, where a

finger-emitter is integrated with gate and anode electrodes in a lateral geometrical configuration. This lateral triode structure is more suitable for high-speed and high-frequency device applications because of their small emitter-to-gate capacitances, compared to the vertical triodes.

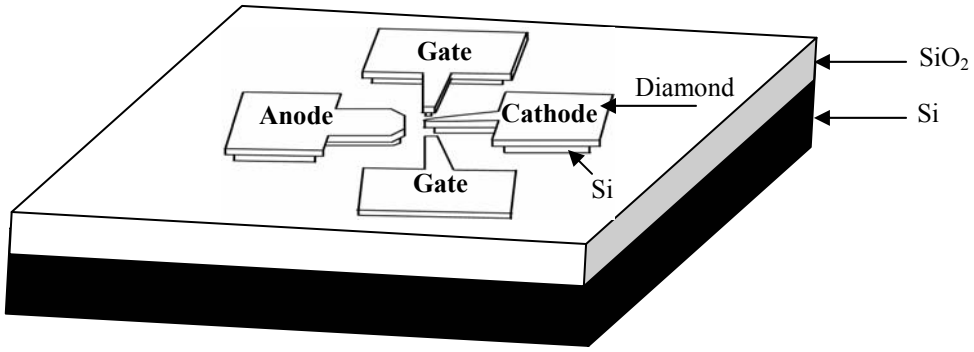

Figure 4.3 Basic design of a nanodiamond lateral field emission triode.

Other important parameters for diamond vacuum triode design are amplification factor and transconductance. Amplification factor determines the ultimate voltage gain and transconductance signifies current driving capability when a diamond triode is operated as an amplifier. For transistor application, the amplification factor and transconductance are desired to be high. To achieve high amplification factor, gate-anode spacing and the gate positioning must be properly chosen such that cathode is effectively shielded from the anode by the gate but anode potential is still capable of collecting all electrons emitted from the cathode. High emission current at low gate voltage from diamond triode is the key requirement to achieve high transconductance. The lateral device approach, with high current per tip capability of the diamond emitter in a small gate-cathode gap construct, can help achieve high transconductance. Different device configurations of the nanodiamond lateral triode featuring a single-emitter

cathode, varying in gate-cathode and anode-cathode separation distances, were fabricated. In this work, only a 1-finger geometry was designed for the triode, so as to clearly study the three-terminal characteristics of a vacuum device in lateral configuration. This design can be later extended to form an array configuration to improve its performance. A detailed analysis was done correlating the device design and electrical characteristics, and it was found that the spacing of the electrode structures can be used to totally control the device characteristics, resulting in either *triode* or *transistor*-type operation.

Overall, the key performance-related aspects of electron field emission focused on in the nanodiamond lateral device included low turn-on electric field and voltage, high emission current and current density, negligible leakage current, emission stability over time and repeatability of device I-V characteristics, diode rectification, and gate-controlled triode and transistor characteristics. The field emission behavior of the lateral emitter was analyzed as a function of the device parameters, viz., emitter geometry, emitter array size, and interelectrode spacing to establish the physical aspects of the vacuum device controlling its electrical performance. To investigate the potential of a vacuum microelectronic technology for extreme environment applications, a thorough experiment was conducted with the nanodiamond lateral device under conditions of high temperatures, and total dose (x-ray) and neutron radiation exposure. Efforts were also directed at developing a nanodiamond lateral emitter device functioning in a vacuum package, with help from the *Kansas City Plant* operated by *Honeywell*®.

CHAPTER V

DEVICE FABRICATION AND EXPERIMENTATION

This chapter describes the process techniques developed for the nanodiamond material, and the fabrication schemes for the development of monolithic nanodiamond lateral field emitter devices, along with the experimental results.

5.1 Deposition and characterization of nanocrystalline diamond thin films

An effective growth rate control technique is identified to grow nanodiamond films with the process of microwave plasma enhanced chemical vapor deposition (MPECVD). It was inferred that a decrease in the growth rate by the control of the CVD process parameters has a direct effect on the reduction of grain size of the diamond film.

5.1.1 Experimental

Nanocrystalline diamond films were deposited in an *ASTeX*® MPECVD system with a 1.5 kW generator, operating at 2.45 GHz. The schematic of a typical MPECVD system is shown in **Figure 5.1 (a)**. The substrate temperature was set using an induction heater independent of the plasma. The growth system was coupled with a controlled gas handling system, allowing for precise control of the flow of all process gases. N-type silicon wafers (ρ=0.001-0.008 Ω-cm) were used as substrates for nanodiamond growth. The substrates were pretreated by mechanically polishing the surface using a 2.5-μm diamond powder, and ultra-sonicating with a 5-20 nm nanodiamond powder in acetone solution to augment diamond nucleation. A gas mixture of $CH_4/H_2/N_2$ was employed for nitrogen-incorporated nanodiamond growth. The gases

at flow rates of 15/8/190 sccm ($CH_4/H_2/N_2$) were introduced into the CVD system at a pressure of 20 Torr. The substrates were heated to a temperature of 800 °C. The microwave plasma was maintained at a power of 550 W. **Figure 5.1 (b)** shows the snapshot of the $CH_4/H_2/N_2$ microwave plasma during the nanodiamond growth process.

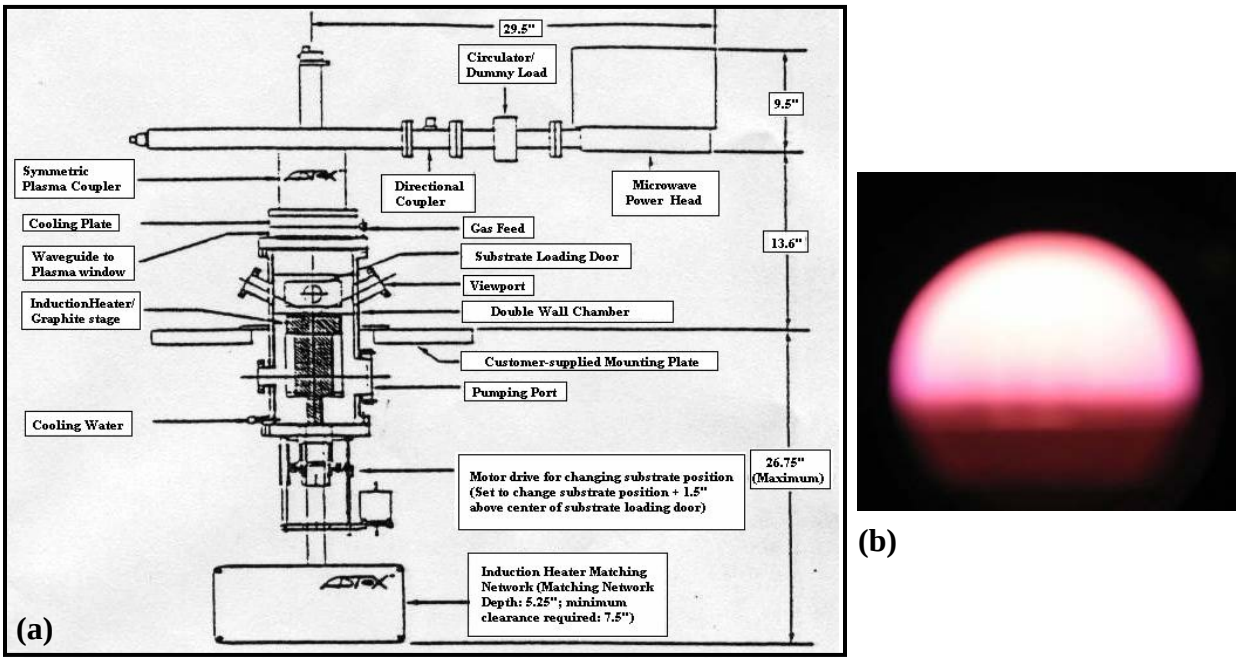

Figure 5.1 (a) ASTeX® PECVD system used for the nanodiamond growth process; (b) snapshot of the $CH_4/H_2/N_2$ plasma during nanodiamond deposition.

The growth rate was then altered by varying the CVD process parameters to investigate the grain size and morphology of the diamond films, and also its composition and electrical properties. To conduct a set of comprehensive trials for nanodiamond growth by $CH_4/H_2/N_2$ plasma CVD, the microwave power was varied between 550 W and 1000 W, methane gas flow rate from 2 sccm–15 sccm with the nitrogen and hydrogen flow rates remaining constant, and the reactant pressure was altered in the range of 13-28 Torr. For comparison, a gas mixture of CH_4/H_2 with flow rates of 15/138 sccm respectively, microwave power of 550 W, and reactant

pressure of 13 Torr maintained at a substrate temperature of 800° C was used for diamond film deposition in the same MPECVD system. The morphology of the CVD diamond films were examined using a field emission-scanning electron microscope (SEM), while the average grain size was determined by scanning across the surface of the film at a high magnification of 150 kX, aided by a nano-scale marker. An atomic force microscope (AFM) was used to analyze the surface roughness profile of the nanodiamond film. The common method of scratch test was used to evaluate the adhesion strength of the nanodiamond film onto the substrate. The composition characterization and structure determination of the diamond films was studied using Raman spectroscopy. Electrical conductivity measurements were performed with the help of a multimeter. Energy dispersive spectrometry (EDS) was used to identify the incorporation of nitrogen in the nanodiamond thin film, where X-rays generated from the diamond film under electron bombardment by the SEM were collected with a liquid nitrogen-cooled solid state Si (Li) detector and analyzed via computer according to their energy. Rutherford backscattering spectrometry (RBS) experiment was also conducted to analyze the chemical composition of the $CH_4/H_2/N_2$-plasma deposited nanodiamond. The technique was used to bombard a small portion of the diamond film with very high energy (1800 keV) helium ions, and measure the yield and energy of backscattered helium. The composition profile and nitrogen concentration in the nanocrystalline diamond were obtained.

5.1.2 Results

Nanodiamond growth: Nanocrystalline diamond films with grain size as small as 5-10 nm were synthesized using the $CH_4/H_2/N_2$ microwave plasma chemical vapor deposition process at a growth rate of 0.1 μm/hr. The grain size of the diamond film was effectively decreased by

lowering the growth rate through the adjustment of the CVD process parameters, viz., microwave power, reactant pressure, and gas flow rate. It was found that a 15 sccm methane flow rate process at 1 μm/hr rate of growth gives a diamond grain size of ~ 200 nm, while a decrease from 15 sccm to 2 sccm results in the drop in the grain size to 10-15 nm. At a constant CH_4 flow rate of 15 sccm, decreasing the microwave power from 1000 W to 550 W produced a grain size reduction from 200 nm to 80 nm, while a decrease in reactant pressure from 28 Torr to 20 Torr with 550 W microwave power yielded a reduction in grain size from 80 nm to 5-10 nm, for which the growth rate was observed to be 0.1 μm/hr. The net result of grain size decrease from 200 nm to 5 nm was brought about by the lowering of growth rate from 1 μm/hr to 0.1 μm/hr. **Table 5.1** summarizes the effect of the adjustment of CVD process parameters on the grain size of the diamond film, while **Figures 5.2** and **5.3** illustrate the result with the help of SEM micrographs. **Figure 5.4** shows the morphology of the as-deposited nanodiamond film, examined at different magnifications in a SEM. The continuity and uniformity of the thin film over a 2-inch wafer area were found to be highly suitable for integration into device forms.

The conventional CH_4/H_2 microwave plasma chemical vapor deposition process also yielded nanocrystalline diamond with grain size of 20-30 nm, when carried out at a low growth rate of 0.2 μm/hr, by controlling the CVD process parameters (see **Figure 5.5**). This result is in contrast to some reports that the CH_4/H_2 microwave plasma technique does not produce nanocrystalline diamond. It is important to note that the grain size of the nanodiamond film remains constant throughout the growth process, irrespective of the thickness of the film. The thickness of the CVD diamond films deposited on flat silicon substrates and applied for this study was ~ 3 μm, though in a different experiment, the nanodiamond film was found to maintain its nanocrystallinity even to a thickness of ~ 20 μm.

By these experimental observations, we infer that an effective means to grow nanocrystalline diamond is to increase the nucleation rate and decrease the growth rate by adjusting the CVD process parameters, viz., microwave power, reactant pressure, and gas flow rate. During the MPECVD diamond growth process, diminishing the microwave power reduces the energy of the plasma, and decreasing the reactant pressure spreads out the microwave plasma in the CVD growth chamber. Reducing the methane flow rate decreases the carbon growth source, thereby slowing the growth rate. When all three parameters forces of the reaction process are decreased, the reaction is starved. Hence, the two events, diamond nucleation and growth compete against each other for the limited amount of energy available. In this condition, the nucleation density will increase and the grain size diminish. Thus, a high density of nano-sized, fine diamond grains conglomerate on the substrate to form the nanocrystalline diamond film. The growth rate control process methodology employed here for nanodiamond thin film deposition can facilitate the synthesis of a very thin and smooth layer of CVD diamond on the surface of several substrates and structures for evaluation in varied applications.

Table 5.1 Reduction of the average grain size of diamond films deposited in $CH_4/H_2/N_2$ microwave plasma conditions through the adjustment of the CVD process parameters

CH_4 flow rate (Power: 1000 W; Pressure: 28 Torr)	**Average grain size**
15 sccm (~ 7 % CH_4)	200 nm
11 sccm (~ 5 % CH_4)	90 nm
5 sccm (~ 2 % CH_4)	50 nm
2 sccm (~ 1 % CH_4)	10-15 nm

Microwave power (CH_4 flow rate: 15 sccm; Pressure: 28 Torr)	**Average grain size**
1000 W	200 nm
800 W	150 nm
550 W	80 nm

Reactant pressure (CH_4 flow rate: 15 sccm; Power: 550 W)	**Average grain size**
28 Torr	80 nm
20 Torr	5-10 nm

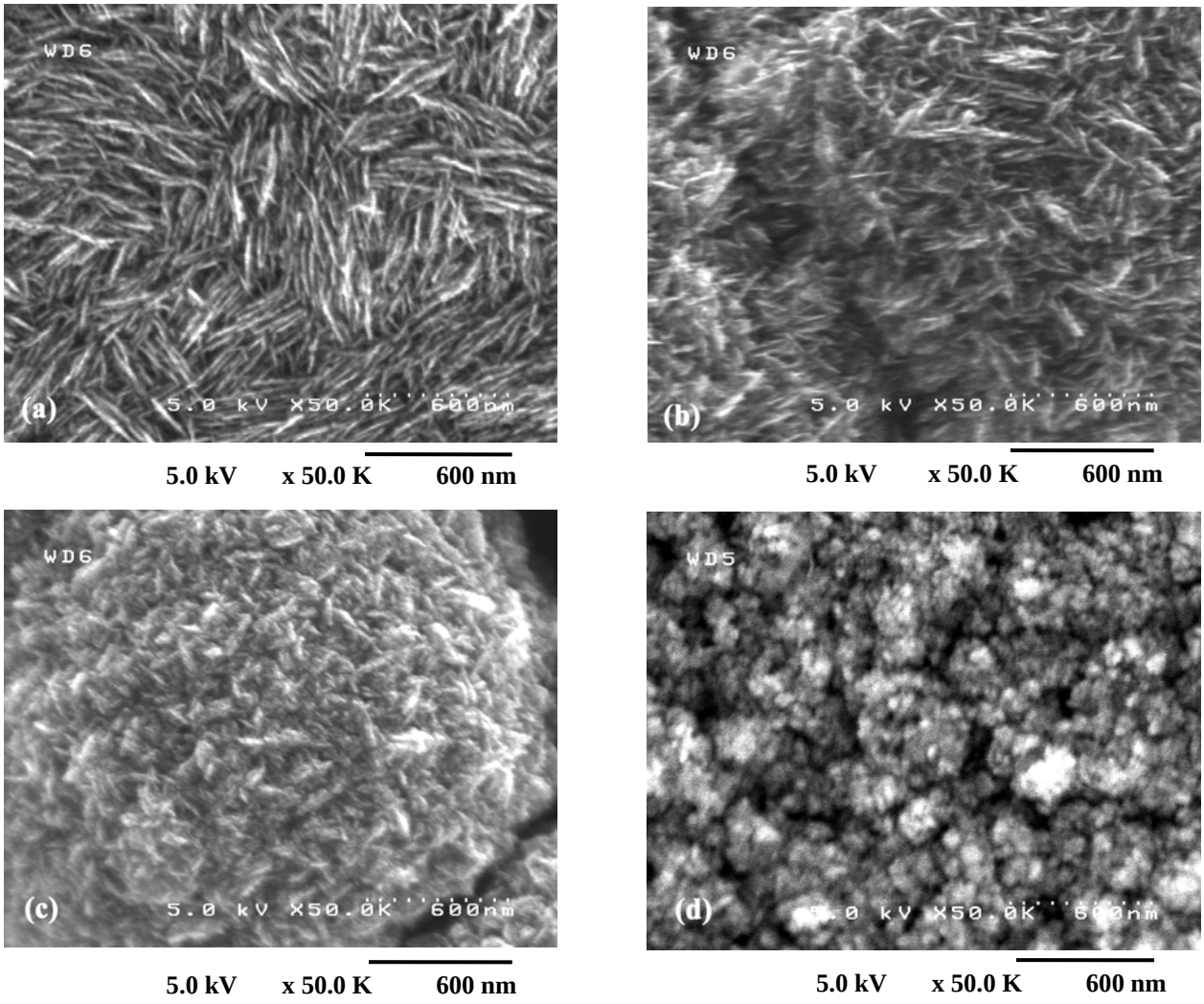

Figure 5.2 SEM micrographs portraying the decrease in diamond grain size due to the reduction in CH_4 flow rate at a constant microwave power of 1000 W and reactant pressure of 28 Torr:

(a) CH_4 flow rate: 15 sccm; grain size: 200 nm;
(b) CH_4 flow rate: 11 sccm; grain size: 90 nm;
(c) CH_4 flow rate: 5 sccm; grain size: 50 nm;
(d) CH_4 flow rate: 2 sccm; grain size: 10-15 nm.

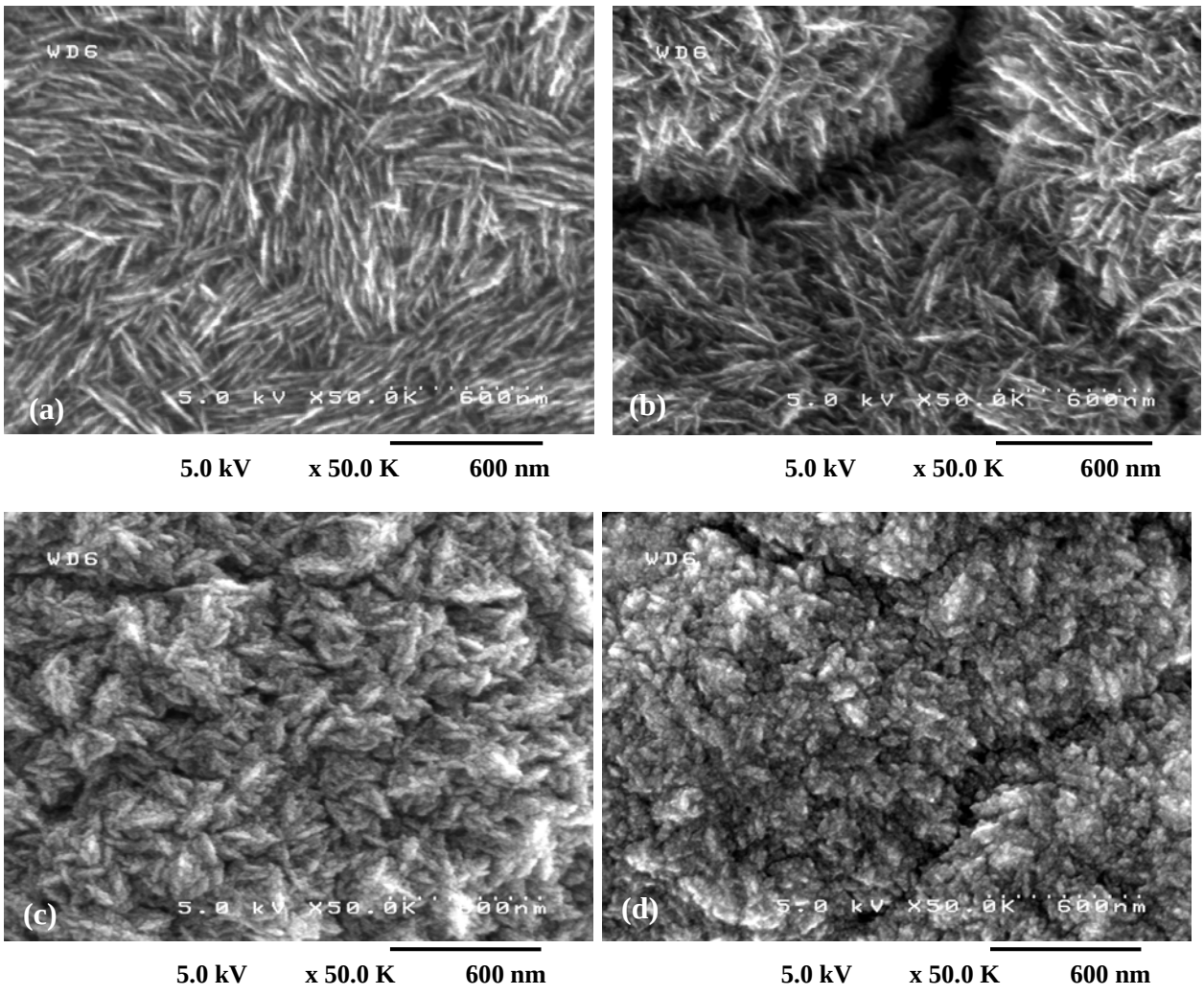

Figure 5.3 SEM micrographs depicting the decrease in diamond grain size due to the reduction in microwave power and reactant pressure at a constant CH_4 flow rate of 15 sccm:

(a) Power: 1000 W, Pressure: 28 Torr; grain size: 200 nm;
(b) Power: 800 W, Pressure: 28 Torr; grain size: 150 nm;
(c) Power: 550 W, Pressure: 28 Torr; grain size: 80 nm;
(d) Power: 550 W, Pressure: 20 Torr; grain size: 5-10 nm.

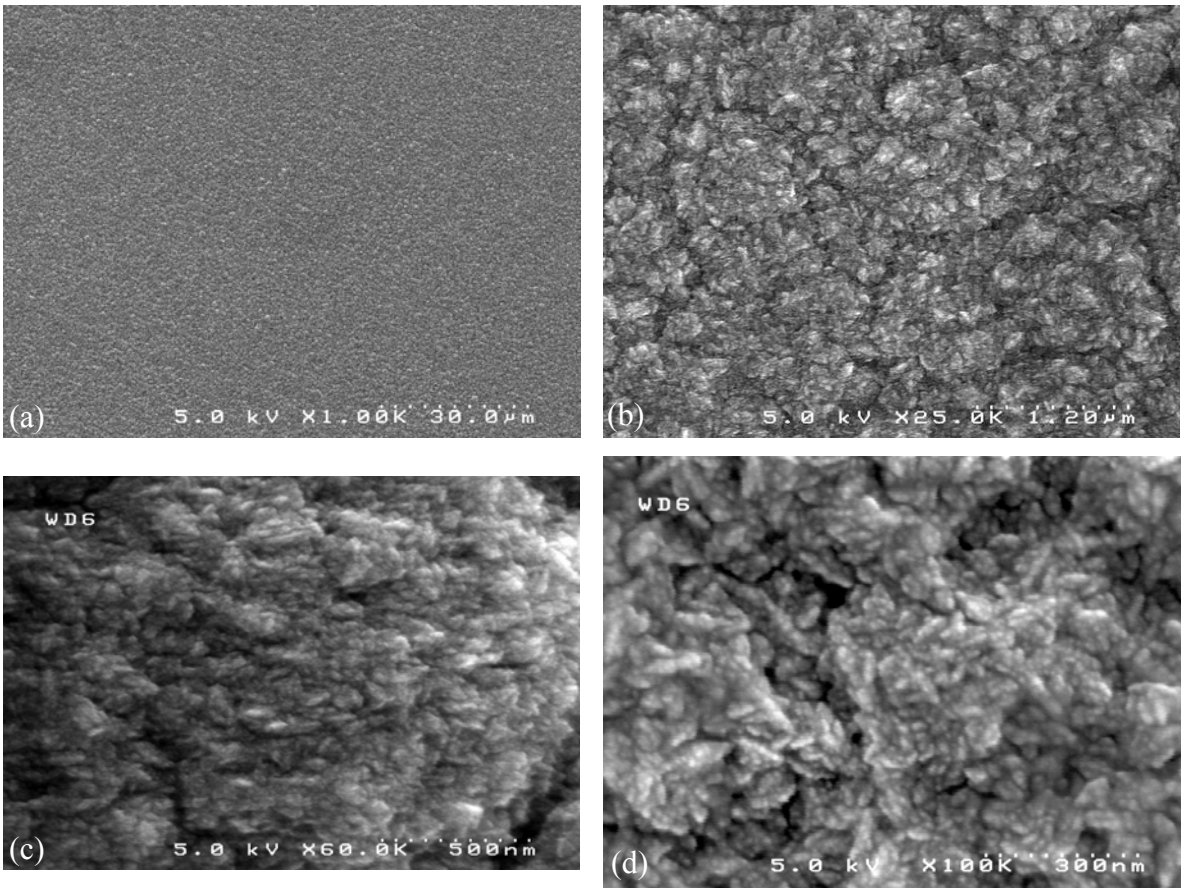

Figure 5.4 SEM micrographs of an as-deposited nanocrystalline diamond film with average grain size of 5-10 nm grown by $CH_4/H_2/N_2$ MPECVD process technique at different magnifications: (a) 1 kX, (b) 25 kX, (c) 60 kX, and (d) 100 kX.

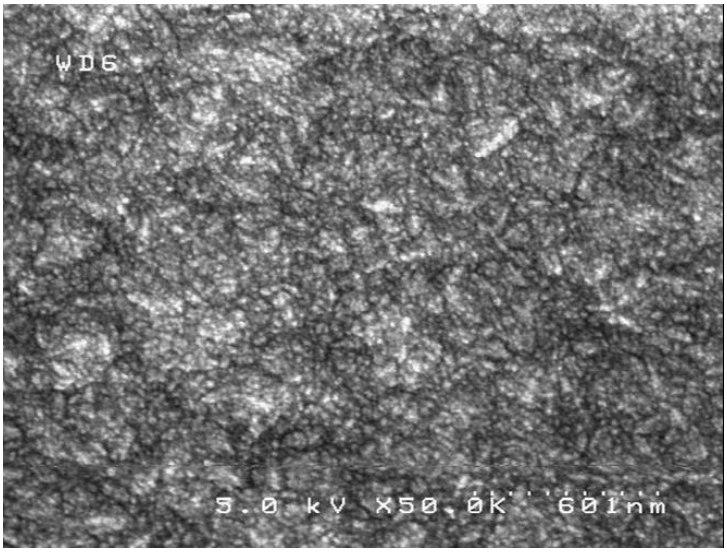

Figure 5.5 SEM image of a nanodiamond film grown by CH_4/H_2 microwave plasma deposition.

Nanodiamond film surface analysis: The SEM and AFM images in **Figure 5.6** show that the nanodiamond film has a smoother and more uniform surface morphology than the microdiamond film, which possesses an increased surface roughness profile. Quantitatively, the RMS roughness of the nanodiamond film was found to be 8-20 nm, while that of the microdiamond film was ~ 115 nm. The low surface roughness is a very important property required for lithographically micropatterning a thin film to realize useful structures for different applications. Hence, nanocrystalline diamond offers better compatibility for process integration and device formation. Also, the scratch test showed that nanodiamond films have good adhesion to the substrate.

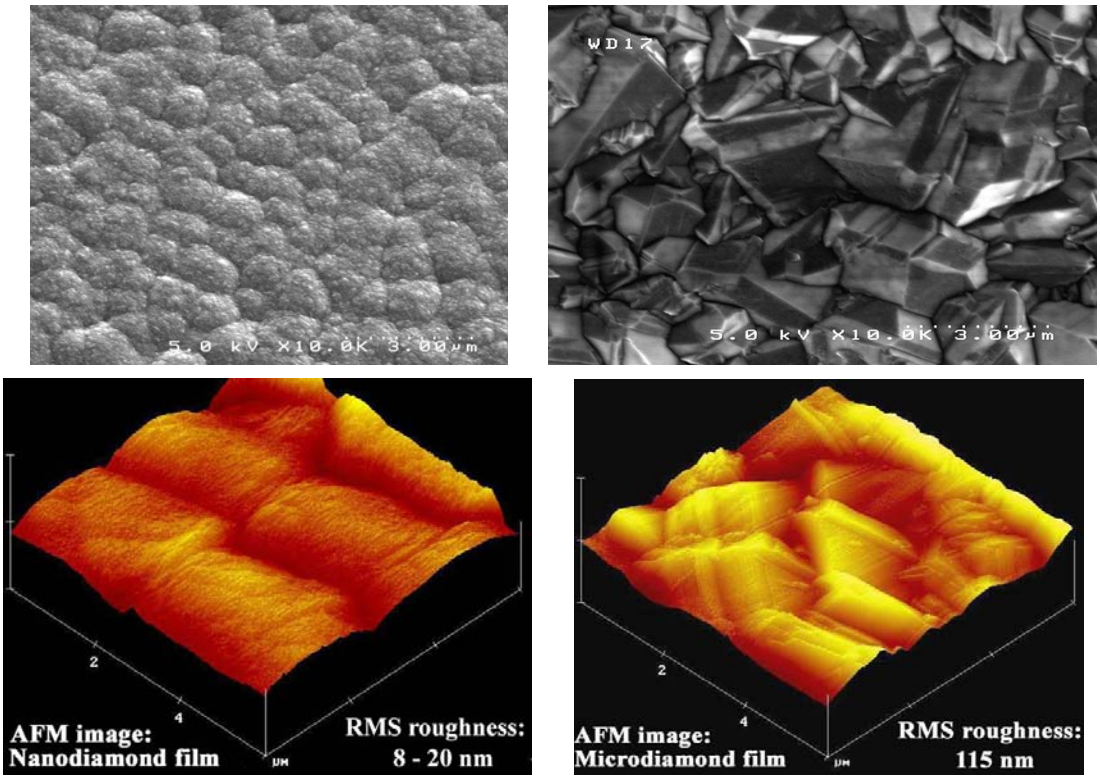

Figure 5.6 SEM and AFM images of nanocrystalline and microcrystalline CVD diamond films.

Composition characterization of nanocrystalline diamond: **Figures 5.7** and **5.8** show the results of the Raman spectroscopic analysis performed on the nanodiamond films. The sp^3-carbon and sp^2-carbon signatures are detected at 1332 cm^{-1} and 1580 cm^{-1} respectively in the Raman spectra.

A small shoulder detected at ~ 1140 or 1160 cm^{-1} indicates the nanocrystalline phase existing in the diamond film [65,185], possibly attributive of the disordered sp^3-bonded carbon distributed in the nano-dimensioned grain boundaries, which are of increased volume-density in the case of nanodiamond [186,201]. **Figure 5.7** compares the Raman spectrum (b) of the 5 nm grain-sized nanodiamond film deposited by $CH_4/H_2/N_2$ MPECVD with that of a larger grain-sized diamond film deposited using the same $CH_4/H_2/N_2$ technique. The spectrum (a) of the latter also shows a shoulder at ~ 1140 cm^{-1} due to the presence of some nano-sized grains and associated grain boundaries interspersed in the diamond film, but the average grain size is 200 nm. Comparing the Raman plots, it can be observed that the degree of sp^2-bonded carbon content in the diamond film increases as the grain size decreases. The sp^2/sp^3 peak ratio of the 5-10 nm grain-sized nanodiamond film ($CH_4/H_2/N_2$ CVD) was found to be ~ 0.97, while that of the 200 nm grain-sized diamond film ($CH_4/H_2/N_2$ CVD) was ~ 0.51. An assumption is often made that the relative peak intensities reflect the volume fractions of diamond and non-diamond carbon present. However, the optical probing depth (*i.e.,* sampled volume) can vary with the microstructure of the carbon phase and the scattering cross sections for the mixtures of sp^2- and sp^3-bonded carbon are also unknown. Therefore, these data should be used in a relative, not an absolute, sense.

A broad sp^3-diamond peak and a higher sp^2-shoulder are typical characteristics of the Raman spectrum of a nanocrystalline diamond film, as described in Chapter III in discussing the properties of the material. Further, it was deduced (see **Figure 5.8**) that the nanodiamond film grown by $CH_4/H_2/N_2$ CVD possesses a higher sp^2-carbon concentration than that obtained by CH_4/H_2 CVD (sp^2/sp^3 peak ratio: 0.76), the reason being nitrogen preferentially enters the network of grain boundaries, and promotes sp^2 bonding in the neighboring carbon atoms [62,65,154]. The exciting wavelength and power of the laser beam used in Raman spectroscopy

was 623.81 nm and 11 mW respectively. The Raman scattering was confined to the ~ 3 μm-thick diamond films, and not the underlying Si substrate. The sp^2-bonding has 50 times higher scattering efficiency than sp^3-bonding in visible range, and hence, the nanodiamond film, though having increased sp^2-carbon concentration, still retains a highly sp^3-bonded diamond structure.

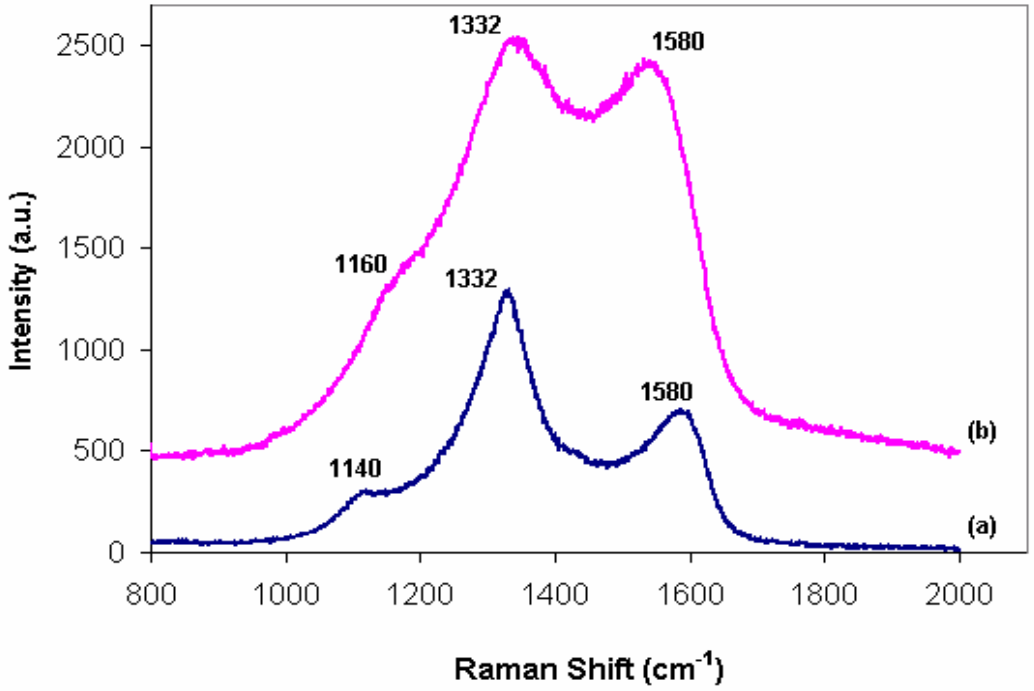

Figure 5.7 Raman spectroscopic analysis of diamond films deposited by $CH_4/H_2/N_2$ MPECVD: (a) 200 nm grain-sized diamond film; (b) 5-10 nm grain-sized nanodiamond film.

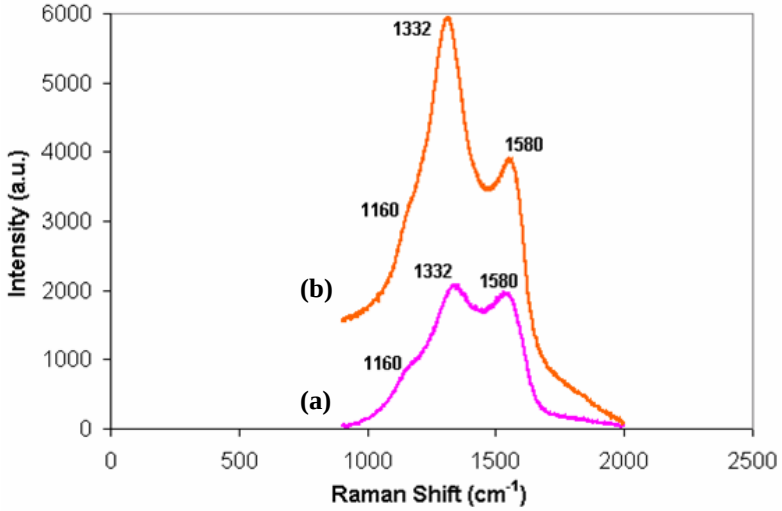

Figure 5.8 Raman spectra of nanodiamond films deposited by (a) $CH_4/H_2/N_2$; (b) CH_4/H_2 CVD.

Electrical conductivity of nanodiamond: The electrical resistance measurements were performed using a multimeter, probed on identical-sized Ti/Au circular electrodes sputter-deposited on the surface of the nanodiamond film. To obtain good Ohmic contacts, a rapid annealing at 350 °C was carried out for 3 min in a vacuum environment. Direct measurement of the electrical conductivity at room temperature (RT) showed that the nanodiamond film grown by $CH_4/H_2/N_2$ MPECVD has a very low resistance of 2 Ω-10 Ω. In contrast, the electrical resistance of the CH_4/H_2-plasma grown nanodiamond film was found to be ~ 25 MΩ. It should be noted that the typical resistivity of intrinsic diamond is ~ 10^{13}-10^{16} Ω-cm, the film resistance of which is measured to be "Open" in a G-ohm multimeter.

The high electrical conductivity of nanodiamond obtained from $CH_4/H_2/N_2$ MPECVD is attributed to the incorporation of nitrogen. Energy dispersive spectrometry X-ray microanalysis revealed the incorporation of nitrogen in the nanodiamond film. **Figure 5.9** represents the corresponding EDS spectrum, displaying a real time histogram of X-ray count per channel versus energy expressed in keV. The nanodiamond film profile exhibits the characteristic carbon and nitrogen elemental peaks at X-ray energies of 0.277 and 0.392 keV, respectively. RBS experiments conducted on the $CH_4/H_2/N_2$-plasma derived nanodiamond film also indicated the incorporation of nitrogen. The semi-log RBS plot, included in **Figure 5.10**, displays a distinct nitrogen edge, thus confirming the presence of nitrogen in the nanodiamond. An idea of the nitrogen distribution profile can be obtained using the graph. While the edge, typically occurring at 565 keV according to the RBS calibration, shows that nitrogen is present at the surface of the film, the step-like profile is indicative of nitrogen also distributed in the nanodiamond bulk. Quantitatively, the nitrogen concentration was found to be ~ 4.5×10^{21} cm^{-3} in the near-surface region (~ 50 Å) of the nanodiamond film. The actual percentage composition of nitrogen in the

diamond was ~ 1.45 %. RBS, being a surface-sensitive technique, could be used to accurately verify the nitrogen concentration in the near-surface region. But, since the nitrogen incorporation technique during nanodiamond thin film deposition is homogeneous, the nitrogen concentration should be uniform throughout the diamond layer. Secondary ion mass spectroscopy (SIMS) analysis can be used to accurately establish the nitrogen n-type dopant concentration. As the increase in electrical conductivity of the nanodiamond film by nitrogen incorporation clearly indicates a decrease in the work function, experimental techniques to estimate this reduction in the work function of the material form a subject of further study.

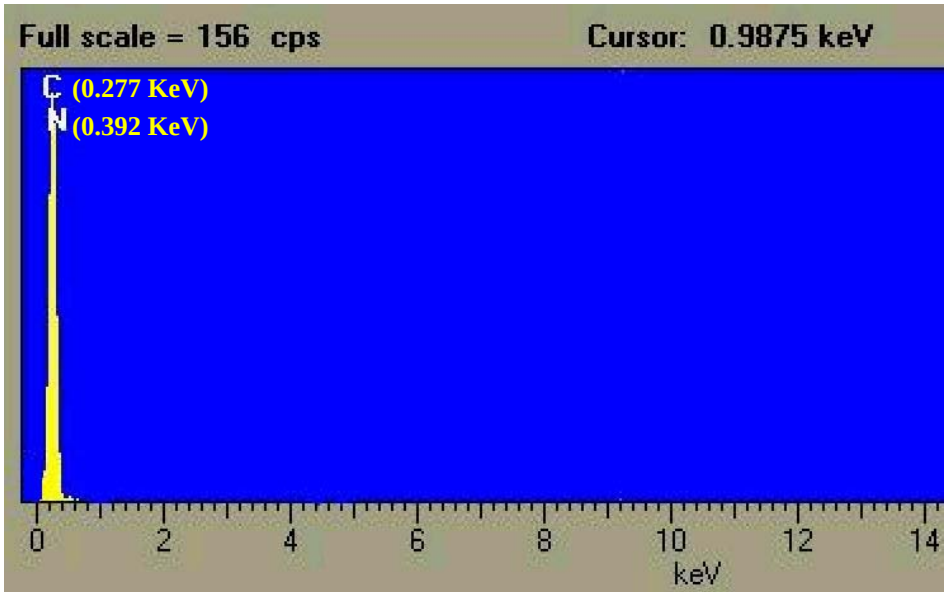

Figure 5.9 EDS x-ray microanalysis composition profile (X-ray count Vs Energy) of the nanodiamond film deposited by $CH_4/H_2/N_2$ MPECVD, indicating the incorporation of nitrogen impurity in the diamond film.

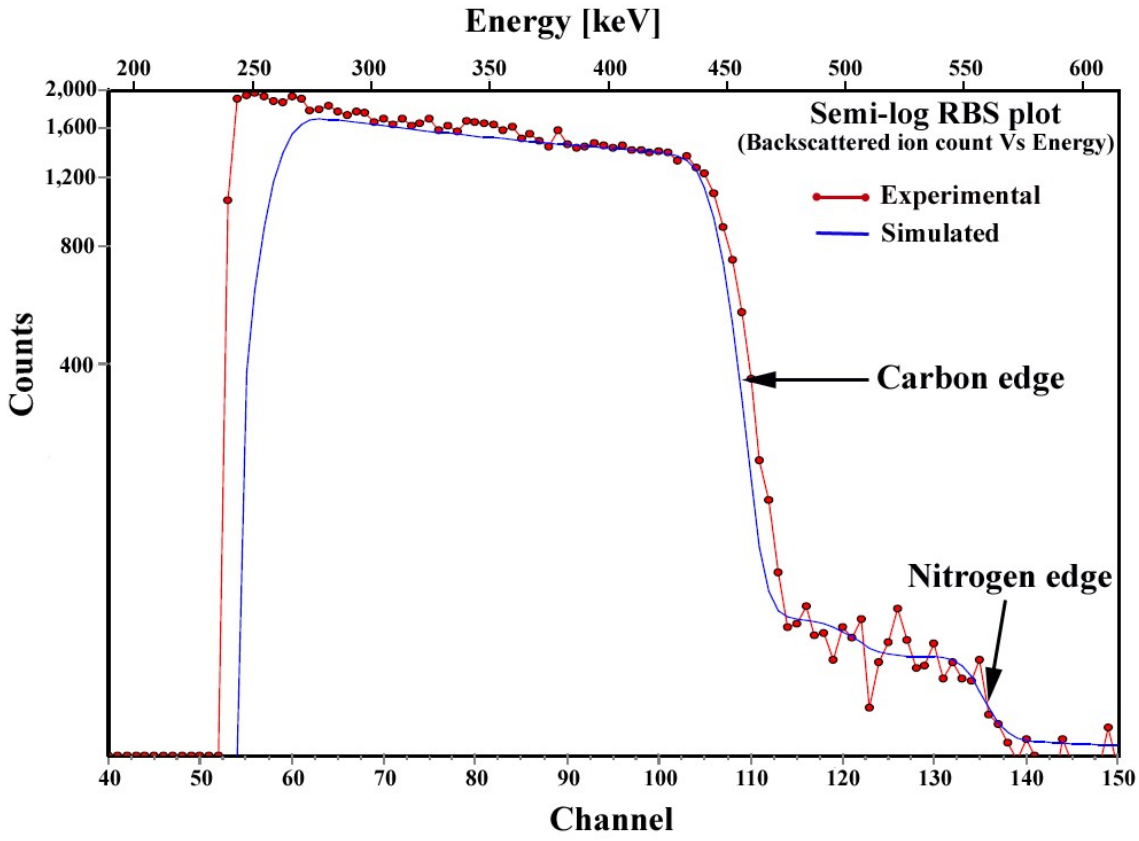

Figure 5.10 Semi-log RBS plot (backscattered ion count vs. energy) obtained from the $CH_4/H_2/N_2$-nanodiamond possessing a distinct nitrogen edge in its composition profile.

Nanodiamond films are incorporated with nitrogen to enhance the electrical characteristics of the material. *In-situ* addition of nitrogen gas to the growth chemistry in the MPECVD process is a suitable method for this purpose. The electrical conductivity of nanodiamond can be enhanced by increasing the percentage of nitrogen included in the growth plasma. Another effective technique to achieve nitrogen-doping in nanocrystalline diamond is to increase the microwave power and pressure at a particular nitrogen gas flow rate. Nitrogen-incorporated nanodiamond films were developed in this research by means of extensive experimentation, where the material deposition process parameters, viz., microwave power,

pressure and nitrogen gas flow rate were effectively controlled to yield a small grain size as well as optimal doping for high conductivity at room temperature.

5.2 Micropatterning of nanocrystalline diamond films

One of the reasons for CVD diamond being less utilized as a field emitter is that it is difficult to pattern diamond films due to the scarcity of appropriate wet or dry etching techniques. Diamond, being the hardest material, requires a well-controlled etch process to be patterned uniformly to realize useful structures for varied applications. Optical lithography on microcrystalline diamond substrates is also a concern, due to its surface roughness. With the nanodiamond films developed in this research, having a small grain size and smooth surface morphology and uniformly controllable thickness, it is possible to overcome many lithography problems. The Vanderbilt Diamond Laboratory has previously created a mold transfer technique to micropattern diamond films and generate topologically managed diamond vacuum field emitters that optimize both the geometrical and quantum aspects of the Fowler-Nordheim governed emission [163]. In this research, a reactive ion etch (RIE) nanodiamond micropatterning process technique is developed, which can be utilized in the fabrication of a variety of diamond-based devices for applications in vacuum microelectronics and beyond, where the geometry directly affects device performance.

Reactive ion etching of diamond has been attempted by different researchers with moderate success. Low etch rate, non-uniform etching, and inadequate mask-defined selectivity for device-level micropatterning have been some of the issues encountered during the diamond etch. This research addresses and overcomes these concerns, with nanodiamond, to develop a consistent and well-controlled micropatterning technique and realize potential electron field

emitter structures. Experimentation involving different plasma technology sources, etchant gas chemistries, power and pressure conditions, and masking materials of varied thicknesses led to the establishment of the nanodiamond micropatterning process. The utilization of an ICP-RIE system, based on the inductively-coupled plasma technology combining a high conductance, high vacuum compatible process chamber with an ICP source to produce very high ion density at controlled low pressures, resulted in a nanodiamond etch process with a high etch rate of ~ 0.5 μm/min. R.F.-assisted pure oxygen plasma chemistry was identified to be a very efficient diamond etchant. An aluminum masking layer of ~ 0.5 μm thickness was found to offer good selectivity, allowing the micropatterned nanodiamond structures to retain the beneficial properties of the material. The ICP-RIE process parameters included a coil R.F. power of 700 W, platen R.F. power of 150 W, oxygen flow rate of 30 sccm, at a pressure of 10 mTorr. The etch conditions of high R.F. power and low pressure helped achieve good anisotropy, the high energy reactive ions with minimum ion scattering giving a high diamond etch rate and directionality. The selective etching ratio of diamond against aluminum was found to be suitably high for device pattern formation. The etching was examined to be uniform over a reasonably large area, leaving a smooth substrate surface with no residue at the end of the RIE process, facilitating high-yield batch-fabrication of devices applying diamond. Nitrogen doping levels in nanodiamond did not have an adverse effect on the etch rate, which can yield field emitter structures of diamond, with no compromise on the material properties. Lateral field emitters fabricated using this nanodiamond micropatterning process are presented in this chapter.

Alternate diamond etch process recipes resulted in very little success. CF_4/O_2 plasma etch chemistry was implemented to investigate its effect on the diamond etch rate. Metal layers of titanium and gold were also applied in different trials to identify the masking material offering

the best selectivity. The experiment employing CF_4/O_2 plasma etchant species for nanodiamond RIE did not increase the etch rate significantly, while the process selectivity suffered. Also, Ti and gold (0.5 μm thick) masks were not reliable, the micropatterned metal layer on the diamond wearing out and peeling off under the same etch process conditions used with Al as mask.

5.3 Cathode fabrication to investigate emission behavior of nitrogen-incorporated nanodiamond

Nitrogen-doped and undoped nanodiamond films grown by the two different gas chemistries, $CH_4/H_2/N_2$ MPECVD and CH_4/H_2 MPECVD respectively, described earlier in this chapter were applied individually in the fabrication of pyramidal diamond tip array cathodes through a mold transfer technique [163]. The physical and electrical characteristics of the diamond microtips have been well explored by Wisitsora-at at Vanderbilt [115]. Although the focus of this research is on planar lateral field emission devices, the potential field emission properties of the developed nitrogen-incorporated nanodiamond material can be evaluated in a conventional cathode form before application in advanced monolithic device configurations, which was the plan behind the application of nanodiamond to the pyramidal tips. The mold transfer process technique used to realize the diamond pyramidal cathode has been documented previously [115]. **Figure 5.11** displays the $CH_4/H_2/N_2$-nanodiamond applied pyramidal tip arrays at different magnifications. The ultra-sharp apex of the nanodiamond tip with a tip radius of curvature of 5 nm and height of 1 μm is displayed in **Figure 5.11 (b)**, indicating that the 5 nm grain size of the $CH_4/H_2/N_2$-nanodiamond film was incorporated in the mold-transfer technique. The microtips seen in **Figure 5.12** are of the CH_4/H_2-nanodiamond. Due to the film's slightly larger grain size, it can be seen that the radius of curvature (~ 25 nm) and height (~ 500 nm) of the tip apex are not as well defined as those in the $CH_4/H_2/N_2$-nanodiamond tip.

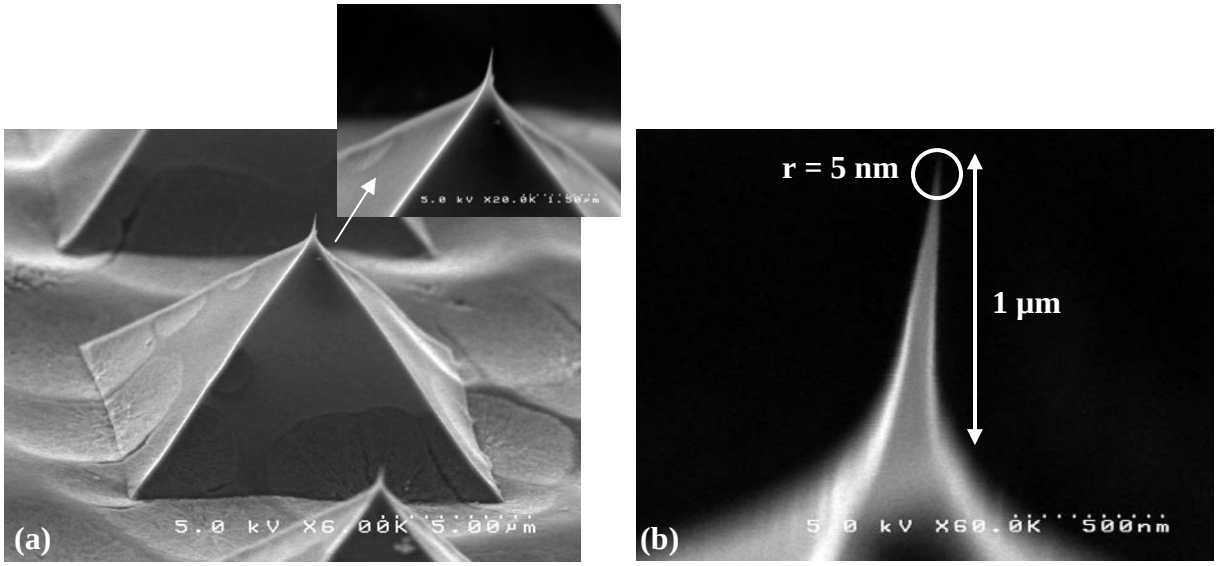

Figure 5.11 SEM micrographs of the $CH_4/H_2/N_2$-nanodiamond microtip array cathode: (a) a single nanodiamond microtip in an emitter array; (b) High magnification image illustrating the high aspect-ratio of the nanodiamond tip geometry with 5 nm radius of curvature.

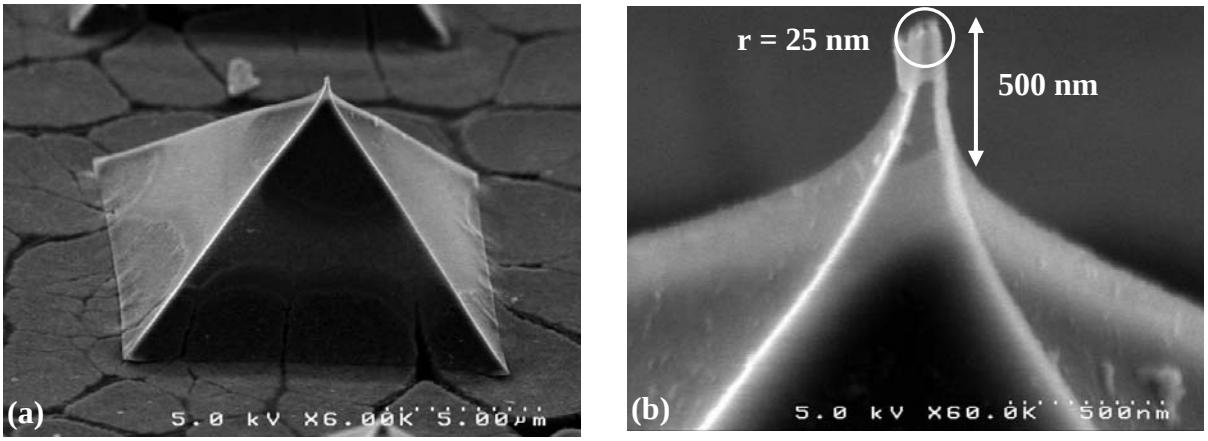

Figure 5.12 SEM images of the CH_4/H_2-nanodiamond microtip array cathode: (a) a single nanodiamond microtip; (b) Illustration of the relatively lower aspect-ratio of the tip with 25 nm radius of curvature.

With the help of these aspect ratio observations of the tips, the geometrical field enhancement factor (β_g) offered by the $CH_4/H_2/N_2$- and CH_4/H_2-nanodiamond films to the microtip arrays was estimated. The two-step field emission enhancement model (TSFE), described in Chapter II, was

taken into consideration. It was found that β_g of the $CH_4/H_2/N_2$-nanodiamond tips (~ 32,000) was about 10 times higher than that of the $CH_4/H_2/N_2$-nanodiamond tips (~ 3,200).

The field emission characteristics of the nanodiamond microtip array cathodes are reported in the next chapter. The nitrogen-incorporated nanocrystalline diamond, when applied in a suitable cathode form, is a candidate for enhanced field emission due to the sharp emitter tips, obtained by virtue of its small grain size, providing a large geometrical field enhancement factor, the presence of deliberate but carefully controlled sp^2-carbon content in the nanodiamond tips, and the incorporation of nitrogen n-type dopant in the nanodiamond.

The ensuing sections in the chapter put forward the fabrication process schemes developed for monolithically integrated nanodiamond lateral field emission devices.

5.4 Fabrication of monolithic nanodiamond lateral field emission devices

A nanodiamond field emission device developed in lateral configuration can result in efficient low-voltage, high-speed and high-frequency electronic performance. Lithographically controlled emitter geometry and small interelectrode separation in a versatile, low-capacitance structure including a built-in anode and insulator, achieved using simple fabrication methods are salient attributes of a lateral field emitter device. By process integration of nitrogen-incorporated nanodiamond film deposition with the controlled micropatterning technique, multiple lateral diamond field emitter arrays have been batch-fabricated on SOI wafers, creating a useful approach to realize potential vacuum electron devices for applications.

5.4.1 Single-mask lateral field emission device fabrication

Device fabrication process: The nanodiamond lateral field emitter devices were physically realized using an uncomplicated single-mask fabrication technique, paralleling conventional IC processing technology. The process schema is shown in **Figure 5.13**. The fabrication begins with the growth of a 1.5 to 2-μm thick nitrogen-incorporated nanodiamond film on a silicon-on-insulator (SOI) wafer (2 μm active Si on 1 or 4 μm buried oxide on a 625 μm Si substrate) by $CH_4/H_2/N_2$ MPECVD. Next, an aluminum metal layer of 0.5 μm thickness is deposited on the nanodiamond by thermal evaporation. The Al layer is then patterned with the lateral device structures using photolithography, the exposed aluminum being etched away by wet chemical processing in commercially available *PAE* (80% phosphoric acid-based etchant) and the photoresist (*AZ 5214-E*) removed. With this aluminum serving as a mask, micropatterning of the nanodiamond film is carried out with RIE in oxygen plasma using an ICP-RIE system to delineate the electrode structures in the diamond. The coil R.F. power is 600 W, platen R.F. power 100 W, with the oxygen flow rate being 30 sccm, at a low pressure of 10 mTorr. A final silicon etch step lets the underlying SiO_2 layer of the SOI substrate serve as the isolating material and sets the interelectrode spacing between the nanodiamond cathode and anode. The process is performed using SF_6/O_2 RIE to ensure no etch of the SiO_2 layer beneath. The process parameters are an R.F. power of 100 W, reactant pressure of 150 mTorr, and gas flow rates of 50/5 sccm (SF_6/O_2). Post-fabrication, the nanodiamond lateral devices are subjected to RCA chemical cleaning procedure, followed in the silicon wafer industry standard process technology, to remove any contaminants present on the emitter surface.

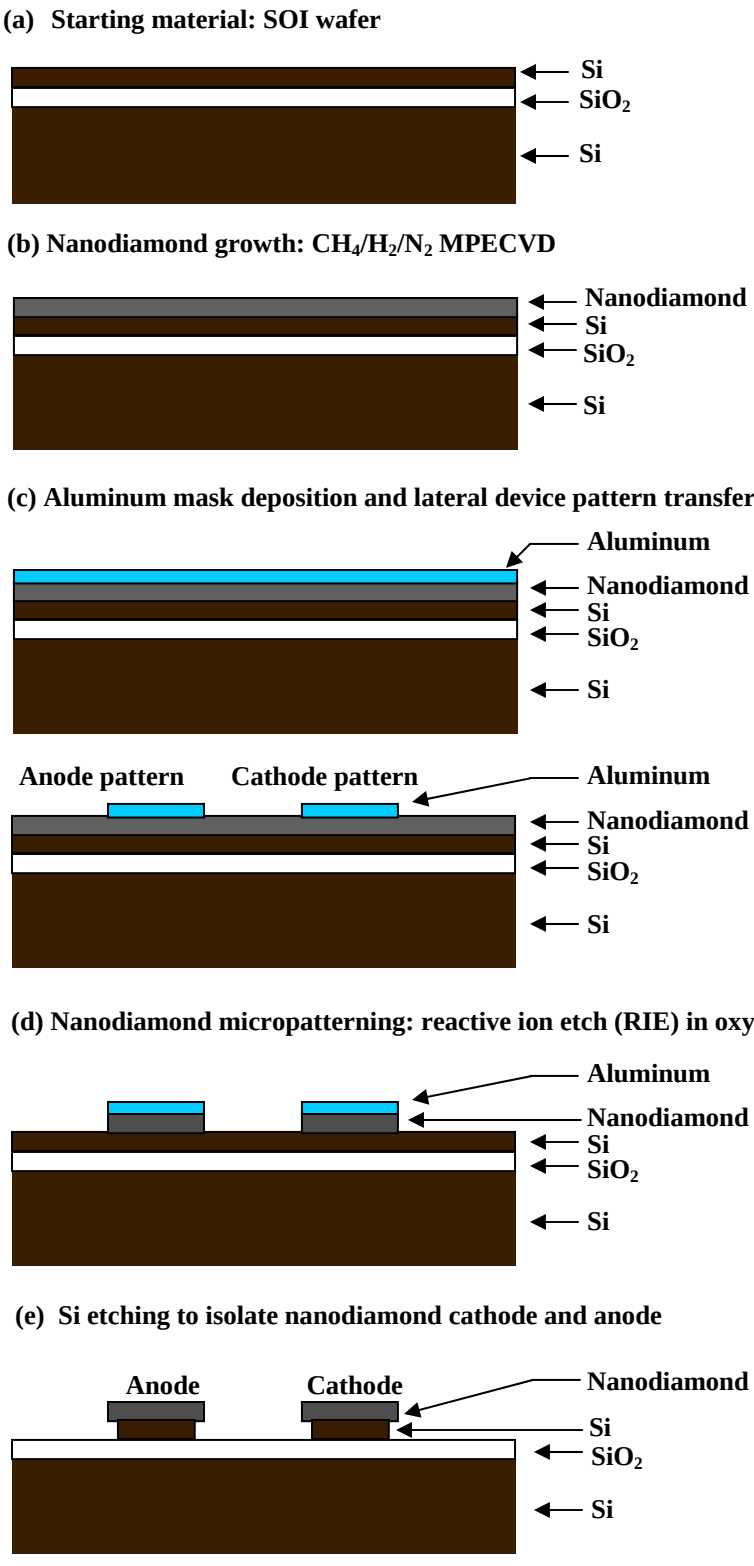

Figure 5.13 Single-mask fabrication process of the nanodiamond lateral field emission device using the reactive ion etch technique.

Device fabrication results: Arrays of nanodiamond lateral diodes have been fabricated with anode-cathode distances ranging from 2 μm to 15 μm. **Figure 5.14** shows the SEM micrographs of a 4-finger and 6-finger nanodiamond lateral diode with 4 μm anode-cathode gap. The nanodiamond cathode is comprised of *finger-like* emitter structures having a high aspect-ratio laterally tapering to end in sharp apexes, increasing the geometrical field enhancement factor (β_g). This β_g factor is estimated to be ~ 1,300 by modeling the nanodiamond finger as a conical tip with lateral tip height of h and tip radius curvature of r, with the factor h/r, defining the lateral aspect ratio. A 15 nm planar lateral radius of curvature of the emitter tip is obtained due to the combination of ultra-small nanodiamond grain size and precise control of the patterning processes in fabrication. The β_g factor calculation is illustrated in **Figure 5.15**. The nanodiamond anode design is a straight edge geometry, giving the cathode the rectifying geometrical field enhancement factor. The 1-4 μm thick buried SiO_2 layer of the SOI wafer forms the dielectric isolation between devices. The interelectrode spacing parameter in the lateral device design can also be well-controlled by lithography to be of any length, while maintaining the cathode tip sharpness, **Figure 5.16**, which determines the turn-on voltage of the diode, per a specific diamond composition and emitter diode configuration, facilitating device operating voltage requirements and IC-compatible device operation. Effective etch bias control is critical during the subtractive processes involved in fabrication, as any lateral over-etch of the masking layers and diamond may result in the widening of the anode-cathode gap, and also a broader and more rounded topology for the emitter tip geometry, which essentially govern the vacuum device performance.

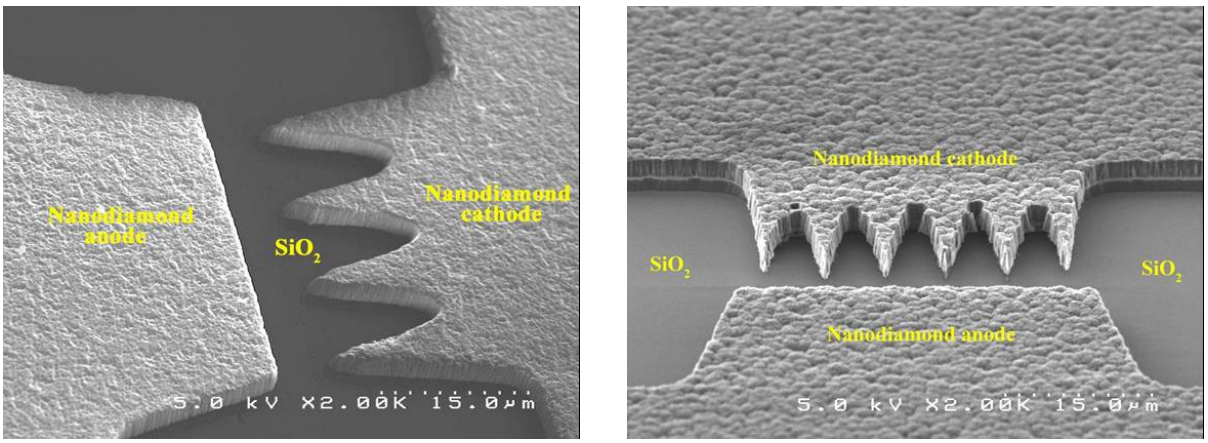

Figure 5.14 SEM micrographs of a 4-finger and 6-finger planar lateral field emission diode with 4 µm anode-cathode spacing fabricated on a SOI wafer.

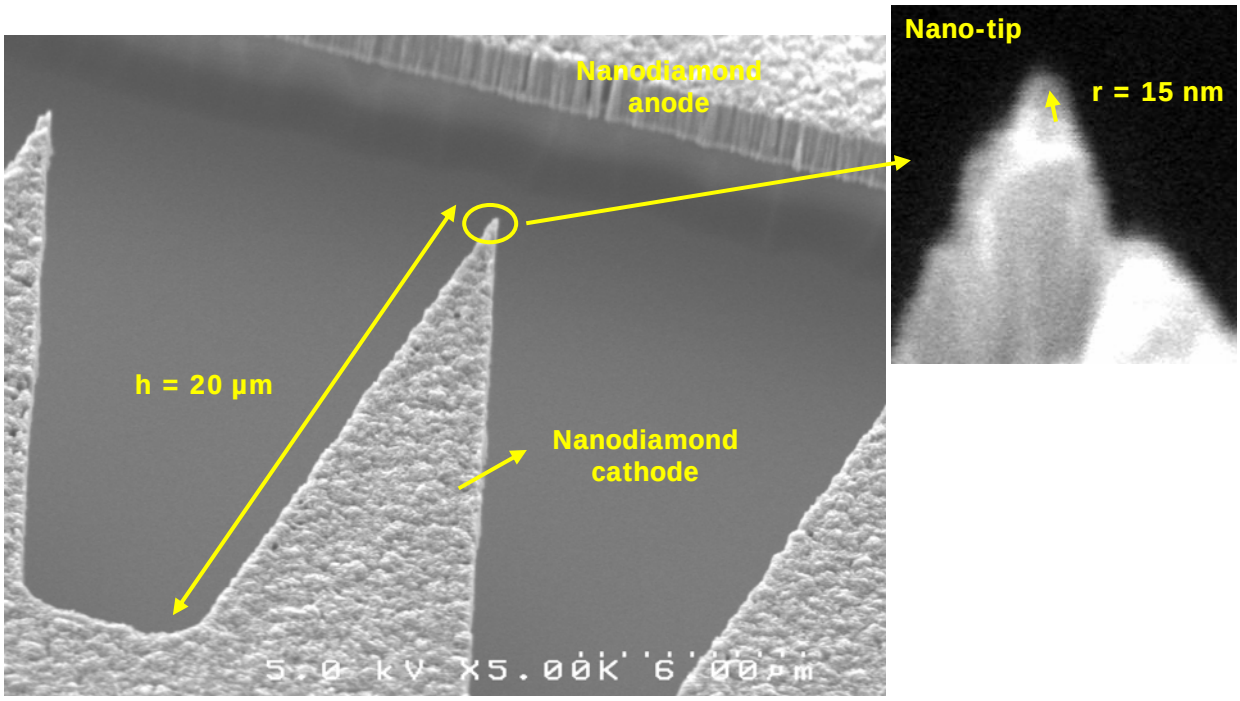

Figure 5.15 Illustration of the geometrical field enhancement factor of the nanodiamond lateral emitter finger.

It is important to note that the SiO_2 dielectric is well protected from any plasma-induced damage during the diamond RIE by the presence of the active Si layer of the SOI substrate. Once the nanodiamond is micropatterned with the lateral electrode structures, the silicon layer beneath the diamond is deliberately under-cut (plasma-etch process recipe chosen accordingly) to promote the nanodiamond layer gap proximity, ensuring that electron emission occurs only from the diamond. The silicon supporting layer also elevates the nanodiamond cathode and anode from the substrate, which results in the path of the emitted electrons to be away from the underlying insulator, minimizing any chance of surface conduction through the oxide. The device SEM images in **Figure 5.17** illustrate the result of the Si etch.

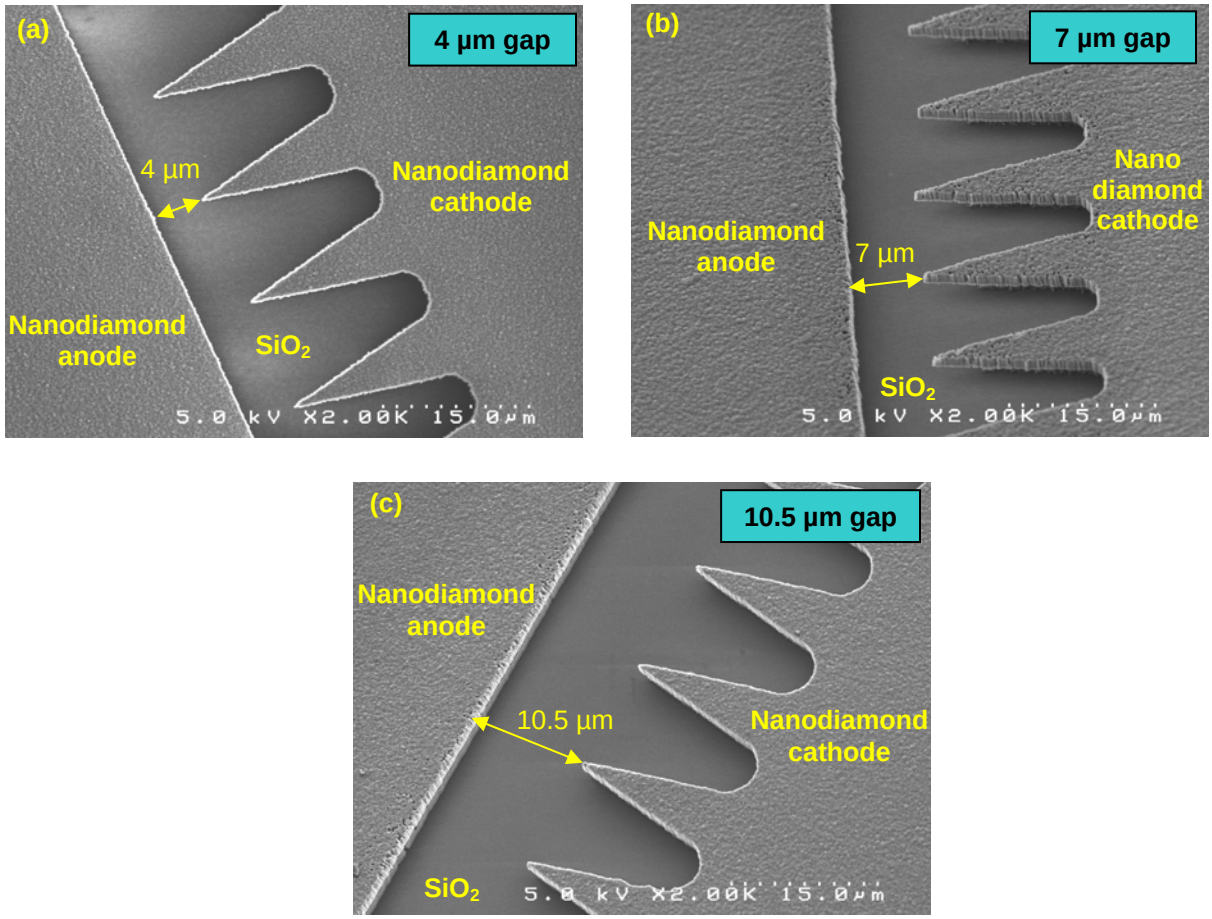

Figure 5.16 SEM images showing three batch-fabricated nanodiamond lateral emitter diodes with lithographically controlled different interelectrode gaps: (a) 4 µm, (b) 7 µm, (c) 10.5 µm.

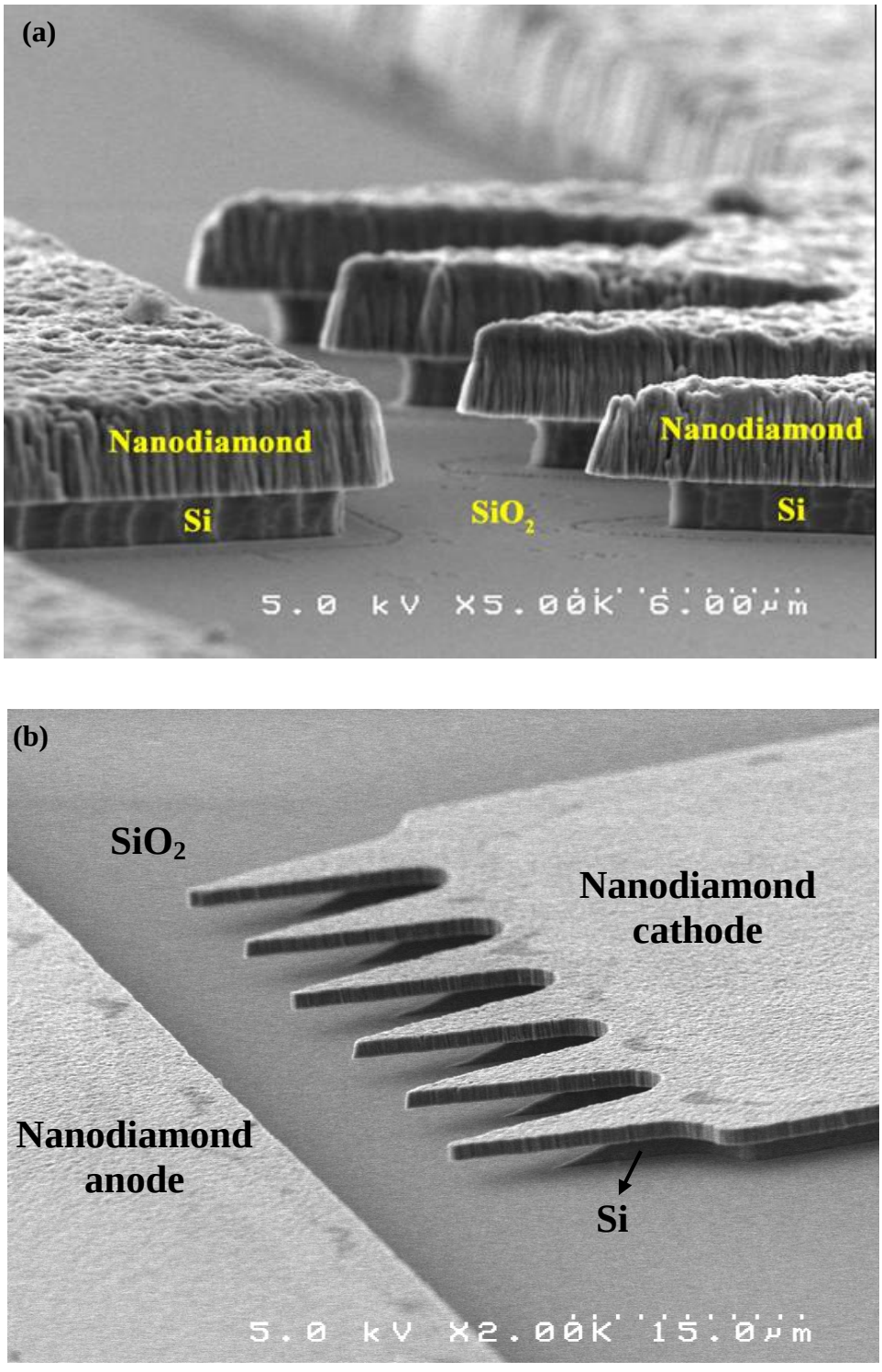

Figure 5.17 High magnification SEM images of the 4-finger and 6-finger lateral device structures, showing the deliberately undercut Si layer beneath the nanodiamond.

Nanodiamond lateral triodes: Different designs of nanodiamond lateral triodes have also been fabricated using the same process scheme. The monolithic lateral vacuum microtriode comprises a single nanodiamond finger as cathode, with a nanodiamond gate symmetrically arranged in close proximity with the emitter, and an integrated nanodiamond anode, all on the same plane. A small gate-cathode gap of 1.5-2 μm was achieved by photolithography and control of subsequent subtractive processes. Fabricated anode-cathode distances per design were set to vary between 10 μm and 1 mm, so as to have a wider range to observe the effect of the collector position on the triode characteristics. The different nanodiamond triode structures are shown in **Figure 5.18**.

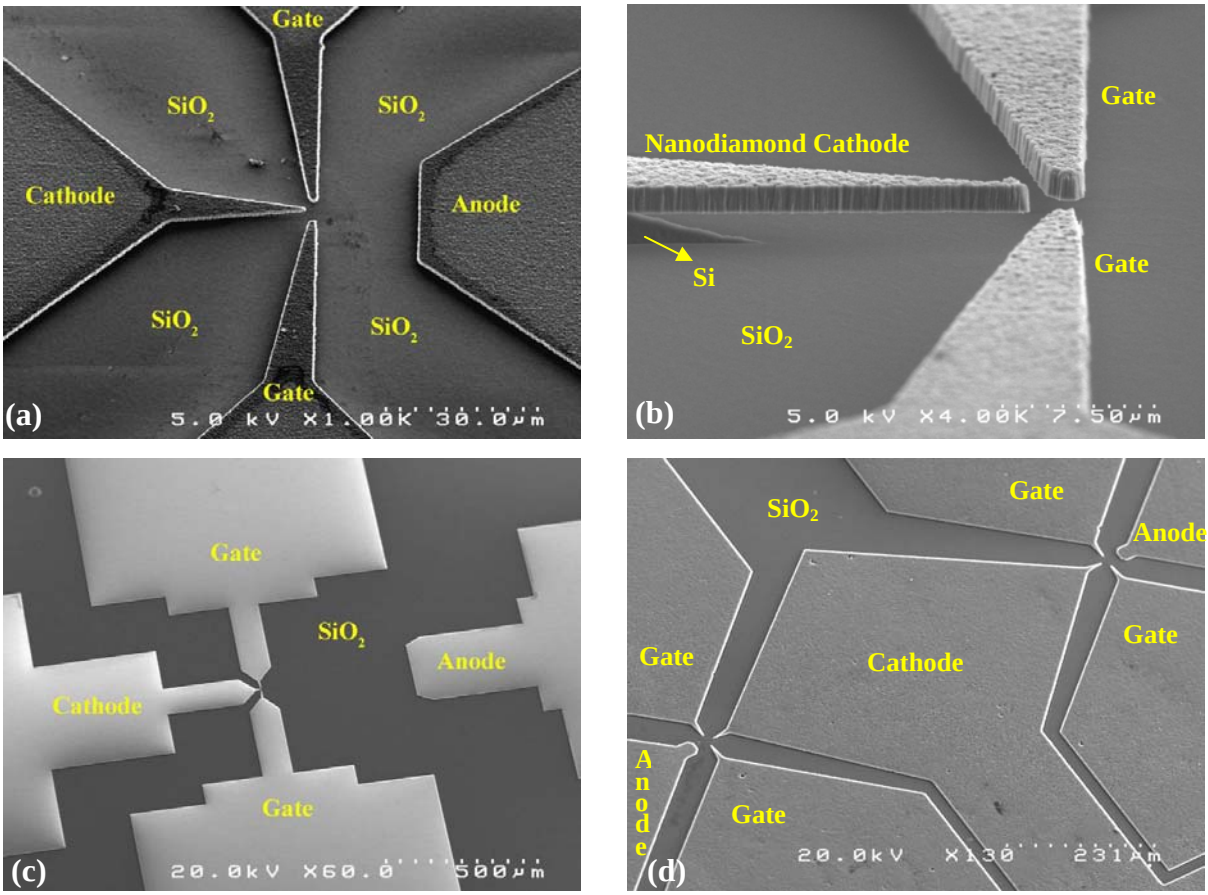

Figure 5.18 (a) A completely integrated nanodiamond lateral field emission triode, with 2 μm gate-cathode and 20 μm anode-cathode spacings; (b) A lateral triode structure, showing a high aspect-ratio nanodiamond finger-emitter in close proximity with the gates, 1.5 μm gate-cathode spacing; (c) A diamond lateral vacuum transistor device with 500 μm anode-cathode separation; (d) An integrated nanodiamond lateral field emission amplifier circuit.

High current lateral emitter device configurations: A suitable design of the lateral emitter diode in array configuration over a large area was devised and implemented to develop a potential vacuum microdevice for high-speed, high-power applications. The objective was to increase the number of nanodiamond fingers in the lateral device structure and investigate how the number of emitters scales with respect to the forward emission current derived from the device.

Nanodiamond comb-shaped lateral field emitter arrays in diode configuration have been fabricated for high current field emission using the single-mask process technique. The nanodiamond film thickness was increased to 3 μm to suit high current applications. **Figures 5.19 (a)** and **(b)** display the construct of the nanodiamond lateral comb array diodes comprising 650 and 9000 emitter fingers respectively. These high power configurations of the lateral device include symmetrically arranged arrays of comb-shaped structures, with each comb composed of 65 nanodiamond finger-like emitters as shown in **Figure 5.20**. The nanodiamond fingers are designed and patterned to possess a high and consistent lateral aspect ratio. A small and uniform anode-cathode separation is maintained throughout the device structure by control and optimization of the micropatterning processes to permit a consistent emission current over the array of fingers. The application of a comb array configuration not only allows for a higher packing density of the emitters, but also ensures a uniform potential distribution to the diamond fingers over a large area. In wafer-scale fabrication, this design can also improve the processing yield to achieve monolithic emitter devices. Precise lithography control over the critical vacuum device parameters, viz., emitter geometry, array structure, and interelectrode gap is achieved in the lateral device. As a result, the device is equipped with well-defined emission sites with a high emission site density over a large area, thus allowing large total emission current to be drawn from a number of finger-tips operated in parallel. The combs are interconnected using large-area

interconnects (500 μm wide by 3 μm thick) of the nitrogen-doped nanodiamond material with high electrical and thermal conductivity to handle the high current efficiently and prevent electromigration. The large contact pads aid visual electrical probing. The cathode is equipped with two contact pads, facilitating the application of current through the electrode structure to clean the diamond finger tips prior to emission testing.

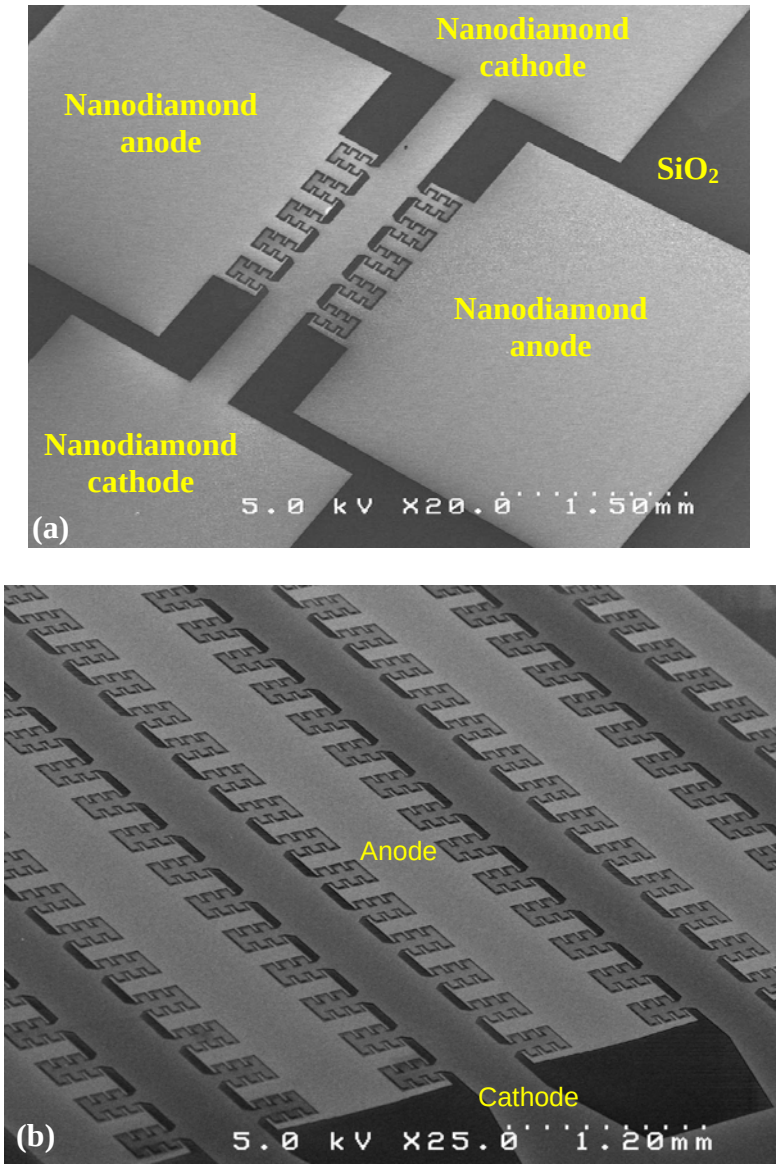

Figure 5.19 SEM micrographs of the nanodiamond lateral comb array high current diodes: (a) 650 emitter finger configuration; and (b) 9000 emitter finger configuration (Device Area: 1 cm^2).

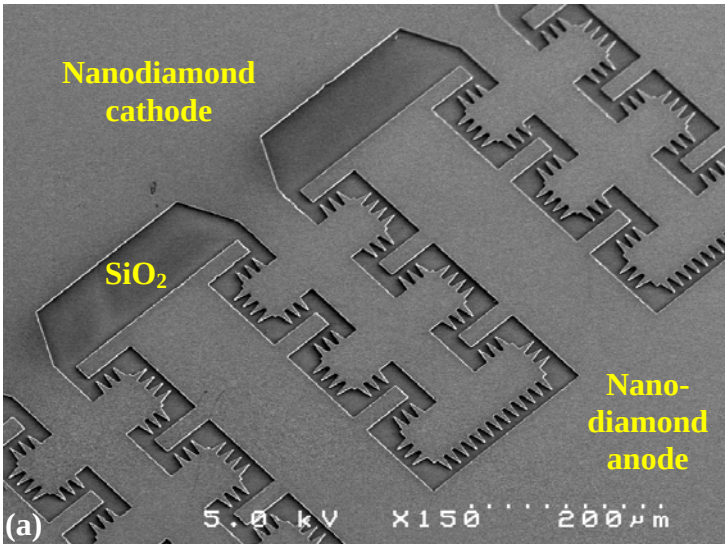

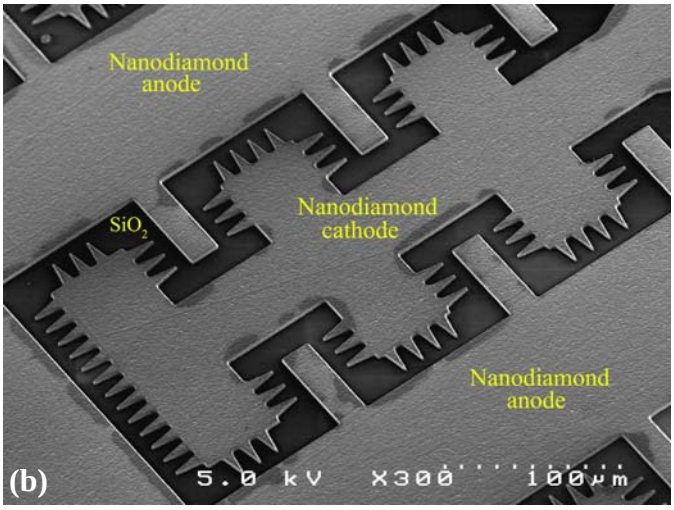

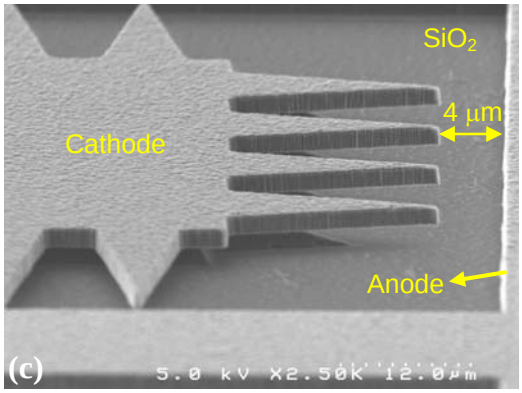

Figure 5.20 SEM images displaying (a) uniformly arranged comb array structures in the nanodiamond lateral diode; and (b) a single comb structure composed of 65 micropatterned nanodiamond lateral emitter fingers with (c) small and equal anode-cathode spacing.

Development of an integrated metal contact layer for nanodiamond: A Ti/Au metal contact layer was applied on the nanodiamond, without the use of an additional mask, to provide more uniform potential to the lateral emitter fingers distributed over a larger device area. The process

step was incorporated into the lateral device fabrication schema and implemented by the deposition of a 1000 Å-thick Ti/Au metal layer over the nanodiamond film, prior to the application of the aluminum mask. Subsequent patterning of the Ti/Au layer was performed by wet chemical processing using the same photoresist as the mask used for aluminum layer etch. The Ti/Au layer was then annealed at 300 °C in vacuum to improve the adhesion strength of the metal contact to the diamond. The integrated Ti/Au metal contact layer (see **Figure 5.21 (a)**) can minimize the potential drop across the large-area lateral emitter array. The high-magnification SEM image in **Figure 5.21 (b)** shows the intentionally over-etched Ti/Au to remove any metal at the nanodiamond fingers. The integration of a metal contact on the diamond, without the use of any additional mask or complicated processes, is an innovative development for the lateral field emission device. The utility of this layer can be extended into the device packaging stage as well, where the Ti/Au on the diamond can aid wire bonding.

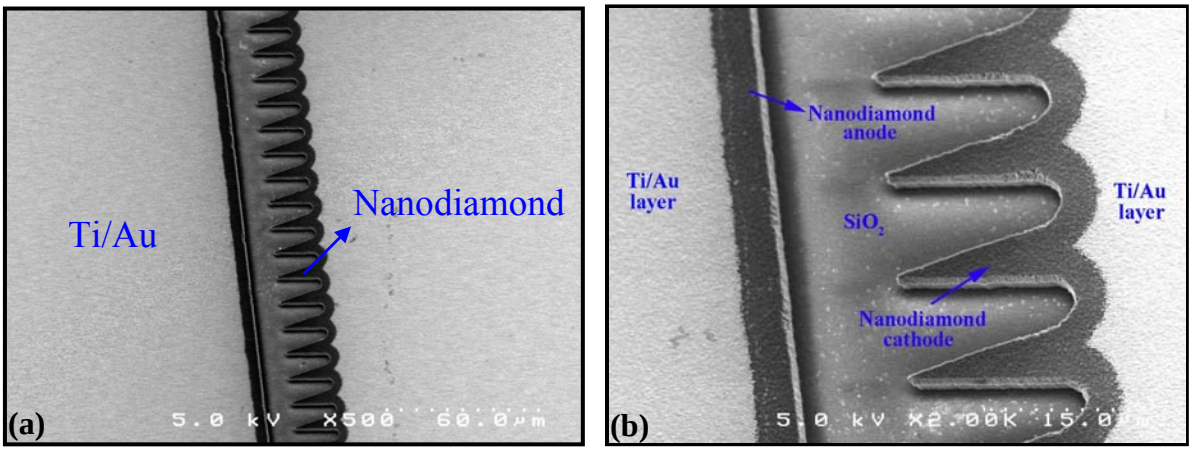

Figure 5.21 (a) A lateral emitter array diode portraying the uniformly integrated Ti/Au metal contact layer on the nanodiamond; (b) High-magnification SEM picture showing that the nanodiamond emission regions are devoid of any Ti/Au metal.

Aluminum nitride insulator for high current nanodiamond lateral devices: In an effort to improve the reliability of the diamond lateral emitter device for high power applications, thicker and robust insulating materials were applied for electrode isolation. We have integrated the nanodiamond device with aluminum nitride insulator to function as a reliable high power vacuum microelectronic device.

The device fabrication involved the deposition of a ~ 2 μm-thick nanodiamond film on the insulating substrate. Several insulator substrates including quartz, sapphire, alumina, and aluminum nitride were considered for this purpose. A 640 μm-thick polished aluminum nitride (AlN), with high thermal conductivity (140-177 W/m-K) and dielectric strength (1.2 MV/cm), was identified to be compatible with the lateral device process scheme. Deposition of a continuous CVD diamond film of reasonable thickness with good adhesion strength to very thick insulators is difficult. Hence, an intermediate 1 μm-thick layer of polysilicon was deposited on the aluminum nitride by low-pressure chemical vapor deposition (LPCVD). The silicon/aluminum nitride sandwich substrate was then pre-treated by ultra-sonicating with a 5–20 nm nanodiamond powder/acetone solution to increase diamond nucleation. No mechanical scratching of the silicon surface was performed prior to nanodiamond deposition. The $CH_4/H_2/N_2$ microwave plasma enhanced chemical vapor deposition (MPECVD) process was used to grow the nanodiamond film on the substrate. The same single-mask nanodiamond lateral device microfabrication technique followed on the SOI substrate was then employed to yield the lateral emitter array device, with aluminum nitride as the spacer.

Figure 5.22 shows the cross-sectional SEM image of an as-deposited nanocrystalline diamond film on a silicon layer over aluminum nitride. The nanodiamond film was found to be dense and continuous with an average grain size of 5-15 nm. Silicon and aluminum nitride have

good thermal matching, which permits strong adhesion of the nanodiamond layer onto the substrate. The integration of diamond thin films to thick insulators has thus been achieved. **Figure 5.23** displays the structure of the nanodiamond lateral comb array diode microfabricated on AlN substrate with silicon as buffer layer. The lateral device processing has again been optimized to undercut the silicon layer beneath the diamond, as shown in **Figure 5.24 (a)**, to insure that the silicon is removed from the high field nanodiamond emitter tip regions. Comb array diode configurations with over 9000 nanodiamond emitter-fingers in the cathode structure have thus been fabricated to evaluate high current testing. Lateral triode device structures have also been developed, **Figure 5.24 (b)**, on the AlN substrate. This development of the lateral vacuum device on an insulator substrate forms an ultra low-capacitance electronic device structure, well-suited for high-frequency operation.

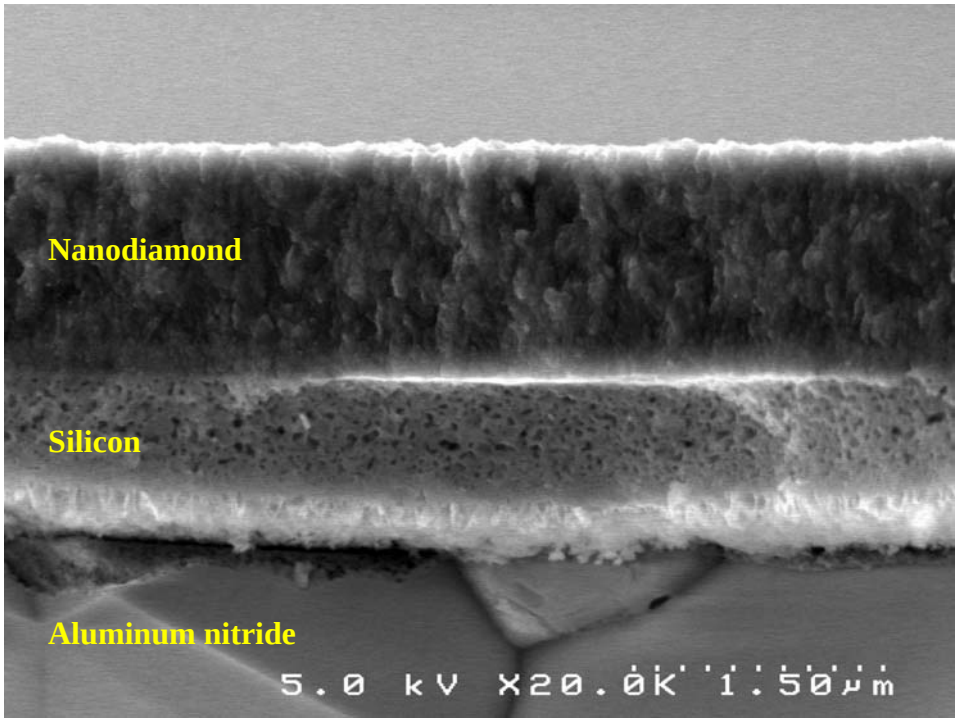

Figure 5.22 Cross-sectional SEM of a uniformly deposited nanodiamond film on Si/Aluminum nitride substrate.

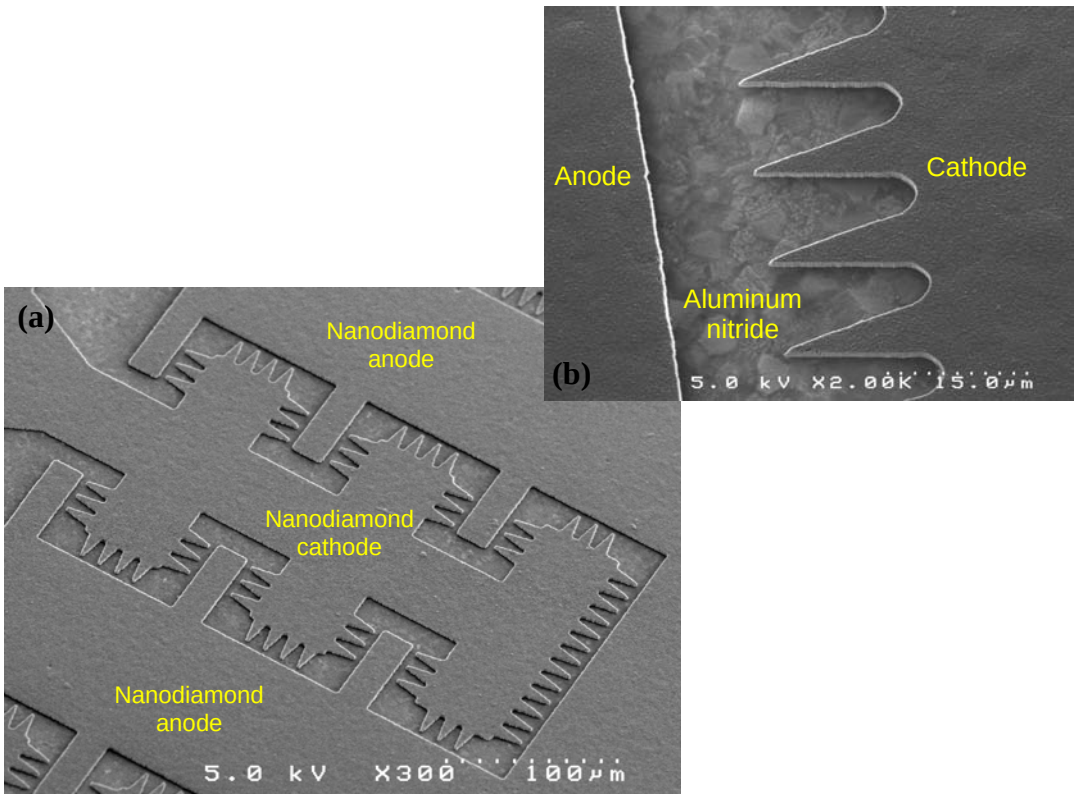

Figure 5.23 (a) Nanodiamond lateral comb array field emitter diode fabricated on aluminum nitride substrate; (b) SEM image showing the device electrodes isolated by aluminum nitride.

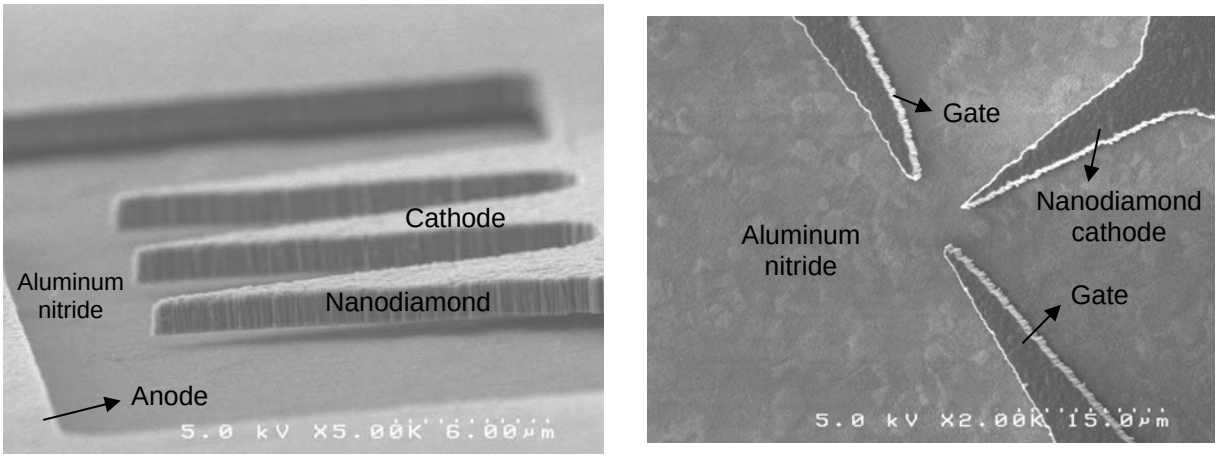

Figure 5.24 (a) SEM picture of the lateral device structure showing the nanodiamond emitter-finger region is devoid of the silicon layer beneath; (b) A gated nanodiamond lateral field emitter transistor device (integrated lateral anode, spaced 500 µm from cathode, not shown in image) isolated by the aluminum nitride substrate.

Lateral device batch-processing: Batch-fabrication of the lateral field emitter devices has been achieved with good repeatability owing to the uniform deposition capability of the nanodiamond film on large area substrates as well as the high etch rate and manufacturability offered by the RIE process. **Figure 5.25** includes a view portraying multiple lateral devices, batch-fabricated using the same mask. One of the advantages of using a lateral emitter configuration is observed here, as several vacuum diode and triode devices are microfabricated monolithically on the same substrate, with no change in the process flow, the device electrode design being defined by the mask (layout) and transferred onto the wafer by lithography processing.

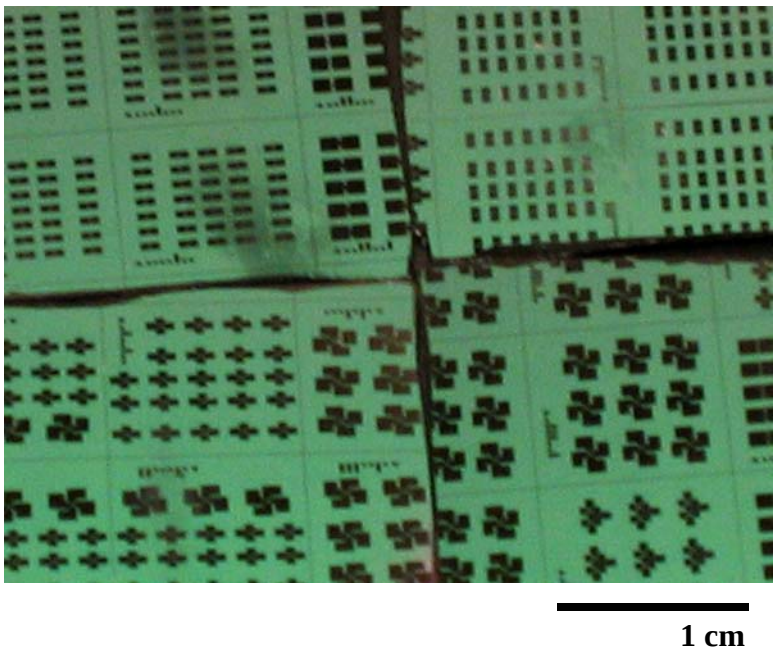

Figure 5.25 Snapshot illustrating the batch-fabrication of multiple monolithic nanodiamond lateral field emission devices, isolated on the same substrate, using a single mask.

Uniformly spaced lateral emitter arrays comprising more than 9000-fingers in the cathode structure over a 1 cm^2 chip area in diode configuration have been realized. Interelectrode distances down to 2 μm achieved with this lateral device processing can be minimized further

when e-beam lithography is employed for device pattern transfer. Further, the fabrication scheme on SOI wafer substrates allows for the integration of the electrode structures, the dielectric, and the metallization contact of the vacuum microdevice, all using a single mask and same processing steps. The process flow parallels integrated circuit production, and by virtue of its single-mask utility, high manufacturability, combined with its reproducibility, is an efficient and cost-effective approach to realize volume production of field emission devices in various configurations in wafer process technology.

5.4.2 Dual-mask lateral field emission device fabrication

A field emission diode with reduced reverse current and high rectification can be realized with a non-diamond anode device approach. Since nitrogen-incorporated nanocrystalline diamond is an excellent electron emitter, a non-diamond material is preferred for the anode component of the lateral device as a diode. We have developed a precise dual-mask micropatterning scheme using an "etch/lift-off" process combination to build such a lateral field emission device, which can be an ideal candidate for low voltage, high rectification vacuum microelectronic diode for harsh environments.

Device fabrication process: The *2-material* lateral device processing follows the described single-mask pattern-etch scheme for the nanodiamond cathode emitter fabrication (mask #1). Next, the lateral anode pattern (mask #2) is transferred onto the substrate using standard photoresist processing, invoking mask alignment with the fabricated cathode. A nickel (Ni) metal layer, with a thin titanium (Ti) adhesion layer beneath, is blanket-deposited over the substrate, followed by a "lift-off" process with acetone to leaves the Ti/Ni only at the patterned anode area. Subsequent silicon etching was performed using SF_6/O_2 RIE to achieve isolation between the

nanodiamond cathode and metal anode using the SiO_2 layer beneath and thereby set the interelectrode spacing. The fabrication process flow is outlined in **Figure 5.26**.

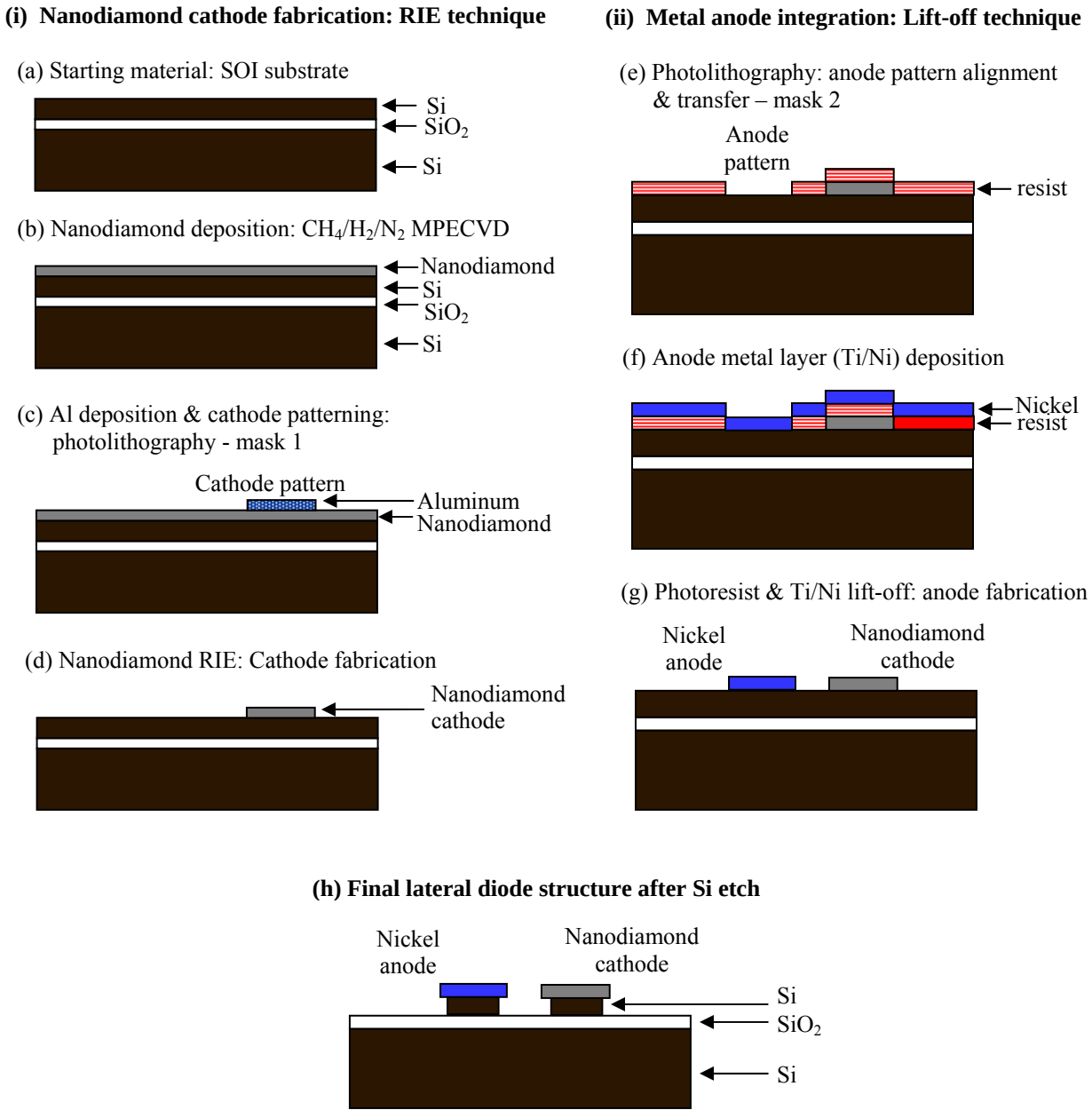

Figure 5.26 Fabrication process schema of the nanodiamond lateral field emission diode by dual-mask micropatterning technique.

Device fabrication results: The dual micropatterning process technique achieved several lateral diodes with nanodiamond cathodes and nickel anodes, batch-fabricated with high yield, as depicted in the inset of **Figure 5.27**. The structure of the developed lateral field emission diode is shown in the main SEM micrograph of **Figure 5.27**, illustrating the diamond cathode and nickel anode are accurately aligned to set a 4 μm interelectrode gap. The selection of preferred anode material depends in part on its electron collecting efficiency. Nickel, a metal with high work function of 5.15 eV, serves as a good electron collector, but an inefficient emitter of electrons. Deposited nickel films also allow for easy micropatterning by "lift-off" process technique.

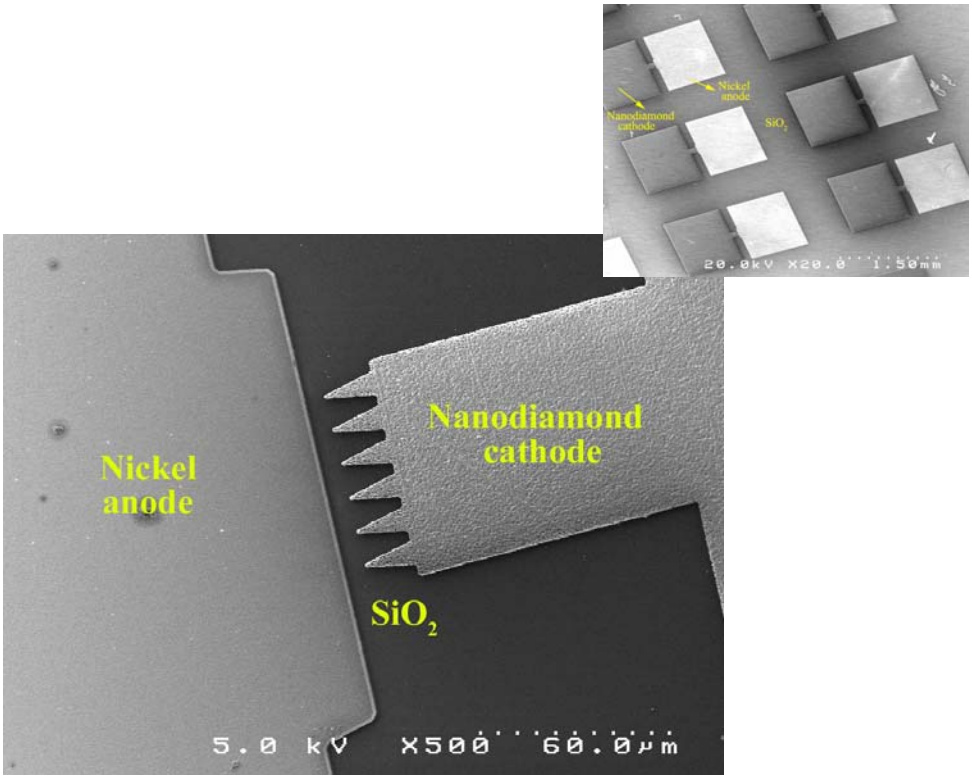

Figure 5.27 SEM micrograph of the lateral field emission diode, equipped with a nanodiamond 6-finger cathode and a nickel anode, precisely aligned to set 4 μm interelectrode spacing; inset: Arrays of lateral diodes batch-fabricated using a dual mask process technique.

Compatibility of diamond films for integration with many other different materials (semiconductors, metals, oxides) is a requisite for realizing active diamond-based devices. The development of the nanodiamond lateral field emission device, involving the integration of a diamond cathode with a metal anode and an insulating spacer, adds veracity to the fact that the many potential performance and reliability advantages of diamond can be successfully realized in device configurations.

5.4.3 Package development for nanodiamond lateral field emission devices

The development of a vacuum package is of practical relevance to field emission devices. The chip-type architecture of the lateral device is well suited for packaging with no device assembly issues involved. In collaboration with the *Honeywell-Kansas City Plant,* a feasible packaging process has been developed for the diamond lateral emitters, where the monolithic devices are die-attached, wire-bonded, and vacuum-encapsulated in a cavity package.

Packaged device development: A 10-pin cavity package made of Kovar (a nickel-cobalt ferrous alloy) has been chosen for this purpose. The die comprising the fabricated nanodiamond lateral devices is attached firmly onto the cavity package. The package was pre-cleaned in Ar(98 %)/O_2(2 %) plasma and vacuum baked at 200 °C for ~ 20 h. For die-attach, a 40000 Å thick Ti/Au film was deposited onto the back surface of the substrate, and attached to a 1-inch square coupon of thick film gold on ceramic by using a AuSn solder preform and run through a belt furnace at ~ 350 °C peak temperature. Aluminum wire bonding is directly onto the nanodiamond contact pads of the lateral devices. A 2 mil aluminum wedge bond was employed for this purpose. **Figure 5.28** shows a die, with several nanodiamond lateral diodes, attached inside the cavity package, while the devices wire-bonded to the contact leads of the package can

be seen in **Figure 5.29**. The smooth surface morphology of nanodiamond plays a critical role in yielding a robust wire-bond. The package is finally vacuum-sealed with a Ni-plated Kovar step lid in a SST® advanced packaging system using a getter material at a process temperature of 360 °C. Fine and gross leak tests are performed and passed per mil-spec levels to confirm the vacuum seal integrity. **Figure 5.30** displays the package developed for the nanodiamond lateral field emitter device.

A practical assembly and package for the diamond vacuum field emission device is thus developed. Field emission characterization results of the lateral device functioning in the package set-up are presented in Chapter VI.

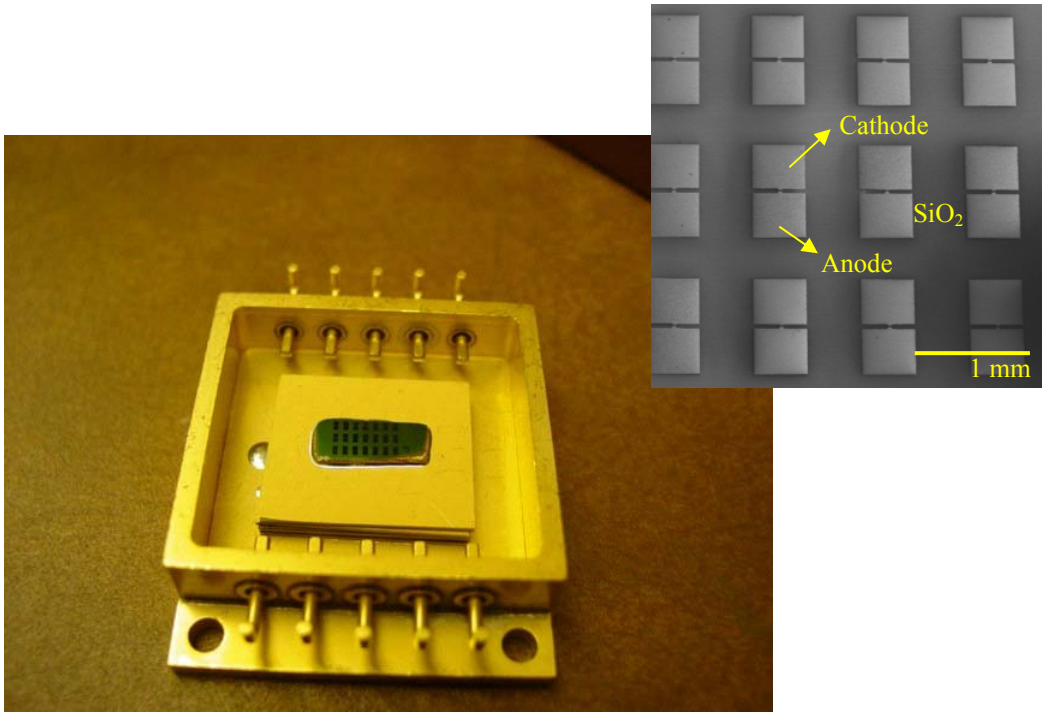

Figure 5.28 Snapshot showing a lateral device die, attached onto a 10-pin cavity package, with an SEM image of the batch-fabricated devices in the die included as inset.

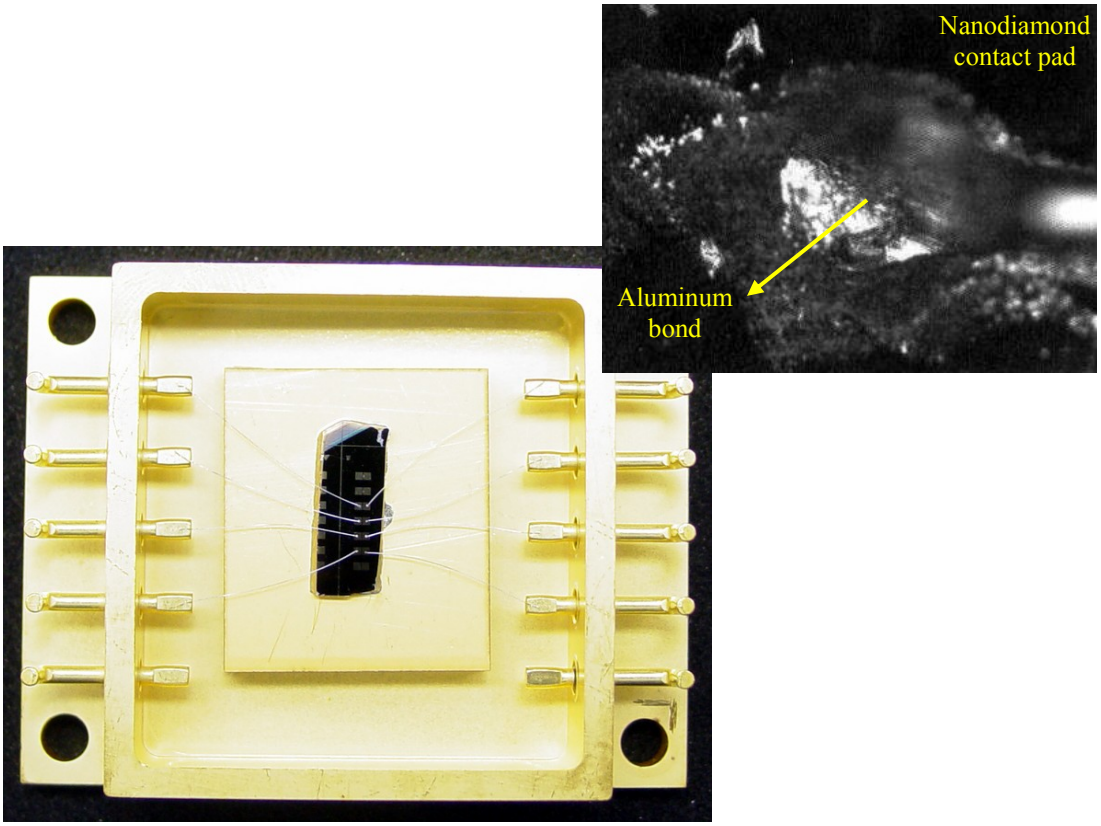

Figure 5.29 Nanodiamond lateral emitter diodes wire-bonded in package; the inset shows the magnified image of the aluminum bond on the nanodiamond contact pad of a device electrode.

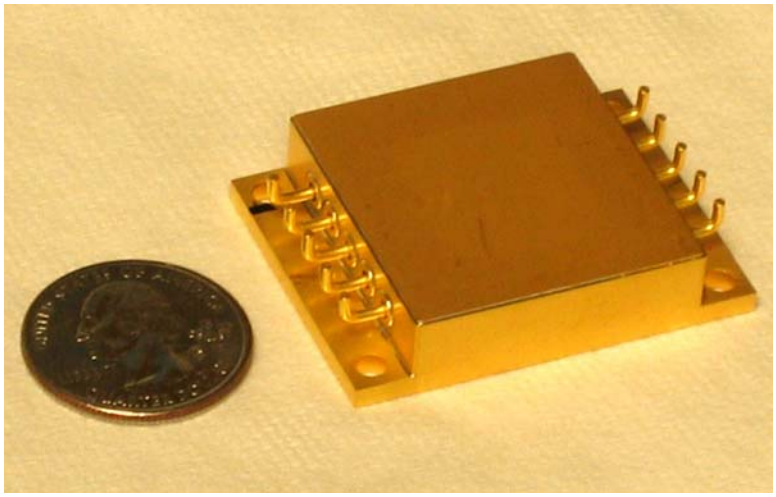

Figure 5.30 Vacuum-sealed package developed for the nanodiamond lateral emitter device.

CHAPTER VI

DEVICE CHARACTERIZATION AND DISCUSSION

This chapter outlines the characterization methods employed for field emission testing of the fabricated cathodes, lateral diodes and triodes, and presents the electrical performance of these nanodiamond devices under vacuum. A discussion on the obtained device characteristics follows the results in each section.

6.1 Device Characterization Techniques

6.1.1 Field emission characterization of nanodiamond films and micro-tip array cathodes in vertical configuration

Emission characteristics of as-deposited nanodiamond films and the fabricated pyramidal nanodiamond microtip array cathodes were investigated in diode configuration with a devised test set-up, involving an external n^{++} silicon anode (ρ=0.002-0.008 Ω-cm), and an alumina spacer. The diode test circuit is shown in **Figure 6.1**.

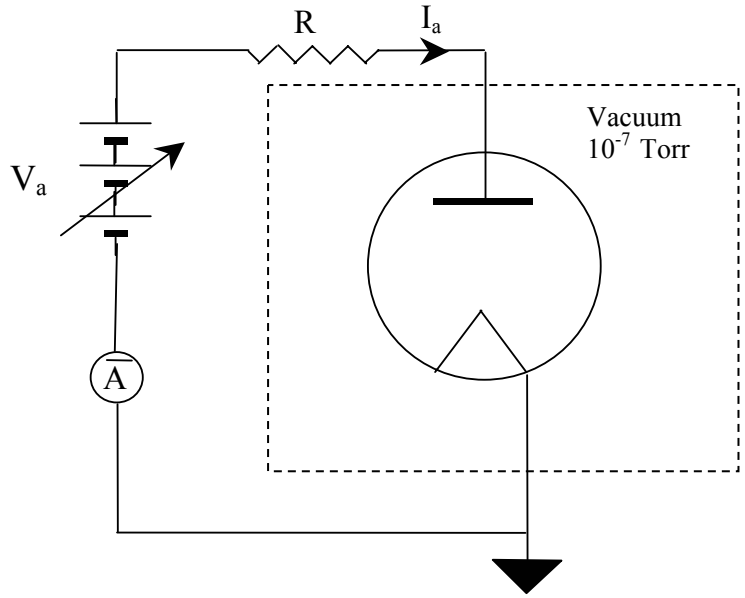

Figure 6.1 Field emission test circuit for nanodiamond cathodes in vertical diode configuration.

A resistor R (1 kΩ-100 MΩ) was used to limit the current in case of a short circuit. The anode and cathode were electrically connected to the circuit via metal probes in a vacuum chamber. The emission testing was performed at room temperature in a vacuum environment of 10^{-7} Torr. The emission current from the nanodiamond emitters was measured as a function of the applied voltage, in both forward and reverse bias directions to confirm the absence of any leakage current in the observed field emission. An ammeter was used to measure the emission current collected by the anode, while computerized data acquisition was available to record the data and generate the I–V and the corresponding F–N plots. The current versus time, at a fixed anode voltage, was also captured by a computer real-time to gauge the stability of the emission current. An average value of current at a fixed anode voltage was then computed and the voltage drop on the limiting current resistor was subtracted from the applied voltage to obtain the true anode voltage. The emission characteristic was obtained by plotting the emission current versus anode voltage and electric field, depending on the anode-cathode gap in the device set-up.

6.1.2 Field emission characterization of nanodiamond lateral diodes

The electrical performance of lateral diode was characterized using the test set-up in **Figure 6.2**. The fabricated device was maintained in a vacuum environment of 10^{-7} Torr. Flat Moly metal dots with large surface area were placed on the contact pads of the cathode and anode of the lateral device, and were electrically connected to the circuit via metal probes. The emission current from the nanodiamond fingered emitter cathode was measured as a function of the applied anode voltage. A continuous D.C. power supply (HP 6035A; 0-500 V; 0-5 A; 1000 W), capable of incrementing the applied voltage in very small intervals (less than 1 V) was used for low-voltage characterization of the lateral diode, designed with a small anode-cathode gap.

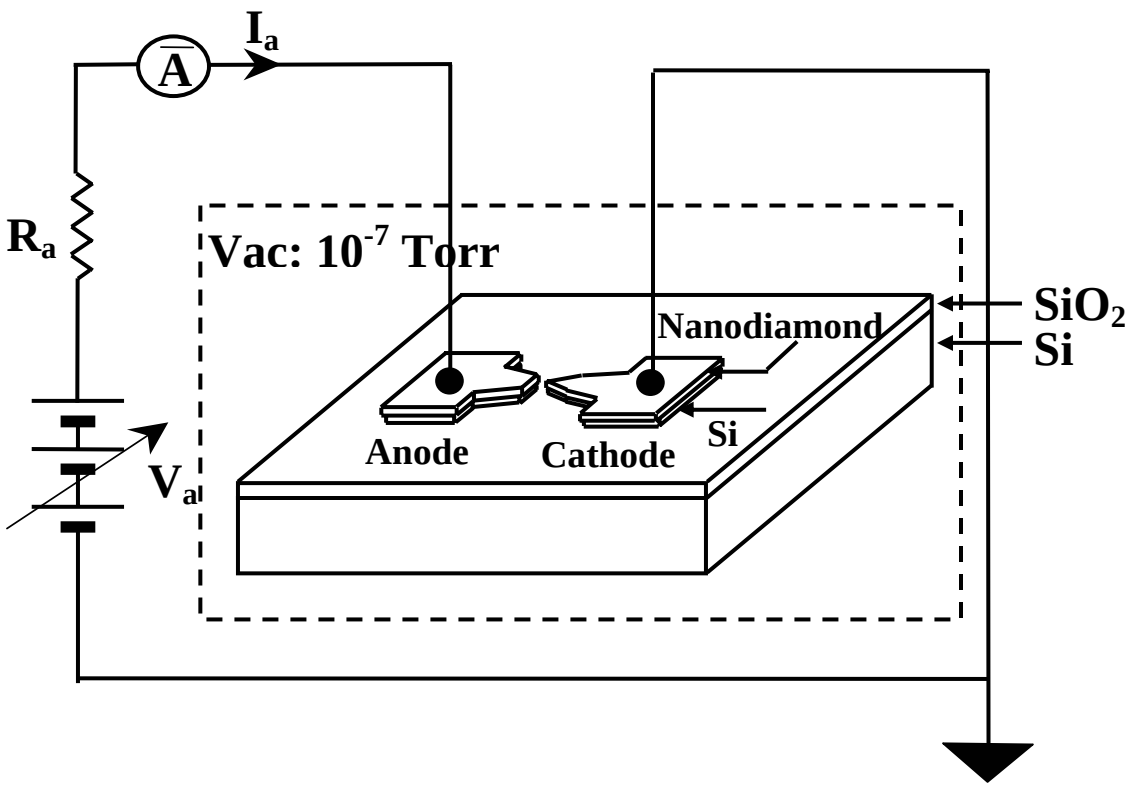

Figure 6.2 Schematic of the vacuum field emission test set-up for the nanodiamond lateral diode.

Prior to emission characterization, the diamond lateral device was subjected to in-situ vacuum tip conditioning by means of thermal desorption to get rid of water vapor or other residual adsorbates on the surface of the nanodiamond accumulated at the terminus of the emitter device processing or by exposure to ambient. With the device on a heated stage, heat treatment was performed at 200 °C for ~ 3 h in a vacuum of 10^{-7} Torr. The device was then cooled down slowly to room temperature. Such post-fabrication processing techniques are also common in conventional silicon IC fabrication technology, such as the rapid thermal annealing (RTA) treatment done following ion implantation to repair the primary crystalline damage in the silicon. Then, without the application of an external heat source, the lateral device was maintained at a particular emission current, say, 3-10 μA (depending on the emitter array size) for ~ 1 h or more during normal vacuum diode operation by adjusting the anode voltage, where the extracted field

emission current was used to execute more localized cleaning of the nanodiamond emitter finger tip. The tip conditioning treatment was terminated when a stable current was obtained for a period of time ~ 1 h. The common activation procedure to enable the device to operate stably at high currents is to very gradually increase the current being drawn from the diamond emitter array from ~ 1 μA to its highest operational level at time intervals determined by the time it takes to reduce the emission fluctuations to a low level. At a given anode voltage, the emission initially increases with time, and the applied voltage must be reduced to maintain the emission level for that step. This procedure was followed to ensure stable emitter-finger operation at high current densities without destroy by an arc, and is analogous to the "burn in" procedures used for MOS devices. After the tip conditioning, the I-V characteristics of the lateral diode were obtained.

6.1.3 Field emission characterization of nanodiamond lateral triodes

The emission testing circuit for the monolithic lateral vacuum triode, in common emitter configuration, is shown in **Figure 6.3**. A load resistor R_a in the anode circuit is used to limit the current in case of short circuit in the anode circuit. A resistor R_g also limits the gate leakage current in case of short circuit in the gate circuit. Anode, gate, and cathode were electrically connected to the circuit via Molybdenum dots and tungsten probes in a vacuum chamber.

The anode emission current was measured as a function of gate and anode voltages under vacuum (10^{-7} Torr). The three-terminal lateral devices were characterized following two procedures depending on the design. In a device with the lateral anode positioned closer to the cathode (~ 10 μm), an anode-induced field emission testing mode was employed, operating in the classical *triode* mode. Initially, the anode voltage was increased to extract electrons from the cathode, with no gate bias applied, until a particular anode current was perceived. Next, the gate

voltage was altered and the subsequent anode current modulation was observed. In an alternative approach, for a device with the anode placed farther (≥ 100 μm) from the cathode and gate electrodes, a gate-induced emission mode was followed, where the gate, by virtue of a very small cathode-gate gap (≤ 2 μm), was used to control the electric field at the emitter finger-tip and extract electrons, with the anode effectively as a collector, in a *transistor*-type operation.

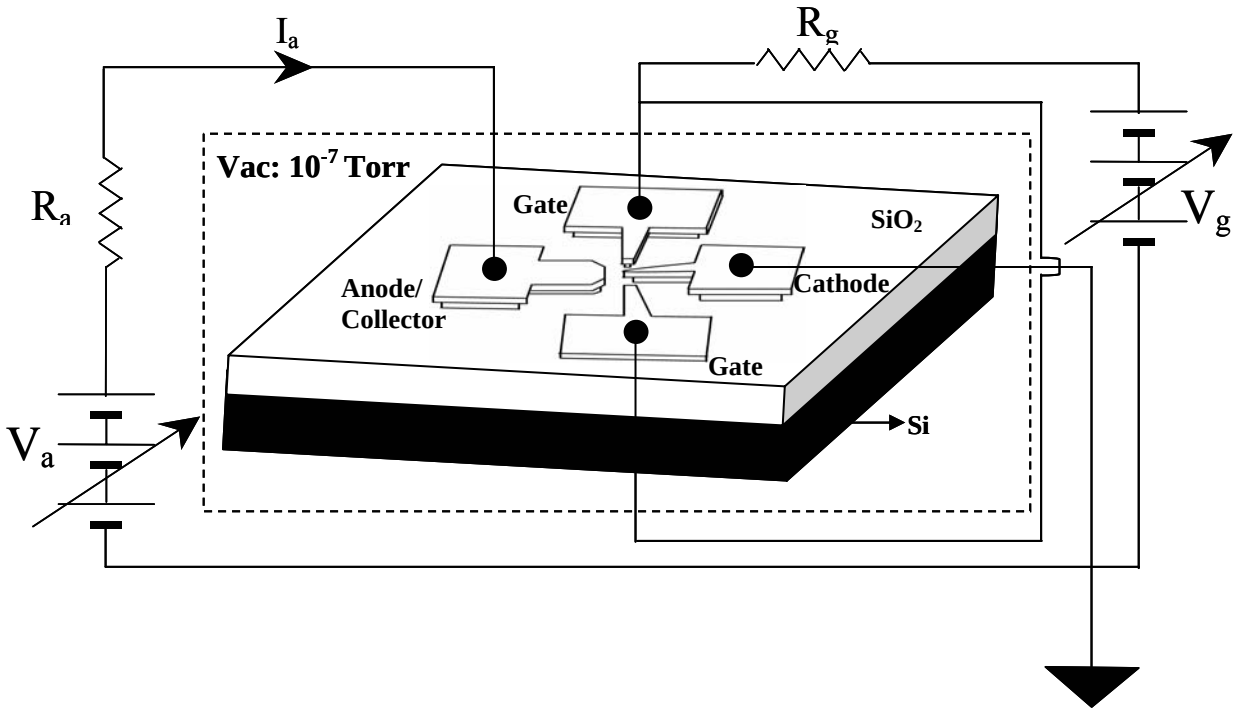

Figure 6.3 Schematic of the lateral triode emission test circuit in common emitter configuration.

The anode currents versus time were taken by a computer data acquisition system. For each set of emission current (I_a) measurement, the anode voltage was scanned manually while keeping the gate voltage constant. The gate voltage was then changed to a new value and the same emission measurement was repeated until a complete data set for all gate voltages in the range of interest were attained. The emission characteristics of triodes were obtained by plotting the anode emission current versus gate and anode voltages.

6.2 Electrical performance of nanodiamond vacuum field emission devices

6.2.1 Field emission characteristics of nanodiamond pyramidal micro-tip array cathode

The microtip array cathodes fabricated applying the nitrogen-incorporated nanodiamond ($CH_4/H_2/N_2$-MPECVD) and the undoped nanodiamond (CH_4/H_2-MPECVD) were tested individually for electron field emission in a high vacuum of 10^{-7} Torr based on the set-up described in the previous section. The undoped nanodiamond tips showed a turn-on electric field of ~14 V/μm and 10 μA emission current was obtained at ~ 23 V/μm. The nitrogen-incorporated nanodiamond tips exhibited significantly enhanced field emission characteristics with a low threshold electric field of 1.6 V/μm and an emission current over 10 μA at ~ 3.3 V/μm, with the resultant onset electric field reduction being greater than 80 %. The turn-on electric field is defined as the electric field at which a threshold emission current of ~ 100 nA is obtained. The graph in **Figure 6.4** illustrates the threshold emission characteristics from the two different cathodes. The linearity of the corresponding F-N plot and the absence of reverse leakage confirms that the observed current is solely due to field emission phenomenon. The drastic reduction in the F-N slope (by a factor of ~ 27) for the $CH_4/H_2/N_2$-nanodiamond indicates the presence of strong field enhancement factors in the nitrogen-incorporated nanodiamond (see inset in **Figure 6.4**). When further subjected to high current testing, the $CH_4/H_2/N_2$-nanodiamond applied microtip array generated an emission current of 19 mA (current density ~ 19 mA/cm^2) at at ~ 6 V/μm, sustainable over time, proving that the nitrogen-incorporated nanodiamond material can yield and handle large electron currents, apart from requiring a very low electric field to emit the electrons.

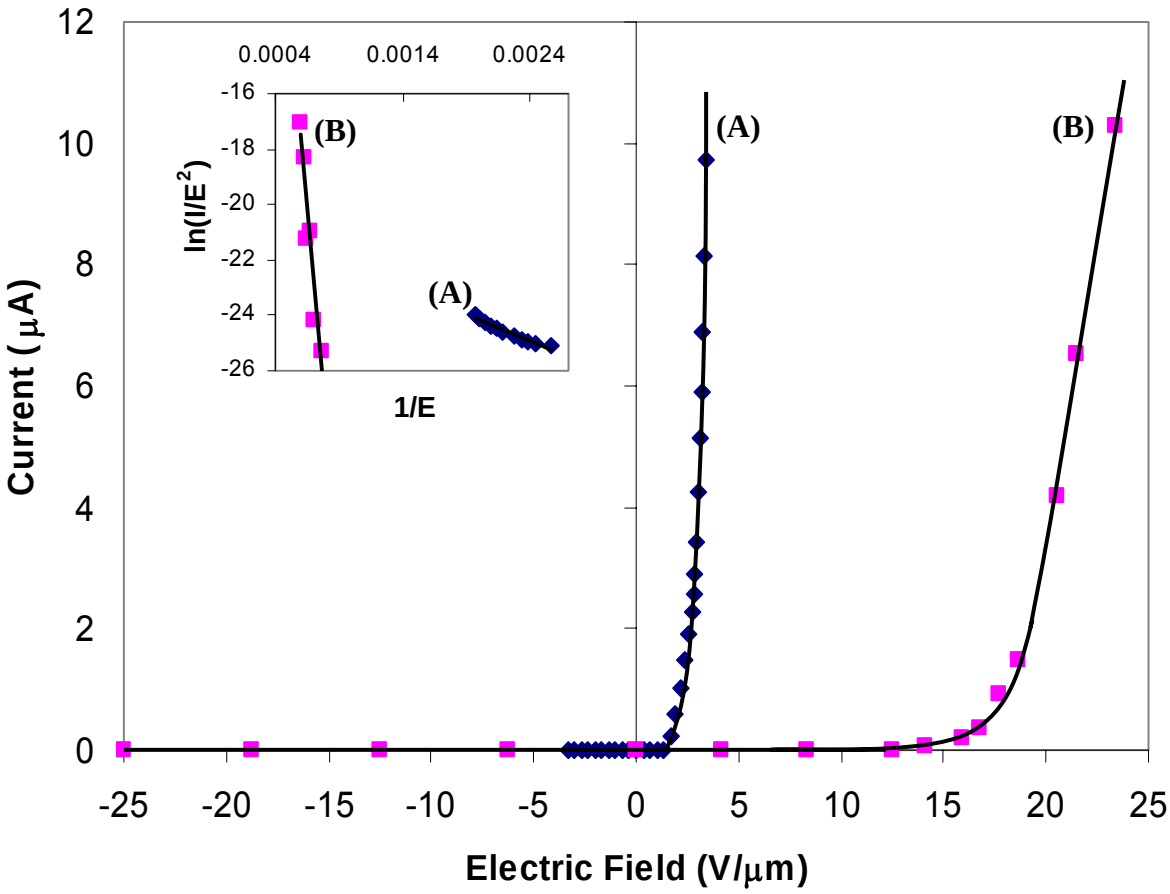

Figure 6.4 Field emission characteristics (I–E) of the pyramidal microtip array cathodes: (A) nitrogen-incorporated nanodiamond tips and (B) undoped nanodiamond tips; inset: corresponding F–N plots.

Discussion of the field emission characteristics of the nanodiamond microtip array cathode: The nitrogen-incorporated nanodiamond is an appealing material for vacuum microelectronic applications. The ultra-small grain size, relatively increased sp^2-bonded carbon content and the high electrical conductivity of the nitrogen-incorporated nanodiamond film offer a combination of properties for efficient field emission devices. The high field enhancement factors of the $CH_4/H_2/N_2$-nanodiamond microtips are summarized in **Table 6.1**. The improved field emission is explained by means of an overall improvement in the total field emission enhancement factor, β, which can be expressed as the product of the following components:

$$\beta = \beta_g \beta_{sp2} \beta_n \quad (6.1)$$

where β_g, β_{sp2}, β_n are the field enhancement factors due to the geometry, sp^2-carbon content, and nitrogen doping respectively, all of which contribute to enhance the electric field and reduce the barrier for electron emission in the diamond cathode. The $CH_4/H_2/N_2$-nanodiamond tip emitter involves these parameters favorably to enhance β, and thereby, exhibits excellent electron field emission characteristics. Similar β enhancement due to geometry, sp^2-content, and boron doping in diamond has been proposed and experimentally verified by Wisitsora-at [115].

Table 6.1 Comparison of the field enhancement factors in $CH_4/H_2/N_2$- and CH_4/H_2-nanodiamond microtip array cathodes

Field enhancement factors	**Analysis technique**	**$CH_4/H_2/N_2$-nanodiamond (nitrogen incorporated) microtips**	**CH_4/H_2-nano diamond (undoped) microtips**
Geometrical field enhancement factor (β_g) of the microtip	SEM: tip radius of curvature & height measurement; TSFE model: βg calculation	32,000	3, 200
sp^2-bonded carbon content in the nanodiamond film (sp^2/sp^3 peak ratio)	Raman spectroscopy	0.97	0.76
Electrical resistance of the nanodiamond emitter surface (measured at RT)	Multimeter	~ 2 Ω	several MΩ
Nitrogen concentration levels in the nanodiamond emitter	Energy dispersive spectrometry (EDS) & Rutherford backscattering spectrometry (RBS)	4.5×10^{21} cm^{-3} in the emitter surface	-

6.2.2 Field emission characteristics of monolithic nanodiamond lateral vacuum diodes

The nanodiamond lateral emitters can form a practical electron device for IC-compatible and general applications in vacuum electronics. Uniformly micropatterned diamond emitters, in conjunction with built-in gates and anode at a small electrode gap form an efficient device structure. The typical electrical characteristics of the developed monolithic nanodiamond lateral diodes are reported in this section. The device was found to have a low operating voltage and electric field, high and stable emission current, reasonable current scaling attributes with emitter area, rectification behavior, and operational temperature and radiation immunity.

(a) Low voltage and electric field operation

The nanodiamond 6-finger lateral diode fabricated with 3 μm anode-cathode spacing was characterized in a vacuum environment of ~ 10^{-6} Torr, a practically attainable vacuum when the device is sealed in a package. A low turn-on voltage of 5.9 V, corresponding to a turn-on electric field of 1.95 V/μm, which are one of the lowest values reported for lateral field emission devices, was demonstrated by the nanodiamond lateral diode. The current value determining the turn-on voltage is 10 nA per finger. Further, a high emission current of ~ 5 μA was derived at an anode voltage of 18 V (applied electric field of 6 V/μm). **Figure 6.5** depicts the turn-on field emission characteristics of the device. The device I-V characteristics were found to be consistent with Fowler–Nordheim (F-N) relationship, as shown by the linear F-N plot, inset of **Figure 6.5**. This result shows that high-performance diamond devices can be designed to meet the operating voltage requirement for IC-compatible and general applications in vacuum microelectronics. Also, it is evident that diamond lateral emitters exhibit excellent field emission characteristics even prior to any use of special, cost-intensive submicron lithography patterning.

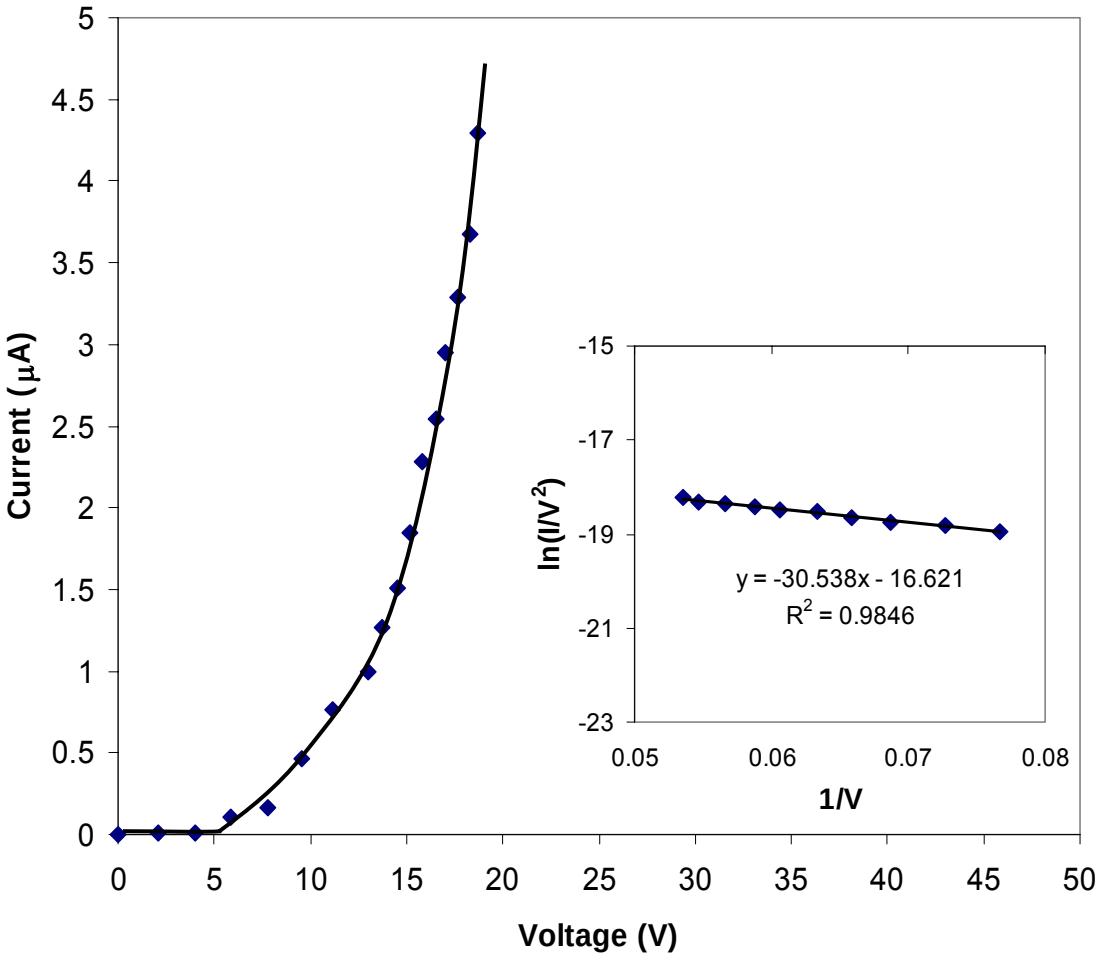

Figure 6.5 Low-voltage field emission characteristics of the nanodiamond 6-finger lateral diode with 3 μm anode–cathode gap; I–V plot indicates turn-on voltage of 5.9 V; inset: linear F–N plot.

At a particular anode-cathode spacing, enhancement of the diode emission characteristics for low voltage performance can be achieved by improving the field enhancement factor (β) of the diamond cathode, resulting in a low turn-on electric field. The lateral emitter was designed to have a higher geometrical aspect-ratio with smaller tip radius of curvature, while the electrical conductivity of the nanodiamond material was increased by appropriate nitrogen incorporation to yield an enhanced β factor. A 125-fingered nanodiamond lateral diode, thus fabricated, exhibited a very low turn-on electric field of 1.1 V/μm. It should be noted that this turn-on electric field is again defined based on 10 nA emission current obtained per finger (1.25 μA for a 125-fingered

cathode). The described emission performance of the lateral device is shown in **Figure 6.6**. The highly linear F-N behavior confirms field emission tunneling mechanism, while shallow slope of the F-N indicates the presence of strong field enhancement constituents (β) in the lateral emitter, viz., finger-tip sharpness, sp^2-carbon and nitrogen concentration in the nanodiamond. The current was then observed to increase exponentially with increasing anode voltages and an emission current of 65 μA was achieved at an applied field of 5.7 V/μm.

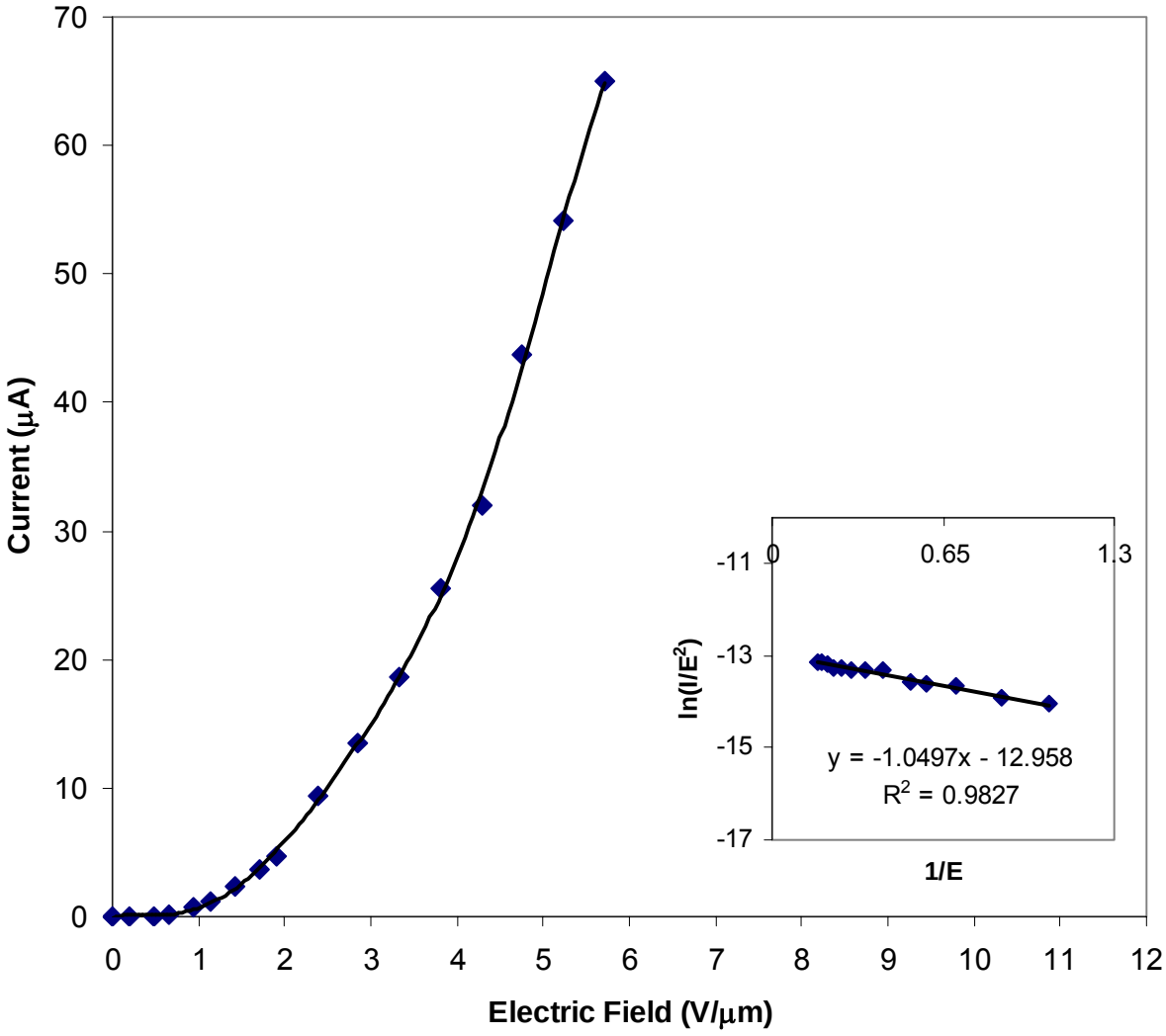

Figure 6.6 Low-electric field emission characteristics of a nanodiamond 125-finger lateral diode; I–E plot shows turn-on field of 1.1 V/μm; inset: linear F–N plot with shallow slope.

The observed turn-on electric field of the nanodiamond lateral emitter is significantly lower than that of a comparable silicon lateral field emitter utilizing a sharp tip apex, which is > 100 V/μm [104]. This is attributed to the superior material properties of nitrogen-incorporated nanocrystalline diamond offering the diamond emitter diode a higher effective field enhancement factor or a lower work function than a silicon field emitter diode. It would be in the bounds of practicality to realize a nanodiamond lateral field emission diode with a nanometer-scale interelectrode gap (20 nm-100 nm) brought about by ultra-high resolution (e-beam) lithography, operable at a subvolt turn-on voltage equivalent to conventional semiconductor p-n junction diodes, triggering a novel candidate for *ultra low-power electronics*. The reported results from silicon lateral field emitters also confirm that for the electric fields at which the nanodiamond lateral diode operates, there can be no emission from the silicon layer beneath the diamond fingers. Moreover, the lateral device processing is optimized to overetch the Si layer, as shown in **Figure 5.17**, which leaves the silicon having a wider gap distance from the anode and also with a larger radius of curvature pattern. Further, the active silicon layer of the SOI substrate was chosen to have a relatively low dopant concentration. All these factors satisfied that the emission characteristics of the lateral diode are contributed solely by nanodiamond.

(b) Geometrical field enhancement factor of the *finger-like* lateral emitters

An organized study was conducted to identify the geometrical field enhancement offered by the finger-like emitter topology to the lateral device. Three different emitter configurations of nanodiamond, viz, the micropatterned 6-finger lateral structure, edge-shaped structure (the anode structure used in the lateral diode) and an as-deposited nanodiamond film were tested for vacuum field emission and their characteristics compared. The effect of the geometrical field

enhancement offered by the micropatterned finger-like emitters over the edge structure and the as-deposited nanodiamond film was established experimentally. *SIMION 7.0*^{TM} simulation software, an industry standard for modeling of electron and ion optics, was subsequently used to model the lateral emitter geometries and study their equipotentials and electric field distributions to corroborate the geometrical field enhancement offered by the fingered emitters.

Characterization procedure: Electron emission from the as-deposited nanodiamond film surface was measured in a vacuum chamber maintained at ~ 10^{-6} Torr, using a heavily doped silicon sample as the anode and a 40 μm-thick mica as the insulator, which defined the anode-cathode spacing (see schematic in **Figure 6.7 (a)**). The micropatterned nanodiamond emitters were characterized for field emission in a vacuum of ~10^{-7} Torr laterally with the integrated adjacent nanodiamond structure serving as the anode (see schematic in **Figure 6.7 (b)**). The separation between two adjacent emitter structures was designed to be 3 μm. The field emission I-E behavior and the corresponding F-N plot were obtained from each of the emitters and compared.

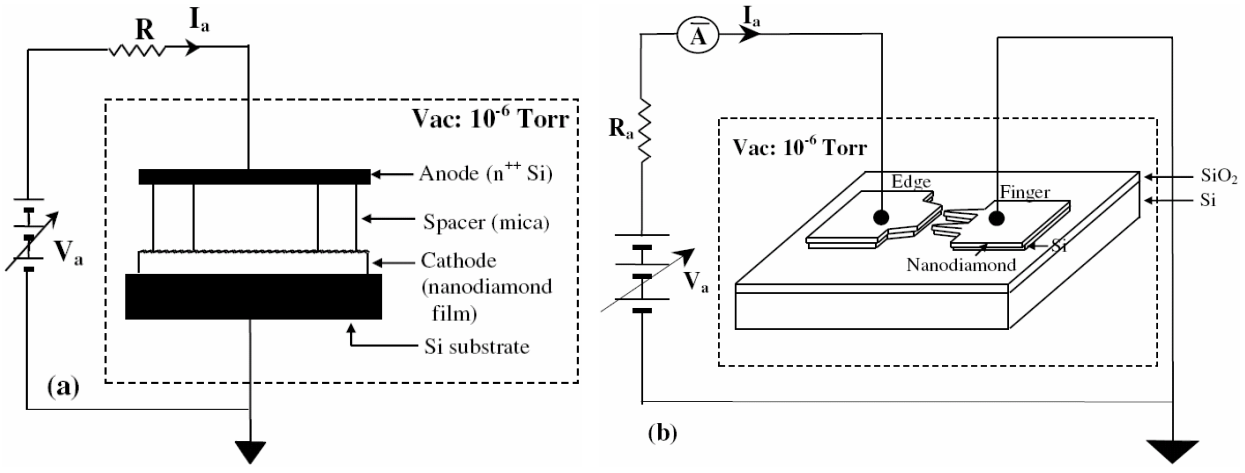

Figure 6.7 Field emission diode characterization testing methods: (a) as-deposited nanodiamond film — vertical configuration; (b) micropatterned nanodiamond emitters — lateral configuration.

Characterization results: The field emission characteristics of the three different emitters are presented in **Figure 6.8**. The linear F-N plots, included as **Figure 6.9**, confirm that the current is attributable to field emission. The electron emission from the as-deposited nanodiamond film could be turned on at an electric field of 18 V/μm, attaining 3 μA emission current at ~ 30 V/μm. The 6-fingered nanodiamond emitter exhibited a very low turn-on electric field of 1.9 V/μm and a high emission current of ~ 100 μA at ~ 20 V/μm, while the nanodiamond edge emitter, with a 6.5 V/μm turn-on field, demonstrated 4.6 μA emission current at the same applied electric field of 20 V/μm. It should be noted that the 6-fingered lateral emitter cathode was characterized for field emission with the adjacent edge structure serving as the anode, while the vice-versa combination was applied for testing the nanodiamond edge emitter.

The effect of the geometry of the high aspect-ratio fingers and the edge emitters on field emission from the nanodiamond film was studied. The emission data of the different emitters was correlated to the modified Fowler-Nordheim equation:

$$\ln(I/E_0^2)=\ln(A^* K_1^* \beta^2/\Phi)-(K_2^*\Phi^{1.5}/\beta)(1/E_0) \qquad (6.2)$$

where K_1 and K_2 are constants, I is the emission current, Φ is the work function of the emitting surface (eV), β is the total field enhancement factor, A is the emitting area, and E_0 is the macroscopic applied electric field (V/cm). Furthermore, the total field enhancement factor β can be expressed in terms of the product of each field enhancement factor as $\beta=\beta_g\ \beta_{sp2}\ \beta_n$, where β_g, β_{sp2}, β_n are the field enhancement factor due to the geometry, sp^2-carbon content, and nitrogen doping, respectively. The slope of the linear F-N plot $\{\ln(I/E^2)$ vs. $1/E\}$ is given by $-K_2\Phi^{1.5}/\beta$. The observed field emission enhancement of the micropatterned nanodiamond emitters can be explained by an increase in the geometrical enhancement factor. This can be deduced from the observation that the F-N slope decreases significantly for the fingered and edge emitters (see

Figure 6.9). The reduction of the F-N slope should mainly arise from the geometric effect because the as-deposited nanodiamond film and the nanodiamond emitters have the same sp^2-carbon and nitrogen concentration and thus should have the same β_{sp2}, and β_n and work function Φ. Considering that Φ, β_{sp2}, and β_n are the same for the nanodiamond films and the micropatterned emitters, β_g can be found from the F-N slopes of emission data. It was found that β_g of the 6-fingered nanodiamond emitter is ~198 times that of the as-deposited nanodiamond film and ~ 35 times that of the nanodiamond edge emitter. It was also deduced that the β_g of the edge emitter was ~ 6 times that of the as-deposited nanodiamond film.

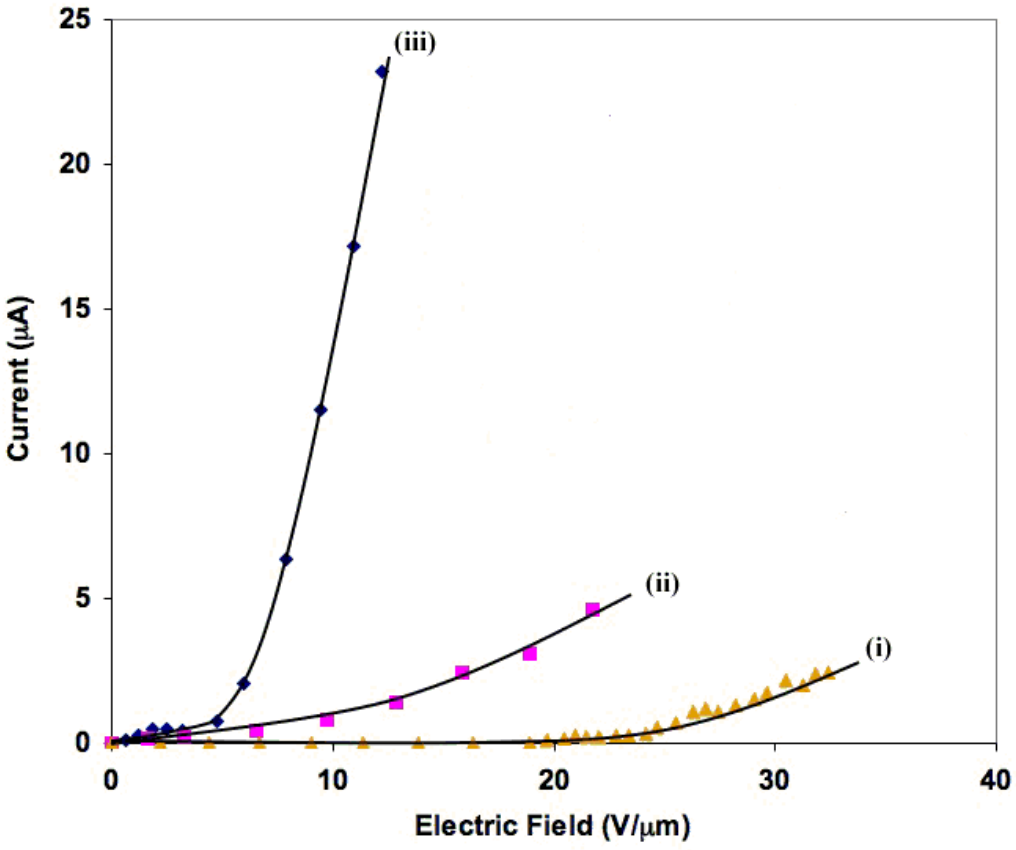

Figure 6.8 Field emission characteristics (I-E) of nanodiamond: (i) as-deposited nanodiamond film; (ii) nanodiamond edge emitter; (iii) nanodiamond 6-finger lateral emitter.

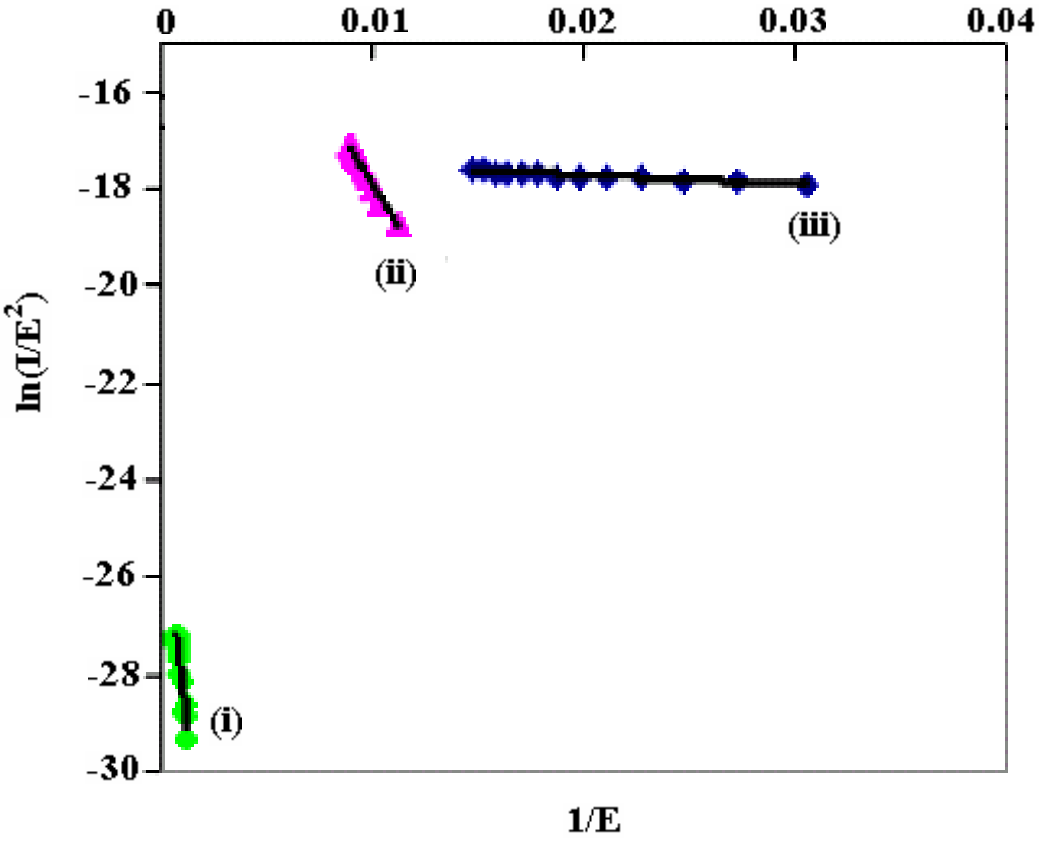

Figure 6.9 Fowler-Nordheim plots for nanodiamond field emission: (i) as-deposited nanodiamond film; (ii) nanodiamond edge emitter; (iii) nanodiamond 6-finger lateral emitter.

Field emission simulations of the lateral emitter structures: SIMION 7.0^{TM} simulation software was used to model the geometries of the fingered and edge lateral emitter structures. The distribution of the equipotentials and electric fields of the lateral emitter geometries for different bias conditions was obtained by solving *Laplace* equations using the tool. The shape of the emitter geometries were the same as that applied for the fabricated ones. The 6-fingered emitter and the edge geometry were considered as the electrodes with an inter-electrode spacing of 5 μm.

The potential arrays, defining the geometry and potentials of electrodes are utilized by *SIMION* [202]. The potentials of points outside electrodes are determined by solving the Laplace equation by finite difference methods:

$$\nabla^2 V = \nabla \cdot \nabla V = 0 \tag{6.3}$$

$$\nabla V = (dV / dx)_I + (dV / dy)_j + (dV / dz)_k = E \tag{6.4}$$

$$\nabla^2 V = \nabla \cdot E = dE_x / dx + dE_y / dy + dE_z / dz = 0 \tag{6.5}$$

The above equation is used to compute electrostatic potential fields. All electrostatic potential fields are constrained by the Laplace equation to conform to a zero charge volume density assumption (no space charge). The electrostatic potential of any point is defined in space in terms of the potentials of surrounding points. For example, in a 2-dimensional electrostatic field represented by a very fine mesh of points, the Laplace equation is satisfied when the electrostatic potential of any point is estimated as the average of its four nearest neighbor points:

$$V = (V_1 + V_2 + V_3 + V_4) / 4 \tag{6.6}$$

This relaxation technique minimizes normal numerical computational errors and produces stable solutions [202].

Figure 6.10 (a) shows the equipotential line plot of the lateral emitters in diode configuration for a given bias condition. The voltage to the edge geometry was set at 25 V, while the fingered geometry was grounded. The plot consists of 10 equipotential lines separated by 2.27 V each. The magnitude of the electric field at the very tip of each finger emitter and the corresponding edge-structured point is listed on the geometries, while the direction of the electric field is denoted by arrowhead. As one would expect, the electric field at the tip of the fingers is greater than that of the edge geometry throughout the device structure, indicating the enhanced

field emission characteristics of the nanodiamond 6-fingered lateral emitters observed in vacuum. When the potentials were reversed, with 25 V applied to the fingers and the edge structure grounded, the magnitude of the electric field on both the electrodes remained the same and the direction of the electric field reversed, being opposite to that of the potential gradient ($E = -\nabla\varphi$), (see **Figure 6.10 (b)**).

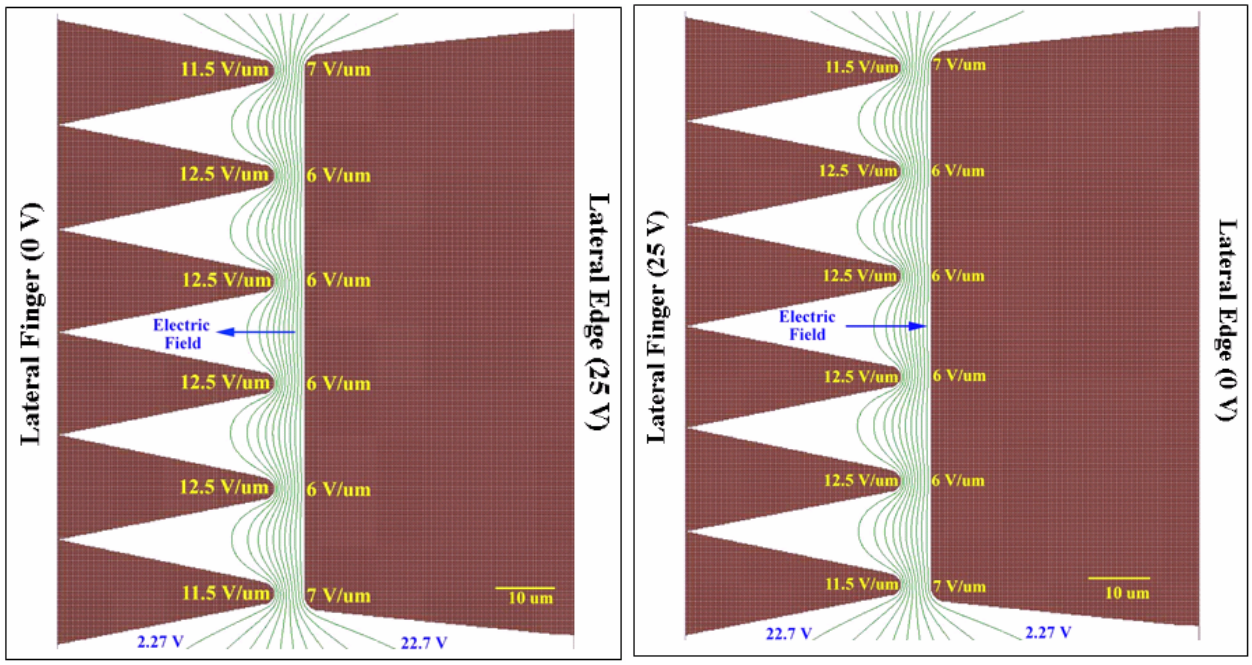

Figure 6.10 Equipotential line plot of the nanodiamond lateral field emitters in diode configuration at a given bias condition, showing the magnitude and direction of the electric field of the chosen geometries: (a) lateral finger at 0 V and edge at 25 V; (b) lateral finger at 25 V and edge at 0 V.

It can also be observed from the electric field distribution of the fingered geometry, that the field at the fingers towards the center of the configuration is greater than the corners. This effect could be more pronounced in reality if the corners of the nanodiamond edge, when serving as the anode, were over-etched during the etch processes in the lateral device fabrication. The influence of increasing the number of fingers in the emitter geometry can be considered in light

of this *"corner-effect"*. Comparing the 6-finger and 4-finger geometries, the former emitter configuration is superior to the latter due to the fact that there is 33.33% of the fingers at lower electric fields due to their location towards the corner of the structure, while the value increases to a notable 50% for the 4-finger electrode. Hence, a higher number of non-corner fingers would be expected to demonstrate more field emission current at a given applied field for the reason that a very small portion of the cathode geometry would be affected by lower electric fields due to the "*corner-effect*".

Figure 6.11 provides a clear view of the equipotential plot around the tip of a single finger, when the bias condition is set as 0 V on the finger and 25 V on the edge. The trajectory of the electrons emitted by a finger (cathode) to reach the edge (anode) at a potential of 25 V is also portrayed. It can be noticed that the density of the equipotential lines around the finger located towards the center of the geometry is higher than that at the corner owing to the lower electric field of the latter. The contours around the finger-tip in **Figure 6.12** indicate the zones at which the electric field distribution is constant. The contours that have been plotted include magnitudes of 2 V/μm to 10 V/μm in increments of 2 V/μm and do not denote the direction of the electric fields. The contour closest to the tip specifies the zone of the 10 V/μm electric field, which is followed by the 8 V/μm field contour. The 6 V/μm contour splits in half and terminates on the anode. The contours matching the electric fields of 4 and 2 V/μm stretch out and terminate on the adjacent fingers. The magnitude of the electric field defined by each contour was found to scale linearly with the anode voltage. These simulations help understand several aspects of electron emission in the lateral emitter geometries. The information obtained from the simulated data was incorporated in the lateral device design to optimize the emitter geometry, spacing between the emitters, and array configuration in the device structure for high performance.

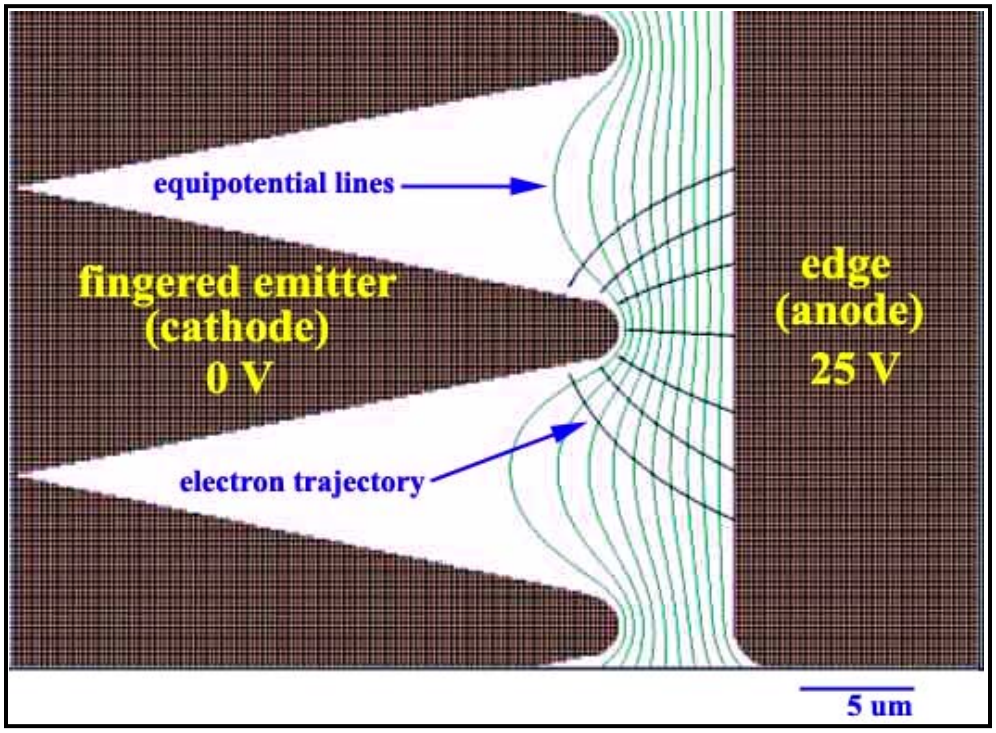

Figure 6.11 Equipotential plot around the tip of a single cathode finger, also showing the emitted electron trajectory to the anode (edge) at a potential of 25 V.

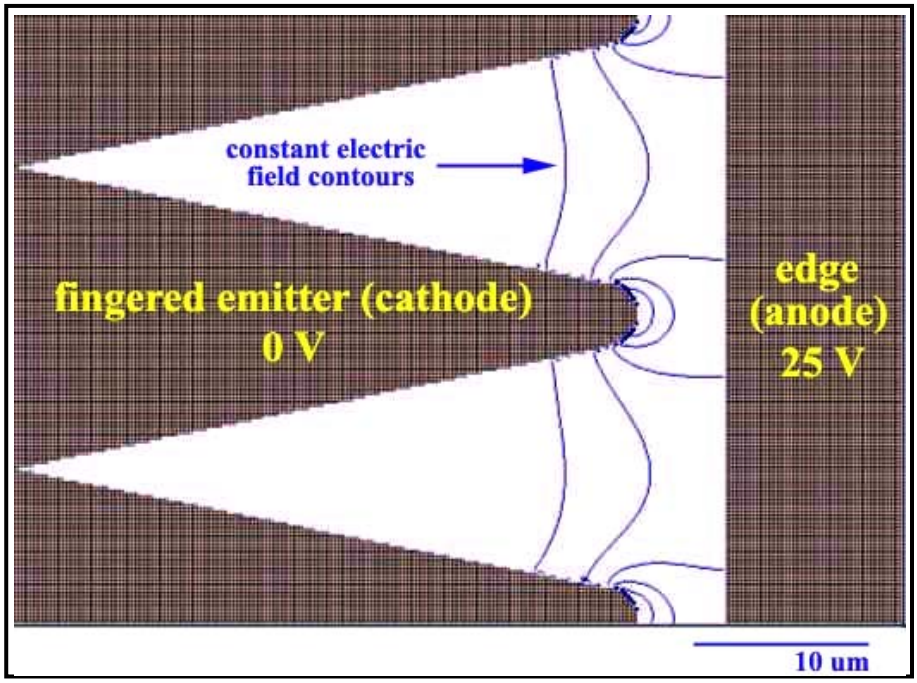

Figure 6.12 Constant-electric field distribution contours around the tip of a cathode fingered emitter.

(c) Observation of high emission current prospect in the nanodiamond lateral device

The nanodiamond 6-finger lateral diode, apart from exhibiting a low turn-on voltage of 5.9 V, achieved high current, which was the first indication in this research that lateral emitters can be a viable candidate for high power applications. As the anode voltage was increased, emission from the 6-fingered cathode was allowed to stabilize over time at different electric fields under vacuum, thus conditioning the tips and consolidating the emission sites participating in electron emission at a given applied field. The diode, then, demonstrated a high emission current of 1.1 mA at an anode voltage of only 98 V (electric field ~ 30 V/μm). The average current extracted per finger was 183 μA (assuming all of the 6 emitters contribute equally to the total current), which is among the highest current/tip values achieved from a lateral emitter geometry. The achievable currents per tip with silicon as the cathode material are reported to be limited to the order of 1 μA [102]. A simple estimate of the current density capability of the lateral device was performed. A 6-fingered cathode occupying a real estate of 270 μm^2, **Figure 6.13**, yielded ~ 1 mA electron current. Extrapolating, it might be possible to achieve ~ 85 A of emission current from a 1 cm^2-area chip possessing multi-fingered (~ 6000 fingers) emitter arrays, with due consideration to the real estate occupied by the anode, interelectrode isolation, and contact pads on the chip. The high current field emission behavior of the nanodiamond 6-finger lateral diode is presented in **Figure 6.14**, with the current density estimate in an I-J-V plot.

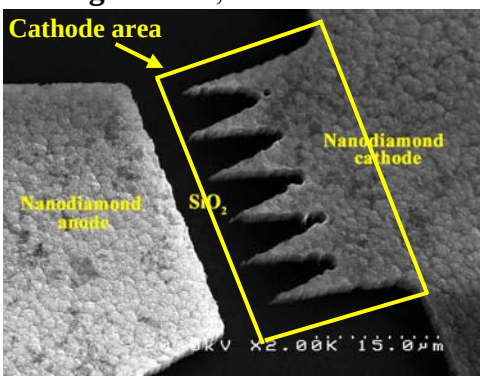

Figure 6.13 SEM image of lateral device specifying the nanodiamond cathode emitter area.

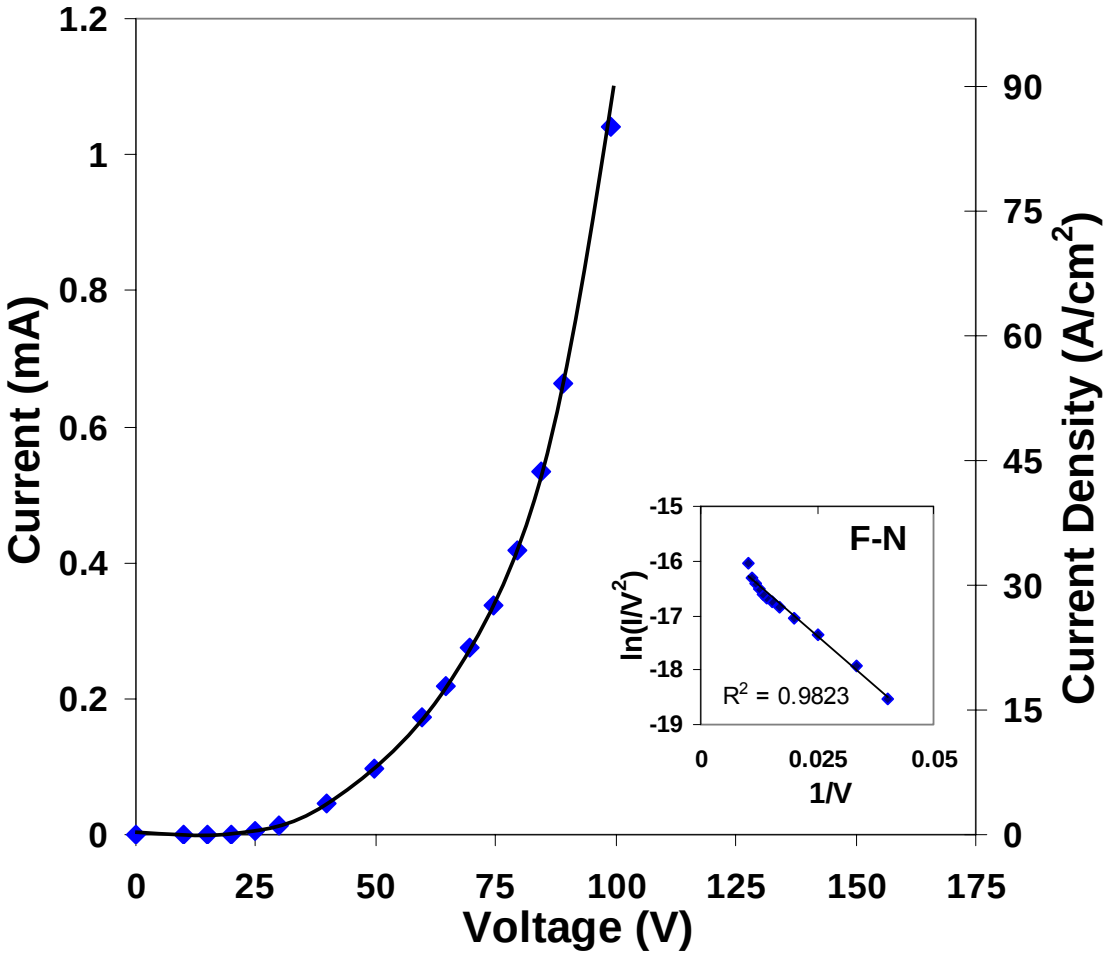

Figure 6.14 High current field emission characteristics of the nanodiamond 6-finger lateral diode with 3 μm anode-cathode gap: 1.1 mA at <100 V; 85 A/cm^2 current density capability based on the real estate occupied by the emitters on a 1 cm^2-area chip; inset: Linear F–N plot.

Alternatively, considering the cross-sectional area of the electron collector in the lateral device structure, the anode current density is found to be as large as 1.5x10^3 A/cm^2. The ~ 1 mA emission current behavior obtained from the 6-finger nanodiamond lateral diode initiated further work on the lateral emitters for high power applications. Versatile designs of the lateral diode equipped with uniformly spaced high aspect-ratio emitters in array configuration over a large area, maintaining a small and equal anode-cathode spacing were devised, processed and characterized for high current.

(d) Emission current scaling behavior in nanodiamond lateral devices

Linear scaling of emission current with emitter area has been challenging to achieve in vacuum microelectronic devices with certain factors affecting reliable array operation, viz., non-uniform geometry of patterned emitter tips in the array, change in interelectrode spacing over the device area due to non-planarity, field screening effect, material issues in handling the high current, to name a few. In this research on nanodiamond lateral devices, these factors have been taken into consideration in the design, material and device processing areas to result in less than 20 % deviation (logarithmic) from ideal linearity in the scaling trend of the emission current. Factors contributing to deviation, and the design/process developments addressed to mitigate the non-ideality are discussed in this section.

Experiment: The experiment involved the batch-fabrication of nanodiamond lateral diodes equipped with three different numbers of emitter fingers, viz., 6, 125, and 2000 to investigate how the forward emission current scales with the number of emitters in the device. The fabricated devices were tested for field emission in a vacuum of 10^{-7} Torr. Their current versus electric field characteristics and the corresponding Fowler-Nordheim behavior were obtained and compared. The emission current scaling results were analyzed.

Results: The nanodiamond lateral devices were tested individually in vacuum upto an emission current of 100 μA to study current scaling behavior. The 6-fingered lateral emitter showed a threshold electric field of 3 V/μm and 100 μA emission current at an electric field of 37 V/μm. The 125-fingered lateral emitter exhibited a lower threshold field of 2.1 V/μm and required ~ 23 V/μm field to generate an emission current of 100 μA. The threshold field of the lateral device with 2000 fingers in a comb-like arrangement was as low as ~ 1.1 V/μm, and the emission current of 100 μA was observed at a much lower electric field of ~ 9.7 V/μm. The emission

current value at the threshold electric field was set at 60 nA, which explains the decrease in threshold field as the number of fingers increases. The field emission characteristics (I-E) of the three devices are presented in **Figure 6.15 (a)**. The semi-log plot in **Figure 6.15 (b)** shows the threshold electric field of the three lateral emitters. The corresponding Fowler-Nordheim data are plotted in **Figure 6.16**. The linear F-N plots with negative slopes prove that the current from the lateral emitters is from field emission, not leakage. The F-N plots have the same slope values, indicating that the field enhancement factor (β) and the work function Φ are essentially the same for all the three lateral emitters, and that the emission behavior enhancement is the result of the increase in the number of emitter fingers in the cathode. It is important to note that the three lateral devices were batch-fabricated, ensuring similar β and Φ factors.

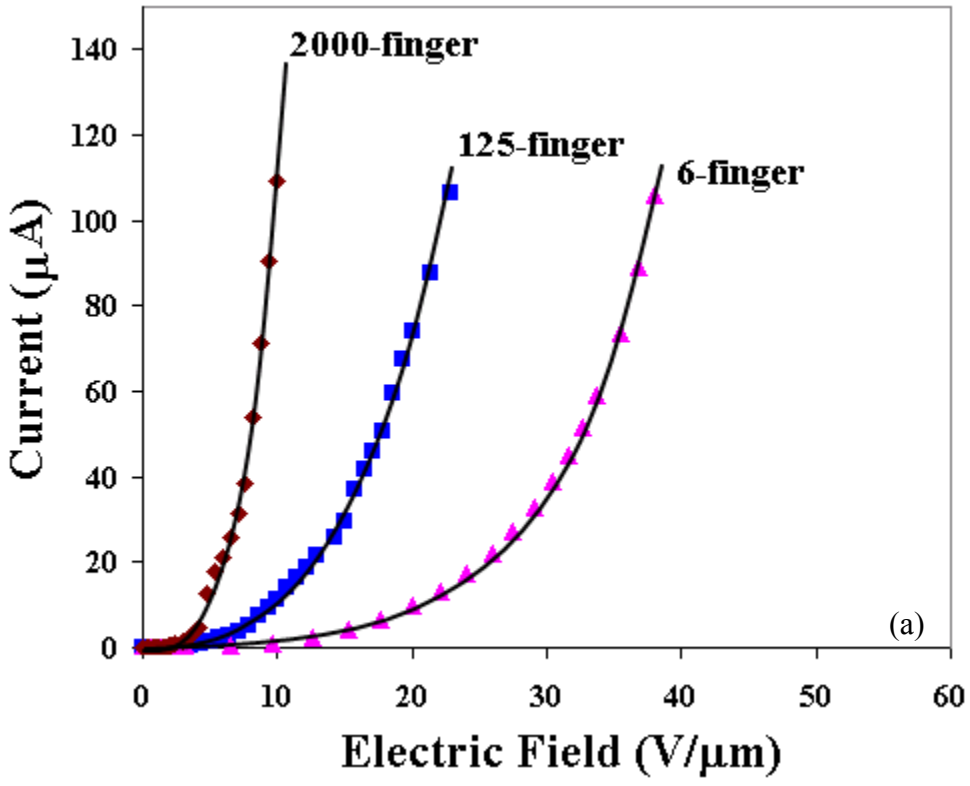

Figure 6.15 - cont.

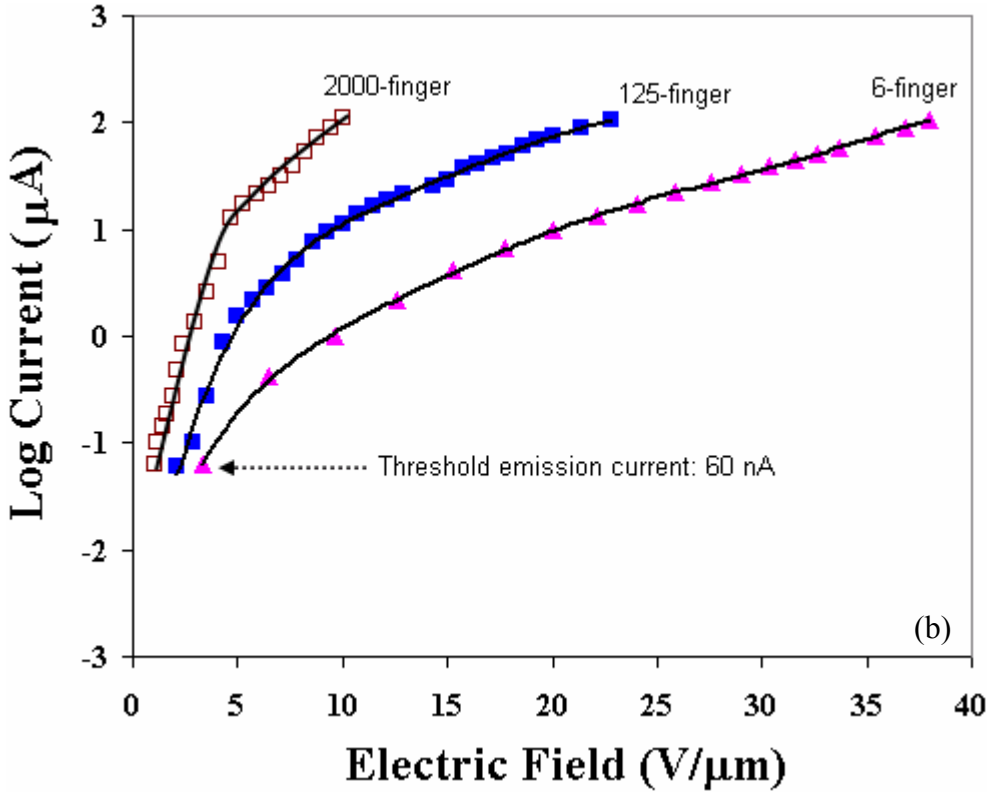

Figure 6.15 (a) Field emission characteristics (I-E) of the nanodiamond lateral devices in discussion, showing the current enhancement obtained by increasing the emitter area; (b) Semi-log plot of the field emission characteristics, showing the threshold electric field of the three lateral emitters.

The current scaling behavior of these devices can be observed at a given electric field. For example, at an electric field of 10 V/μm, the 6, 125, and 2000-fingered lateral emitters demonstrated 1.1 μA, 11.3 μA, and 109 μA respectively. The augmentation in overall emission current capability of the multi-fingered lateral emitters is attributed to the increase in the emitter area and thereby the number of potential emission sites in the cathode.

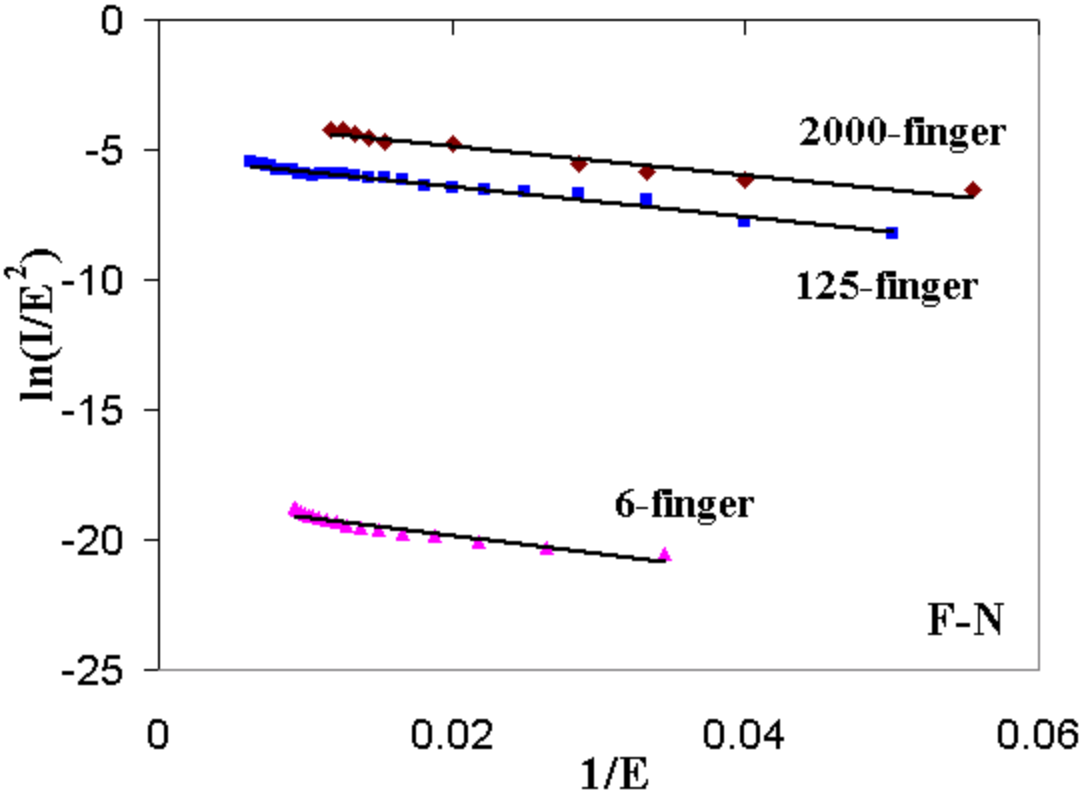

Figure 6.16 Fowler-Nordheim behavior of the nanodiamond lateral devices with identical slopes, indicating an unchanged β factor.

Analyzing the current scaling trend in these diamond lateral devices, the deviation from the ideal scaling factor was calculated by logarithmically plotting the number of emitter fingers in the cathode structure with the observed emission current at a particular electric field for the three devices in discussion. It was found that the emission current from the nanodiamond lateral device scales with less than 20 % deviation from the *ideal* linear scaling phenomenon, in a logarithmic trend. **Figure 6.17** graphically illustrates this statement, taken as a forward sign toward a high current lateral field emission device.

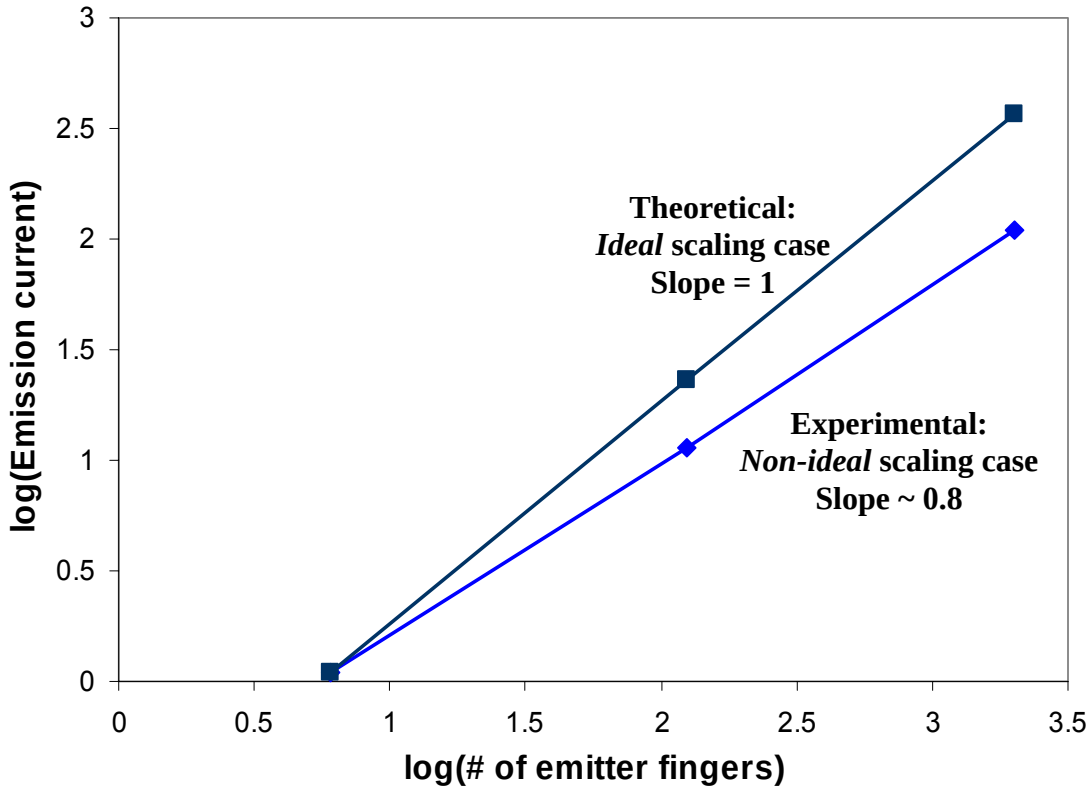

Figure 6.17 Logarithmic plot illustrating the deviation from ideal linear current scaling, observed in the nanodiamond lateral field emission devices.

An effort to study the device aspects possibly causing the non-ideality in current scaling was undertaken and practical solutions have been recognized and addressed. One probable phenomenon could be the field screening effect [203], occurring in electron field emitters, where electric field shielding can arise between closely packed emitters in a dense array. Though the ND fingers are spaced uniformly in the comb array device, the separation between the tips is lesser than twice the tip height. A wider inter-emitter separation in the present lateral device configuration can help minimize the screening effect [203], but the solution would be a compromise on the emitter packing density. A determination of the suitable lateral finger length and inter-tip spacing for high current arrays is currently underway. Another issue affecting emission over large areas is the voltage drop across the lateral device. Increasing the electrical

conductivity of the nanodiamond film further and application of a Ti/Au metal contact layer on the nanodiamond can help mitigate this effect. An integrated Ti/Au metallization technique, as shown in **Figure 5.21**, has been applied with this regard to the lateral device. These ongoing design and process developments can further enhance the emission current scaling behavior, thus making the nanodiamond lateral comb array device a viable candidate for high current.

(e) High power nanodiamond lateral comb array emitter diode

Based on the current scaling results, it was observed that the nanodiamond lateral comb array device, possessing well-defined emission sites and a high emission site density with equal anode-cathode spacing over a large area, has the potential to generate large total emission current through a number of parallely-operated finger tips. A 9000-fingered nanodiamond lateral comb array diode with 8 μm anode-cathode spacing, occupying a device area of 1 cm^2, was characterized for field emission under a vacuum of 10^{-7} Torr. To derive high current from the diamond device, the emitter fingertips were conditioned by allowing the emission current to improve and stabilize over time at different applied electric fields. Consequently, the 9000-fingered lateral emitter demonstrated high emission current performance with ~ 25 mA derived at an anode voltage of 260 V (electric field ~ 32 V/μm, gap ~ 8 microns). The field emission (I-V) behavior of the device is presented in **Figure 6.18**. The linear Fowler-Nordheim (F-N) plot, included as an inset in **Figure 6.18**, confirms that the current from the lateral emitter is attributable to field emission. The F-N plot exhibits a dual linear slope. The line with the shallower slope corresponds to low emission current regime (low emission field), while the one with the steeper slope corresponds to the high emission current zone (high emission field). This F-N behavior can be possibly explained by a change in the effective β factor during the field

emission. At lower electric fields, emission of electrons occurs only from the sharp apex area of each nanodiamond finger in the lateral emitter array. This leads to a case of smaller emission area (i.e. smaller extrapolated y-intercept value per the F–N equation) with very high field enhancement factor β, a shallow F–N slope. At higher electric fields, a larger area of the emitter finger contributes to the electron emission, which decreases the effective overall β. A higher emission area (i.e. bigger extrapolated y-intercept value per the F–N equation) and an augmentation in the number of emission sites with lower field enhancement factor is the reason for the observed high current and a steeper F–N slope.

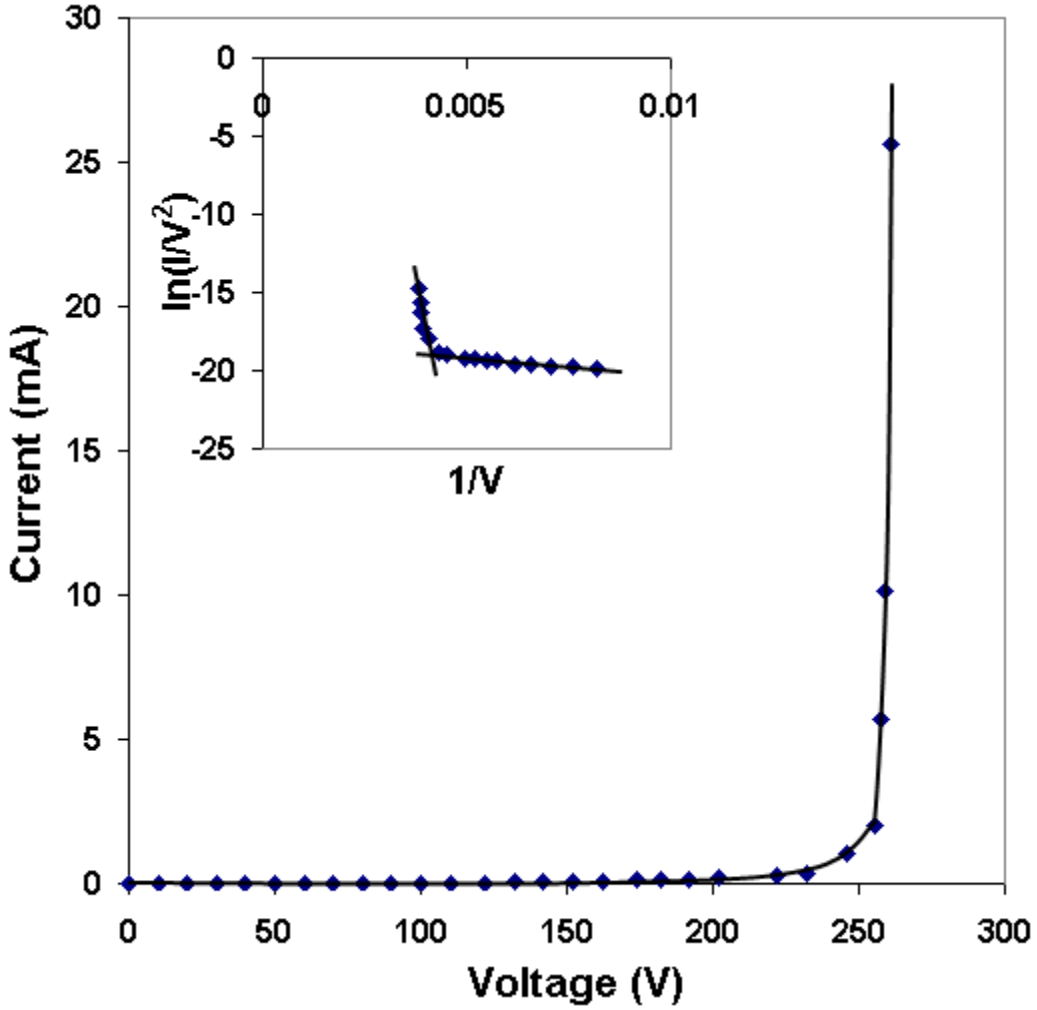

Figure 6.18 25 mA high current field emission behavior of the 9000-fingered nanodiamond lateral comb array diode; inset: F-N plot.

The potential of the nanodiamond lateral comb array emitter for higher current is demonstrated by its truly exponential I-V characteristics in the mA emission current regime at low anode voltage increments; no emission current saturation is observed, as depicted in **Figure 6.19**. The high degree of linearity in the corresponding F-N behavior verifies that the high current measured adheres to the field emission theory. The high emission current capability of this diamond lateral vacuum diode is attributed to the efficiency of the process in yielding uniformly micropatterned emitter fingers in array configuration with controlled geometry along with small and equal anode-cathode interdistance, and the material properties, viz., high electrical and thermal conductivity of the nitrogen-incorporated nanodiamond. A nanodiamond vacuum diode operable at high current over 25 mA at reasonable voltages in lateral configuration has thus been demonstrated in this research. This device behavior represents the highest emission current value reported from comparable lateral field emitter arrays to date.

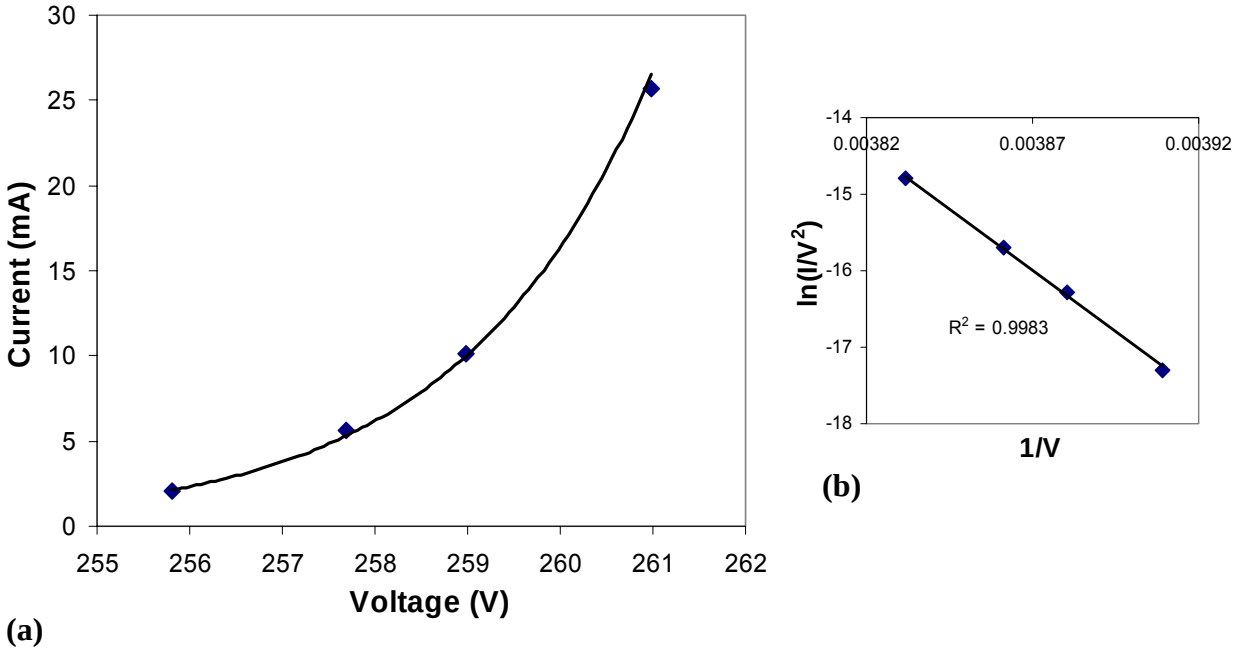

Figure 6.19 Expand representation of Figure 6.18 at high emission current regime (a) I-V field emission characteristics; (b) F-N behavior at high current (mA range).

(f) Reliability-enhanced nanodiamond high power vacuum diode on aluminum nitride insulator

The practical realization of the high-power potential of vacuum field emission devices has been hindered by issues such as over-heating of emitter tips owing to material properties, non-uniform current density over a large emitter array, and importantly, insulator breakdown at high current and associated high electric fields. With diamond lateral emitter array devices demonstrating high current capability, a robust insulator, alternative to SiO_2, is essential to reliably operate the device at high power with long lifetime. With this regard, nanodiamond lateral comb array diodes were fabricated on a thick aluminum nitride insulating substrate, the process specifications of which have been described in Chapter V.

Field emission characterization results: A 325-fingered diode was one of the devices built on aluminum nitride substrate and characterized for vacuum field emission. The diode had a turn-on voltage of ~ 30 V and the emission current was found to increase exponentially with the applied voltage. The device then demonstrated a high emission current of 1 mA at an anode voltage of 360 V. **Figure 6.20** includes the field emission I-V behavior of the lateral emitter array device. The highly linear F-N plot indicates that the observed current is due to field emission from the nanodiamond emitter-fingers. The emission current was found to be stable over time, around 1 mA at constant applied voltage. The high current behavior was also sustainable, with no emission degradation resulting in monotonic decrease of current with time observed.

Temperature tests were also conducted on the diode to verify the integrity of aluminum nitride for device functionality at high current. Since heat generation can occur in the emitter tip regions during high current operation, these temperature tests can provide indication of the device reliability for high power. At a constant applied electric field, no significant change was observed in the current obtained from the lateral emitter device as the substrate temperature was

increased from 27 °C to 350 °C, as depicted in **Figure 6.21 (a)**. The temperature insensitivity behavior observed was also stable with time, as shown in the current-time plots in **Figure 6.21 (b)**, captured at different temperatures of 27 °C and 200 °C, with the applied voltage is kept constant. In addition to the verification of F-N behavior of the observed field emission, these temperature tests are necessary to rule out *Frenkel-Poole* conduction via the insulator in the lateral device structure, should it be present. The results presented in **Figure 6.21** denote the absence of leakage current through the aluminum nitride.

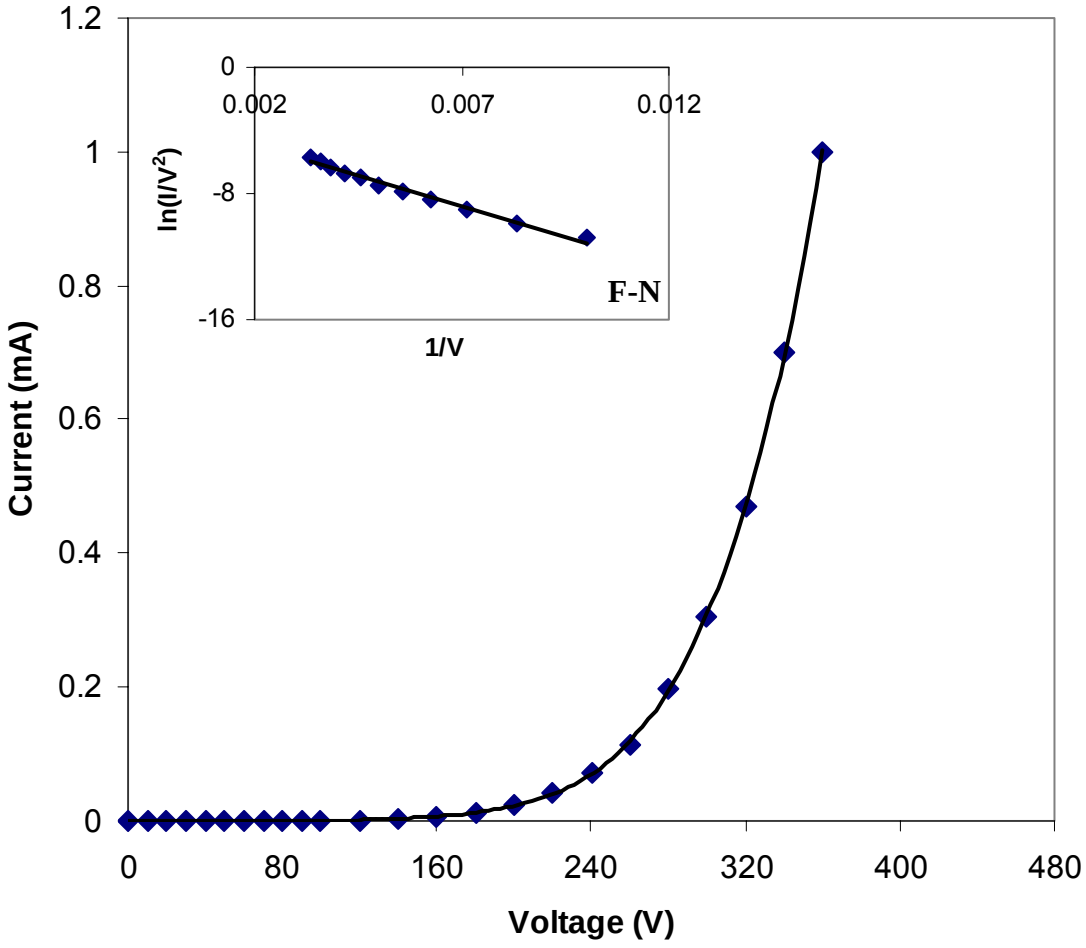

Figure 6.20 Field emission behavior of a 325-fingered nanodiamond lateral diode fabricated on aluminum nitride substrate; inset: F-N plot.

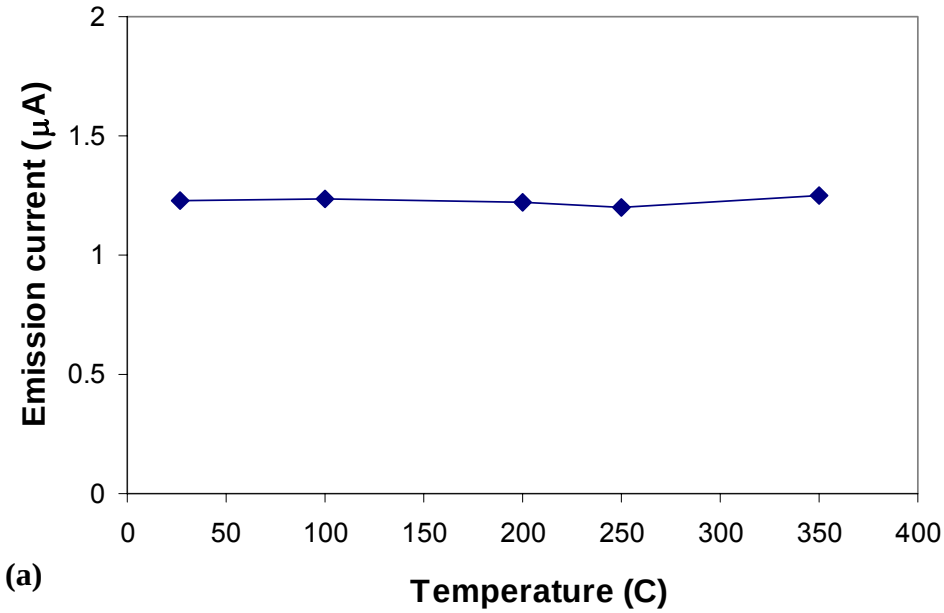

(a)

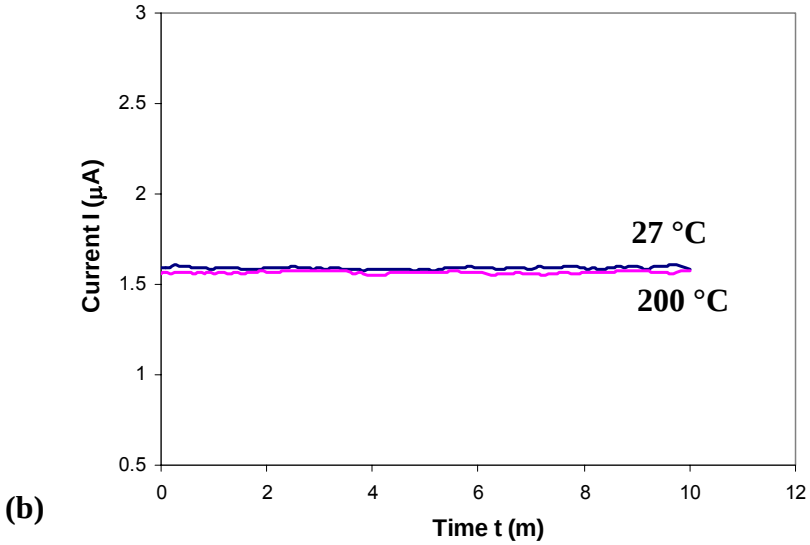

(b)

Figure 6.21 Temperature insensitivity behavior of the nanodiamond lateral field emission device developed on aluminum nitride substrate.

The observed electrical characteristics can enhance the applicability offered by the nanodiamond lateral field emitter array device for high power microelectronics, even under conditions of high temperature and radiation.

(g) Effect of interelectrode spacing on field emission in lateral devices

The dependence of the emission current on the electrode spacing in the device structure was investigated. A strong sensitivity of 10 V μm^{-1} observed in the field emission behavior of the nanodiamond lateral device as a function of the cathode-anode distance can be utilized in the development of novel sensors and NEMS, reliably operable in harsh environments.

Experiment: Three batch-fabricated nanodiamond lateral diodes, with a 125-finger emitter array, were chosen for this experiment (SEM images shown in **Figure 5.16**). The design parameters, viz., emitter geometry, array size and anode-cathode spacing were all mask layout-defined and transferred onto the nanodiamond device by lithography, following the single-mask lateral device fabrication process. The lateral devices differ only in their interelectrode distance, with the nanodiamond composition, emitter geometry and area controlled to be almost the same by parallel processing. The three devices, with different interelectrode gaps of 4 μm, 7 μm, and 10.5 μm were individually characterized for field emission under the same vacuum environment of 10^{-7} Torr. The current-voltage (I-V) and current-electric field (I-E) curves were obtained for each device and the results compared.

Results: The effect of changing the anode-cathode gap was observed in the I-V characteristics, with a distinct reduction in the device turn-on and operating voltages with a decrease in the gap, inversely altering the electric field at the emitter fingers. The nanodiamond lateral diode with 10.5 μm interelectrode separation exhibited a turn-on voltage of 23 V and achieved an emission current of ~ 5 μA at an anode voltage of 85 V. The lateral diode with 7 μm anode-cathode spacing showed 15 V turn-on voltage and yielded an anode current of ~ 5 μA at a lower anode voltage of 55 V. When the device with the smallest gap of 4 μm was tested for field emission, the turn-on voltage was as low as 9 V, and an applied anode voltage of 30 V yielded ~ 5 μA

emission current. The threshold current value used to determine the turn-on voltage is 60 nA. The I-V characteristics of the devices are graphically presented in **Figure 6.22**. The derived current in the devices was found to be stable over time. The emission current from the lateral emitters conforms to Fowler-Nordheim behavior, shown in **Figure 6.23**. The parameters extracted from the linear F-N plots indicate that the field enhancement factor (β) and the work function (Φ), by virtue of almost identical F-N slope values, and the emitter area (same extrapolated y-intercept value per the F-N equation) are essentially the same for the three lateral emitters, and that the change in the emission behavior between the devices is the result of the variation in the interelectrode spacing. Further confirmation to this is provided by the fact that all the nanodiamond emitter devices demonstrate the same low turn-on electric field of ~ 2 V/μm and closely matched I-E characteristics, depicted in **Figure 6.24**. The semi-logarithmic plot, included as an inset in **Figure 6.24**, provides verification for the turn-on field of the three lateral emitter devices. The scaling of the emission current with the interelectrode gap can be observed at a given electric field. For example, at an applied electric field of ~ 8 V/μm, the 4 μm, 7 μm and 10.5 μm lateral-gap devices yielded 5.109 μA, 5.11 μA, and 5.10 μA respectively. The linearity in the relationship between the applied anode voltage and the interelectrode distance for a particular measured emission current was examined graphically. The slope of this line, at a constant current of 5.1 μA, was found to be ~ $1x10^{-7}$ m/V, which can be extrapolated [204] to a displacement sensitivity value of 10 V μm^{-1}. Sensitivity expresses the amount of signal change (V) in proportion to the change in the device (or sensing) parameter, in this instance, the interelectrode spacing (microns). The combination of diamond cathode in Fowler-Nordheim emission has demonstrated a higher sensitivity factor than reported for, e.g., silicon vertical field emitters [205-206].

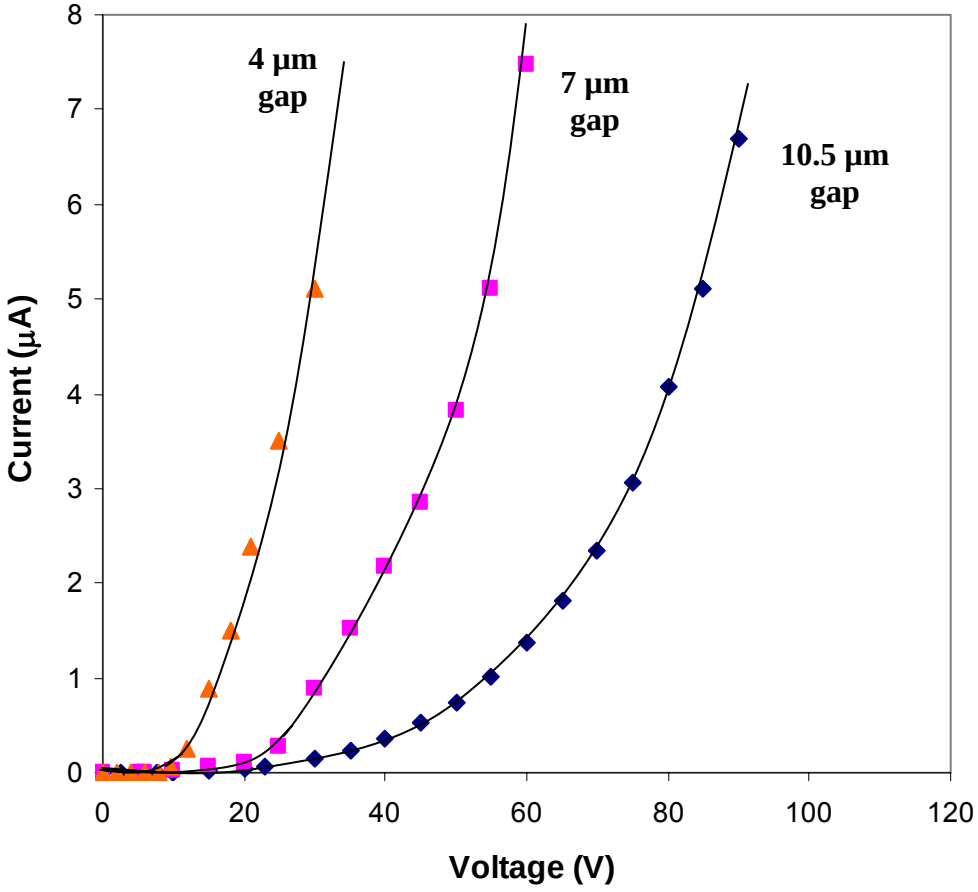

Figure 6.22 Field emission (I-V) characteristics exhibited by the nanodiamond lateral field emission devices with different anode-cathode spacings.

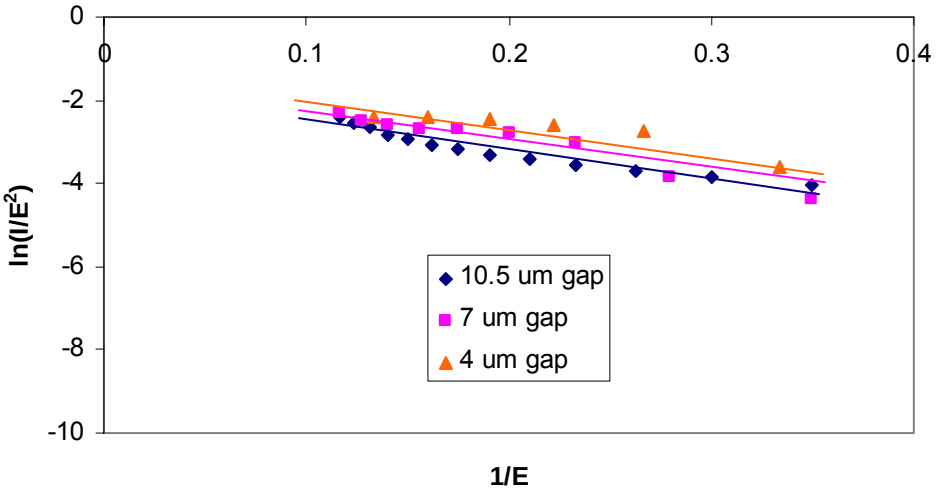

Figure 6.23 Fowler-Nordheim behavior of the three nanodiamond lateral field emitters with different interelectrode separation.

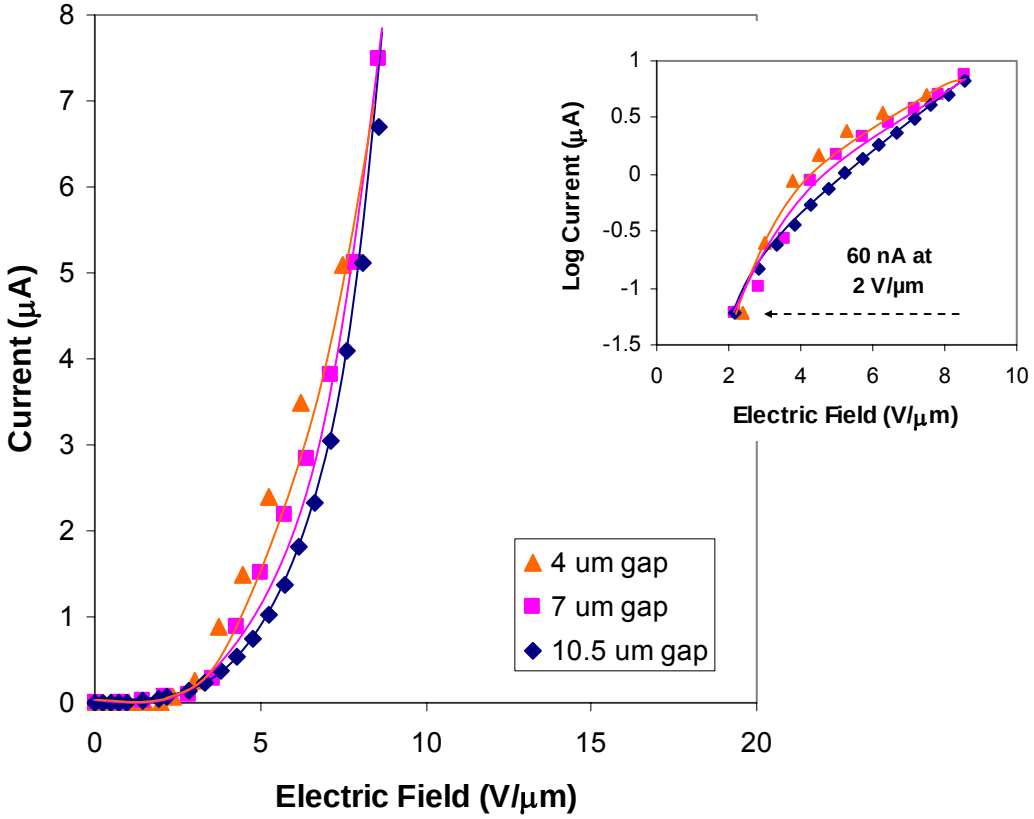

Figure 6.24 Virtually unchanged field emission (I-E) characteristics obtained from the lateral vacuum devices; inset is the semi-logarithmic plot showing the turn-on electric field of ~ 2 V/μm for the three diodes.

According to Fowler-Nordheim theory, the emission current is correlated with the electric field strength (E), which is a function of the anode-cathode distance (d) for a fixed applied voltage (V), given by the equation $E=\beta(V/d)$, where β is the field enhancement factor. This effect can be utilized for efficient sensing applications. For example, deformation caused by pressure, vibration, or acceleration can result in a variation in the interelectrode distance and thereby the electric field, leading to a change in the emitted current. **Figure 6.25** illustrates an approach using the lateral device, where the deflection of a cantilever can be transduced into electrical current signals by means of field emission. Sensors and NEMS based on this detection principle can offer several advantages such as high sensitivity and measurement range, operational

temperature and radiation immunity over conventional capacitive, piezoresistive, or piezoelectric sensors. Field emission sensing has been studied previously [207-211], but achieving a linear scaling relationship of the emission behavior with the separation distance between the electrodes is a challenge. The sensitivity of the nanodiamond lateral emitter device to the interelectrode spacing, along with its ease of fabrication and integration with on-chip circuitry, low voltage operation, and high frequency sensing capability, implies a novel IC-compatible candidate for "smart sensors".

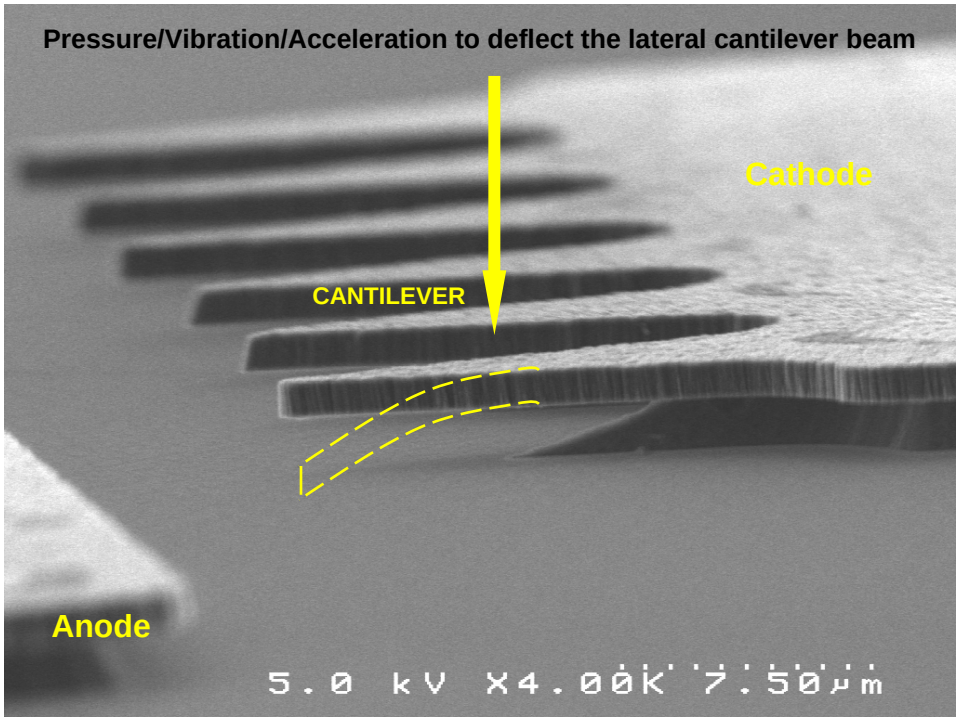

Figure 6.25 Illustration of a cantilever sensing application based on the effect of anode-cathode distance on field emission in a monolithic nanodiamond lateral vacuum microelectronic device.

Further, this exhibited dependence of the turn-on and operating voltages on the anode-cathode spacing indicates the strong potential for achieving an ultra-low voltage vacuum diode, when a nanoscale-gap is achieved in the lateral device structure.

(h) Emission current stability characteristics of the nanodiamond lateral device

The emission behavior of the nanodiamond lateral emitter was found to be repeatable and stable over time. An idea of the emission stability of the lateral device can be obtained from **Figure 6.26**, with a current fluctuation of ~ 2 % over a time period of 80 min under a vacuum of 10^{-6} Torr for a given applied electric field. No monotonic current decrease with time is observed. The electron emission stability was found to be reasonable even at high current, with the fluctuation value about 4 % at an emission current of 1 mA maintained over 10 hours. The observed current fluctuation is considerably smaller than the fluctuation of 50 % at the emission current of approximately 1 μA from a typical single silicon tip [212]. **Figure 6.27** presents the high current stability (I-t) plot obtained from the nanodiamond lateral emitter array diode.

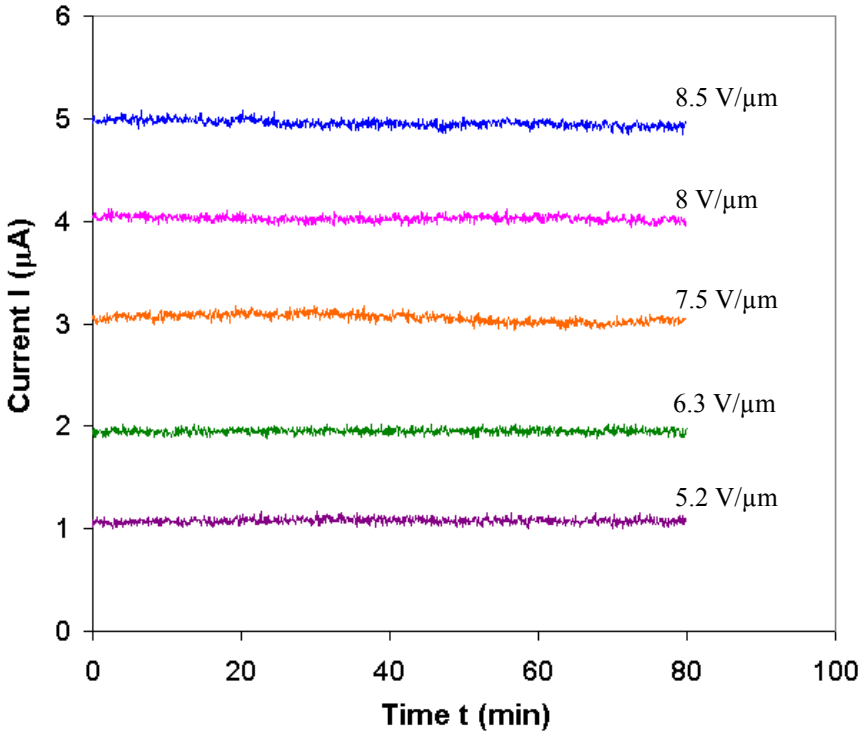

Figure 6.26 Current-time plots extracted from a nanodiamond lateral field emitter at various applied electric fields depicting its emission current stability over time.

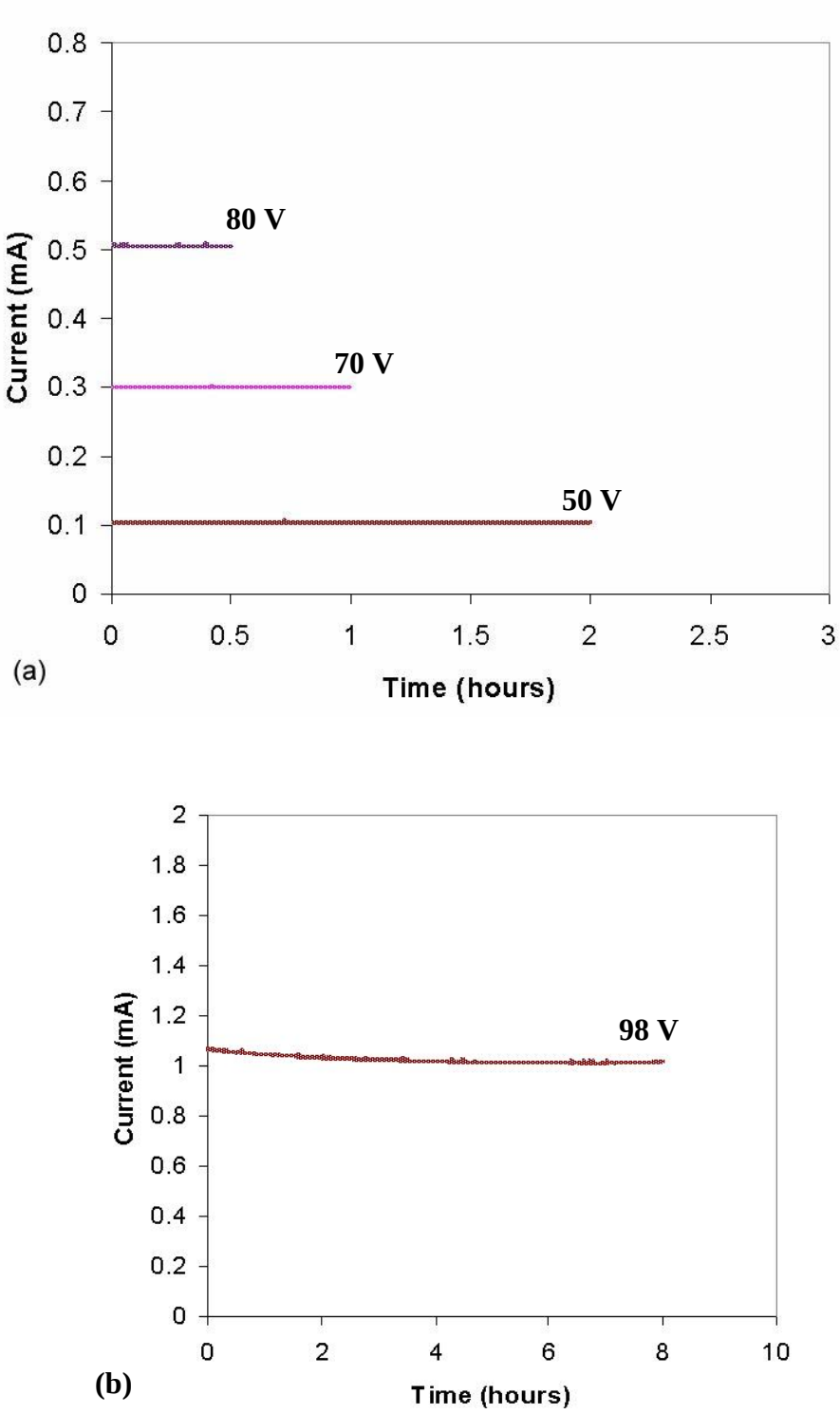

Figure 6.27 High current stability (I vs. t) plots: (a) nanodiamond lateral emitter array diode at several hundreds of μA emission currents at various anode voltages during device operation; (b) nanodiamond lateral vacuum diode at 1 mA for 10 h at a constant anode voltage of 98 V.

(i) Nanodiamond lateral VFEM technology for harsh environments

Orvis *et. al* [29] state that "the usefulness of miniature vacuum tubes will derive mainly from their radiation and temperature tolerance." They point to potential applications in nuclear reactor instrumentation, accelerator instrumentation, and space power systems. Gray also speculated on the radiation hardness of vacuum microelectronic devices [213]. However, little if any actual experimental data on the radiation response of vacuum field emission microelectronic devices has been published. Through this research, we have developed the first vacuum field emission microelectronics (VFEM) technology, with the diamond lateral device, capable of operating efficiently at both low and high temperatures (350 °C), with an inherent "hardness" to radiation exposure as high as 20 Mrad(SiO_2) total dose and $4.4x10^{13}$ neutrons/cm^2, signifying an emerging electronics for extreme environment.

Sensitivity to high temperatures and radiation in solid-state electronics is caused by bulk generation of charge carriers in the active regions of the devices [29]. These charge carriers can cause transient artifacts in the operation of the device (soft errors), and in some cases, permanent damage (hard errors). Most electrical properties in silicon solid-state devices are temperature-dependent. Likewise, radiation damage observed in these devices has been attributed to electron-hole pair generation, lattice displacement, and carrier removal effects [16]. With vacuum as the active volume (signal carrier medium), a field emission device is not susceptible to thermal- or radiation-induced bulk carrier generation or permanent damage by exposure to radiation. There can be carrier generation or damage involving other parts of the device that may be injected into the vacuum, but this will be a small effect, which can be minimized by proper device design and material choice. Particularly, with the electron emitter being diamond, a wide band-gap material

with high thermal conductivity and mechanical hardness, a diamond field emission device has suitable elements for achieving operational high temperature and radiation immunity.

Temperature tolerance characteristics: To evaluate the *temperature insensitivity* of the nanodiamond lateral VFEM, several of the nanodiamond lateral diodes were subjected to temperature testing in a vacuum chamber maintained at 10^{-7} Torr. With the device seated on a heated stage, the operating temperature of the diode was measured and controlled by means of thermocouple feedback at close proximity of the device. **Figures 6.28 (a)** and **(b)** depict the temperature response of two different nanodiamond lateral field emission diodes operating at various temperatures upto 200 °C. No leakage current via the SiO_2 layer was observed in the emission current and the electrical behavior of the diode was unaffected by the varied temperatures. Note the total *independence* of the device forward current on temperature, which signifies the operational temperature immunity of the nanodiamond lateral vacuum device. The corresponding linear Fowler-Nordheim (F-N) plots, as seen in the inset of the two graphs, confirm that the observed current is attributable to field emission. Though the operational temperature immunity of the diamond lateral device has been tested here only up to 200 °C, it is expected that the diode characteristics will be unaffected up to an ambient temperature of ~ 600 °C, at which, *thermionic* controlled emission may overcome the *field* controlled emission and change the diode characteristics. The results presented in **Figure 6.28** and earlier in **Figure 6.21** (temperature tolerance behavior upto 350 °C) demonstrate the performance offered by the nanodiamond lateral vacuum device for high temperature electronics.

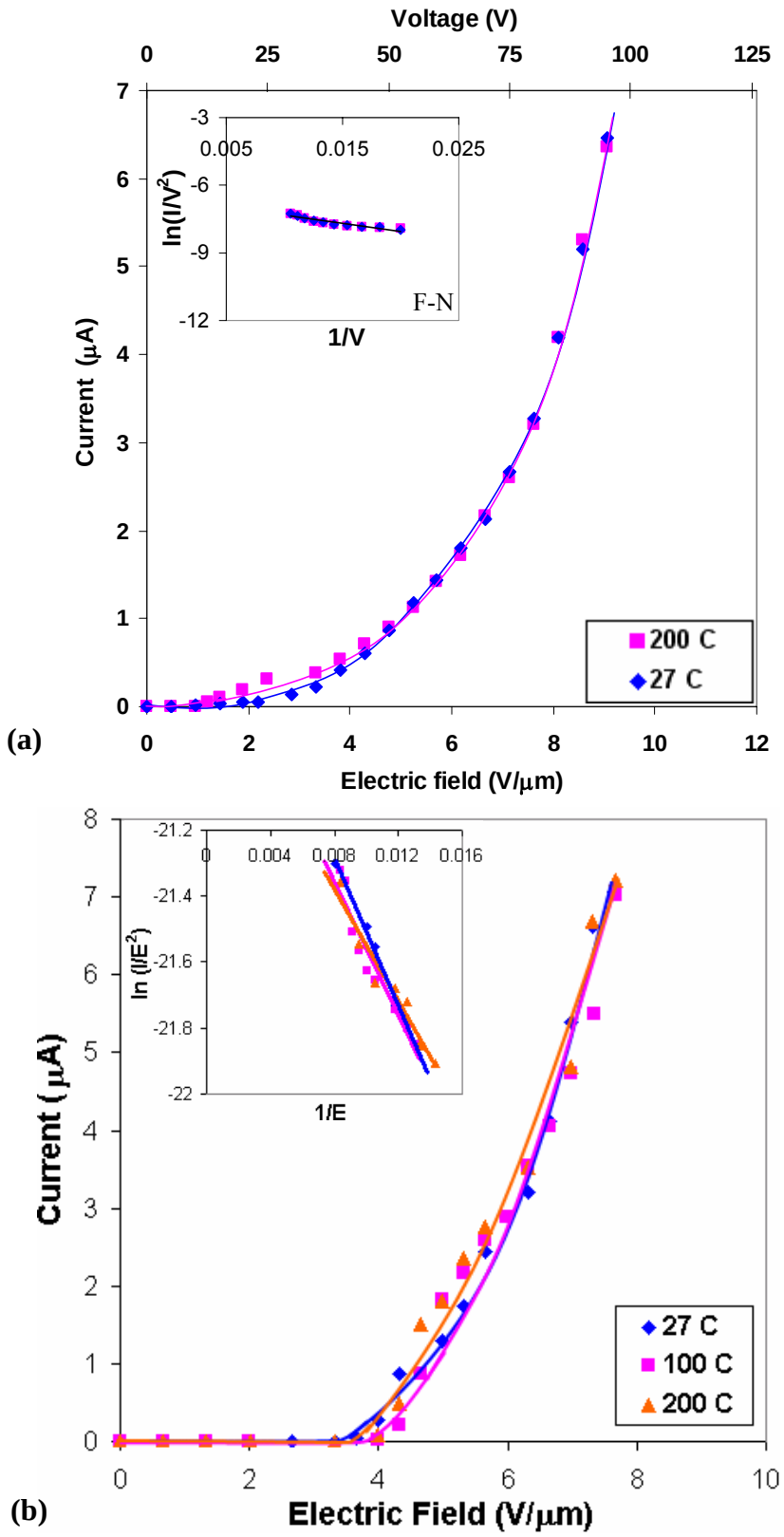

Figure 6.28 Typical temperature insensitivity characteristics exhibited by the nanodiamond lateral vacuum field emission diodes.

Radiation tolerance characteristics (X-ray exposure experiment): Total dose *radiation hardness* tests were conducted on two nanodiamond lateral diodes, separately. Irradiation was performed with an ARACOR 10 keV x-ray source at a dose rate of 31.5 krad(SiO_2)/min. Incremental irradiations were carried out to achieve total doses of 1,5, and 15 Mrad(SiO_2). A bias of 2 V was applied to the diodes during the radiation exposure. **Figures 6.29** and **6.30** show the results of x-ray irradiation on the devices. Essentially no changes in I-V characteristics are observed as a function of total dose. And, the radiation dose has no effect on the diode turn-on voltage.

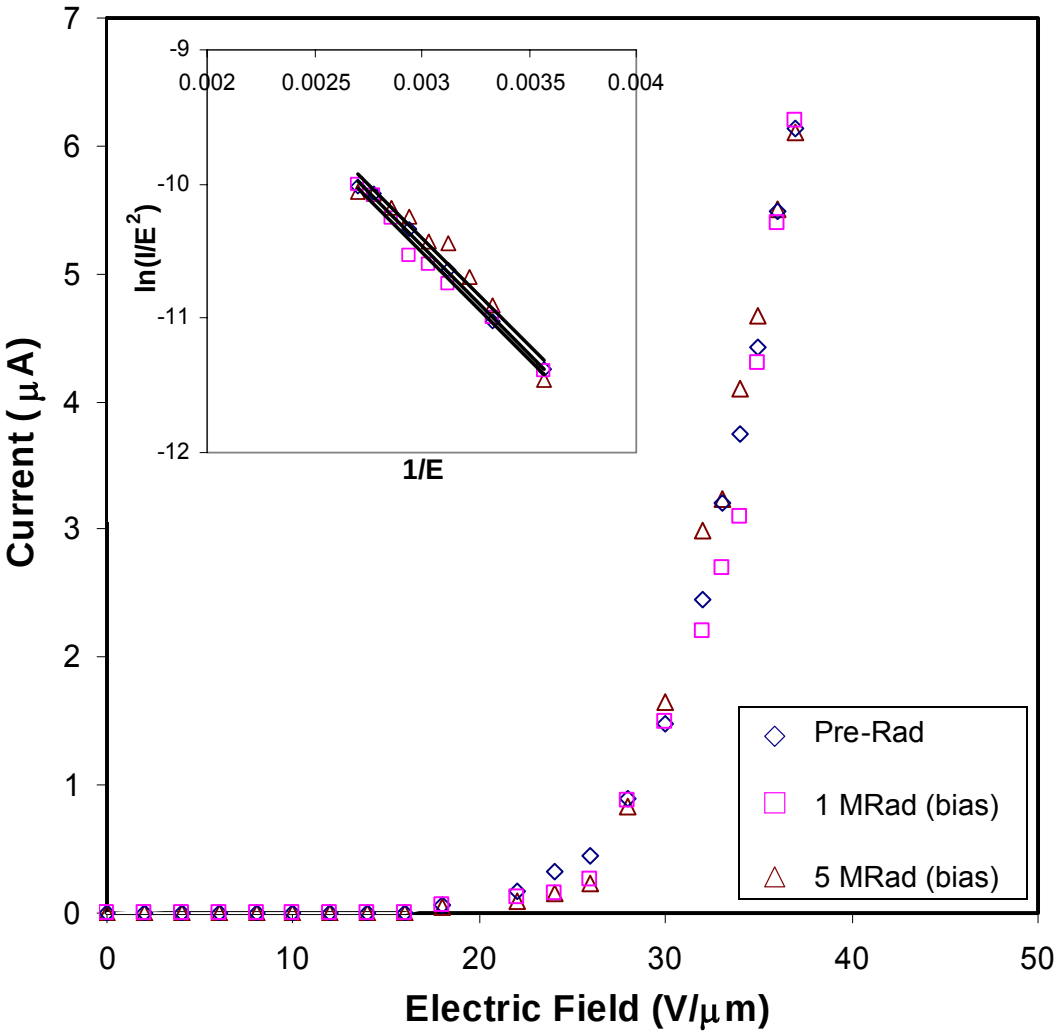

Figure 6.29 Field emission behavior of the nanodiamond lateral diode (Pre-Rad, 1, 5 Mrads); inset: corresponding F-N plots.

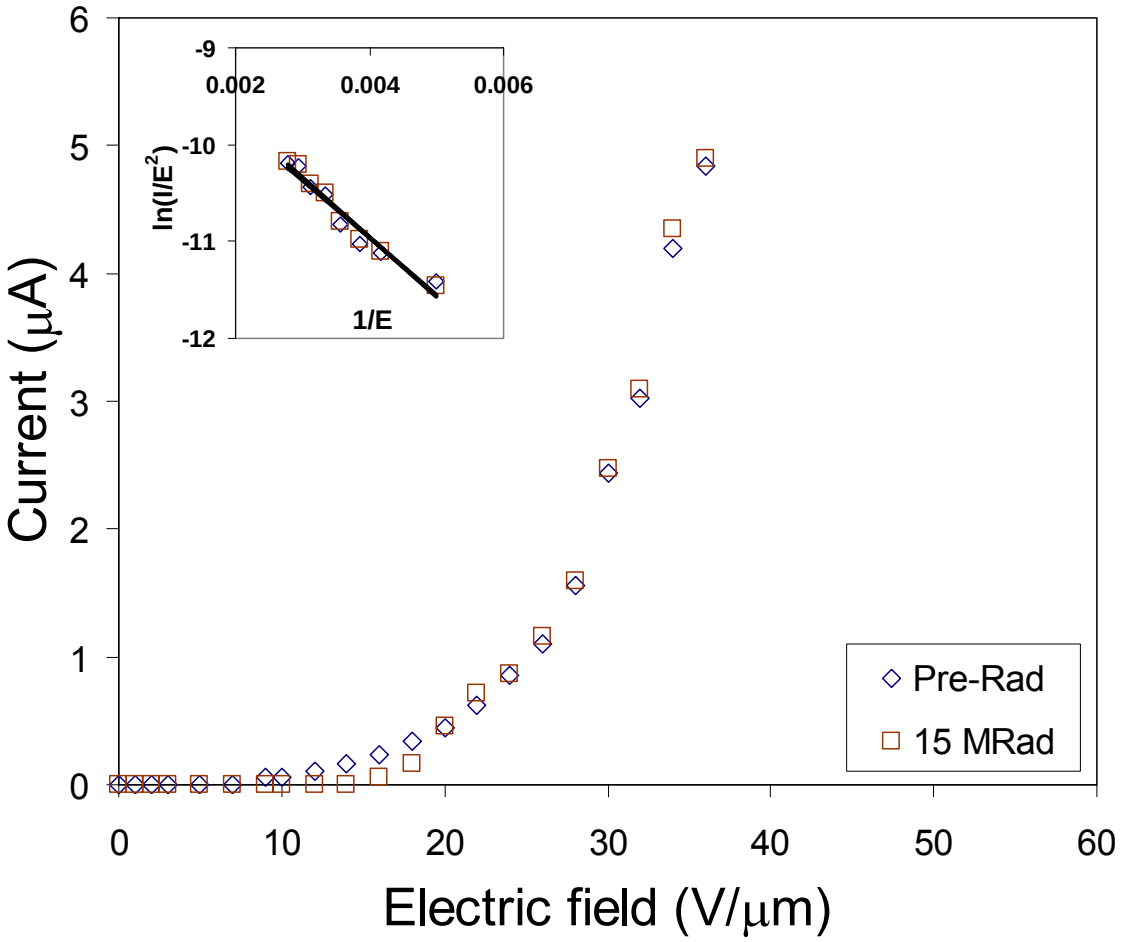

Figure 6.30 Field emission behavior of the nanodiamond lateral diode (Pre-Rad, 15 Mrad); inset: corresponding F-N plots.

The negative linear slopes of the FN plots (inset of **Figures 6.29** and **6.30**) indicate that the emission data conforms to field emission behavior. Moreover, the linear slopes remain unchanged as a function of radiation dosage confirming the irradiation caused no change in work function or field enhancement factor of the emitting surface.

Figures 6.31 (a) and **(b)** show the emission current of the diode as a function of irradiation, using an average dose rate of 31.5 krad(SiO_2)/min, operating at several applied

electric fields. The data confirms the field emission behavior of VFEM is indeed insensitive to irradiation.

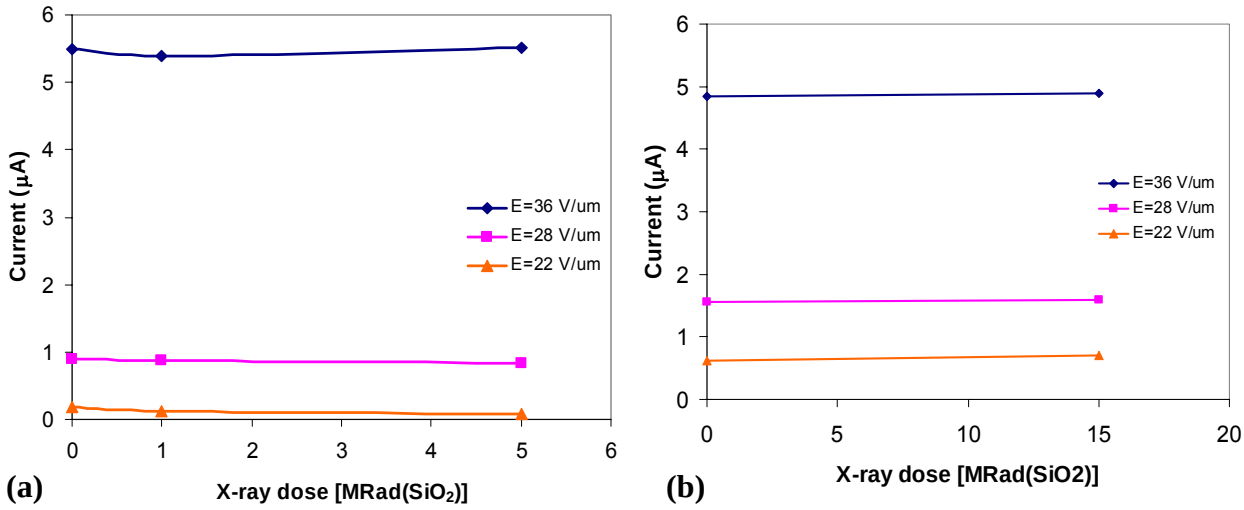

Figure 6.31 Change in diode emission current as a function of total ionizing dose at 31.5 krad(SiO_2)/min.

Since the nanodiamond lateral VFEM is fabricated on a SOI substrate, C-V measurements of the SOI structure were made to investigate the effect of charge trapping in the SiO_2 layer and its subsequent effect on VFEM performance. **Figure 6.32** shows the C-V characteristics of the SOI structure before and after 10 Mrad(SiO_2) irradiation. It can be observed that the absolute value of the capacitance has changed, which shows that significant radiation-induced hole trapping has occurred in the buried oxide and SiO_2-Si interface. The post-radiation C-V measurements indicate fast-trapped mobile charges in the SOI substrate However, this disturbance does not affect the performance of the nanodiamond lateral VFEM (**Figures 6.29-6.31**), which operates on the SOI substrate.

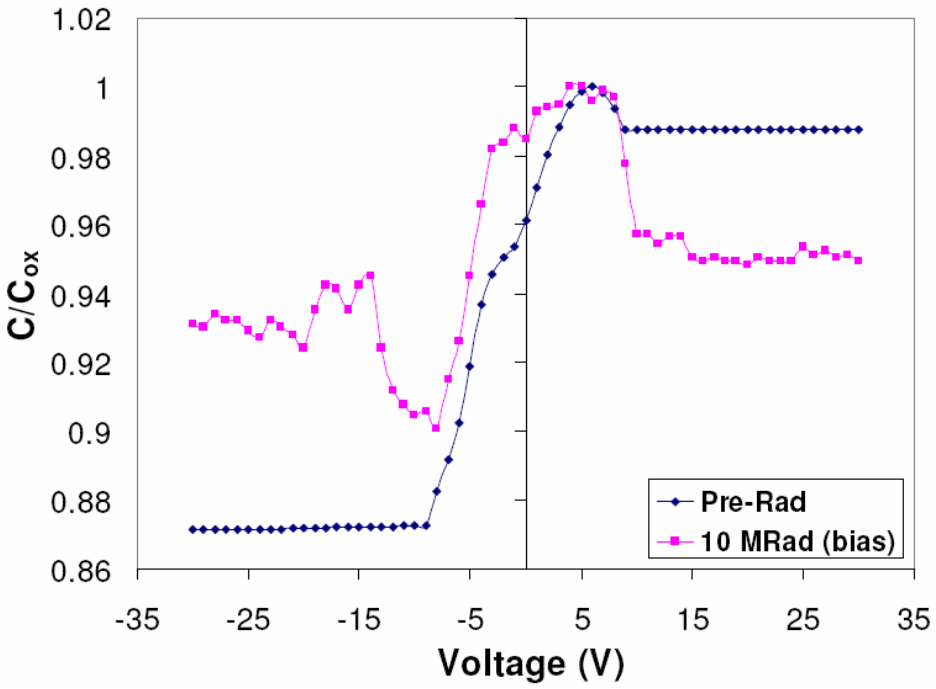

Figure 6.32 C-V plot of SOI structure; Pre-Rad and 10 Mrad(SiO_2) irradiation.

Radiation tolerance characteristics (Neutron exposure experiment): We have also performed neutron irradiation on the nanodiamond lateral emitter devices for their possible application in very high fluence neutron conditions. The devices were examined in the SEM and measured electrically under vacuum before and after exposure to high fluences of neutrons. Neutron irradiation was conducted at the U. S. Army White Sands Missile Range Fast Burst Reactor. One set of the diamond lateral devices was subjected to a total fluence of 1.25(10^{12}), (> 3MeV was 1.46(10^{11}) and a second set of devices was subjected to a higher total fluence of 4.4(10^{13}), (> 3MeV was 5.6(10^{12}), neutrons/cm^2.

The devices were subsequently examined via SEM for any noticeable material post-rad alterations such as expansion or contraction, and then for any change in resistivity or electrical performance. Although prior work on a polished sapphire surface [214] indicated expansion

upwards of a micron due to 1 dpa, as detected with a *Dectac* microstylus mechanical profiler (1 displacement per atom (dpa) is equivalent to about $1(10^{21})$ 14 MeV neutrons/cm^2), no discernable difference in physical size or appearance of the diamond devices was observed in the SEM, post fluence examination. Given that the diamond lateral emission structures are very sensitive to the cathode to anode spacing, any dilation (expansion or contraction) in the material should result in a change in the emission current as a function of field (voltage). This could provide a means of conducting reproducible dosimetry in very high neutron fluences. However, no change in resistivity of the film pre vs. post exposure was observed. Likewise, no significant difference in the I-V behavior was observed before and after neutron exposure, the current at higher voltages being identical pre vs. post radiation, as typically seen in **Figure 6.33**. The small difference at very low currents is within measurement variations for the device.

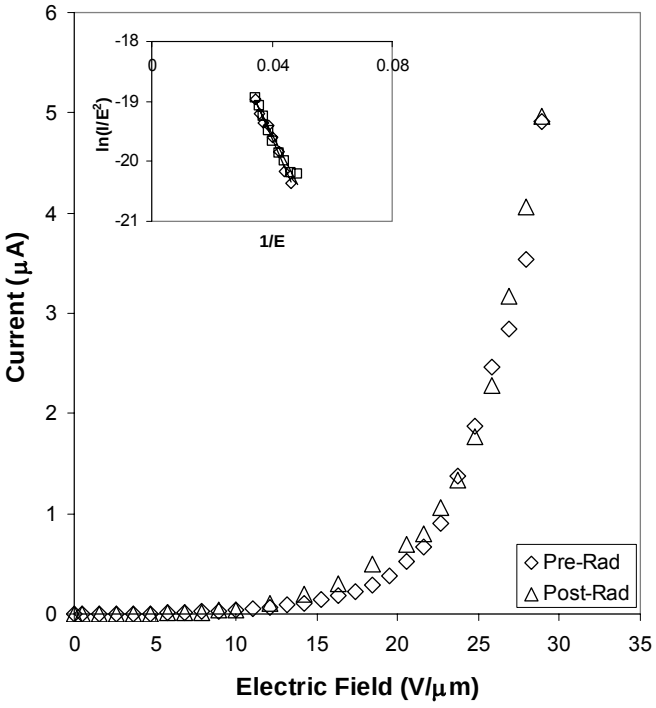

Figure 6.33 Field emission behavior of a nanodiamond lateral diode before and after neutron irradiation; inset: Corresponding F-N plots.

We have performed the first total dose and neutron exposure tests on nanocrystalline diamond lateral vacuum field emission microelectronics (VFEM) technology. No measurable change was observed in the diode device response after 15 Mrad(SiO_2) total dose and $4.4x10^{13}$ neutrons/cm^2 radiation exposure. Radiation hardness was also observed in the vacuum transistor, when a gated nanodiamond lateral device was subjected to 20 MRad total dose (x-ray) exposure and characterized for field emission, results presented in **Figures 6.39** and **6.40**. This is consistent with the analysis and speculations of others. Adams and Holms-Siedle [215] estimate that VFEM devices can withstand conditions as high as 10^{13} rads(SiO_2), 10^{22} n/cm^2, and 10^{13}rad/s stating that "At these values, there will be some swelling of materials and uncontrolled electron emission." The data presented here indicates that nanodiamond VFEM devices are *very resistant to radiation* and *high temperature* exposure, and that the technology is well-suited for application in harsh environments, encountered in radar, electronic warfare and space-based communication systems, and also in extreme-demand terrestrial electronics, where solid-state devices are impractical or inconvenient due to their inherent sensitivity to hostile environments.

Present solutions for "rad-hard" ICs are to use a radiation shielding material, or to apply hardened fabrication techniques or SOI substrates for the solid-state devices, which have been shown to reduce radiation-induced failures. These methods require very conservative circuit design techniques to take into account the maximum predicted radiation damage (i.e., threshold voltage shifts due to radiation damage). Also, a more brute-force approach of built-in self testing (BIST) and redundancy is used to mitigate the failures due to radiation, which increases the complexity and power consumption of any given system, without actually addressing the problem of radiation damage [216]. With a vacuum channel for signal propagation, vacuum microelectronic devices are relatively immune to radiation damage, making them suitable for

high radiation environments. Further, there are crucial applications, such as aircraft and machine sensing applications, requiring high temperature operation. Currently, high temperature sensing requires the electronics to be placed in a shielded location away from the sensor, reducing the system efficiency and accuracy. Fuel cooling is often used in aerospace to cool these electronics. It has been estimated that high-temperature stable electronics on an F-16 fighter, would bring about savings in the order of hundreds of pounds of weight and millions of dollars per aircraft [217]. Diamond Vacuum Microelectronics has shown the potential for much higher temperature stability than silicon and SiC based devices. This immunity to high temperature can allow closer placement of the device for high temperature measurements and also reduced need for heat transfer accessories (heat sinks, etc) in power electronics.

Thus, the material system and device construct of the nanodiamond lateral field emission vacuum device is relevant for extremely hardened electronics and can be beneficial to the scientific, defense, and commercial high-temperature and *rad-hard* communities.

(j) Rectification behavior of the nanodiamond lateral field emission diode

As mentioned in item (b) of this section, by comparing the field emission characteristics of different nanodiamond lateral emitter geometries, the superior geometrical field enhancement of the high aspect-ratio finger-like emitter structure over the edge structure has been established experimentally. When these structures are combined to form an all-diamond diode, with the 6-finger emitter as cathode and the straight edge as anode, the rectification factor was found to be ~ 26. A non-diamond straight edge anode in the lateral device configuration can help realize a field emission diode with higher rectification factor with negligible or no reverse emission current, since it gives the nanodiamond cathode a superior field enhancement factor materially as well as geometrically. Nickel with a high work function (Φ=5.15 eV) was considered a suitable choice for the anode material, and the nanodiamond lateral diode was fabricated using the dual-mask micropatterning methodology described in the previous chapter.

Figure 6.34 shows the field emission diode characteristics of a 6-finger *2-material* lateral vacuum device (diode structure shown in **Figure 5.27**). Under forward bias, the diode shows a reasonable threshold electric field, and an emission current over 5 μA extracted from the nanodiamond emitter at an electric field of ~ 8 V/μm. No measurable emission from the nickel, or leakage current, was observed under reverse bias condition at the corresponding applied electric field. The emission was found to obey F-N behavior, per the linear F-N plot with negative slope, inset of **Figure 6.34**. The shallow slope is indicative of a high β factor of the nanodiamond emitter of the lateral device.

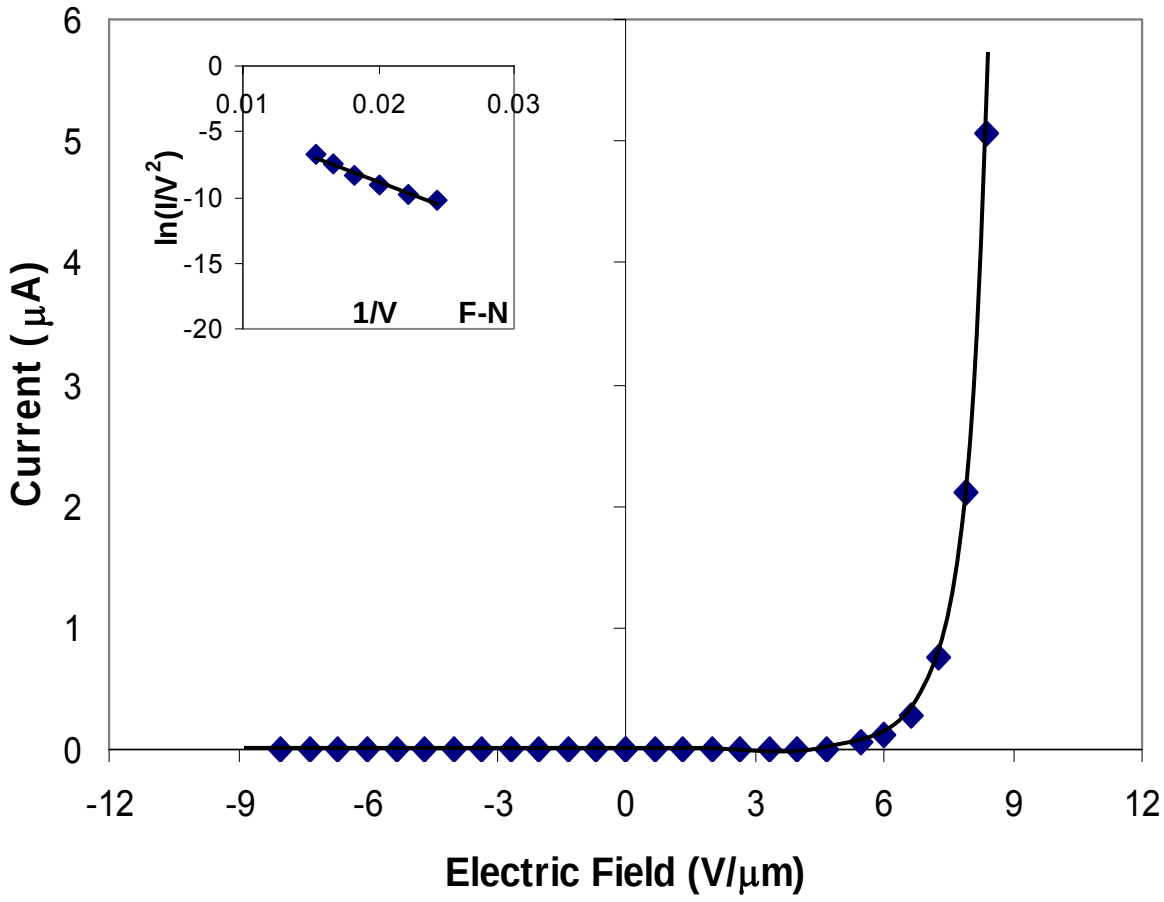

Figure 6.34 Rectifying diode behavior obtained from a lateral vacuum diode with nanodiamond 6-finger emitter array as the cathode and nickel as the anode; inset: corresponding F-N plot.

These diode characteristics demonstrate that the nanodiamond lateral device with the non-diamond anode configuration can perform as an excellent diode with rectification ratio $>10^4$, suitable for practical microelectronic circuit applications.

6.2.3 Field emission characteristics of monolithic nanodiamond lateral vacuum triodes

Field emission diodes and triodes are critical building blocks in the development of ultra-fast, temperature- and radiation-immune vacuum microelectronics. Having examined the nanodiamond lateral device as a vacuum diode, the research was continued to study the device in a triode configuration. Lateral triodes with a gate-cathode spacing as small as 2 μm, and anode-cathode spacings ranging from 10 μm to 1 mm were developed. The different three-terminal lateral configurations were tested to investigate the triode characteristics of the device. It was identified that the position of the electrodes in the device design plays a significant role in determining its characteristics.

The functionality of the lateral emitter device as a *triode* or a *transistor* could be manipulated by lithographically altering the design of the three-terminal structure. The lateral anode, when placed closer to the cathode (~ 10 μm) can induce the electron emission and result in gate-modulated *triode* characteristics. By moving the anode farther (> 100 μm) from the cathode and gate electrodes, the anode effectively acts as a collector, with the gate, owing to a very small cathode-gate gap (≤ 2 μm), principally controlling the electric field at the emitter finger-tip and significantly shielding the collector field from the emitter, leading to *transistor*-type characteristics. The operation of the nanodiamond lateral field emission device in triode and transistor modes is described in this section.

(a) Vacuum triode characteristics

A 1-finger nanodiamond lateral microtriode with 3 μm gate-cathode and 12 μm anode-cathode spacings (device structure shown in **Figure 6.35 (a)**) was characterized for electron field emission in a vacuum condition of 10^{-6} Torr. The gate electrodes are separated laterally by an

equal distance of 3 μm from the cathode to have effective emission modulation at low gate voltages, while minimizing intercepted gate current. The device was operated similar to the classical thermionic triode, where the electron emission from the cathode is induced by the anode and modulated by the gate electrode. The only difference in this case is the gate voltage modulates the electric field at the emitter tip and hence the tunneling probability, whereas in the thermionic triode, the gate controls the space charge near the emitter. **Figure 6.35** shows the I-V characteristics of the triode device as a function of the gate and anode biasing voltages. The gate-controlled current modulation behavior is clearly observed, whereby higher applied gate voltages give rise to higher emission currents induced by a given anode voltage. A large anode current of ~ 4 μA was thus obtained from a single nanodiamond lateral emitter at an anode voltage of ~ 65 V, when the gate bias was 40 V. The low applied electric fields required to initiate and modulate the electron emission between the electrodes are attributed to the geometry and material composition of the nanodiamond lateral emitter. For a given anode voltage, the anode current was found to change by more than an order of magnitude with a ±10 V alteration in the gate bias. The transconductance, g_m, relates the current driving capability, voltage gain, and high frequency response when the diamond triode is operated as an amplifier. It is defined as the change in the anode current due to a change in the gate voltage at a given anode voltage:

$$g_m = \left.\frac{\partial I_a}{\partial V_g}\right|_{V_a=\text{const}} \tag{6.7}$$

This transconductance parameter was determined to be ~ 0.3 μS at V_a=65 V, one of the highest reported for lateral-type devices involving a single emitter, especially with the cathode-gate separation in microns. This value can be further improved by applying a larger nanodiamond

finger array as emitter. The g_m was also found to increase exponentially with V_g, as the device electron current is strongly affected by the gate voltage.

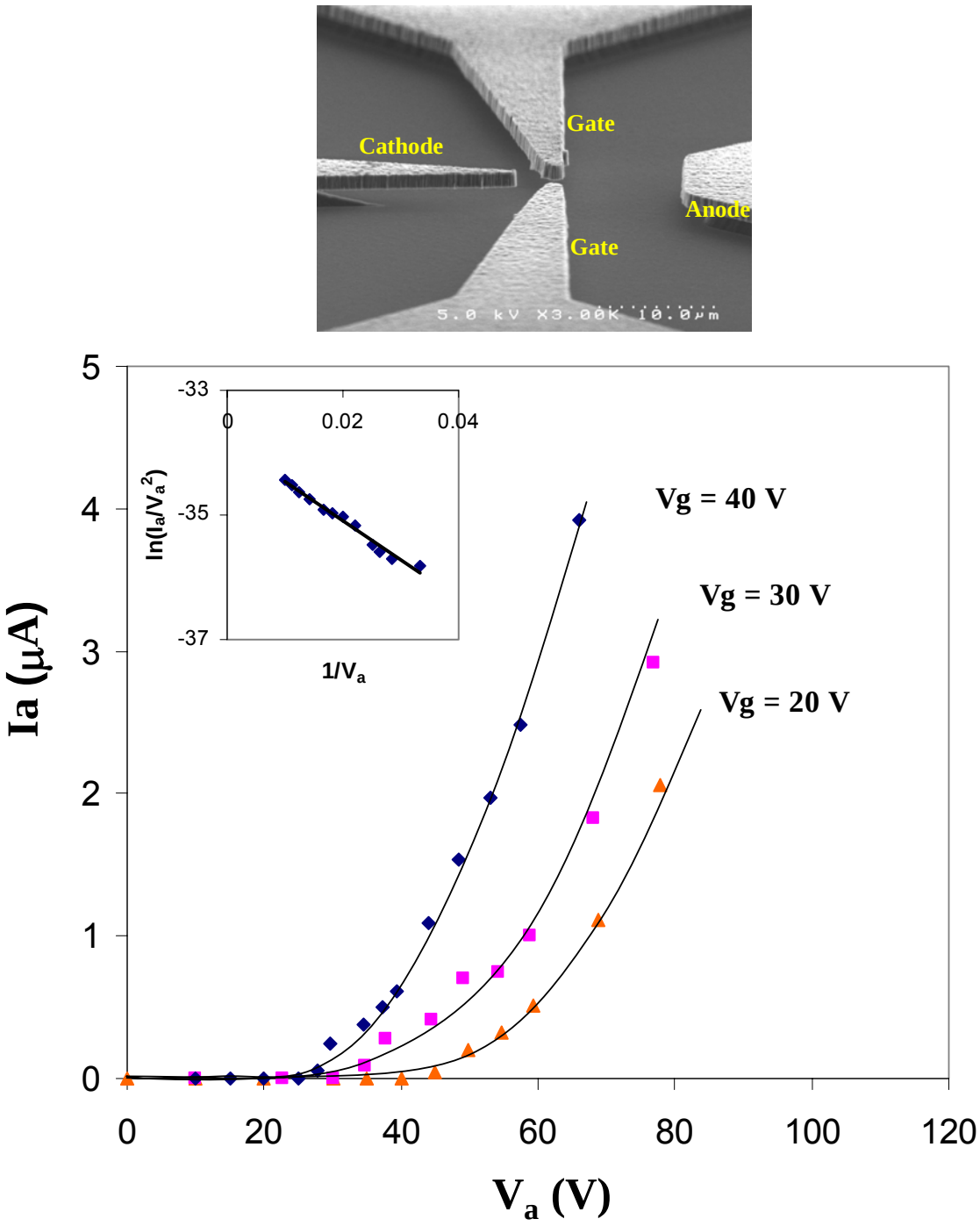

Figure 6.35 (a) Structure of the integrated nanodiamond lateral field emitter vacuum microtriode with 3 µm gate-cathode and 12 µm anode-cathode spacings; (b) Triode characteristics of the 1-finger lateral device; inset: F-N plot of one of the I-V curves shown in the main figure.

The device characteristics were found to follow Fowler-Nordheim relationship (inset, **Figure 6.35**), which confirms that the extracted anode current is due to the field emission mechanism. For optimum device performance, the gate-intercepted current must be small relative to the anode current. Operation in triode mode can allow for a low gate current, especially for negative and moderate positive gate voltages. The gate current for this lateral triode was below the measurable limit of 0.1 nA. The achieved triode device behavior is congruent with the simulated electrical characteristics [90] reported from lateral field emitter triodes, where an increase in gate voltage leads to a subsequent increase in the anode current, owing to the enhancement in the electric field at the emitter tip.

(b) Vacuum transistor characteristics

The demonstration of a lateral field emission transistor at microelectronic scale is essential to the development of the vacuum IC. Transistor characteristics have been reported from *vertical* emitter devices utilizing different cold cathode materials [164-166,218-220]. This work involves the development of a vacuum transistor, designed and fabricated in a completely integrated, planar, lateral configuration, achieving an advanced, alternative electron device.

A 1-finger nanodiamond lateral device with 2 μm gate-cathode and 500 μm anode-cathode spacings (device structure shown in **Figure 5.18 (c)**) was tested under vacuum for dc field emission characteristics in a common emitter amplifier configuration. The device was operated in a gate-induced emission mode, with the anode (collector) potential contributing an insignificant component to the electric field at the tip of the emitter-finger. A positive gate voltage (V_g) was applied on the gate electrode to extract electrons from the emitter and a fixed voltage (V_a) was applied to the anode to collect the emitted electrons. The anode emission

current (I_a) was then recorded as a function of the anode (collector) voltages while holding the gate voltage constant. The measurements were repeated for different V_g to obtain a family of I_a-V_a-V_g curves. **Figure 6.36** shows the dc characteristics curves of the lateral vacuum device. Gate-controlled current modulation behavior was clearly observed, whereby higher applied gate voltages, by means of field enhancement at the emitter-finger tip, gave rise to higher emission current collected by the anode. The gate turn-on voltage was 40 V, defined as the voltage required to obtain 1 nA of emission current from the 1-finger cathode. Saturation of the collector currents was observed at anode voltages above ~ 180 V, where the current stays constant, independent of the applied collector voltage. Overall, the field emission data demonstrated basic transistor characteristics of the nanodiamond lateral device with distinct cutoff, linear, and saturation regions in a triode configuration.

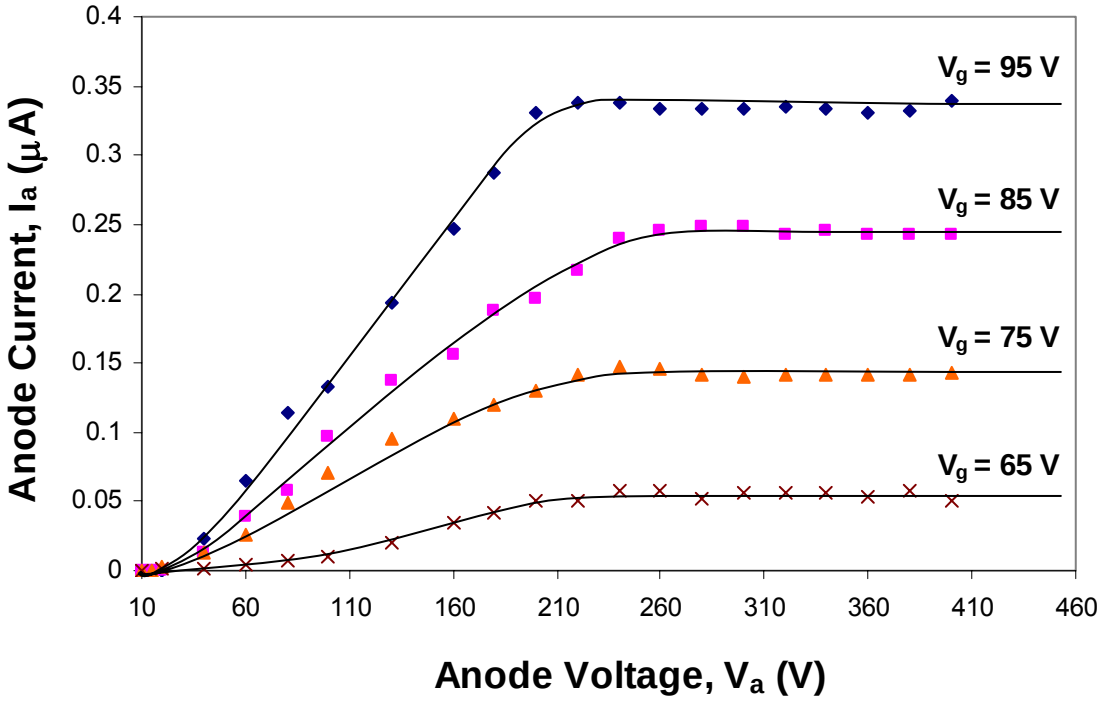

Figure 6.36 DC transistor characteristics of the nanodiamond lateral field emission device.

A plot of gate voltage vs. anode emission current of the transistor is shown in **Figure 6.37**, neglecting the effect of the applied anode voltage. The linearity of the corresponding FN plot (inset, **Figure 6.37**) indicates that the electron emission is induced by the gate voltage and the anode acts exclusively as an electron collector, due to the close proximity of the former to the cathode in the device design. Hence, a positive amplification factor can be expected of the transistor amplifier. The negative linear slope of the FN further indicates that the device current is due to the field emission tunneling mechanism. A large anode current of 1.1 μA was obtained from the 1-finger nanodiamond emitter device, with the macroscopic current density calculated to be ~ 1 A/cm^2 based on the cross-sectional area of the lateral anode. Gate currents were recorded at different V_g and V_a values to interpret the trajectory of the electrons emitted from the cathode. Gate intercepted current, **Figure 6.37**, amounted to a very small (I_g/I_a) ratio of 0.001 % at gate voltages lower than 100 V, and 0.7 % at higher gate voltages. This small (I_g/I_a) ratio would maximize the power gain by permitting a substantial output current gain, and also ensure reliable long-term operation of the transistor. Also, the sum of the gate and collector currents was almost constant over the entire voltage range of the transistor characterization. The emission behavior was found to be stable over time (tested for several hours), with low fluctuations and no monotonic decrease in the current observed at given anode and gate voltages. A typical current stability plot obtained from the nanodiamond lateral transistor device is given in **Figure 6.38**. The electrical isolation integrity of the cathode-gate-anode in the monolithic transistor device was confirmed from the observation of zero leakage.

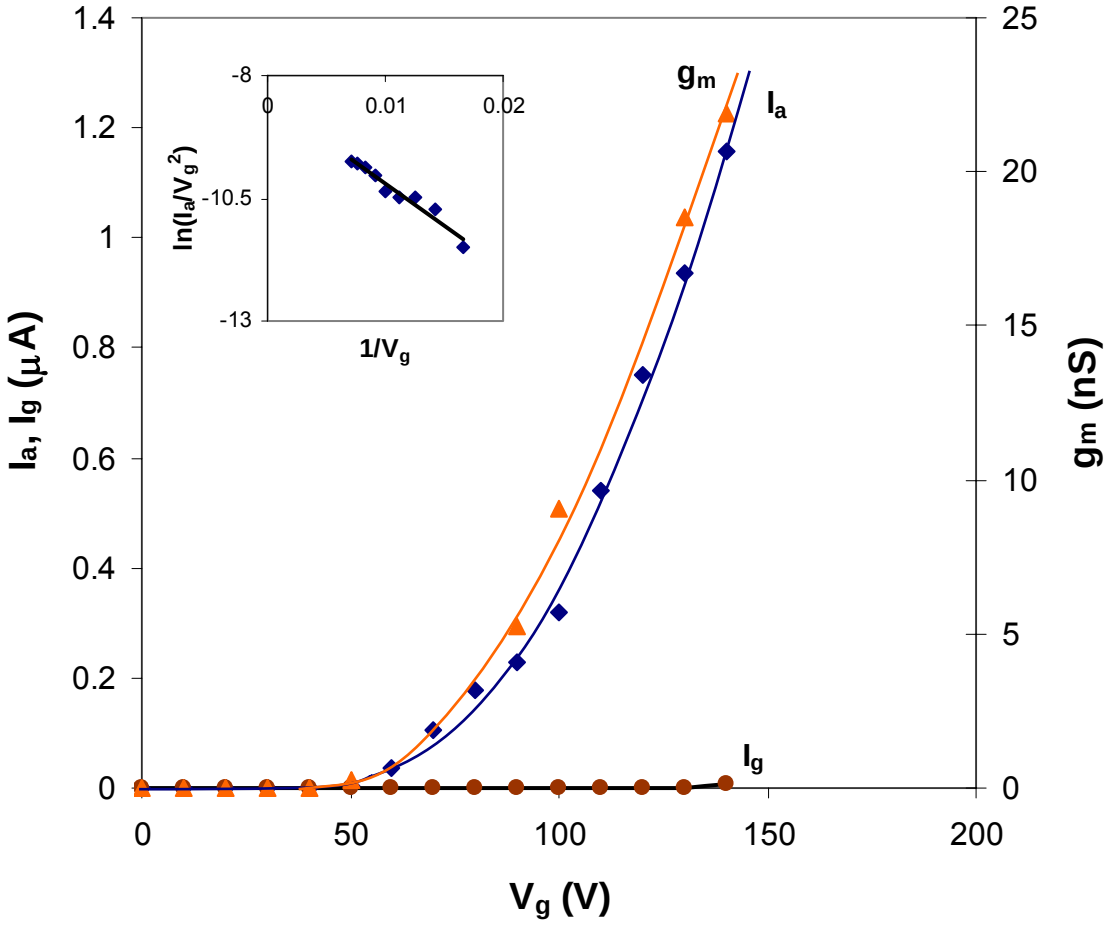

Figure 6.37 Plot of the anode currents, I_a, gate currents, I_g, and transconductance, g_m vs. the gate voltage, V_g of the nanodiamond lateral field emission transistor at an applied anode voltage, V_a=380 V (saturation region); inset: F-N plot of the corresponding data of I_a vs. V_g.

The transistor parameters of the triode amplifier were determined graphically from the dc characteristics curves. The amplification factor, μ is a parameter used to enumerate how much effect the gate voltage has on the anode emission current over anode voltage. For a vacuum field-emitter triode, the controlling gate has more influence on the electric field at the emitter than the anode due to the proximity of the gate to the cathode. Thus, the amplification factor describes

how the gate voltage influences the cathode electric field more so than the anode voltage. The amplification factor, μ is defined as the change in the anode voltage due to a change in the gate voltage at a given anode current level and μ can be expressed as:

$$\mu = -\left.\frac{\partial V_a}{\partial V_g}\right|_{I_a=\text{const}} \tag{6.8}$$

It is an important parameter for small signal amplification applications because it defines a limit for voltage gain as can be implied from the above equation. The transconductance, g_m, as defined by Equation 6.7 as ($g_m=\partial I_a/\partial V_g$), signifies current driving capability, the voltage gain, and high frequency response of the amplifier. For transistor application, the amplification factor and transconductance are desired to be high. Also, the anode or plate resistance, r_a is a parameter determining the output resistance/impedance (r_o) and voltage gain of the device. It is a measure of the effectiveness of V_a in controlling I_a and can be expressed as:

$$r_a = \left.\frac{\partial V_a}{\partial I_a}\right|_{V_g=\text{const}} = \mu/g_m \cong r_o \tag{6.9}$$

Note that the amplification factor can be expressed as a product of the anode resistance and the transconductance, $\mu=r_a.g_m$.

An estimated μ at a constant current of 0.3 μA, from **Figure 6.36**, is determined to be ~ 200, indicating this transistor can provide high voltage gain when operated as an amplifier. The g_m is found to be ~ 22 nS at V_a=380 V. This value can be significantly improved by using an array of fingers as the emitter or employing e-beam lithography to set a submicron gate-cathode gap. Higher transconductance from the 1-finger lateral diamond device is achievable, but we limited the emission current to ~ 1 μA in order to demonstrate operation of the device, not maximize collector current. Further, the g_m was observed to increase exponentially with V_g,

Figure 6.37, substantiating that the emission current is affected by the gate voltage. The anode resistance, r_a of the transistor is computed to be ~ 10 GΩ, useful in amplification applications requiring high output impedance.

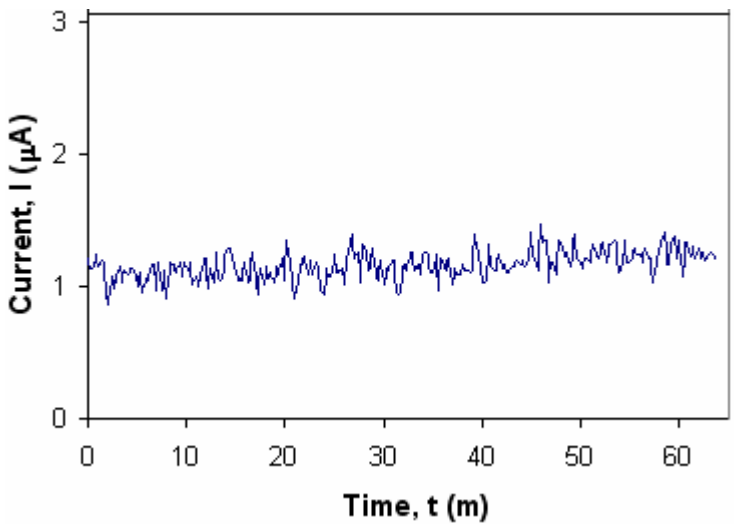

Figure 6.38 Current-time plot extracted from the nanodiamond lateral vacuum field emitter transistor at constant gate (V_g=140 V) and anode (V_a=380 V) applied voltages.

Transistor characteristics were also observed from a lateral device involving a 100 μm anode-cathode separation and the same 2 μm gate-cathode gap, with the anode current saturation occurring at a relatively lower voltage due to the decreased interdistance between the collector and the emitter in the device structure. Optimization of the lateral transistor design for lower operating voltages and higher g_m is the subject for further study. The application of diamond and the low voltage potential in the lateral vacuum transistor can allow for a practical electron device, with reduced power requirements, minimized probability of device damage due to thermal issues, and operational stability in a vacuum-sealed package.

Thus, a monolithic vacuum transistor has been developed applying the diamond lateral field emitter. The lateral device configuration facilitates device fabrication and integration, with simple and few process steps. Transistor characteristics, exhibiting good gate control and modulation of the anode current in the device, with well-defined cut-off, linear, and saturation regions have been demonstrated. An important characteristic of this diamond lateral transistor is the very flat saturation of the current that occurs with increasing anode voltages, making for ideal current-limiting devices. The negligible gate intercepted current observed can ensure reliable operation of the device. The diamond transistor shows a high amplification factor and output impedance, and with further reduction of the threshold voltage and enhancement of the transconductance, the low-capacitance property of the lateral emitter device can enable the development of IC-equivalent high-frequency amplifiers, logic gates, electronic switches, and sensors, possessing temperature- and radiation-insensitivity. Unlike a conventional solid-state MOSFET, where reduction in the threshold voltage of the device requires a decrease in the gate oxide thickness, which is accompanied by reliability issues such as increased leakage current and insulator breakdown, the turn-on voltage of the vacuum lateral emitter device is independent of the thickness of the spacer material. Simple lithography process control over the lateral gate-cathode spacing will directly regulate the threshold voltage of the vacuum transistor.

A nanodiamond lateral field emission transistor, fabricated on aluminum nitride insulator substrate (device structure shown in **Figure 5.24 (b)**), was subjected to high total dose radiation to investigate the potential of the gated vacuum device for *rad-hard* electronics. DC field emission characteristics were captured in common emitter amplifier configuration under vacuum, prior to and after x-ray irradiation to a level of 20 MRad total dose and compared. A bias of 2 V was applied between the gate and cathode electrodes during the radiation exposure.

Similar to the results achieved with the lateral diode, no effect of radiation was observed in the field emission I-V characteristics of the monolithic diamond vacuum transistor. The electrical characterization results obtained from the device are depicted in **Figures 6.39** and **6.40**. The turn-on voltage of the transistor was unaffected after exposure to radiation, while no significant change was perceived in the gate-controlled anode current modulation characteristics. Overall, the basic transistor characteristics remained *unaltered* as a function of total dose, signifying the robustness of the device in extreme operating conditions.

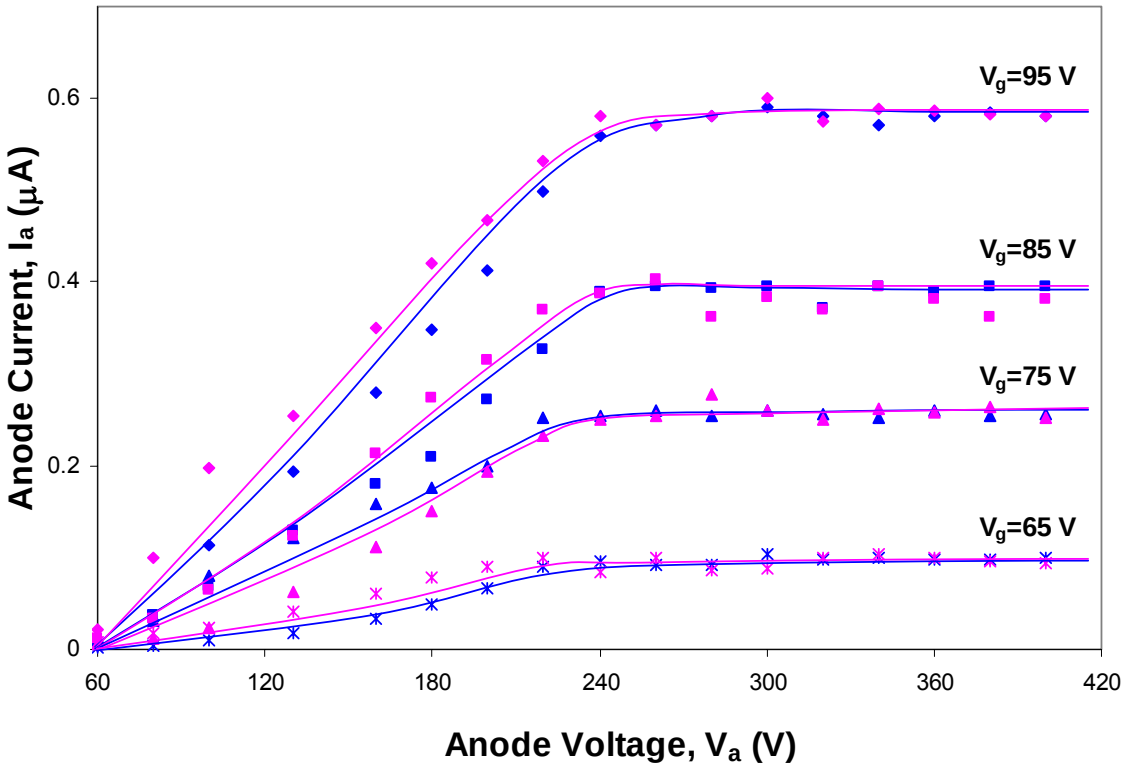

Figure 6.39 DC transistor characteristics of a nanodiamond lateral field emission device built on aluminum nitride insulator substrate before and after 20 MRad total dose x-ray irradiation; data points in blue indicate *pre-rad* I-V characteristics and points in pink denote *post-rad* I-V data.

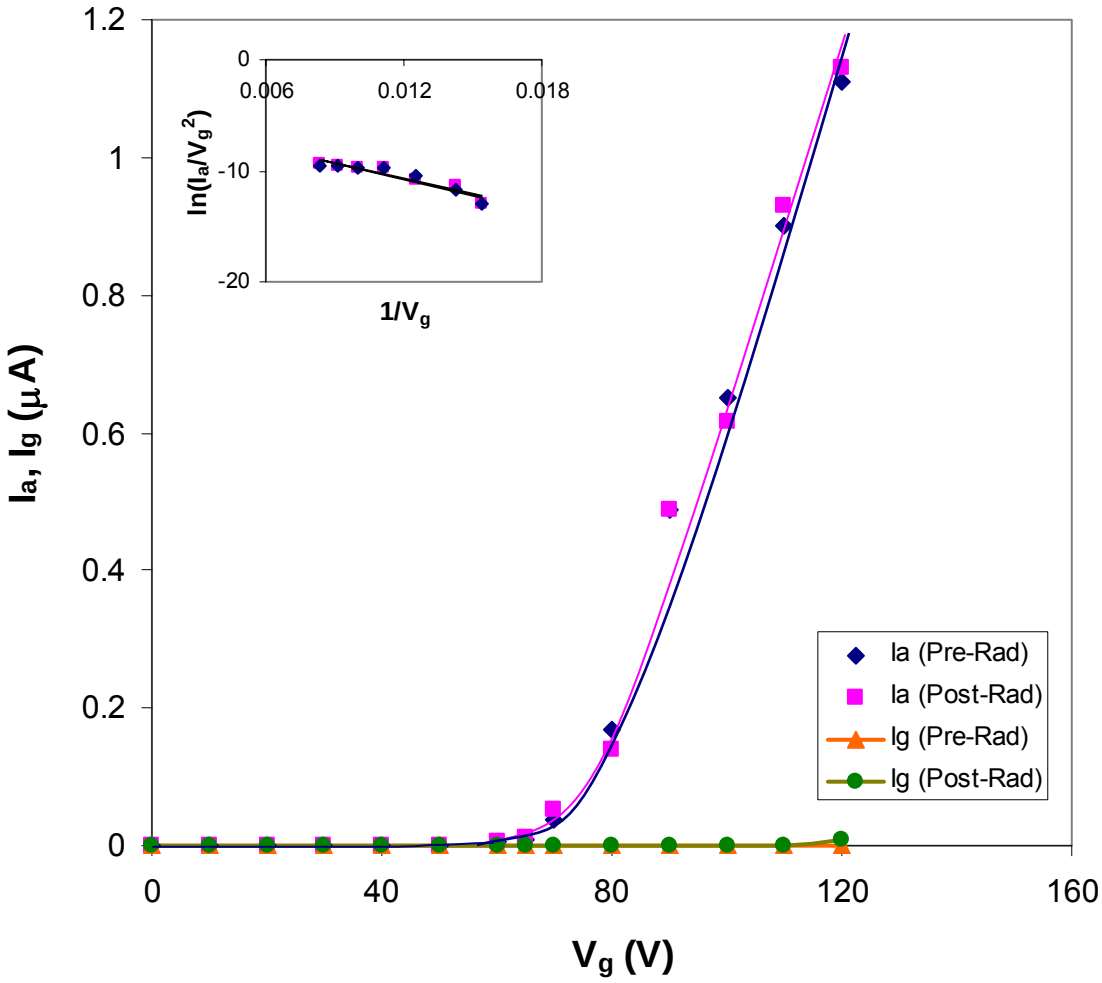

Figure 6.40 Unchanged I_a-I_g-V_g plots obtained from the nanodiamond lateral field emission transistor at an applied anode voltage, V_a=360 V (saturation region) before and after x-ray exposure; inset: corresponding F-N plots of the data of I_a vs. V_g.

A lateral emitter array structure can be developed in future to improve the performance of the vacuum transistor. As demonstrated by the current scaling behavior of the nanodiamond lateral field emitters in this research, increasing the cathode area with uniformly micropatterned arrays of fingers will lower the operating electric field and voltage and enhance the current, resulting in increased transconductance suitable for achieving high signal gain from the device,

when operated as an amplifier. **Table 6.2** estimates some of the potential performance parameters of the lateral emitter array transistor device, when developed. These estimates are based on the field emission characteristics observed in a typical multi-fingered nanodiamond lateral device in diode configuration on a SOI substrate. A safe and reliable long-term device operating mode at reasonable current densities and voltages is chosen for determining these values, even though better performance can be achieved by maximizing the current from each diamond finger tip.

Table 6.2 Estimated performance specifications of a 125-fingered nanodiamond lateral field emission transistor designed with a 2 μm gate-cathode spacing on a SOI substrate

Parameter	Estimated value
Gate turn-on voltage (V_{th})	2.2 V (1.1 V/μm turn-on electric field)
Transconductance (g_m)	~ 11 μS
A.C. voltage gain [$A_v = gm * (R_a//R_L//r_a)$] Anode resistor R_a: 6 MΩ Load Resistor R_L: 100 MΩ Anode resistance: 10 GΩ	~ 61 or 35 dB
Cut-off frequency [$f_t = g_m/2\pi C_g$] C_g = cathode-gate capacitance: ~ pF	1.75 MHz

A possible design of the lateral emitter array transistor can involve a bottom-gate structure, where the array of nanodiamond emitter-fingers is present at a distance of 2 μm from a bottom layered gate (Si or metal), with an integral anode (nanodiamond) on the same plane as the cathode. The device can be fabricated using the same dual-mask process technique developed for the lateral diode in this research.

6.2.4 Vacuum device operation in a package

Field emission characterization measurements were performed on vacuum-packaged nanodiamond lateral devices. The initial results indicate a practical device and package for vacuum electronic applications.

Figure 6.41 presents the electrical characteristics of a 6-finger nanodiamond lateral diode in package environment, yielding an emission current over 3 μA at an anode voltage of 95 V (electric field: ~10 V/μm). The F-N linear plot with negative slope (see inset, **Figure 6.41**) confirms that the current is due to field emission. The current was found to be stable with no emission degradation over a time period greater than 2 h at a constant applied voltage, indicating that the vacuum environment in package is suitable for device operation. The current-time behavior, shown in **Figure 6.42**, also verifies that diamond electron field emitters, with their ability to withstand ion bombardment and also remain immune to gas adsorption and desorption, can operate with relative stability at practical vacuum levels achievable in a package. The package was then transferred into a bell-jar vacuum chamber maintained at a base pressure of $2x10^{-7}$ Torr and the same device tested for field emission. The I-V characteristics were observed to be unchanged, as depicted in **Figure 6.41**, thus verifying that the vacuum seal of the package is not leaking. These results imply a portable candidate for temperature and radiation immune electronics. Packaging high power lateral emission device configurations and also testing them in extremely harsh conditions is a subject for future study. Efficient vacuum field emission device operation warrants a pressure level of ~ 10^{-5} to 10^{-6} Torr sealed in package cavity. Available techniques should be employed to analyze the constituents of the sealed vacuum environment and accurately measure the pressure in package, apart from assessing the same based on the emission behavior of the devices in the package. Efforts need to be focused on the development

of an advanced packaging process involving materials with low outgassing properties to routinely achieve optimal vacuum level in package.

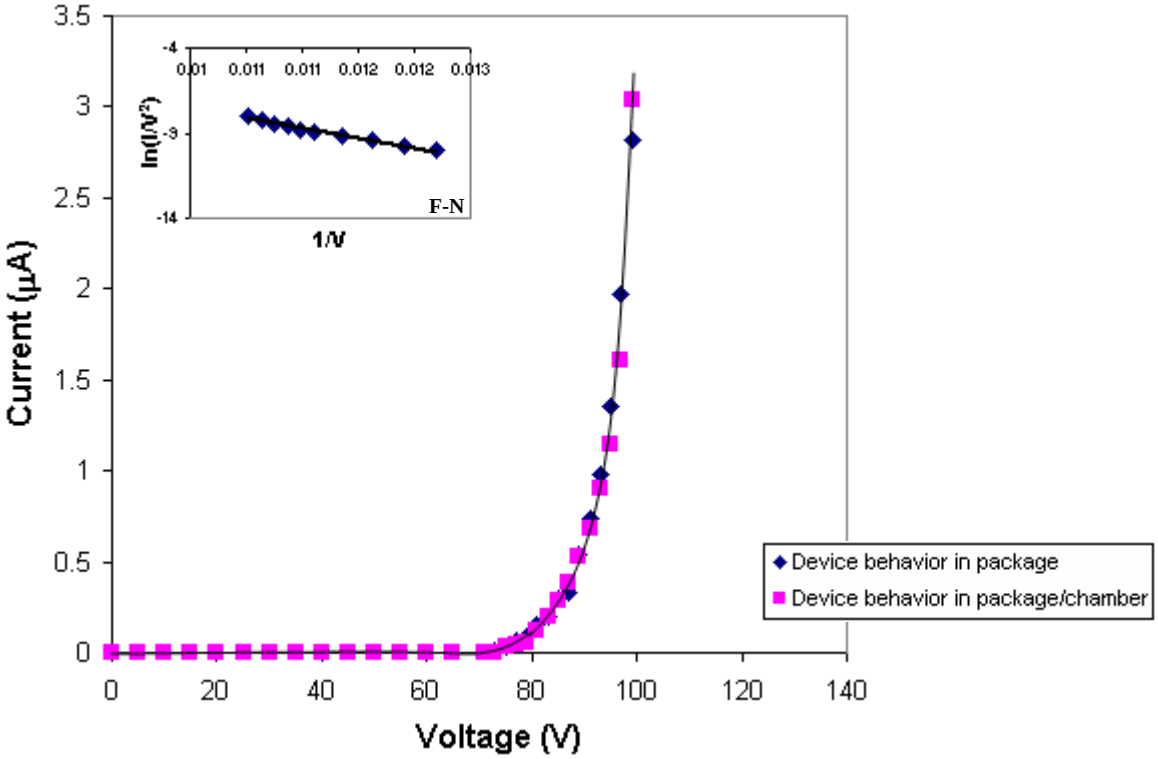

Figure 6.41 Field emission behavior of a 6-finger nanodiamond lateral device operating in package, with *unchanged* characteristics when tested inside a vacuum chamber; inset: F-N plot.

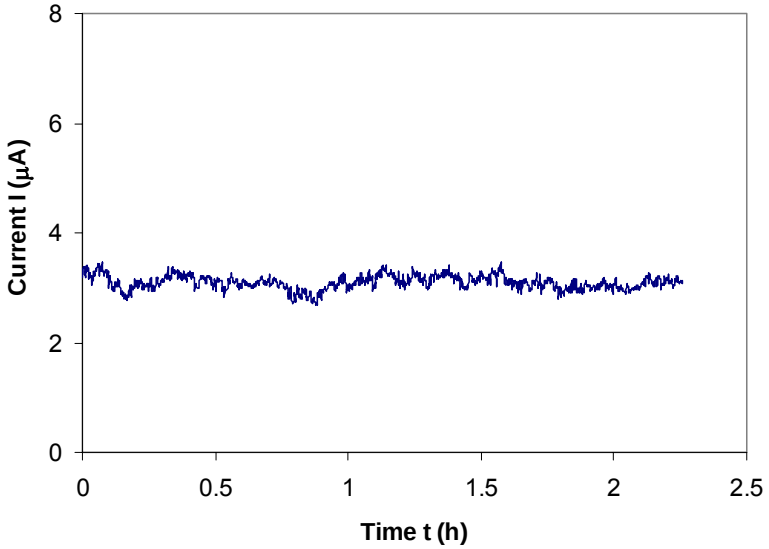

Figure 6.42 Current-time emission stability behavior of the nanodiamond lateral device in package at a constant applied voltage of 95 V.

6.2.5 Verification of field emission from nanodiamond lateral emitter devices

It is important to verify that the measured current in the lateral device is indeed a field emission current from nanodiamond finger tips, and not leakage current**.** Several techniques have been adopted to achieve absolute clarification of field emission phenomenon in lateral devices. The Fowler-Nordheim behavior of each and every lateral emitter device discussed in this research was verified. The emission was found to conform to F-N behavior; the F-N plots of the nanodiamond lateral diodes are straight lines with a negative slope. The F-N slopes are also indicative of the estimated β and Φ factors of the emitter. A conclusive idea of the electron field emission current was achieved by conducting temperature insensitive tests on the diamond lateral devices to rule out *Frenkel-Poole* conduction via SiO_2 defects. The emission characteristics of the nanodiamond lateral diodes are temperature insensitive at 200 ^{o}C, which totally confirm the absence of any leakage current via the SiO_2 layer (dielectric strength: 5 MV/cm) [221], and also signify the reliability offered by the nanodiamond vacuum device for high temperature electronics. The typical *unchanged* field emission behavior of the device at various temperatures has been shown earlier in this chapter (see **Figure 6.28**), which is the first operational temperature-immunity data presented in field emission literatures for the lateral emitters to show that there is no leakage through the supporting oxide layer in the device.

In addition, current conduction due to F-N tunneling through silicon dioxide is highly unlikely, because tunneling through a silicon dioxide layer would occur at a much higher electric field typically 1000 V/μm [222] contradicting to the low turn-on of 1-5 V/μm obtained in the diamond lateral emitter device. Conductivity measurements of the lateral devices in an open-air environment before and after emission testing were also conducted to examine the quality of the silicon dioxide layer. If the measured current is a leakage current or hopping conduction current

via SiO_2, it must remain unchanged in open air as well as in vacuum environments because leakage and hopping are conduction currents in solid-state devices. No current was observed in open air environment. Reverse bias measurements were done to confirm that the observed forward current is attributed to field emission. In an all-diamond lateral diode, there can be emission current in the reverse direction due the use of a nanodiamond anode. Hence, a nickel anode has been applied to show that there is no emission or leakage current in the lateral diode under reverse bias. Furthermore, it should be noted that leakage conduction currents via SiO_2 layer were observed from defective samples. These leakage conduction currents through the oxide were found to be strongly temperature sensitive, symmetric under applied voltage, and remained the same in both vacuum and open-air environment.

Therefore, it is sufficient to conclude from these experimental measurements that the measured current from the lateral device is indeed the emission current from nanodiamond fingers into vacuum.

CHAPTER VII

CONCLUSIONS AND RECOMMENDATIONS

In this research, nanocrystalline diamond has been developed as an applicable microelectronic material. Thin film processing techniques have been identified for nitrogen-incorporated nanodiamond and integrated for device fabrication for utilization in vacuum field emission microelectronics (VFEM) technology. The upshot of these techniques is the development of monolithic diamond diode, triode, and transistor devices in lateral configuration, demonstrating enhanced electron emission characteristics of low turn-on voltage and electric field, high and stable emission current, operational temperature and radiation tolerance, making them potential candidates for realizing IC-compatible high-speed, high-power, extreme environment electronics, sensors, and nanoelectromechanical systems (NEMS). The important results obtained from the experiments conducted are summarized in this chapter, followed by recommendations for future studies on the nanodiamond lateral vacuum field emission devices.

7.1 Conclusions

7.1.1 Nanodiamond thin film processing and characterization

Controlled and consistent process techniques have been developed to deposit and micropattern nanocrystalline diamond thin films with properties favorable for vacuum field emission. Factors contributing to electron field emission from diamond were identified and a suitable form of the material offering these field enhancement factors realized. An effective growth-rate control method has been devised and implemented to deposit nanodiamond films with grain size as small as 5 nm and low RMS surface roughness of 8-20 nm by $CH_4/H_2/N_2$

microwave plasma-enhanced chemical vapor deposition (MPECVD). Nitrogen, a suitable n-type dopant in nanocrystalline diamond films, has been incorporated successfully to realize high electrical conductivity at room temperature and thereby enhanced electron transport and electron emission properties. Through characterization of the electrical behavior of nanodiamond cathodes under vacuum, it was found that field emission from diamond is significantly enhanced by properties of increased sp^2 carbon content and nitrogen impurity concentration in the nanodiamond material. To apply nanodiamond as an efficient electron emitter, a micropatterning process was developed to derive geometrical field enhancement. The difficulty in patterning diamond films to build micron-scale devices, has been resolved by the development of a highly selective and uniform nanodiamond etch process using an oxygen plasma reactive ion etch (RIE) technique. A high diamond etch rate of 0.5 μm/min was achieved, and various electron field emitter micro/nanostructures of nanodiamond realized.

7.1.2 Nanodiamond lateral field emitter device fabrication

A process flow, compatible with conventional semiconductor integrated circuit (IC) process technology and integration, has been developed to fabricate nanodiamond lateral field emitter devices on a SOI wafer. Monolithic lateral diodes and triodes are consistently batch-fabricated using a single mask, and other advanced vacuum microelectronic devices and circuits, in a chip-type architecture, could be built without employing excessive or arcane process steps. The deposition and micropatterning techniques developed for nanodiamond were applied with precise lithography processing to yield the lateral device features. High aspect-ratio *finger-like* nanodiamond lateral emitters having a ~ 15 nm tip radius of curvature form the cathode geometry, with a nanodiamond lateral edge structure as the anode, isolated by an SiO_2 layer.

Anode-cathode spacings down to 2 μm have been achieved with the device, enabling the potential for low voltage operation. Versatile lateral comb array diode configurations comprising 9000 uniformly micropatterned emitter-fingers with small inter-electrode separation over a large area for high current applications have been realized. The same process was applied to build monolithic lateral vacuum triodes, with the lateral cathode, gate, and anode integrated on the same substrate, with 2 μm gate-cathode spacing. The diamond device has also been provided with an integrated gold contact layer for equal potential distribution over a large-area structure. Further, an advanced dual-mask microprocessing scheme has been utilized to fabricate lateral field emission devices integrating a nanodiamond cathode with a nickel anode for high rectification diode applications, signifying the feasibility of materials integration offered by nanocrystalline diamond. The 1 μm-thick oxide layer used for lateral device isolation has also been upgraded to an aluminum nitride substrate of 640-μm thickness for reliable high power vacuum microelectronics. High-resolution lithography control over critical device parameters, viz., emitter geometry, interelectrode spacing, and array structure in the lateral configuration provides a potential solution to some of the significant barriers in vacuum micro/nanoelectronics.

7.1.3 Nanodiamond lateral vacuum diode characteristics

Several aspects of the field emission behavior of the nanodiamond lateral diodes have been investigated. A low turn-on voltage of 5.9 V has been achieved from a lateral device with interelectrode spacing in the micron range. An extremely low threshold electric field of 1.1 V/μm is observed, attributed to the strong field enhancement factors in the nanodiamond lateral emitter. These characteristics enhance operational reliability and indicate the potential of the device for ultra-low power electronics, when a sub-micron anode-cathode distance is obtained by

an e-beam lithography-based process technique. The effect of the device design (emitter geometry, array size, and electrode gap) on the electrical performance is studied and quantified.

The potential of the nanodiamond lateral device for high power applications was established. A high emission current of 1 mA from a 6-finger nanodiamond lateral device at an anode voltage under 100 V, with a current per finger of 183 μA, and current density of 85 A/cm^2 has been achieved. Increasing the cathode area, emission current scaling behavior was observed, with less than 20 % deviation from ideal linearity measured logarithmically. A nanodiamond vacuum diode operable at high emission current over 25 mA at reasonable voltages, with potential for generating much higher current from the device, has been demonstrated using a monolithic lateral comb array emitter structure, possessing well-defined emission sites and a high emission site density with equal anode-cathode spacing over a large area. Improved reliability of the lateral device for high power has been demonstrated, when aluminum nitride insulator is applied for electrode isolation. Excellent diode behavior with high rectification factor (> 10^4) has been achieved in the lateral field emission device, involving a non-diamond anode, implying viable candidacy for low voltage microelectronic circuit applications.

7.1.4 Nanodiamond lateral vacuum triode characteristics

A monolithically integrated nanodiamond lateral field emission microtriode has been developed in this work on SOI as well as aluminum nitride substrates. It was identified that the behavior of the lateral emitter device can be completely varied as a *triode* or a *transistor* by lithographically altering the design of the three-terminal structure. The lateral anode can induce the electron emission, when placed closer to the cathode (~ 10 μm), and result in gate-modulated *triode* characteristics, as in a classical triode. When the anode is located at a large inter-distance

($\geq$ 100 μm) from the cathode and gate electrodes, it effectively acts as a collector, with the gate, by virtue of its proximity ($\leq$ 2 μm) to the cathode, principally controlling the electric field at the emitter finger-tip, leading to *transistor* characteristics.

Transistor characteristics have been achieved for the first time in a lateral device configuration, exhibiting distinct cut-off, linear, and saturation regions, with good gate controlled modulation of the device current. The flat saturation region and negligible gate current attributes obtained are suited for practical and reliable applications. The diamond lateral transistor shows a high amplification factor (D.C. voltage gain) and output impedance, with low capacitance, and a clear path to further enhancement of the transconductance. This fabrication and demonstration of a monolithic lateral field emission transistor is an essential step in the development of IC-equivalent high-frequency signal or power amplifiers, logic gates, switches, oscillators, modulators, sensors and control devices, having temperature- and radiation-immunity.

The devices have undergone evaluation for their behavior at extended operational levels such as temperature and radiation. We have performed the first total dose and neutron radiation exposure tests on nanodiamond lateral vacuum field emission microelectronics (VFEM) technology. Exposure to high levels of x-ray radiation flux (upto 20 Mrad(SiO_2) total dose), that would have damaged silicon solid-state devices, had no effect on device performance. The pre- and post-neutron radiation behavior of the diamond devices was examined to a total fluence of 4.4×10^{13} neutrons/cm^2. Property changes, including resistivity, dilation and emission characteristics were sought, but no changes were observed. The diamond lateral vacuum emission devices are determined to be insensitive to neutron irradiation to this level of exposure. Operational temperature tolerance was also observed in the field emission performance of the lateral device over a wide temperature range between 27 °C and 350 ºC. These results,

portraying the inherent temperature tolerance and radiation hardness of the diamond vacuum microelectronics technology, represent the development of an electron device of choice for a whole large realm of applications warranting extreme operational limits in their system specifications, such as radar, electronic warfare and space-based communications, and also certain specialized terrestrial electronic systems.

The emission characteristics of the nanodiamond lateral devices were observed to be stable and repeatable over time. Low current fluctuations were observed in the μA emission current regime, which increased slightly at high currents (mA regime), operating in a vacuum condition of ~ 10^{-6}-10^{-7} Torr. Further improvement in the current stability behavior of the diamond lateral emitters can be expected at very high vacuum levels of 10^{-9}-10^{-11} Torr. Nevertheless, the ability of the diamond emitter to function with good stability even at medium vacuum levels was noticed, when the lateral devices were assembled in vacuum cavity packages.

Overall, nanocrystalline diamond is a favorable material for electron field emission, with its properties well suited for use in a broad range of applications. With the emergence of nanodiamond, the utility of CVD diamond can now be vastly expanded to perpetuate the development of robust devices and products from the material. One such application is explored in this research in the form of lateral vacuum field emission microelectronics. The nanodiamond lateral emitter device represents a new category of diamond-based electronics, made possible from the development of a consistent microfabrication process capable of achieving desirable micro/nanostructures from the material. The development of monolithic nanodiamond lateral field emission diode, triode and transistor devices signifies a novel approach to accomplish vacuum integrated circuits and electronic systems for terrestrial and space-based applications.

7.2 Recommendations for future work

The present work on the nanodiamond lateral vacuum microelectronic devices can be extended to investigate the following:

(i) Design, simulate, fabricate, and characterize a nanodiamond lateral field emission array transistor and examine its transconductance and gain performance for high frequency amplifiers

(ii) Apply the diamond lateral vacuum diode, triode, and transistor devices monolithically in integrated circuits (ICs) and build digital logic gates, differential amplifiers, and complex electronic systems

(iii) Develop a 100 nm interelectrode-gap diamond lateral field emission diode employing e-beam lithography patterning process and demonstrate ultra-low voltage device turn-on and operation

(iv) Pursue the reliability and high current potential shown by the nanodiamond lateral comb array emitter diode on aluminum nitride substrate for high power applications

(v) Develop an advanced package for the lateral device with high vacuum sealing for portable and commercial utilization of the device and technology

(vi) Extend the temperature insensitivity and radiation hardness performance of the diamond lateral vacuum device into a packaged device and for custom applications such as space communication electronics and sensors

(vii) Study the field emission response of the lateral vacuum device at very low (freezing) temperatures for cryogenic electronic circuits.

LIST OF PUBLICATIONS

Research works related to this dissertation have been published in or submitted to the following peer-reviewed journals as listed below.

[1] K. Subramanian, W. P. Kang, and J. L. Davidson, "Development of a Monolithic Nanodiamond Lateral Field Emission Vacuum Transistor", *IEEE Electron Device Letters*, 2008 (submitted).

[2] K. Subramanian, W. P. Kang, and J. L. Davidson, "Nanocrystalline Diamond Lateral Vacuum Microtriode", *Applied Physics Letters*, 2008 (submitted).

[3] J.L. Davidson, W.P. Kang, K. Subramanian, A. Holmes-Siedle, R.A. Reed, and K.F. Galloway, "Diamond electronic device behavior after high neutron fluence exposure", *IEEE Transactions on Nuclear Science*, 2008 (submitted).

[4] K. Subramanian, R. Schroeder, W.P. Kang, and J.L. Davidson, "Development of a vacuum packaged nanodiamond lateral field emission device", *Journal of Vacuum Science and Technology B: Microelectronics and Nanometer Structures*, Article In Review, 2008.

[5] K. Subramanian, W.P. Kang, J.L. Davidson, and B.K. Choi, "The effect of interelectrode spacing on field emission in nanodiamond lateral vacuum devices", *Diamond and Related Materials*, Article In Press, Corrected Proof, Available online 16 April 2008.

[6] K. Subramanian, W.P. Kang, J.L. Davidson, and M. Howell, "Nanodiamond lateral field emitter devices on thick insulator substrates for reliable high power applications", *Diamond and Related Materials*, vol. 17, pp. 786-789, 2008.

[7] K. Subramanian, W. P. Kang, and J. L. Davidson, "Emission current scaling in nanodiamond lateral field emission devices", *Journal of Vacuum Science and Technology B: Microelectronics and Nanometer Structures*, vol. 25, pp. 532-535, 2007.

[8] W. P. Kang, J. L. Davidson, K. Subramanian, B. K. Choi, and K. F. Galloway, "Nanodiamond Lateral VFEM Technology for Harsh Environments", *IEEE Transactions on Nuclear Science*, vol. 54, pp. 1061-1065, 2007.

[9] K. Subramanian, W. P. Kang, J. L. Davidson, Y.M. Wong, and B. K. Choi, "Nanodiamond lateral field emission diode fabrication by dual micropatterning technique", *Diamond and Related Materials*, vol. 16, pp. 1408-1412, 2007.

[10] K. Subramanian, Y.M. Wong, W.P. Kang, J.L. Davidson, B.K. Choi, and M. Howell**, "**Field emission devices for advanced electronics comprised of lateral nanodiamond or carbon nanotube emitters, *Diamond and Related Materials*, vol. 16, pp. 1997-2002, 2007.

[11] K. Subramanian, W.P. Kang, J.L. Davidson, B.K. Choi, and M. Howell, "Nanodiamond lateral comb array field emission diode for high current applications", *Diamond and Related Materials*, vol. 15, pp. 1994-1997, 2006.

[12] K. Subramanian, W.P. Kang, J.L. Davidson, R.S. Takalkar, B.K. Choi, M. Howell, and D.V. Kerns, "Enhanced electron field emission from micropatterned pyramidal diamond tips incorporating $CH_4/H_2/N_2$ plasma-deposited nanodiamond", *Diamond and Related Materials*, vol. 15, pp. 1126-1131, 2006.

[13] R.S. Takalkar, W.P. Kang, J.L. Davidson, B.K. Choi, W.H. Hofmeister, and K. Subramanian, "Field emission characteristics of diamond edge-shaped emitters fabricated using nitrogen–methane plasma", *Diamond and Related Materials*, vol. 15, pp. 329-333, 2006.

[14] K. Subramanian, W. P. Kang, J. L. Davidson, B. K. Choi, and M. Howell, "Single-mask multiple lateral nanodiamond field emission devices fabrication technique", *Journal of Vacuum Science and Technology B: Microelectronics and Nanometer Structures,* vol. 24, pp. 953-957, 2006.

[15] K. Subramanian, W.P. Kang, J.L. Davidson, J.D. Jarvis, W.H. Hofmeister, B.K. Choi, and M. Howell, "Geometrical field enhancement on micropatterned nanodiamond film for electron emissions", *Diamond and Related Materials,* vol. 15, pp. 417-425, 2006.

[16] K. Subramanian, W.P. Kang, J.L. Davidson, W.H. Hofmeister, B.K. Choi, and M. Howell, "Nanodiamond planar lateral field emission diode", *Diamond and Related Materials,* vol. 14, pp. 2099-2104, 2005.

[17] K. Subramanian, W. P. Kang, J. L. Davidson, and W. H. Hofmeister, "Growth aspects of nanocrystalline diamond films and their effects on electron field emissions", *Journal of Vacuum Science and Technology B: Microelectronics and Nanometer Structures,* vol. 23, pp. 786-792, 2005.

[18] K. Subramanian, W.P. Kang, J.L. Davidson, W.H. Hofmeister, "The effect of growth rate control on the morphology of nanocrystalline diamond", *Diamond and Related Materials*, vol. 14, pp. 404-410, 2005.

[19] W.P. Kang, J.L. Davidson, A. Wisitsora-at, Y.M. Wong, R. Takalkar, K. Subramania, D.V. Kerns, and W.H. Hofmeister, "Diamond and carbon-derived vacuum micro- and nano-electronic devices", *Diamond and Related Materials*, vol. 14, pp. 685-691, 2005.

REFERENCES

[1] T. Utsumi, “Vacuum Electronics: What’s New and Exciting”, *IEEE Trans. Electron Devices*, vol. 38, pp. 2276-2283, 1991.

[2] P.R. Schwoebel and I. Brodie, “Surface-science aspects of vacuum microelectronics”, *J. Vac. Sci. Technol. B*, vol. 13, pp. 1391-1410, 1995.

[3] J. Bardeen and W.H. Brattain, “The Transistor, A Semi-Conductor Triode”, *Phys. Rev.*, vol. 74, pp. 230-231, 1948.

[4] R.N. Noyce, “Semiconductor Device-and-Lead Structure”, *US Patent* 2,981,877, 1959.

[5] J.S. Kilby, “Invention of the Integrated Circuit”, *IEEE Trans. Electron Devices*, vol. ED-23, pp. 648-654, 1976.

[6] I. Brodie and C.A. Spindt, “Vacuum Microelectronics”, *Adv. Electron. Electron Phys.*, vol. 83, pp. 1-106, 1992.

[7] H.H. Busta, “Review-Vacuum Microelectronics”, *J. Micromech. Microeng.*, vol. 2, pp. 42-74, 1992.

[8] I. Brodie and P.R. Schwoebel, “Vacuum Microelectronic Devices”, *Proc. IEEE*, vol. 82, pp. 1006-1034, 1994.

[9] A. Wisitsora-at, W.P. Kang, J.L. Davidson, C. Li, D.V. Kerns, and M. Howell, “Modeling of the transistor characteristics of a monolithic diamond vacuum triode”, *J. Vac. Sci. Technol. B,* vol. 21, pp. 1665-1670, 2003.

[10] W.P. Kang, Y.M. Wong, J.L. Davidson, D.V. Kerns, B.K. Choi, J.H. Huang, and K.F. Galloway, “Carbon nanotubes vacuum field emission differential amplifier integrated circuits”, *Electronics Letters*, vol. 42, p. 210, 2006.

[11] D.A. Buck and K.R. Shoulders, “An approach to microminiature systems”, *Proc. Eastern Joint Computer Conference, Amer. Inst. of Elect. Engrs: New York*, p.55, 1958.

[12] K.R. Shoulders, “Microelectronics using electron beam activated machining techniques”, *Advances in Computers,* vol. 2, p. 135, 1961.

[13] C. A. Spindt and K. R. Shoulders, “Research in micron-size field-emission tubes”, *IEEE 1966 Eight Conference on Tube Techniques*, p.143, 1966.

[14] C. A. Spindt, “A Thin Film Field Emission Cathode”, *J. Appl. Phys.*, vol. 39, p. 3504, 1968.

[15] R. Meyer, A. Ghis, P.C. Rambaud, and F. Muller, "Microchip fluorescence display", *Proc. Japan Display*, p. 513, 1986.

[16] H.F. Gray, G.J. Campisi, and R.F. Greene, "A vacuum field effect transistor using silicon field emitter arrays", *Proc. IEDM 86*, Los Angeles, CA, p. 776, 1986.

[17] C. A. Spindt, C. E. Holland, and R. D. Stowell, "Field emission cathode array development for high current density applications", *Proc. 29th International Field Emission Symposium*, p. 119, 1982.

[18] I. Brodie, "Physical Considerations in Vacuum Microelectronics Devices", *IEEE Trans. on Electron Devices*, vol. 36, p. 2641, 1989.

[19] B. C. Djubua and N. N. Chubun, "Emission properties of Spindt-type cold cathodes with different emission cone material", *IEEE Trans. on Electron Devices*, vol. 38, p. 2314, 1991.

[20] C. A. Spindt, C. E. Holland, A. Rosengreen, and I. Brodie, "Field emitter arrays for vacuum microelectronics", *IEEE Trans. on Electron Devices*, vol. 38, no.10, p. 2355, 1991.

[21] E. A. Adler, Z. Bardai, R. Forman, D. M. Goebel, R. T. Longo, and M. Sokolich, "Demonstration of low voltage field emission", *IEEE Trans. on Electron Devices*, vol. 38, p. 2304, 1991.

[22] C. A. Spindt and I. Brodie, "Molybdenum field emitter array", *IEDM 96 Technical Digest*, S.F., CA, Dec 8-11, 1996.

[23] G. N. Fursey, L. M. Baskin, D. V. Glazanov, A. O. Yevgen'ev, A. V. Kotcheryzhenkov, and S. A. Polezhaev, "Specific features of field emission from submicron cathode surface areas at high current densities", *J. Vac. Sci. Technol. B*, vol. 16, p. 232, 1998.

[24] T. Sakai, T. Ono, M. Nakamoto, and N. Sakuma, "Self-align Si gate field emitter arrays using the transfer mold technique", *J. Vac. Sci. Technol. B*, vol. 16, p. 770, 1998.

[25] F. Ito, K. Konuma, and A. Okamoto, and A. Yano, "Effects of thermal annealing on emission characteristics and emitter surface properties of a Spindt-type field emission cathode", *J. Vac. Sci. Technol. B*, vol. 16, p. 783, 1998.

[26] C. W. Oh, C. G. Lee, B. G. Park, J. D. Lee, and J. H. Lee, "Fabrication of metal field emitter arrays for low voltage and high current operation", *J. Vac. Sci. Technol. B*, vol. 16, p. 807, 1998.

[27] H. F. Gray, "Silicon field emitter array technology", *Proc. 29th International field emission symposium*, p. 111, 1982.

[28] R. A. Lee, "Electron emission at GEC", *The 1st International Vacuum Microelectronics Conference*, June 13-15, 1988.

[29] W. J. Orvis, C. F. McConaghy, D. R. Ciarlo, J. H. Yee, and E.W. Hee, "Modeling and Fabricating Micro-Cavity Integrated Vacuum Tubes", *IEEE Trans. on Electron Devices*, vol. 36, p. 2615, 1989.

[30] C. E. Hunt, J. T. Trujillo, and W. J. Orvis, "Structure and Electrical Characteristic of Silicon Field Emission Microelectronic Devices", *IEEE Trans. on Electron Devices*, vol. 38, p. 2309, 1991.

[31] Q. Li, W. P. Kang, M. Y. Yuan, J. F. Xu, D. Zhang, and J. L. Wu, "Fabrication and characterization of silicon field emission diodes and triodes", *J. Vac. Sci. Technol. B*, vol. 12, p. 676, 1994.

[32] D. B. King, J. G. Fleming, and R. J. Walko, "The potential of Vacuum microelectronics for space reactor applications", *AIP Conference Proceedings*, vol. 324, part 1, p. 19, 1995.

[33] S. Kang, J. H. Lee, Y. H. Song, B. G. Yu, K. I. Cho, and H. J. Yoo, "A novel structure of silicon field emission cathode with sputtered TiW for gate electrode and TEOS Oxide for gate dielectric", *IEDM 96 Technical Digest*, S.F., CA, Dec 8-11, 1996.

[34] S. Kang, J. H. Lee, Y. H. Song, B. G. Yu, K. I. Cho, and H. J. Yoo, "A novel lateral field emitter triode with insitu vacuum encapsulation", *IEDM 96 Technical Digest*, S.F., CA, Dec 8-11, 1996.

[35] J. H. Lee, S. Kang, Y. H. Song, K. I. Cho, S. Y. Lee, and H. J. Yoo, "Fabrication and characterization of silicon field emitter arrays by spin-on-glass etch-back process", *J. Vac. Sci. Technol. B*, vol. 16, p. 238, 1998.

[36] S. Kang, J. H. Lee, B. G. Yu, K. I. Cho, and H. J. Yoo, "Novel structure of silicon field emission cathode with sputtered TiW for gate electrode", *J. Vac. Sci. Technol. B*, vol. 16, p. 242, 1998.

[37] K. Higa, K. Nishii, and T. Asano, "Gated Si field emitter arrays prepared by using anodization", *J. Vac. Sci. Technol. B*, vol. 16, p. 651, 1998.

[38] P. Bruschi, A. Diligenti, F. Iani, A. Nannini, and M. Piotto, "Fabrication of a silicon-vacuum field emission microdiode with a moving anode", *J. Vac. Sci. Technol. B*, vol. 16, p. 665, 1998.

[39] H. Lee, S. Park, D. Park, S. Hahm, J. O. Lee, and J. Y. Lee, "Nanometer-scale gap control for low voltage and high current operation of field emission array", *J. Vac. Sci. Technol. B*, vol. 16, p. 762, 1998.

[40] M. R. Rakhshandehroo and S. W. Pang, "Fabrication of self-aligned silicon field emission devices and effects of surface passivation on emission current", *J. Vac. Sci. Technol. B*, vol. 16, p. 765, 1998.

[41] J. H. Lee, Y. Song, S. Kang, K. I Cho, S. Y. Lee, and H. J. Yoo, "Polycrystalline silicon field emitter arrays prepared by silicidation-sharpening technique at low temperature", *J. Vac. Sci. Technol. B*, vol. 16, p. 773, 1998.

[42] J. R. Jessing, H. R. Kim, D. L. Parker, and M. H. Weichold, "Fabrication and characterization of gated porous silicon cathode field emission arrays", *J. Vac. Sci. Technol. B*, vol. 16, p. 777, 1998.

[43] S. E. Huq, M. Huang, P. R. Wilshaw, and P. D. Prewett, "Microfabrication and characterization of gridded polycrystalline silicon field emitter devices", *J. Vac. Sci. Technol. B*, vol. 16, p. 796, 1998.

[44] J. H. Lee, Y. Song, S. Kang, Y. Lee, K. I. Cho, and H. J. Yoo, "Fabrication and characterization of silicon field emitter arrays with focusing electrode by chemical mechanical polishing process", *J. Vac. Sci. Technol. B*, vol. 16, p. 811, 1998.

[45] J. van der Weide, Z. Zhang, P. K. Baumann, M.G. Wemnsell, J. Bernholc, and R. J. Nemanich, "Negative-electron affinity effects on the diamond (100) surfaces", *Phys. Rev. B*, vol. 50, p. 5803, 1994.

[46] F. J. Himpsel, J. A. Knapp, J. A. Van Vechten, and D. E. Eastman, "Quantum photoyield of diamond(111)—A stable negative-affinity emitter", *Phys. Rev. B*, vol. 20, p.624, 1979.

[47] M. W. Geis, J. A. Gregory, and B.B. Pate, "Capacitance-voltage measurements on metal-SiO_2-diamond structures fabricated with (100)- and (111)-oriented substrates", *IEEE Trans. Electron Devices*, vol. 38, pp. 619-626, 1991.

[48] R. J. Nemanich, P. K. Baumann, and J. Van der Weide, "Diamond negative electron affinity surfaces, structures and devices", *Proc. Applied Diamond Conference*, vol. 1, p17, 1995.

[49] C. Bandis and B. B. Pate, "Photoelectric emission form negative-electron-affinity diamond (111) surfaces: exciton breakup versus conduction band", *Phys. Rev. B*, vol. 52, no. 16, p. 12056, 1995.

[50] I. L. Krainsky, V. M. Asnin, G. T. Mearini, and J. A. Dayton, "Negative-electron affinity effect on the surface of chemical-vapor-deposited diamond polycrystalline films", *Phys. Rev. B*, vol. 53, no. 12, p. 7650, 1996.

[51] C. Bandis and B. B. Pate, "Simultaneous field emission and photoemission from diamond", *Appl. Phys. Lett.*, vol. 69, no. 3, p. 366, 1996.

[52] J. Liu, V. V. Zhirnov, W. B. Choi, G. J. Wojak, A. F. Myers, J. J. Cuomo, and J. J. Hren, "Electron emission from a hydrogenated diamond surface", *Appl. Phys. Lett.*, vol. 69, no. 26, p. 4038, 1996.

[53] T. P. Humphreys, R. E. Thomas, D. P. Malta, J. B. Posthill, M. J. Mantini, R. A. Rudder, G. C. Hudson, R. J. Markunas, and C. Pettenkofer, "The role of atomic hydrogen and its influence on the enhancement of secondary electron emission from C(001) surfaces", *Appl. Phys. Lett.*, vol. 70, p. 1257, 1997.

[54] J. E. Yater, A. Shih, and R. Abrams, "Electron transport and emission properties of C(100)", *Phys. Rev. B*, vol. 56, p. 56, 1997.

[55] I. L. Krainsky and V. M. Asnin, "Negative electron affinity mechanism for diamond surfaces", *Appl. Phys. Lett.*, vol. 72, p. 2574, 1998.

[56] A. Wisitsora-at, W. P. Kang, J. L. Davidson, Y. Gurbuz, and D. V. Kerns, "Field emission enhancement of diamond tips utilizing boron doping and surface treatment", *Diamond Relat. Mater.*, vol. 8, pp. 1220-1224, 1999.

[57] K. R. Cheruparambil, B. Farouk, J. E. Yehoda, and N. A. Macken, "Thermal Conductivity Measurement of CVD Diamond Films Using a Modified Thermal Comparator Method", *Trans. ASME, Ser. C: J. Heat Transfer*, vol. 122, p. 808, 2000.

[58] K. M. Leung, A. C. Cheung, B. C. Liu, H. K. Woo, C. Sun, X. Q. Shi, and S. T. Lee, "Measuring thermal conductivity of CVD diamond and diamond-like films on silicon substrates by holographic interferometry", *Diamond Relat. Mater.*, vol. 8, p.1607, 1999.

[59] A. N. Obraztsov, I. Yu. Pavlovsky, H. Okushi, and H. Watanabe, "Direct measurement of CVD diamond film thermal conductivity by using photoacoustics", *Diamond Relat. Mater.*, vol. 7, p. 1513, 1998.

[60] A. Denisenko, Department of Electron Devices and Circuits, *University of Ulm*, 89069 Ulm, Germany.

[61] J. Liu, V. V. Zhirnov, A. F. Myers, G. J. Wojak, W. B. Choi, J. J. Hren, S. D. Wolter, M. T. McClure, B. R. Stoner, and J. T. Glass, "Field emission characteristics of diamond coated silicon field emitter", *J. Vac. Sci. Technol. B*, vol. 13, p. 422, 1994.

[62] T.D. Corrigan, D.M. Gruen, A. R. Krauss, P. Zapol, and R. P. H. Chang, "The effect of nitrogen addition to Ar/CH_4 plasmas on the growth, morphology and field emission of ultrananocrystalline diamond", *Diamond Relat. Mater.*, vol. 11, pp. 43-48, 2002.

[63] A. R. Krauss, O. Auciello, M. Q. Ding, D. M. Gruen, Y. Huang, V. V. Zhirnov, E. I. Givargizov, A. Breskin, R. Chechen, E. Shefer, V. Konov, S. Pimenov, A. Karabutov, A. Rakhimov, and N. Suetin, "Electron field emission for ultrananocrystalline diamond films", *J. Appl. Phys.*, vol. 89, pp. 2958-2967, 2001.

[64] X. Xiao, O. Auciello, H. Cui, D. H. Lowndes, V. L. Merkulov, and J.A. Carlisle, "Synthesis and field emission properties of hybrid structures of ultrananocrystalline diamond and vertically aligned carbon nanofibers", *Diamond Relat. Mater.*, vol. 15, pp. 244-247, 2006.

[65] S.G. Wang, Q. Zhang , S.F. Yoon , J. Ahn , Q. Zhou , Q. Wang , D.J. Yang , J.Q. Li, and S.Z. Shanyong, "Electron field emission enhancement effects of nano-diamond films", *Surface and Coatings Technology*, vol. 167, pp. 143-147, 2003.

[66] A. V. Karabutov, V. I. Konov, V. G. Pereverzev, I. I. Vlasov, E. V. Zavedeev, S. M. Pimenov, and E. N. Loubnin, "Competition of nitrogen doping and graphitization effect for field electron emission from nanocrystalline diamond films", *J. Vac. Sci. Technol. B*, vol. 22, pp.1319-1326, 2004.

[67] K. Wu, E. G. Wang, J. Chen, and N. S. Xu, "Nitrogen-incorporated distorted nanocrystalline diamond films: Structure and field emission properties", *J. Vac. Sci. Technol. B*, vol. 17, pp. 1059-1063, 1999.

[68] Yu-Che Yu, Jin-Hua Huang, and I-Nan Lin, "Electron field emission properties of nanodiamonds synthesized by the chemical vapor deposition process", *J. Vac. Sci. Technol. B*, vol. 19, pp. 975-979, 2001.

[69] Yu-Fen Tzeng, Yen-Chih Lee, Chi-Young Lee, Hsin-Tien Chiu, and I-Nan Lin, "Electron field emission properties on UNCD coated Si-nanowires", *Diamond Relat. Mater.*, vol. 17, pp. 753-757, 2008.

[70] K.L. Ma, W.J. Zhang, Y.S. Zou, Y.M. Chong, K.M. Leung, I. Bello, and S.T. Lee, "Electrical properties of nitrogen incorporated nanocrystalline diamond films", *Diamond Relat. Mater.*, vol.15, pp. 626 – 630, 2006.

[71] N. A. Fox, W. N. Wang, T. J. Davis, J. W. Steeds, and P. W. May, "Field emission properties of diamond films of different qualities", *Appl. Phys. Lett.*, vol. 71, pp. 2337-2339, 1997.

[72] J. M. Garguilo, F. A. M. Koeck, and R. J. Nemanich, X. C. Xiao, J. A. Carlisle, and O. Auciello, "Thermionic field emission from nanocrystalline diamond-coated silicon tip array", *Physical Rev. B*, vol. 72, p. 165404, 2005.

[73] J.W. Baldwin, M.K. Zalalutdinov, T. Feygelson, B.B. Pate, J.E. Butler, and B.H. Houston, "Nanocrystalline diamond resonator array for RF signal processing", *Diamond Relat. Mater.*, vol. 15, pp. 2061-2067, 2006.

[74] T. Zimmermann, K. Janischowsky, A. Denisenko, F.J. Hernández Guillén, M. Kubovic, D.M. Gruen, and E. Kohn, "Nanocrystalline diamond pn-structure grown by Hot-Filament CVD", *Diamond Relat. Mater.*, vol. 15, pp. 203-206, 2006.

[75] Y.C. Lee, S.J. Lin, V. Buck, R. Kunze, H. Schmidt, C.Y. Lin, W.L. Fang, and I.N. Lin, "Surface acoustic wave properties of natural smooth ultra-nanocrystalline diamond characterized by laser-induced SAW pulse technique", *Diamond Relat. Mater.*, vol. 17, pp. 446-450, 2008.

[76] O. Elmazria, F. Bénédic, M. El Hakiki, H. Moubchir, M.B. Assouar, and F. Silva, "Nanocrystalline diamond films for surface acoustic wave devices", *Diamond Relat. Mater.*, vol. 15, pp. 193-198, 2006.

[77] B. Bi, W.-S. Huang, J. Asmussen, and B. Golding, "Surface acoustic waves on nanocrystalline diamond", *Diamond Related Mater.*, vol. 11, pp. 677-680, 2002.

[78] O. Auciello, J. Birrell, J.A Carlisle, J.E Gerbi1, X. Xiao, B. Peng, and H.D. Espinosa, "Materials science and fabrication processes for a new MEMS technology based on ultrananocrystalline diamond thin films", *J. Phys.: Condens. Matter 16*, p. R539, 2004.

[79] A. R. Krauss, O. Auciello, D. M. Gruen, A. Jayatissa, A. Sumant, J. Tucek, D. C. Mancini, N. Moldovan, A. Erdemir, D. Ersoy, M. N. Gardos, H. G. Busmann, E. M. Meyer, and M. Q. Ding, "Ultrananocrystalline diamond thin films for MEMS and moving mechanical assembly devices", *Diamond Relat. Mater.*, vol. 10, pp. 1952-1961, 2001.

[80] Q. Chen, D.M. Gruen, A.R. Krauss, T.D. Corrigan, M. Witek, and G.M. Swain, "The Structure and Electrochemical Behavior of Nitrogen-Containing Nanocrystalline Diamond Films Deposited from CH_4/N_2/Ar Mixtures", *J. Electrochem. Soc.*, vol. 148, pp. E44-E51, 2001.

[81] A.E. Fischer, M.A. Lowe, and G.M. Swain, "Preparation and Electrochemical Characterization of Carbon Paper Modified with a Layer of Boron-Doped Nanocrystalline Diamond", *J. Electrochem. Soc.*, vol. 154, pp. K61-K67, 2007.

[82] W. Yang, J.E. Butler, W. Cai, J.A. Carlisle, D.M. Gruen, T. Kickerbocker, J. N. Russell, L.M. Smith, and R.J. Hamers, "Covalent Attachment of Hybridization of DNA at Nanocrystalline Diamond Thin films", *Nature-Materials*, vol.1, p. 253, 2002.

[83] H.H. Busta, "Lateral cold cathode triode structures fabricated on insulating substrates", Vac. *Microelectron. 89*, pp. 29-32, 1989.

[84] H.F. Gray, J.L. Shaw, A.I. Akinwande, and P. Bauhahn, "Field Edge Emitters: The Basis for a New Vacuum Transistor", *Proc. IEDM 91,* pp. 201-204, 1991.

[85] J.A. Oro and D.D. Ball, "Lateral field-emission devices with subtenth-micron emitter to anode spacing", *J. Vac. Sci. Technol. B*, vol. 11, pp. 464-467, 1993.

[86] S. Kanemaru and J. Itoh, "Fabrication and Characterization of Lateral Field-Emitter Triodes", *IEEE Trans. Electron Devices*, vol. 38, pp.2334-2336, 1991.

[87] J. Itoh, K. Tsuburaya, S. Kanemaru, T. Watanabe. S. Itoh, "Fabrication and Characterization of Comb-Shaped Lateral Field-Emitter Arrays", *Jpn. J. Appl. Phys*, vol. 32, pp. 1221-1226, 1993.

[88] M. Araragi and C. Nureki, "Planar field emission devices with three-dimensional gate structures", *J. Micromech. Microeng.*, vol. 2, pp. 5-9, 1992.

[89] H. Komatsu, "Fabrication and characterization of vacuum microelectronic devices with a lateral field electron emission cathode", *Tech. Digest 4th Int. Vacuum Microelectronics Conf* Nagahama, Japan, pp. 48-49, 1991.

[90] S.-S. Park, D.-I. Park, S.-H. Hahm, J.-H. Lee, H.-C. Choi, and J.-H. Lee, "Fabrication of a Lateral Field Emission Triode with a High Current Density and High Transconductance using the Local Oxidation of the Polysilicon Layer", *IEEE Trans. Electron Devices*, vol. 46, pp. 1283-1289, 1999.

[91] M-S. Lim, C-M. Park, M-K. Han, and Y-I. Choi, "In-situ vacuum-sealed lateral FEAs with low turn-on voltage and high transconductance", *IEEE Trans. Electron Devices*, vol. 48, pp. 161-165, 2001.

[92] J-H. Lee, M-B. Lee, S-H. Hahm, J-H. Lee, H-I. Seo, D-H. Kwon, J-S. Kim, and K-M. Choi, "Lateral field emitter arrays with high emission currents and wide operation region by high field activation", *J. Vac. Sci. Technol. B,* vol. 21, pp. 506-510, 2003.

[93] A. Kaneko, T. Kanno, K. Tomii, M. Kitawaga, and T. Hirao, "Wedge-shaped field emitter arrays for flat display", *IEEE Trans. Electron Devices*, vol. 38, pp. 2395-2397, 1991.

[94] A. Kaneko, I. Sumita, H. Kimura, J. Matsuura, and Y. Kondo, "Emission property and current fluctuation of star-like thin-film field emitter array with self-feedback function", *J. Vac. Sci. Tech. B*, vol. 13, pp. 494-499, 1995.

[95] S.B. Lee, A.S. Teh, K.B.K. Teo, M. Chhowalla, D.G. Hasko, W.I. Milne, G.A.J. Amaratunga, and H. Ahmed, "Fabrication of carbon nanotube lateral field emitters", *Nanotechnology 14*, pp. 192-195, 2003.

[96] K. Yamashita, W. Sun, K. Kakushima, H. Fujita, and H. Toshiyoshi, "rf microelectromechanical system device with a lateral field-emission detector", *J. Vac. Sci. Technol. B*, vol. 24, pp. 927-931, 2006.

[97] Q. Mei, S. Zurn, and D.L. Polla, "Process characterization and analysis of sealed vacuum microelectronic devices", *J. Vac. Sci. Technol. B*, vol. 12, pp. 638-643, 1994.

[98] J.C. Tucek, A.R. Krauss, D.M. Gruen, O. Auciello, N. Moldovan, D.C. Mancini, S. Zurn, and D. Polla, "Development of edge field emission cathodes based on low work function Cu-Li alloy coatings", *J. Vac. Sci. Technol. B,* vol. 18, pp. 2427-2432, 2000.

[99] W.N. Carr and J.M. Kim, "Field emission diodes with tungsten wedge cathode", *Proc. IEDM 91,* pp. 225-228, 1991.

[100] C. Ochiai, A. Sawada, H. Noriyasu, M. Takai, A. Hosono, and S. Okuda, "Wedge emitter fabrication using focused ion beam", *J. Vac. Sci. Technol. B*, vol. 19, pp. 904-906, 2001.

[101] C-S. Lee, J-D. Lee, and C-H. Han, "A new lateral field emission device using chemical-mechanical polishing", *IEEE Electron Device Lett.*, vol. 21, pp. 479-481, 2000.

[102] V. Milanović, L. Doherty, D.A. Teasdale, S. Parsa, and K.S.J. Pister, "Micromachining Technology for Lateral Field Emission Devices", *IEEE. Trans. Electron Devices,* vol. 48, pp.166-173, 2001.

[103] I. Puchades, R.J. Langley, and M.D. Potter, "An Integrated Thin Film Phosphor Lateral Field Emission Display Device", *Proc. Twelfth Biennial University/Government/Industry Microelectronics Symposium*, pp. 133 – 136, 1997.

[104] S. Han, S-a. Yang, T. Hwang, J. Lee, J.D. Lee, and H. Shin, "Lateral silicon field-emission devices using electron beam lithography", *Jpn. J. Appl. Phys*, vol. 39, pp. 2556-2559, 2000.

[105] W.J. Zang, J.H. Lee, J.H. Lee, Y.H. Bee, C.A. Choi, and S.H. Hahm, "Lateral field-emission diode with wedge-type tip and nanogap on separation by implantation of oxygen silicon", *J. Vac. Sci. Technol.* B, vol. 18, pp.1006-1008, 2000.

[106] J. Itoh, K. Ushiki, K. Tsuburaya, and S. Kanemaru, "Vacuum microtriode with comb-shaped lateral field-emitter array", *Jpn. J. Appl. Phys*, vol. 32, pp. L809-L812, 1993.

[107] M.S. Lim, C.M. Park, M.K. Han, and Y.I. Choi, "Investigation of field emission characteristics for Si-base materials: Titanium silicide, poly-Si, and single-crystal Si", *J. Vac. Sci. Technol. B* 17, pp. 635-637, 1999.

[108] A.C.F. Hoole, D.F. Moore, and A.N. Broers, "Directly patterned low voltage planar tungsten lateral field emission structures", *J. Vac. Sci. Technol. B*, vol. 11, pp. 2574-2578, 1993.

[109] J. Itoh, K. Tsuburaya, S. Kanemaru, T. Watanabe, and S. Itoh, "Low-operation-voltage comb-shaped field emitter array", *Jpn. J. Appl. Phys*, vol. 31, pp. L884-L886, 1992.

[110] J.-H. Park, H.-I. Lee, H.-S. Tae, J.-S. Huh, and J.-H. Lee, "Lateral field emission diodes using SIMOX wafer", *IEEE Trans. Electron Devices,* vol. 44, pp. 1018-1021, 1997.

[111] V. Milanović, L. Doherty, D. A. Teasdale, C. Zhang, S. Parsa, V. Nguyen, M. Last, and K. S. J. Pister, "Deep reactive ion etching for lateral field emission devices", *IEEE Electron Device Lett.* 21, pp. 271-273, 2000.

[112] M. Yun, A. Turner, R. J. Roedel, and M.N. Kozicki, "Novel lateral field emission device fabricated on silicon-on-insulator material", *J. Vac. Sci. Technol.* B, vol. 17, pp. 1561-1564, 1999.

[113] Y. Gotoh, K. Inoue, T. Ohtake, H. Ueda, Y. Hishida, H. Tsuji, and J. Ishikawa, "Application of focused ion beam techniques to the fabrication of lateral-type thin-film edge emitters", *Jpn. J. Appl. Phys*, vol. 33, pp. L63-L66, 1994.

[114] W.P. Kang, J.L. Davidson, A. Wisitsora-at, M. Howell, A. Jamaludin, Y.M. Wong, K.L. Soh, and D.V. Kerns, "Fabrication and field emission characteristics of lateral diamond field emitter", *J. Vac. Sci. Technol.* B, vol. 21, pp.593-596, 2003.

[115] A. Wisitsorat-at, "Micropatterned Diamond Vacuum Field Emission Devices", *PhD Dissertation*, Department of Electrical Engineering, Vanderbilt University, USA, 2002.

[116] R. H. Fowler, and L. Nordheim, "Electron emission in intense electric fields", *Proc. Royal Soc. London*, vol. 119, p. 173, 1928.

[117] Rother, *Ann. Der Physik*, vol. 81, p. 316, 1926.

[118] N. Garcia, M. I. Marques, A. Asenjo, and A. Correia, "Experimental and theoretical characterization of integrated field emission nanotips", *J. Vac. Sci. Technol. B*, vol. 16, no. 2, p. 654, 1998.

[119] G. N. Fursey and D. V. Glazanov, "Deviation from the Folwer-Nordhiem theory and peculiarities of field electron emission from small-scale objects", *J. Vac. Sci. Technol. B*, vol. 16, p. 910, 1998.

[120] J. Jung, B. Lee, and J. D. Lee, "Effective three-demensional simulation of field emitter array and its optimal design methodology using an evolution strategy", *J. Vac. Sci. Technol. B*, vol. 16, p. 920, 1998.

[121] Wei Zhu, Vacuum Microelectronics, *Wiley Interscience*, 2001.

[122] W. P. Kang, A. Wisitsora-at, J. L. Davidson, D. V. Kerns, Q. Li, J. F. Xu, and C. K. Kim, "Effect of sp^2 content and tip treatment on the field emission of micropatterned pyramidal diamond tip", *J. Vac. Sci. Technol. B*, vol. 16, pp. 684-688, 1998.

[123] A. Wisitsora-at, W. P. Kang, J. L. Davidson, M. Howell, W. Hofmeister, and D. V. Kerns, "High current diamond field emission diode", *J. Vac. Sci. Technol. B*, vol. 21, pp. 1671-1674, 2003.

[124] P. K. Baumann and R. J. Nemanich, "Electron affinity and schottky barrier height of metal-diamond (100), (111) and (110) interfaces", *J. Appl. Phys.*, vol. 82, p. 5148, 1997.

[125] P. K. Baumann and R. J. Nemanich, "Negative electron affinity effects and Schottky barrier height measurements of Cobalt on diamond (100) surfaces", *Proc. Applied Diamond Conference*, vol. 1, p. 41, 1995.

[126] J. van der Weide and R. J. Nemanich, "Influence of interfacial hydrogen and oxygen on the Schottky barrier height of nickel on (111) and (100) diamond surfaces", *Physical Rev. B*, vol. 49, p. 13629, 1994.

[127] C. Bandis, D. Haggerty, and B. B. Pate, "Electron emission properties of the negative electron affinity (111)2x1 diamond-TiO interface", *Proc. Material Research Society*, vol. 339, p. 75, 1994.

[128] W.E. Pickett, "Negative-electron-affinity and low work function surface cesium on oxygenated diamond (100)", *Phys. Rev. Lett.*, vol. 73, p. 1664, 1994.

[129] W. P. Kang, J. L. Davidson, M. Howell, B. Bhuva, D. L Kinser, and D. V. Kerns, "Micro-pattern polycrystalline diamond field emitter diode arrays", *J. Vac. Sci. Technol. B*, vol. 14, p. 1, 1996.

[130] S. Kim, B. K. Ju, Y. H. Lee, B. S. Park, Y. Baik, S. Lim, and M. H. Oh, "Electron emission of diamond-tip field emitter arrays fabricated by transfer mold technique", *J. Vac. Sci. Technol. B*, vol. 15, p. 499, 1997.

[131] E. I. Givargizov, V. V. Zhirnov, A. N. Stepanova, E. V. Rakova, A. N. Kiselev, and P. S. Plekhanov, "Microstructure and field emission of diamond particles on silicon tips," *Appl. Surf. Sci.*, vol. 87-88, p. 24, 1995.

[132] M. W. Geis, J. C. Twichell, J. Macaulay, and K. Okano, "Electron field emission from diamond and other carbon materials after H_2 , O_2 , and Cs treatment," *Appl. Phys. Lett.*, vol. 67, pp.1328-1330, 1995.

[133] W. Zhu, G.P. Kochanski, S. Jin, and L. Seibles, "Defect-enhanced electron field emission from chemical vapor deposited diamond", *J. Appl. Phys.*, vol. 78, p. 2707, 1995.

[134] M.W. Geis, J.C. Twichell, J. Macaulay, and K. Okano, *Science* 67, p. 1328, 1995.

[135] W. Zhu, G.P. Kochanski, S. Jin, L. Seibles, D. Jacobson, M. McCormack, and A. White, "Electron field emission from ion-implanted diamond", *Appl. Phys. Lett.*, vol. 67, p. 1157, 1995.

[136] Z.H. Huang, P.H. Cutler, N.M. Miskovsky, and T.E. Sullivan, "Theoretical study of field emission from diamond", *Appl. Phys. Lett.,* vol. 65, p. 2562, 1994.

[137] R.M. Hill, *Phil. Mag* 23, p. 59, 1971.

[138] Y. Muto, T. Sugino, J. Shirafuji, and K. Kobachi, "Electrical conduction in undoped diamond films prepared by chemical vapor deposition", *Appl. Phys. Lett.*, vol. 59, p. 843, 1991.

[139] J.B. Cui, J. Ristein, and L. Ley, "Low-threshold electron emission from diamond", *Phys. Rev. B*, vol. 60, p. 16135, 1999.

[140] C.S. Athwal, K.H. Bayliss, R. Calder, and R.V. Latham, "Field-Induced Electron Emission from Artificially Produced Carbon Sites on Broad-Area Copper and Niobium Electrodes", *IEEE. Trans. Plasma Sci.*, vol. 13, pp. 226-229, 1985.

[141] N.S. Xu and R.V. Latham, “Coherently scattered hot electrons emitted from MIM graphite microstructures deposited on broad-area vacuum-insulated high-voltage electrodes”, *J. Phys. D: Appl. Phys.*, vol. 19, pp. 477-482, 1986.

[142] C. Wang, A. Garcia, D.C. Ingram, M. Lake, and M.E. Kordesch, “Cold field emission from CVD diamond films observed in emission electron microscopy”, *Electron Lett.*, vol. 27, pp. 1459-1461, 1991.

[143] N.S. Xu, Y. Tzeng, and R.V. Latham, “Similarities in the 'cold' electron emission characteristics of diamond coated molybdenum electrodes and polished bulk graphite surfaces”, *J. Phys. D: Appl. Phys.*, vol. 26, pp. 1776-1780, 1993.

[144] N.S. Xu, R..V. Latham, and Y. Tzeng, “Field-dependence of the area-density of 'cold' electron emission sites on broad-area CVD diamond films”, *Electron Lett.*, vol. 28, pp. 1596-1597, 1993.

[145] N.S. Xu, Y. Tzeng, and R.V. Latham, “A diagnostic study of the field emission characteristics of individual micro-emitters in CVD diamond films”, *J. Phys. D: Appl. Phys.*, vol. 27, pp. 1988-1991, 1994.

[146] O.M. Kuttel, O. Groening, and L. Schlapbach, “Surface conductivity induced electron field emission from an indium cluster sitting on a diamond surface”, *J. Vac. Sci. Technol. A*, vol. 16, pp. 3464-3470, 1998.

[147] K.H. Bayliss and R.V. Latham, “An Analysis of Field-Induced Hot-Electron Emission from Metal-Insulator Microstructures on Broad-Area High-Voltage Electrodes”, *Proc. R. Soc. A*, vol. 403, pp. 285-311, 1986.

[148] J.D. Shovlin and M.E. Kordesch, “Electron emission from chemical vapor deposited diamond and dielectric breakdown”, *Appl. Phys, Lett.*, vol. 65, p. 863, 1994.

[149] Y.D. Kim, W. Choi, H. Wakimoto, S. Usami, H. Tomokage, and T. Ando, “Direct observation of electron emission site on boron-doped polycrystalline diamond thin films using an ultra-high-vacuum scanning tunneling microscope”, *Appl. Phys. Lett.*, vol. 75, p. 3219, 1999.

[150] B. Fiegl, R. Kuhnert, M. Ben-Chorin, and F. Koch, “Evidence for grain boundary hopping transport in polycrystalline diamond films”, *Appl. Phys, Lett.*, vol. 65, p. 371, 1994.

[151] I. Andrienko, A. Cimmino, D. Hoxley, S. Prawer, and R. Kalish, “Field emission from boron-doped polycrystalline diamond film at the nanometer level within grains”, *Appl. Phys, Lett*, vol.. 77, p. 1221, 2000.

[152] K. Okano and K. K. Gleason, “Electron emission from phosphorus and boron doped polycrystalline diamond films”, *Electron. Lett.*, vol. 31, p. 74, 1995.

[153] C. Kimura, S. Koizumi, M. Kamo, and T. Sugino, "Behavior of electron emission from phosphorus-doped epitaxial diamond films", *Diamond Relat. Mater.*, vol. 8, pp. 759-762, 1999.

[154] D. Zhou, A. R. Krauss, L. C. Qin, T. G. McCauley, D. M. Gruen, T. D. Corrigan, R. P. H. Chang, and H. Gnaser, "Synthesis and electron field emission of nanocrystalline diamond thin films grown from N_2/CH_4 microwave plasmas", *J. Appl. Phys.*, vol. 82, p. 4546, 1997.

[155] M. W. Geis, J. C. Twichell, and T. M Lyszcazarz, "Diamond Emitters Fabrication and Theory", *J. Vac. Sci. Technol. B*, vol. 14, p. 2060, 1996.

[156] K. Okano, T. Yamada, H. Ishihara, S. Koizumi, and J. Itoh, "Electron field emission from nitrogen-doped pyramidal-shape diamond and its battery operation", *Appl. Phys. Lett.*, vol. 70, p. 2201, 1997.

[157] P. Lerner, P. H. Cutler, and N. M. Miskovsky, "Theoretical analysis of field emission from a metal diamond cold cathode emitter", *J. Vac. Sci. Technol. B*, vol. 15, p. 337, 1997.

[158] P. Lerner, N. M. Miskovsky, and P. H. Cutler, "Model calculation of internal field emission and J-V characteristics of a composite n-Si and N-diamond cold cathode source", *J. Vac. Sci. Technol. B*, vol. 16, p. 900, 1998.

[159] M. W. Geis, J.C. Twichell, N.N. Efremow, K. Krohn, and T.M. Lyszczarz, "Comparison of electric field emission from nitrogen-doped, type Ib diamond, and boron-doped diamond", *Appl. Phys. Lett.*, vol. 68, p. 2294, 1996.

[160] O. Groning, O.M. Kuttel, P. Groning, and L. Schlapbach, "Field emitted electron energy distribution from nitrogen-containing diamondlike carbon", *Appl. Phys. Lett.*, vol. 71, p. 2253, 1997.

[161] P. W. May, S. Hohn, M. N. R. Ashfold, W. N. Wang, N. A. Fox, T. J. Davis, and J. W. Steeds, "Field emission from chemical vapor deposited diamond and diamond-like carbon films: Investigations of surface damage and conduction mechanisms", *J. Appl. Phys.*, vol. 84, p. 1618, 1998.

[162] M.W. Geis, N. Efremow, J. Woodhouse, M. Mcalese, M. Marchywka, D. Socker, and J. Hochedez, "Diamond cold cathode", *IEEE. Electron Device Lett.*, vol. 12, pp. 456-459, 1991.

[163] W. P. Kang, J. L. Davidson, and D. V. Kerns Jr., "Mold method for forming vacuum field emitters and methods for forming diamond emitters", *US Patent* 6,132,278, 2000.

[164] A. Wisitsora-at, W. P. Kang, J. L. Davidson, D. V. Kerns, and T. Fisher, "Diamond field-emission triode with low gate turn-on voltage and high gain", *J. Vac. Sci. Technol. B*, vol. 21, pp. 614-617, 2003.

[165] W.P. Kang, J.L. Davidson, A. Wisitsora-at, Y.M. Wong, R. Takalkar, K. Holmes, and D.V. Kerns, "Diamond vacuum field emission devices", *Diamond Relat. Mater.*, vol. 13, pp. 1944-1948, 2004.

[166] C.E. Holland, A. Rosengreen, and C.A. Spindt, "A study of field emission microtriodes", *IEEE Trans. Electron Devices*, vol. 38, pp. 2368-2372, 1991.

[167] N. Tatsumi, A. Ueda, Y. Seki, Y. Nishibayashi, and T. Imai, "Fabrication of highly uniform diamond electron emitter devices", *SEI Tech. Review*, pp. 15-20, April 2007.

[168] P. R. Schwoebel, C. A. Spindt, and C. E. Holland, "High current, high current density field emitter array cathodes*", J. Vac. Sci. Technol. B*, vol. 23, pp. 691-693, 2005.

[169] W. Zhu, G.P. Kochanski, and S. Jin, *Science* 282, p. 1471, 1998.

[170] D.M. Gruen, "Nanocrystalline Diamond Films", *Annu. Rev. Mater. Sci.*, vol. 29, p. 211, 1999.

[171] T. G. MaCauley, T.D. Corrigan, A.R. Krauss, O. Auciello, and D. Zhou, *Mater. Res. Soc. Symp. Proc.* 498, p. 227, 1998.

[172] A.R. Krauss, D.M. Gruen, D. Zhou, T.G. McCauley, and L.C. Lin, *Mater. Res. Soc. Symp. Proc.* 495, p. 299, 1998.

[173] O. Groning, O.M. Kuttel, P. Groning, and L. Schlapbach, "Field emission properties of nanocrystalline chemically vapor deposited-diamond films", *J. Vac. Sci. Technol. B*, vol. 17, pp. 1970-1986, 1999.

[174] J. Liu, V. V. Zhirnov, G. J. Wojak, A. F. Myers, W.B. Choi, J. J. Hren, S.D. Wolter, M.T. McClure, B.R. Stoner, and J.T. Glass, "Electron emission from diamond coated silicon field emitters", *Appl. Phys. Lett.*, vol. 65, p. 2842, 1994.

[175] W. B. Choi, J. J. Cuomo, V. V. Zhirnov, A. F. Myers, and J. J. Hren, "Field emission from silicon and molybdenum tips coated with diamond powder by dielectrophoresis", *Appl. Phys. Lett.*, vol. 68, p. 720, 1996.

[176] W. B. Choi, J. Liu, M.T. McClure, A. F. Myers, V. V. Zhirnov, J. J. Cuomo, and J. J. Hren, "Field emission from diamond coated molybdenum field emitters", *J. Vac. Sci. Technol. B*, vol. 14, pp. 2050-2055, 1996.

[177] V. Raiko, R. Spizl, B. Aschermann, D. Theirich, J. Engemann, N. Puteter, T. Habermann, and G. Müller, „Field emission observations from CVD diamond-coated silicon emitters", *Thin Solid Films*, vol. 290-291, pp. 190-195, 1996.

[178] V.V. Zhirnov, "On the Cold Emission Mechanism of Diamond Coated Tips", *J. de Physique* IV 6, C5, 1996.

[179] T. Sharda**,** M. M. Rahaman, Y. Nukaya, T. Soga, T. Jimbo and M. Umeno, "Structural and optical properties of diamond and nano-diamond films grown by microwave plasma chemical vapor deposition", *Diamond Relat. Mater.*, vol. 10, pp. 352-357, 2001.

[180] Advanced Diamond Technologies webpage: http://www.thindiamond.com/technical.asp

[181] Argonne National Lab website: http://www.msd.anl.gov/groups/sc/research/ntf/index.html

[182] O.A. Williams, M. Daenen, J. D'Haen, K. Haenen, J. Maes, V.V. Moshchalkov, M. Nesládek, and D.M. Gruen, "Comparison of the growth and properties of ultrananocrystalline diamond and nanocrystalline diamond", *Diamond Relat. Mater.*, vol. 15, pp. 654–658, 2006.

[183] J. Birrell, J.E. Gerbi, O. Auciello, J.M. Gibson, J. Johnson, and J.A. Carlisle, "Interpretation of the Raman spectra of ultrananocrystalline diamond", *Diamond Relat. Mater.*, vol. 14, pp. 86-92, 2005.

[184] Y.C. Chen, N.H. Tai, and I.N. Lin, "Substrate temperature effects on the electron field emission properties of nitrogen doped ultra-nanocrystalline diamond", *Diamond Relat. Mater.*, vol. 17, pp. 457-461, 2008.

[185] M. Stammler, J. Ristein, T. Habermann, A. Göhl, K. Janischowsky, D. Nau, G. Müller, and L. Ley, "Field emission measurements with micrometer resolution on carbon nanostructures", *Diamond Relat. Mater.*, vol. 8, pp. 792-797, 1999.

[186] E.D. Obraztsova, K. G. Korotushenko, S. M. Pimenov, V. G. Ralchenko, A. A. Smolin, V. I. Konov, and E. N. Loubnin, "Raman and photoluminescence investigations of nanograined diamond films", *Nanostructured Materials*, vol. 6, pp. 827-830, 1995.

[187] Y.K. Liu, P.L. Tso, D. Pradhan, I.N. Lin, M. Clark, and Y. Tzeng, "Structural and electrical properties of nanocrystalline diamond (NCD) heavily doped by nitrogen", *Diamond Relat. Mater.*, vol. 14, pp.2059-2063, 2005.

[188] S. Bhattacharyya, O. Auciello, J. Birrell, J.A. Carlisle, L.A. Curtiss, A.N. Goyette, D.M. Gruen, A.R. Krauss, J. Schlueter, A. Sumant, and P. Zapol, "Synthesis and characterization of highly-conducting nitrogen-doped ultrananocrystalline diamond films", *Appl. Phys. Lett.*, vol. 79, p.1441, 2001.

[189] Y. Dai, D. Dai, C. Yan, B. Huang, and S. Han, "*N*-type electric conductivity of nitrogen-doped ultrananocrystalline diamond films", *Phys. Rev. B*, vol. 71, p. 075421, 2005.

[190] S. Bhattacharyya, "Mechanism of high *n*-type conduction in nitrogen-doped nanocrystalline diamond", *Phys. Rev. B*, vol. 70, p.125412, 2004.

[191] P. Zapol, M. Sternberg, L.A. Curtiss, T. Frauenheim, and D.M. Gruen, "Tight-binding molecular-dynamics simulation of impurities in ultrananocrystalline diamond grain boundaries", *Phys. Rev. B*, vol. 65, p. 045403, 2001.

[192] V.I. Polyakov, A.I. Rukovishnikov, N.M. Rossukanyi, V.G. Pereverzev, S.M. Pimenov, J.A. Carlisle, D.M. Gruen, and E.N. Loubnin, "Charge-based deep level transient spectroscopy

of undoped and nitrogen-doped ultrananocrystalline diamond films", *Diamond Relat. Mater*., vol. 12, pp. 1776-1782, 2003.

[193] D.M. Gruen, A.R. Krauss, O.H. Auceillo, and J. A. Carlisle, "N-type doping of nanocrystalline diamond films with nitrogen and electrodes made therefrom", *US Patent* 6,793,849, 2004.

[194] O.A. Williams, "Ultrananocrystalline diamond for electronic applications", *Semicond. Sci. Technol.*, vol. 21**,** pp. R49–R56, 2006.

[195] X. Xiao, J. Birrell, J. E. Gerbi, O. Auciello and J. A. Carlisle, "Low temperature growth of ultrananocrystalline diamond", *J. Appl. Phys.*, vol. 96, pp. 2232-2239, 2004.

[196] D. Pradhan, Y.C. Lee, C.W. Pao, W.F. Pong and I.N. Lin, "Low temperature growth of ultrananocrystalline diamond film and its field emission properties", *Diamond Relat. Mater*., vol. 15, pp. 2001-2005, 2006.

[197] Advanced Diamond Technologies webpage: http://www.thindiamond.com/uncd.asp

[198] J. E. Gerbi, O. Auciello, J. Birrell, D. M. Gruen, B. W. Alphenaar, and J. A. Carlisle, "Electrical contacts to ultrananocrystalline diamond", *Appl. Phy. Lett.*, vol. 83, pp. 2001-2003, 2001.

[199] M. Hajra, C. E. Hunt, M. Ding, O. Auciello, J. Carlisle, and D. M. Gruen, "Effect of gases on the field emission properties of ultrananocrystalline diamond-coated silicon field emitter arrays", *J. Appl. Phys.*, vol. 94, pp. 4079-4083, 2003.

[200] M. Q. Ding, O. Auciello, J. A. Carlisle, and D. M. Gruen, "Effect of oxygen on field emission properties of ultrananocrystalline diamond-coated ungated Si tip arrays", *J. Vac. Sci. Technol. B*, vol. 21, pp. 1644-1647, 2003.

[201] F. A. M. Köck, J. M. Garguilo, Billyde Brown and R. J. Nemanich, "Enhanced low-temperature thermionic field emission from surface-treated N-doped diamond films", *Diamond Relat. Mater*., vol. 11, pp. 774-779, 2002.

[202] D.A. Dahl, SIMION 3D Version 7.0, *User's Manual*, pp. 2-5, 2000.

[203] K. B. K. Teo, M. Chhowalla, G. A. J. Amaratunga, W. I. Milne, G. Pirio, P. Legagneux, F. Wyczisk, D. Pribat, and D. G. Hasko, "Field emission from dense, sparse, and patterned arrays of carbon nanofibers", *Appl. Phy. Lett.*, vol. 80, p. 2011, 2002.

[204] C. K. Yang, A. J. le Fèbre, G. Pandraud, E. van der Drift, and P. J. French, "Field emission for resonance sensing in MEMS/NEMS", *20th Intl. Vacuum Nanoelectronics Conf. (IVNC)*, Tech. Digest , p. 72, 2007.

[205] H.H. Busta, D.W. Jenkins, B.J. Zimmerman, and J.E. Pogemiller, "Triode operation of a vacuum transistor", *Proc. IEDM*, pp. 213-215, 1991.

[206] H.H. Busta, J.E. Pogemiller, and B.J. Zimmerman, "The field emitter triode as a displacement/pressure sensor", *J. Micromech. Microeng.*, vol. 3, pp.49-56, 1993.

[207] D. Arslan, A. Dehé, and H.L. Hartnagel, "New concept of lateral GaAs field emitter for sensor applications", *J. Vac. Sci. Technol. B*, vol. 17, pp. 784-787, 1999.

[208] K. Qian, T. Chen, B. Yan, Y. Lin, D. Xu, Z. Sun, and B. Cai, "Studies on vacuum microelectronic pressure sensors based on carbon nanotubes arrays", *Physica E*, vol. 31, pp.1-4, 2006.

[209] S.H. Xia, J. Liu, D.F. Cui, J.H. Han, S.F. Chen, and L. Wang, "Investigation on a novel vacuum microelectronic pressure sensor with stepped field emission array", *J. Vac. Sci. Technol. B*, vol. 15, pp. 1573-1576, 1997.

[210] H-C Lee and R-S Huang, "A theoretical study on field emission array for microsensors", *IEEE Trans. Electron Devices*, vol. 39, p. 313-324, 1992.

[211] J.C. Jiang, R.C. White, and P.K. Allen, *Intl. Conf. Solid-State Sensors and Actuators (TRANSDUCERS 91)*, Digest of Tech. Papers, p. 238, 1991.

[212] T. Hirano, S. Kanemaru, and J. Itoh, "A MOSFET-structured Si tip for stable emission current," *IEDM 96 Tech. Digest*, S.F., CA, Dec 8-11, 1996.

[213] H.F. Gray, "Vacuum Microelectronics – Hope for Ultra-Radiation Hardness", Invited talk at the *IEEE Nuclear and Space Radiation Effects Conference,* Reno, NV, 1990.

[214] P.Pells, Private communication, *Harwell Dosimeters, Ltd*.

[215] A. Holmes-Siedle and L. Adams, "Handbook of Radiation Effects", *Oxford University Press*, 1993.

[216] B.P. Otis, "Integrated Vacuum Microelectronics", *Univ. of Berkeley*: http://bwrc.eecs.berkeley.edu/People/Grad_Students/botis/documents/papers/243_botis.pdf

[217] NASA webpage: http://www.grc.nasa.gov/WWW/SiC/aircraftbenefit.html

[218] Y.M. Wong, W.P. Kang, J.L. Davidson, W. Hofmeister, S. Wei, and J.H. Huang, "Transistor characteristics of thermal chemical vapor deposition carbon nanotubes field emission triode", *J. Vac. Sci. Technol. B,* vol. 23, pp. 868-873, 2005.

[219] H.H. Busta, B.J. Zimmerman, M.C. Tringides, and C.A. Spindt, "DC *I-V* characteristics of field emitter triodes", *IEEE Trans. Electron Devices*, vol. 38, pp. 2558-2562, 1991.

[220] K. Betsui, “Fabrication and characteristics of Si field emitter arrays”, *Tech. Digest 4th Int. Vacuum Microelectronics Conf.*, Nagahama, Japan, p. 26, 1991.

[221] S.M. Sze, “Semiconductor Physics & Technology”, *John Wiley & Sons, Inc.*, p. 358, 1985.

[222] S.M. Sze, “Modern semiconductor device physics”, *John Wiley & Sons, Inc.*, 4th ed., 1998.